

MECHANISTIC-EMPIRICAL PAVEMENT
DESIGN GUIDE FLEXIBLE PAVEMENT
PERFORMANCE PREDICTION MODELS
FOR MONTANA: *VOLUME II REFERENCE
MANUAL*

FHWA/MT-07-008/8158-2

Final Report

prepared for
THE STATE OF MONTANA
DEPARTMENT OF TRANSPORTATION

in cooperation with
THE U.S. DEPARTMENT OF TRANSPORTATION
FEDERAL HIGHWAY ADMINISTRATION

August 2007

prepared by
Harold L. VonQuintus, PE
Applied Research Associates, Inc.

James S. Moulthrop, PE
Fugro Consultants, Inc.



RESEARCH PROGRAMS

Montana Department of Transportation



You are free to copy, distribute, display, and perform the work; make derivative works; make commercial use of the work under the condition that you give the original author and sponsor credit. For any reuse or distribution, you must make clear to others the license terms of this work. Any of these conditions can be waived if you get permission from the sponsor. Your fair use and other rights are in no way affected by the above.

**Mechanistic-Empirical Pavement Design Guide
Flexible Pavement Performance Prediction Models
for Montana**

**Volume II
Reference Manual**

**Prepared for:
Research Programs
Montana Department of Transportation
2701 Prospect Avenue
Helena, Montana 59620**

**Prepared by:
Harold L. Von Quintus, PE, Applied Research Associates, Inc.
James S. Moulthrop, PE, Fugro Consultants, Inc.
Fugro Consultants, Inc.
8613 Cross Park Drive
Austin, Texas 78754
Project 1101-3074**

August 2007

Technical Report Documentation Page

1. Report No. FHWA/MT-07-008/8158-2		2. Government Accession No.		3. Recipient's Catalog No.	
4. Title and Subtitle Mechanistic-Empirical Pavement Design Guide Flexible Pavement Performance Prediction Models Volume II Reference Manual		5. Report Date August 2007			
		6. Performing Organization Code			
7. Author(s) Harold L. Von Quintus, PE, Applied Research Assoc. Inc. James S. Moulthrop, PE, Fugro Consultants, Inc.		8. Performing Organization Report No.			
9. Performing Organization Name and Address Fugro Consultants, Inc. 8613 Cross Park Drive Austin TX 78754		10. Work Unit No. (TRAIS)			
		11. Contract or Grant No. Montana Department of Transportation Contract HWY-30604-DT, Project #8158			
12. Sponsoring Agency Name and Address Research Programs Montana Department of Transportation 2701 Prospect Avenue PO Box 201001 Helena MT 59620-1001		13. Type of Report and Period Covered Final Report 2001-2007			
		14. Sponsoring Agency Code 5401			
15. Supplementary Notes Research performed in cooperation with the Montana Department of Transportation and the United States Department of Transportation, Federal Highway Administration. This report can be found at http://www.mdt.mt.gov/research/projects/pave/pave_model.shtml .					
16. Abstract The objective of this research study was to develop performance characteristics or variables (e.g., ride quality, rutting, fatigue cracking, transverse cracking) of flexible pavements in Montana, and to use these characteristics in the implementation of the distress prediction models or transfer functions included in the Mechanistic-Empirical Pavement Design Guide (MEPDG) software that was developed under NCHRP Project 1-37A. Reliable distress prediction models will enable the Montana Department of Transportation (MDT) to use Mechanistic-Empirical (ME) based principles for flexible pavement design and in managing their highway network. The work conducted within this study included using the MEPDG software to develop local calibration factors in the use of that software for Montana climate, structures, and materials for flexible pavements. The report is comprised of three volumes: Volume I – Executive Research Summary; Volume II – Reference Manual (which includes Selection of Distress Prediction Models, Traffic Characterization and Analyses, and Database for Calibration of ME Distress Prediction Models); and Volume III – Field Guide – Calibration and User's Guide for the Mechanistic-Empirical Pavement Design Guide.					
17. Key Words Flexible Pavements, Pavement Design, Mechanistic-Empirical, Fatigue Cracking, Rutting, Thermal Cracking, IRI, Smoothness, Surface Initiated Cracks, Bottom Initiated Cracks, Calibration, Transfer Functions, Distress Prediction Models.			18. Distribution Statement Unrestricted. This document is available through the National Technical Information Service, Springfield, VA 21161.		
19. Security Classif. (of this report) Unclassified.		20. Security Classif. (of this page) Unclassified.		21. No. of Pages 170	
22. Price					

DISCLAIMER STATEMENT (MDT)

This document is disseminated under the sponsorship of the Montana Department of Transportation and the United States Department of Transportation in the interest of information exchange. The State of Montana and the United States Government assume no liability of its contents or use thereof.

The contents of this report reflect the views of the authors, who are responsible for the facts and accuracy of the data presented herein. The contents do not necessarily reflect the official policies of the Montana Department of Transportation or the United States Department of Transportation.

The State of Montana and the United States Government do not endorse products of manufacturers. Trademarks or manufacturers' names appear herein only because they are considered essential to the object of this document.

This report does not constitute a standard, specification, or regulation.

ALTERNATIVE FORMAT STATEMENT (MDT)

MDT attempts to provide accommodations for any known disability that may interfere with a person participating in any service, program, or activity of the Department. Alternative accessible formats of this information will be provided upon request. For further information, call (406) 444-7693, TTY (800) 335-7592, or Montana Relay at 711.

ACKNOWLEDGEMENTS

This report was prepared under sponsorship of the Montana Department of Transportation. The project team recognizes and appreciates the services provided by the Montana Department of Transportation. These services included profile and deflection basins measurements, materials sampling, traffic control, and assistance with project activities to recover construction properties from selected project segments. Other individuals and organizations involved in the work and in preparation and review of the report are listed below.

Dragos Andrei, PhD, PE
Brian Killingsworth, PE
Matthew Witczak, PhD

Weng-On Tam, PhD, PE
Amy Simpson, PhD, PE
Mark Hallenbeck, PhD

SI* (MODERN METRIC) CONVERSION FACTORS				
APPROXIMATE CONVERSIONS TO SI UNITS				
Symbol	When You Know	Multiply By	To Find	Symbol
LENGTH				
in	inches	25.4	millimeters	mm
ft	feet	0.305	meters	m
yd	yards	0.914	meters	m
mi	miles	1.61	kilometers	km
AREA				
in ²	square inches	645.2	square millimeters	mm ²
ft ²	square feet	0.093	square meters	m ²
yd ²	square yard	0.836	square meters	m ²
ac	acres	0.405	hectares	ha
mi ²	square miles	2.59	square kilometers	km ²
VOLUME				
fl oz	fluid ounces	29.57	milliliters	mL
gal	gallons	3.785	liters	L
ft ³	cubic feet	0.028	cubic meters	m ³
yd ³	cubic yards	0.765	cubic meters	m ³
[NOTE: volumes greater than 1,000 shall be shown in m ³]				
MASS				
oz	ounces	28.35	grams	g
lb	pounds	0.454	kilograms	kg
T	short tons (2000 lb)	0.907	megagrams (metric tons)	Mg (or t)
TEMPERATURE (exact degrees)				
°F	Fahrenheit or (F-32)/1.8	5 (F-32)/9	Celsius	°C
ILLUMINATION				
fc	foot-candles	10.76	lux	lx
fl	foot-Lamberts	3.426	candela/m ²	cd/m ²
FORCE and PRESSURE or STRESS				
lbf	pounds	4.45	Newtons	N
lbf/in ² (psi)	pounds per square inch	6.89	kiloPascals	kPa
k/in ² (ksi)	kips per square inch	6.89	megaPascals	MPa
DENSITY				
lb/ft ³ (pcf)	pounds per cubic foot	16.02	kilograms per cubic meter	kg/m ³
APPROXIMATE CONVERSIONS FROM SI UNITS				
Symbol	When You Know	Multiply By	To Find	Symbol
LENGTH				
mm	millimeters	0.039	inches	in
m	meters	3.28	feet	ft
m	meters	1.090	yards	yd
km	kilometers	0.621	miles	mi
AREA				
mm ²	square millimeters	0.0016	square inches	in ²
m ²	square meters	10.764	square feet	ft ²
m ²	square meters	1.195	square yards	yd ²
ha	hectares	2.47	acres	ac
km ²	square kilometers	0.386	square miles	mi ²
VOLUME				
mL	Milliliters	0.034	fluid ounces	fl oz
L	liters	0.264	gallons	gal
m ³	cubic meters	35.314	cubic feet	ft ³
m ³	cubic meters	1.307	cubic yards	yd ³
MASS				
g	grams	0.035	ounces	oz
kg	kilograms	2.202	pounds	lb
Mg (or t)	megagrams (metric tons)	1.103	short tons (2000 lb)	T
TEMPERATURE (exact degrees)				
°C	Celsius	1.8C+32	Fahrenheit	°F
ILLUMINATION				
lx	lux	0.0929	foot-candles	fc
cd/m ²	candela/m ²	0.2919	foot-Lamberts	fl
FORCE and PRESSURE or STRESS				
N	Newtons	0.225	pounds	lbf
kPa	kiloPascals	0.145	pounds per square inch	lbf/in ² (psi)
MPa	megaPascals	0.145	kips per square inch	k/in ² (ksi)
DENSITY				
kg/m ³	pounds per cubic foot	0.062	kilograms per cubic meter	lb/ft ³ (pcf)

*SI is the symbol for the International System of Units. Appropriate rounding should be made to comply with Section 4 of ASTM E 380. (Revised March 2003)

TABLE OF CONTENTS

PART I: INTRODUCTION	1
PART II: SELECTION OF DISTRESS PREDICTION MODELS	4
CHAPTER II-1: INTRODUCTION.....	4
CHAPTER II-2: LOAD RELATED CRACKS	6
II-2.1 TYPES OF LOAD RELATED CRACKS.....	6
II-2.2 MECHANISMS OF LOAD RELATED CRACKS	7
II-2.2.1 Bottom-Up Fatigue Cracking – Alligator Cracks.....	7
II-2.2.2 Top-Down Fatigue Cracking – Longitudinal Cracks Within Wheel Path	7
II-2.3 LOAD RELATED FATIGUE CRACKING PREDICTION MODELS	8
II-2.3.1 MEPDG: Load Related Fatigue Cracking	8
II-2.3.2 Asphalt Institute.....	12
II-2.3.3 Shell International Model	13
II-2.3.4 Probabilistic Distress Models for Asphalt Pavements	13
II-2.3.5 FHWA Cost Allocation Study	14
II-2.3.6 Asphalt Aggregate Mixture Analysis System.....	15
II-2.3.7 Virginia Research Council	17
II-2.3.8 Transport and Road Research Laboratory.....	18
II-2.3.9 Illinois	18
II-2.3.10 Michigan.....	19
CHAPTER II-3: RUTTING.....	20
II-3.1 RUTTING MECHANISMS	20
II-3.2 TYPES OF RUTTING PREDICTION MODELS.....	21
II-3.2.1 Layered Permanent Strain Approach.....	21
II-3.2.2 Plastic-Elastic Vertical Strain Ratio Approach.....	22
II-3.2.3 Permanent Strain Rate Approach	22
II-3.3 HMA PERMANENT DEFORMATION MODELS.....	24
II-3.3.1 MEPDG: HMA Permanent Deformation.....	24
II-3.3.2 WesTrack Permanent Deformation Model	25
II-3.3.3 VESYS Permanent Deformation Model	27
II-3.3.4 Ohio State University Model	28
II-3.3.5 Asphalt Institute Model	29
II-3.3.6 Leahy, Ayers, and Kaloush and Witczak Models	29
II-3.3.7 Flow Model.....	31
II-3.3.8 Allen and Deen Model	32
II-3.3.9 Asphalt-Aggregate Mixture Analysis System	33
II-3.3.10 Michigan State Model.....	34
II-3.3.11 Shell International Model	34
II-3.3.12 Verstraeten Plastic Strain Model.....	35
II-3.4 UNBOUND LAYERS PERMANENT DEFORMATION MODELS.....	36
II-3.4.1 MEPDG	36
II-3.4.2 WesTrack Model	38
II-3.4.3 Limiting Vertical Compressive Strain Approach	39
II-3.4.4 Limiting Modulus Ratio Approach for Unbound Layers	40

CHAPTER II-4: TRANSVERSE CRACKS	42
II-4.1 TRANSVERSE CRACKING MECHANISMS	42
II-4.1.1 Low Temperature Cracking	42
II-4.1.2 Thermal Fatigue Cracking	43
II-4.2 TRANSVERSE CRACKING PREDICTION MODELS	43
II-4.2.1 MEPDG: Transverse Cracking	43
II-4.2.2 Other Models.....	50
CHAPTER II-5: HMA DISINTEGRATION – RAVELING	52
CHAPTER II-6: SMOOTHNESS / RIDE QUALITY MODELS	54
II-6.1 SITE VARIABLES AND DISTRESSES THAT INFLUENCE FLEXIBLE PAVEMENT SMOOTHNESS	54
II-6.2 ROUGHNESS PREDICTION MODELS	55
II-6.2.1 MEPDG – Smoothness Prediction Models	55
II-6.2.2 LTPP Smoothness Prediction Models	57
II-6.2.3 AASHTO Serviceability Equation	58
II-6.2.4 FHWA Zero-Maintenance Pavements Study	59
II-6.2.5 World Bank HDM-III.....	59
II-6.2.6 FHWA/Illinois Department of Transportation Study.....	60
CHAPTER II-7: SUMMARY AND CONCLUSIONS – SELECTION OF DISTRESS PREDICTION MODELS SUMMARY	61
PART III: TRAFFIC CHARACTERIZATION AND ANALYSES	63
CHAPTER III-1: INTRODUCTION.....	63
CHAPTER III-2: GENERAL LOADING PATTERNS	64
CHAPTER III-3: TRUCK VOLUME PATTERNS.....	67
III-3.1 SEASONAL PATTERNS FOR SINGLE UNIT TRUCKS.....	69
III-3.2 SEASONAL PATTERNS FOR MULTI-TRAILER TRUCKS	72
III-3.3 MONTHLY SEASONAL FACTORS FOR COMBINATION TRUCKS.....	76
III-3.4 RECOMMENDATIONS FOR SEASONAL TRUCK VOLUME FACTORING.....	78
CHAPTER III-4: TRUCK WEIGHT PATTERNS.....	79
III-4.1 GENERAL AXLE LOAD DISTRIBUTION FINDINGS	80
III-4.2 PRIMARILY LOADED – SIGNIFICANT LOAD	80
III-4.3 BIMODAL LOADED – PRIMARILY HEAVY LOAD	85
III-4.4 BIMODAL LOADED – PRIMARILY EVEN LOAD	89
III-4.5 LIGHTLY LOADED – PRIMARILY EMPTY	93
III-4.6 FLAT DISTRIBUTION – EVEN LOAD	97
CHAPTER III-5: SUMMARY AND CONCLUSIONS – TRAFFIC.....	101
III-5.1 SEASONAL FACTORING OF VEHICLE VOLUMES BY CLASSIFICATION	101
III-5.2 TRUCK WEIGHT ROAD GROUPS – TWRG'S	101
PART IV: DATABASE FOR CALIBRATION OF MECHANISTIC-EMPIRICAL PAVEMENT DISTRESS PREDICTION MODELS	103
CHAPTER IV-1: INTRODUCTION	103
IV-1.1 BACKGROUND.....	103
IV-1.2 DATABASE OBJECTIVE.....	103

CHAPTER IV-2: OVERVIEW OF DATABASE.....	104
IV-2.1 DATABASE DESIGN.....	104
IV-2.2 DATABASE ELEMENTS	105
IV-2.3 DATABASE STRUCTURE.....	105
IV-2.4 DATABASE OPERATION AND UPGRADES	106
CHAPTER IV-3: DATABASE POPULATION.....	107
PART V: REFERENCES.....	109
APPENDIX II-A LOAD RANGES USED FOR NCHRP PROJECT 1-37A LOAD SPECTRA	116
APPENDIX II-B: MONTANA DATABASE SCHEMA.....	118
APPENDIX II-C: TABLES DESCRIBING THE DATA ELEMENTS INCLUDED IN MONTANA'S ME DATABASE	120
APPENDIX II-D LTPP TABLES DOCUMENTATION – DATABASE OPERATION AND UPGRADES	147

LIST OF TABLES

Table II-1 Comparison of HMA Fatigue Cracking Equations Using Mechanistic Pavement Response Parameters (<i>NHI 2002</i>).....	9
Table II-2 Suggested Values of <i>K</i> as Function of HMA Layer Thickness	27
Table II-3 Typical Values of <i>A</i> and <i>m</i> in the Ohio State Rut Depth Prediction Model	29
Table II-4 Regression Coefficients for the Allen and Deen Rutting Prediction Model.....	32
Table II-5 Correction Factors, <i>C_m</i> , for the Shell International Procedure to Predict Rutting.....	35
Table II-6 Field Calibration Constants and Subgrade Strain Criteria for Permanent Deformation Models	40
Table II-7 Design Features and Site Condition Variables Affecting Flexible Pavement Roughness	55
Table II-8 Distress Variables Affecting Flexible Pavement Smoothness/Serviceability	55
Table II-9 Percentage of Load Caused by Primary Truck Classes.....	65
Table II-10 Monthly Volume Factors.....	68
Table II-11 Assignment of WIM Sites to Truck Weight Road Groups.....	102
Table II-12 Data from the LTPP and Non-LTPP Test Sections Located in Montana Included in the MDT ME Database	107
Table II-13 Data from the LTPP Test Sections Located in States Adjacent to Montana Included in the MDT ME Database.....	108

LIST OF FIGURES

Figure II-1 Relationship between tensile strain at failure and indirect tensile total resilient modulus (<i>Von Quintus et al. 1991</i>).....	17
Figure II-2 Limiting modulus criteria of unbound aggregate base and subbase layers.....	41
Figure II-3 Example of thermal effects or drops in temperature on the tensile strength and thermal stress development in HMA mixtures.	42
Figure II-4 Illustration of the formation of a master creep compliance curve.	45
Figure II-5 Truck Seasonal Patterns for All Sites Combined.....	68
Figure II-6 Seasonal Traffic Patterns for Single Unit Trucks.....	71
Figure II-7 FHWA Class 5 and Class 6 Monthly Volume Patterns.....	72
Figure II-8 Monthly Multi-Trailer Truck Volume Patterns by Site.....	74
Figure II-9 Comparison of Eastern and Non-Eastern Monthly Seasonal Patterns for Multi-Trailer Trucks.....	75
Figure II-10 Monthly Seasonal Factors for Combination Trucks.....	77
Figure II-11 Average Annual Tandem Axle Load Distribution for Class 9 Trucks, Primarily Loaded Truck Weight Road Group.....	81
Figure II-12 Average Annual Tandem Axle Load Distribution for Class 13 Trucks, Primarily Loaded Truck Weight Road Group.....	83
Figure II-13 Average Annual Tandem Axle Load Distribution for Class 6 Trucks, Primarily Loaded Truck Weight Road Group.....	84
Figure II-14 Average Annual Tandem Axle Load Distribution for Class 9 Trucks, Heavy-Bimodal Truck Weight Road Group.....	86
Figure II-15 Average Annual Tandem Axle Load Distribution for Class 13 Trucks, Heavy-Bimodal Truck Weight Road Group.....	87
Figure II-16 Average Annual Tandem Axle Load Distribution for Class 6 Trucks, Heavy-Bimodal Truck Weight Road Group.....	88
Figure II-17 Average Annual Tandem Axle Load Distribution for Class 9 Trucks, Bimodal Truck Weight Road Group.....	90
Figure II-18 Average Annual Tandem Axle Load Distribution for Class 6 Trucks, Bimodal Truck Weight Road Group.....	91
Figure II-19 Average Annual Tandem Axle Load Distribution for Class 13 Trucks, Bimodal Truck Weight Road Group.....	92
Figure II-20 Monthly Single Axle Load Distribution for Class 9 Trucks, at Site 102.....	94
Figure II-21 Average Annual Tandem Axle Load Distribution for Class 9 Trucks, Lightly Loaded Truck Weight Road Group.....	95
Figure II-22 Average Annual Tandem Axle Load Distribution for Class 6 Trucks, Lightly Loaded Truck Weight Road Group.....	96
Figure II-23 Average Annual Tandem Axle Load Distribution for Class 9 Trucks, Flat Truck Weight Road Group.....	98
Figure II-24 Average Monthly Tandem Axle Load Distribution for Class 9 Trucks, Site 113.....	99
Figure II-25 Average Monthly Tandem Axle Load Distribution for Class 9 Trucks, Site 113.....	100

PART I: INTRODUCTION

A Mechanistic-Empirical (ME) based design method is a rational engineering approach that has been used by some agencies to replace the empirical American Association of State Highway and Transportation Officials (AASHTO) design procedure (*AASHTO 1993*). Illinois, Kentucky, Texas, and Washington Departments of Transportation (DOTs) are all agencies that use an ME based approach for pavement design. The main advantage of an ME based design system is that it is based on pavement fatigue and deformation characteristics of all layers, rather than solely on the pavement's surface condition (ride quality). The concepts of ME based methods allow the pavement design engineer to quantify the effect of changes in materials, load, climate, age, pavement geometry, and construction practices on pavement performance. Such a rational engineering design approach provides a more accurate and cost effective method of diagnosing pavement problems, and forecasting maintenance, repair, and rehabilitation needs.

The Montana Department of Transportation (MDT) recognized the benefits and advantages of using an ME based design method. Therefore, Montana began the process of identifying the modeling tools (e.g., pavement response model, climatic model, distress prediction models) and developing a pavement performance database for storing standard inputs. The distress prediction models (or transfer functions) provide a benefit for optimizing the rehabilitation strategies and the predictions inherent in a pavement management system that involve the forecasting of maintenance, repair, rehabilitation, and reconstruction costs. The pavement performance database can be used to determine the robustness and accuracy of the transfer functions to Montana's materials and local conditions.

The objective of this project was to develop performance characteristics for variables (e.g., ride quality, rutting, fatigue cracking, transverse cracking) of flexible pavements in Montana, and to use these characteristics in the verification and calibration of the distress prediction models (transfer functions) included in the Mechanistic-Empirical Pavement Design (MEPDG) software developed under National Cooperative Highway Research Program (NCHRP) Project 1-37A (*ARA 2004a,b*). The MEPDG software includes a uniform and comprehensive set of procedures for the design of new and rehabilitated flexible pavements. Reliable distress prediction models will enable the MDT to use ME principles for flexible pavement design and in managing their highway network.

To achieve the project objective, the project was divided into two phases, each with a series of tasks to achieve the above objective. The specific tasks for each Phase are listed below.

- PHASE I provided the initial identification of the test sections, established the data collection policies and procedures, and included the preparation of a draft document defining the data collection procedures to be implemented in Phase II. Phase I was divided into four tasks, which included:
 - Task 1 – Literature Review of Distress Prediction Models.
 - Task 2 – Review of MDT Pavement-Related Data.
 - Task 3 – Develop the Experimental Plan and Factorial.
 - Task 4 – Develop Work Plan for Monitoring and Testing.

- PHASE II included the data collection and analysis efforts required for the local calibration of the distress prediction models to Montana's climate, materials, and design strategies. Phase II was divided into four tasks, which included:
 - Task 5 – Presentation of Work Plan to MDT.
 - Task 6 – Implement Work Plan – Conduct Field Investigations and Collect Data.
 - Task 7 – Data Analyses and Calibration of Performance Prediction Models.
 - Task 8 – Final Report and Presentation of Results to MDT.

Results from this research project are contained in a three-volume report. Following is a list that describes each report volume from this project:

- **Volume I** is the Executive Research Summary for the overall project and summarizes all work completed under this project, Phases I and II, (*Von Quintus and Moulthrop 2007a*). Volume I is divided into eight chapters.
 - Chapter I-1 is the introduction to the project report.
 - Chapter I-2 presents the experimental plan and matrix that was used to ensure that a sufficient number of test sections were selected to cover the range of conditions encountered in Montana.
 - Chapter I-3 presents the performance indicators and the prediction models selected for pavement design and management purposes.
 - Chapter I-4 establishes the climatic and environmental inputs and default values needed for predicting all distresses.
 - Chapter I-5 summarizes the traffic analyses to determine the inputs for the load related distress prediction models.
 - Chapter I-6 summarizes the materials testing and characterization to determine the inputs for each prediction model.
 - Chapter I-7 summarizes the verification and calibration procedure for each distress prediction model.
 - Chapter I-8 provides the conclusions and recommendations from this research project.
 - Chapter I-9 is the reference section for Volume I.
- **Volume II** (included herein) is a Reference Manual that documents some of the Supplemental Research Studies and Products that resulted from this project. Volume II is divided into five parts – each part summarizing a specific product from this study.
 - Part I of Volume II is an introduction to Volume II.
 - Part II of Volume II summarizes the literature review (Task 1 of Phase I) of ME based distress prediction models and recommends specific equations to be used for each distress.
 - Part III of Volume II was prepared by the University of Washington, Washington State Transportation Center (TRAC), and discusses the analyses completed on the traffic data provided by the MDT and summarizes the input values recommended for use in pavement design in Montana.
 - Part IV of Volume II discusses the ME database created for Montana. This part provides an overview of the database and defines the format for each data field and category. Part IV also lists the tests sections, both within and outside of

- Montana, that were used to populate the database with data used in the local calibration process.
- Part V of Volume II is the reference section for Volume II.
 - **Volume III** is the Field Guide (Calibration and User Guide) presenting standard practices for updating and enhancing the distress prediction models that were calibrated under this research project (*Von Quintus and Moulthrop 2007b*). This volume is divided into five chapters.
 - Chapter III-1 is the introduction to Volume III.
 - Chapter III-2 provides an overview of the MEPDG.
 - Chapter III-3 is a user manual for the MEPDG.
 - Chapter III-4 presents the local calibration factors that were determined from this research project for immediate use by the MDT for designing pavements and managing their highway network.
 - Chapter III-5 is the reference section for Volume III.

PART II: SELECTION OF DISTRESS PREDICTION MODELS

CHAPTER II-1: INTRODUCTION

Distress prediction models are critical in managing, designing, and analyzing flexible pavement structures. A literature review was conducted to identify prediction models that have been developed for those distresses that MDT considers within their Pavement Management System, (*MDT 2000*). Those distresses are listed below.

- Alligator Cracking: Predicted in the Mechanistic-Empirical Pavement Design Guide (MEPDG) software, developed under NCHRP Project 1-37A (*ARA 2004a,b*).
- Longitudinal Cracking: Predicted in the MEPDG software.
- Transverse Cracks: Predicted in the MEPDG software as thermal cracking.
- Block Cracking: Not predicted in the MEPDG software.
- Rutting: Predicted in the MEPDG software for each paving layer and foundation.
- Raveling and Weathering: Considered but not predicted in the MEPDG software.
- Patching: Not predicted in the MEPDG software.

Volume II Part II provides a review of ME based prediction models. This review of distress prediction models for these distresses and other performance indicators is not meant to be exhaustive, but includes those models that can be used to make design and management decisions. Chapters II-2 through II-6 reviews selected prediction models for specific distresses.

- Chapter II-1 Introduction.
- Chapter II-2 Load Related Cracks (Includes both bottom-initiated and surface-initiated cracks).
- Chapter II-3 Rutting (Includes permanent deformation within the HMA layers and unbound layers and foundation).
- Chapter II-4 Transverse (Non-Load Related) Cracks (Includes both low temperature and thermal fatigue cracking).
- Chapter II-5 HMA Disintegration, Raveling.
- Chapter II-6 Smoothness and Ride Quality Models.
- Chapter II-7 Summary.

The review focused on the distress prediction models that are incorporated in the MEPDG that were developed and calibrated under NCHRP Projects 1-37A (*ARA 2004a,b*) and 1-40D (*NCHRP 2006*). A detailed review and discussion of those prediction models are included in the final reports for NCHRP Project 1-37A (*ARA 2004a,b*) and NCHRP Project 9-30 (*Von Quintus et al. 2004*). The prediction model for each distress included in the MEPDG software is listed first within this document and is then followed by other ME based models. If the MEPDG prediction models are selected and used, Montana will be prepared to put into practice the products from

NCHRP Project 1-37A (*ARA 2004a,b*) and NCHRP 9-19 (*Witczak et al. 2002*). In NCHRP Project 9-19, Witczak et al. (2002) developed the simple performance test for designing Hot Mix Asphalt (HMA) mixtures in accordance with the Superpave design method. Both NCHRP projects used the same material properties to tie HMA mixture design to flexible pavement structural and rehabilitation design.

CHAPTER II-2: LOAD RELATED CRACKS

A longer-term distress mode considered by most design/evaluation procedures is fatigue or load related cracks. Fatigue cracks are a series of longitudinal and/or interconnected cracks caused by the repeated application of wheel loads resulting in fatigue failure (some level of cracking) of the HMA surface and/or base mixtures.

II-2.1 TYPES OF LOAD RELATED CRACKS

There are predominantly two types of fatigue cracks that occur in flexible pavements and HMA overlays that are defined based on the direction of crack propagation: bottom-up and top-down fatigue cracks. Top-down fatigue cracking is considered the more critical, because once the crack occurs it is visible and allows water to infiltrate the HMA mixture. Conversely, fatigue cracks that initiate at the bottom of the HMA layer must propagate to the surface before they become visible. It is difficult to identify where the fatigue cracks initiate without taking cores or excavating test pits to observe the direction of crack propagation.

Fatigue cracks that initiate at the bottom of the HMA layer and propagate to the surface are the more classical defined alligator area cracks, as defined by the Long Term Pavement Performance (LTPP) Distress Identification Manual (*SHRP 1993, FHWA 2003*). This type of fatigue cracking first shows up as short longitudinal or transverse cracks in the wheel path that quickly spread and become interconnected to form a cracking pattern defined as alligator cracks. The following is the definition of alligator or fatigue cracks (measured on an area basis), as included in the LTPP Distress Identification Manual.

“A series of interconnected cracks in early stages of development. Develops into many-sided, sharp-angled pieces, usually less than 0.3 m (1 ft) on the longest side, characteristically with a chicken wire/alligator pattern, in later stages.”

Fatigue cracks that initiate at or near the surface of the HMA layer and propagate downward through the HMA layers are believed to be less common. This type of fatigue cracking is longitudinal cracks that occur adjacent to the tires. This type of load related cracking is characteristic of one to three longitudinal cracks in the wheel path that are not interconnected, and is referred to as Longitudinal Cracking Within the Wheel Path (LCWP) by some agencies. Crack deterioration occurs with continued wheel loadings, but this type of cracking does not exhibit the alligator cracking pattern. LTPP recognized this difference and established a separate distress category. As defined in the LTPP Distress Identification Manual, the definition for these cracks is given below.

“Cracks predominantly parallel to the centerline and within wheel path versus non-wheel path.”

II-2.2 MECHANISMS OF LOAD RELATED CRACKS

II-2.2.1 Bottom-Up Fatigue Cracking – Alligator Cracks

Load related cracks that initiate at the bottom of the HMA layer are characteristic of alligator or area cracks. This type of cracking starts as short longitudinal or transverse cracks in the wheel path and progress to an alligator-cracking pattern (interconnected cracks), and is a result of the repeated bending of the HMA layer under traffic. The pavement and HMA layer deflects under wheel loads that result in tensile strains and stresses at the bottom of the layer. With continued bending, the tensile stresses and strains cause cracks to initiate at the bottom of the layer and then propagate to the surface. As bending continues, greater tensile strains and stresses and fewer numbers of repeated wheel loads are required to cause the cracks to initiate at the bottom of the layer and propagate to the surface. The following briefly lists some of the reasons for higher tensile strains and stresses to occur at the bottom of the HMA layer.

- Relatively thin or weak HMA layers for the magnitude of the wheel loads.
- Higher wheel loads and higher tire pressures.
- Soft spots or areas in unbound aggregate base materials or in the subgrade soil.
- Weak aggregate base/subbase layers caused by inadequate compaction or increases in moisture contents.

II-2.2.2 Top-Down Fatigue Cracking – Longitudinal Cracks Within Wheel Path

As noted above, most fatigue cracks initiate at the bottom of the HMA layer and propagate upward to the surface of the pavement. However, there is increasing evidence that suggests load-related cracks do initiate at the surface and propagate downward. There are various opinions on the mechanisms that cause these types of cracks, but there are no conclusive data to suggest that one is more applicable than the other is. Some of the suggested mechanisms are:

- Tearing of the HMA surface mixture from radial tires with high contact pressures near the edge of the tire, causing the cracks to initiate and propagate both in shear and in tension.
- Severe aging of the HMA mixture near the surface resulting in high stiffness and when combined with high contact pressures, adjacent to the tire loads, cause the cracks to initiate and propagate in shear.
- The combination of wheel load induced tensile stresses and strains with the thermal stresses and strains that occur at the surface when the temperature decreases causing the cracks to initiate and propagate in tension. Aging of the HMA surface mixture accelerates this crack initiation-propagation process. The stiffer (more brittle) the surface in combination with the higher tire pressures and greater temperature changes, the larger the tensile and shear stresses and strains and the fewer the number of wheel loads to cause the cracks to initiate at the top of the layer. The following lists some of

the reasons or conditions under which load-related cracks can initiate at the surface and propagate downward:

- o High tire and contact pressures and/or heavy wheel loads.
- o HMA layers with large modulus gradients – high modulus at the surface (because of aging or sudden large drops in temperature) that decreases with depth.
- o Combination of thermal stresses with those induced from wheel loads.

II-2.3 LOAD RELATED FATIGUE CRACKING PREDICTION MODELS

Traditional ME approaches that are used to design or evaluate flexible pavements and mixtures are based on the initial pavement response parameter to determine the number of load cycles to a defined extent and severity level of fatigue cracks. Tensile strain is the most common response parameter used to predict alligator cracking, however, tensile stress and the maximum surface deflection have been used. Table II-1, from the National Highway Institute Course 131064 (*NHI 2002*), lists and compares some of the more commonly used prediction models using a basic pavement response parameter.

Nearly all of these models have been developed and calibrated with the assumption that the fatigue cracks initiate at the bottom of the HMA layer and propagate to the surface, with the exception of the MEPDG. This assumption may be incorrect for those flexible pavements with thick HMA layers greater than 250 mm (10 inches). Most of Montana's roadways have HMA thicknesses less than 250 mm (10 inches).

II-2.3.1 MEPDG: Load Related Fatigue Cracking

The MEPDG predicts both bottom and surface initiated fatigue cracks (refer to Table II-1) using an incremental damage index approach. It is the only design/analysis procedure that uses this incremental damage index approach for predicting bottom and surface initiated fatigue cracks. The methodology assumes that the same mechanism results in both types of fatigue cracks, which is similar to the Asphalt Institute equation for bottom initiated fatigue cracks (refer to Equation II-7).

Table II-1 Comparison of HMA Fatigue Cracking Equations Using Mechanistic Pavement Response Parameters (NHI 2002)

HMA Fatigue Equation	Response Parameter	HMA Fatigue Constants			Other Parameters in Equation	Mixture Dependent	Cracking Prediction		Definition of Failure, % Cracking
		Coefficient, K_1	Response Exponent, K_2	Modulus Exponent, K_3			Bottom-Up; Alligator Cracking	Top-Down; Longitudinal Cracking	
MEPDG	ϵ_t	f(Air Voids, Asphalt Volume)	-3.9492	-1.281	Dynamic Modulus; Air Voids; Effective % Asphalt by Volume	Yes	Yes	Yes	f(DI)
Asphalt Institute	ϵ_t	f(Air Voids, Asphalt Volume)	-3.291	-0.854	Dynamic Modulus; Air Voids; Effective % Asphalt by Volume	Yes	All Combined	No	20 @ DI=1.0
Shell	ϵ_t	0.0685	-5.671	-2.363	Dynamic Modulus	Yes	All Combined	No	50 @ DI=1.0
PDMAP	ϵ_t	6.601×10^{-14}	-3.291	-0.854	Flexure Modulus	Yes	All Combined	No	Lab, Crack Initiation
	ϵ_t	8.851×10^{-15}	-3.291	-0.854	Flexure Modulus				10 @ DI=1.0
	ϵ_t	1.219×10^{-16}	-3.291	-0.854	Flexure Modulus				45 @ DI=1.0
Ontario	ϵ_t	8.86×10^{-14}	-5.12	0.000	Dynamic Modulus	Yes	All Combined	No	20 @ DI=1.0
Cost Allocation	ϵ_t	f(E_r)	f(K_1)	0.000	Indirect Tensile Resilient Modulus	Yes	All Combined	No	f(DI)
Virginia	ϵ_t	f(σ_t)	f(σ_t)	0.000	Indirect Tensile Strength @ 70°F	Yes	All Combined	No	NA
MICH-PAVE	ϵ_t	f(h_{HMA})	-1.0964	0.000	Subgrade Resilient Modulus; Base Resilient Modulus; Base Equivalent Thickness; HMA Thickness & Air Voids; Kinematic Viscosity; Aggregate Angularity	Yes	All Combined	No	---
	ϵ_v		1.173						
	Δ		-2.799						
TRRL	ϵ_t	1.66×10^{-10}	-4.32	0.000		No	All Combined	No	---
Belgian	ϵ_t	4.92×10^{-14}	-4.76	0.000		No	All Combined	No	---
Illinois, Full-Depth	ϵ_t	5.00×10^{-6}	-3.00	0.000		No	All Combined	No	---
Illinois	Δ	5.60×10^{-11}	-4.60	0.000		No	All Combined	No	---
ϵ_t = Tensile strain in the HMA mixture. $N_f = K_1 (\epsilon_t)^{K_2} (E)^{K_3}$ = Allowable number of axle load applications. E_r = Resilient modulus measured from the indirect tensile test. DI = Damage Index.					ϵ_v = Compressive strain at the bottom of the HMA layer. h_{HMA} = Thickness of the HMA layer. σ_t = Tensile stress in the HMA mixture. Δ = Maximum deflection at the surface of the flexible pavement.				

The MEPDG fatigue cracking prediction model was calibrated using over 100 test sections from the LTPP program. Confirmation of the mechanism for surface initiated cracks, however, has yet to be completed. Trenches were not used within the calibration process to confirm the direction of crack propagation. The MEPDG calculates the number of allowable strain applications for the incremental damage index approach using Equation II-1.

$$N_f = k_{f1}(C)(C_H)\beta_{f1}(\epsilon_t)^{k_{f2}\beta_{f2}}(E)^{k_{f3}\beta_{f3}} \quad (II-1)$$

Where:

- N_f = Allowable number of load repetitions.
 ϵ_t = Tensile strain at the critical location.
 E = Dynamic modulus measured in compression.
 k_{f1}, k_{f2}, k_{f3} = Global field calibration parameters (from the NCHRP Project 1-37A (ARA 2004a,b) calibration effort: $k_{f1}=0.00432$, $k_{f2}=-3.9492$, and $k_{f3}=-1.281$; from the NCHRP Project 1-40D (NCHRP 2006) recalibration effort: $k_{f1}=0.007566$, and the other parameters remained unchanged).
 $\beta_{f1}, \beta_{f2}, \beta_{f3}$ = Local or mixture specific field calibration parameters, all set to 1.0 during the calibration efforts under NCHRP Projects 1-37A and 1-40D (ARA 2004a,b; NCHRP 2006).
 C = Correction factor, 10^M , when:
 $M = 4.84 \left(\frac{V_b}{V_a + V_b} - 0.69 \right)$
 V_a = Percent Air Void volume in HMA mixture.
 V_b = Percent asphalt volume in HMA mixture.
 C_H = Thickness correction term, dependent on type of cracking:
 For bottom-up or alligator cracking:

$$C_H = \frac{1}{0.000398 + \frac{0.003602}{1 + e^{(11.02 - 3.49H_{HMA})}}}$$

H_{HMA} = Total HMA thickness, inches.

For top-down or longitudinal cracking:

$$C_H = \frac{1}{0.01 + \frac{12.00}{1 + e^{(15.676 - 2.8186H_{HMA})}}}$$

H_{HMA} = Total HMA thickness, inches.

The incremental damage index (DI) is calculated for each axle load interval for each axle type and truck type that is applied within a month that is subdivided into five average temperatures. The cumulative damage index is determined by summing the incremental damage indices (refer to Equation II-2).

$$DI = \sum \left(\frac{n}{N_f} \right)_{j,m,l,p,T} \quad (II-2)$$

Where:

- DI = Incremental damage index.
- n = Actual number of axle load applications within a specific time period.
- N_f = Load applications to failure.
- j = Axle load interval.
- m = Axle load type (single, tandem, tridem, quad, or special axle configuration).
- l = Truck type using the truck classification groups included in the MEPDG.
- p = Month.
- T = Median temperature for the five temperature intervals used to subdivide each month.

The MEPDG calculates the amount of alligator area cracking and the length on LCWP based on the incremental damage index that are summed with time and different truck loadings (Equation II-2). Different relationships were developed between the amounts of cracking and damage indices. Equation II-3 is the relationship to predict area alligator cracking based on total lane area, while Equation II-4 is the relationship to predict length of longitudinal cracking in the wheel paths.

Bottom Initiated Fatigue Cracks:

$$FC_{Bottom} = \left(\frac{1}{60} \right) \left(\frac{C_4}{1 + e^{(C_1 C_1^* + C_2 C_2^* \text{Log}(DI_{Bottom} * 100))}} \right) \quad (II-3)$$

Where:

- FC_{Bottom} = Bottom initiated fatigue cracks.
- C_4 = Calibration coefficients of 6,000.
- C_1 = Calibration coefficients of 1.00.
- C_2 = Calibration coefficients of 1.00.
- C_1^* = $-2C_2^*$.
- C_2^* = $-2.40874 - 39.748(1 + h_{HMA})^{-2.856}$.
- h_{HMA} = Total HMA thickness.
- DI_{Bottom} = Bottom incremental damage index.

Surface Initiated Fatigue Cracks:

$$FC_{Top} = 10.56 \left(\frac{C_4}{1 + e^{(C_1 - C_2 \text{Log} DI_{Top})}} \right) \quad (II-4)$$

Where:

- FC_{Top} = Surface (top) initiated fatigue cracks.
- C_4 = Calibration coefficients of 1,000.
- C_1 = Calibration coefficients of 7.00.
- C_2 = Calibration coefficients of 3.5.
- $\text{Log} DI_{Top}$ = Incremental damage index.

The MEPDG has the capability to predict the fatigue cracking of cement treated bases. Montana has built and plans to continue building these composite pavements. Equation II-5 provides the equation used to calculate the number of allowable load application for the cement treated bases, and Equation II-6 is the equation relating the incremental damage index to the amount of fatigue cracks exhibited at the surface of the HMA layer. Unfortunately, this

prediction model was not calibrated under NCHRP Project 1-37A (*ARA 2004a,b*) or within the re-calibration work completed under NCHRP 1-40D (*NCHRP 2006*). Sections will need to be used to calibrate this prediction model to Montana's conditions and materials.

$$N_{f-CTB} = 10^{\left(\frac{K_{c1}\beta_{c1}1 - \left(\frac{\sigma_t}{M_r} \right)}{K_{c2}\beta_{c2}} \right)} \quad (II-5)$$

Where:

- N_{f-CTB} = Allowable number of strain repetitions for the Cement Treated Base (CTB) layer.
- β_{c1}, β_{c2} = Field calibration factors (local).
- σ_t = Tensile stress at the bottom of the CTB layer, psi.
- M_r = Modulus of rupture for the CTB layer, psi.
- K_{c1} = 0.972 global field calibration factor.
- K_{c2} = 0.0825 global field calibration factor.

$$FC_{CTB} = C_1 + \frac{C_2}{1 + e^{(C_3 - C_4(DI_{CTB}))}} \quad (II-6)$$

Where:

- FC_{CTB} = Fatigue cracks for the CTB layer, psi.
- C_1, C_2 = Calibration coefficients of 1.0.
- C_3 = Calibration coefficients of 0.0.
- C_4 = Calibration coefficients of 1,000.
- DI_{CTB} = Incremental damage index for the CTB layer, psi.

II-2.3.2 Asphalt Institute

The Asphalt Institute developed a fatigue-cracking prediction model based on constant stress criterion using the American Association of State Highway Officials (AASHTO) Road Test data (*AI 1983, 1991*). The prediction equation was based on using the cumulative damage approach for an alligator cracking level of 20 percent, which is given by Equation II-7 (*AI 1991*).

$$N_f = 0.00432C (\epsilon_t)^{-3.291} (E)^{-0.854} \quad (II-7)$$

Where:

- N_f = Number of strain applications to failure (20 percent fatigue cracking over the entire pavement area).
- C = Correction factor, 10^M , when:

$$M = 4.84 \left(\frac{V_b}{V_a + V_b} - 0.69 \right)$$
 - V_a = Percent Air Void volume in HMA mixture.
 - V_b = Percent Asphalt volume in HMA mixture.

$$E = \text{HMA dynamic modulus, lb/in}^2.$$

$$\epsilon_t = \text{Tensile strain at the bottom of the HMA layer.}$$

II-2.3.3 Shell International Model

Shell developed a fatigue cracking prediction model (*Shell 1978*), Equation II-8, similar to that of the Asphalt Institute, but using a different level of cracking as the definition for fatigue failure (50 percent).

$$N_f = 0.0685(\epsilon_t)^{-5.671} (E)^{-2.363} \quad (II-8)$$

Where:

$$N_f = \text{Number of constant strain applications to failure.}$$

$$\epsilon_t = \text{Tensile strain at the bottom of the HMA layer.}$$

$$E = \text{HMA dynamic modulus, lb/in}^2.$$

Shell developed separate equations for determining the tensile strain for both constant stress and constant strain conditions. The constant stress and constant strain equations, based on 146 fatigue curves covering a wide range of mixtures, asphalts, and testing conditions, are shown in Equations II-9 and II-10, respectively.

$$\epsilon_t = (4.102PI - 0.205PIV_b + 1.094V_b - 2.7807) S_m^{-0.36} N^{-0.2} \quad (II-9)$$

and

$$\epsilon_t = (0.300PI - 0.015PIV_b + 0.080V_b - 0.198) S_m^{-0.28} N^{-0.2} \quad (II-10)$$

Where:

$$\epsilon_t = \text{Tensile strain at the bottom of the HMA layer, mm/mm.}$$

$$PI = \text{Penetration index of the bitumen.}$$

$$V_b = \text{Percentage of bitumen by volume in the HMA layer.}$$

$$S_m = \text{Stiffness modulus of the HMA layer.}$$

$$N = \text{Allowable number of load applications to fatigue cracking.}$$

II-2.3.4 Probabilistic Distress Models for Asphalt Pavements

Probabilistic Distress Models for Asphalt Pavements (PDMAP) developed by Finn et al. (1973, 1986) is a computer program that predicts the amount of fatigue cracking expected in a given pavement under specific environmental and traffic conditions. This fatigue model was developed using a set of laboratory fatigue curves as a basis for crack initiation and applying a shift factor to correlate the laboratory results with the AASHO Road Test. The laboratory curves used were first developed by Monismith et al. (1972) for an HMA mixture with five percent air voids and six percent asphalt by weight. Through the use of shift factors, two fatigue equations were developed to predict the number of load applications required to cause 10 and 45 percent area fatigue cracking (alligator cracking) are shown in Equations II-11 and II-12, respectively.

$$\log N_f(10\%) = 15.947 - 3.291 \log \left(\frac{\epsilon}{10^{-6}} \right) - 0.854 \log \left(\frac{E}{10^3} \right) \quad (II-11)$$

and

$$\text{Log}N(45\%) = 16.086 - 3.291 \text{Log} \left(\frac{\epsilon}{10^{-6}} \right) - 0.854 \text{Log} \left(\frac{E}{10^3} \right) \quad (II-12)$$

Where:

- $\log N_f$ = 10% load applications to 10% area fatigue cracking.
- $\text{Log}N$ = 45% load applications to 45% area fatigue cracking.
- N_f = Load applications of constant stress to cause fatigue failure.
- ϵ = Initial tensile strain at the bottom of the HMA layer, in/in.
- E = HMA modulus, lb/in².

II-2.3.5 FHWA Cost Allocation Study

A Federal Highway Administration (FHWA) study of cost allocations for pavement damage functions, found that the fatigue constants K_1 and K_2 were related for many of the fatigue relationships that had been developed using both constant strain and constant stress tests (*Rauhut et al. 1984a,b*). The FHWA Cost Allocation fatigue cracking relationship adopted the PDMAP form of the equation, but combined the results from many laboratory fatigue tests. This study found that the coefficient and response exponent of the laboratory and field test results were related. That relationship between the coefficients and exponents was used in developing a more universal fatigue equation (Equation II-13), which is given below.

$$N_f = K_1 (\epsilon_t)^{K_2} \quad (II-13)$$

Where:

- N_f = Allowable load applications of constant stress to cause fatigue failure.
- $K_1 = K_{1R} \left(\frac{E_r}{E_{Rr}} \right)^{-4}$.
- K_{1R} = Fatigue constant.
- E_r = Resilient modulus of the HMA, using the indirect tensile test, psi.
- E_{Rr} = Reference resilient modulus of the HMA measured at the reference temperature, (500,000 psi was used in the calibration work), psi.
- ϵ_t = Tensile strain at the bottom of the HMA layer.
- $K_2 = 1.75 - 0.252 [\text{Log} (K_1)]$.

As part of the fatigue cracking prediction model, Rauhut, et al. (1984a,b) found more than 40 test sections from roadways around the United States (U.S.) with significantly different site features were used to develop a relationship between the damage index, computed with the above fatigue equation (Equation II-13), and observed cracking on those test sections (*Rauhut*

et al. 1984b). The conversion of the predicted fatigue damage to percent area cracking (based on tensile strains at the bottom of the HMA layer) is shown below in Equation II-14. This equation is applicable to fatigue cracking areas of 0 to 50 percent of the wheel path area.

$$A_c = 0.191(e)^{(3.958DI(t))} \quad (II-14)$$

Where:

A_c = Alligator cracking, percent of wheel path area.

$DI(t)$ = Damage index with time, t , when:

$$DI(t) = \frac{n_{ESAL}}{N_f}$$

n_{ESAL} = Number of actual cumulative equivalent single axles loads with time, t .

N_f = Load applications of constant stress to cause fatigue failure.

II-2.3.6 Asphalt Aggregate Mixture Analysis System

The Asphalt Aggregate Mixture Analysis System (AAMAS) adopted the PDMAP and FHWA Cost Allocation fatigue cracking relationships for evaluating and designing HMA mixtures (*Von Quintus et al. 1991*). Those fatigue cracking relationships, however, were modified based on HMA mixture properties from the indirect tensile strength and resilient modulus tests. Equation II-15 gives the relationship used to modify the PDMAP fatigue cracking relationship for 10 percent alligator cracks (Equation II-11) using results from the indirect tensile test.

$$\text{Log}N_f(T_i) = 15.947 - K_r [\text{Log}\epsilon_i(T_i)] - C_r \text{Log}E_R(T_i) \quad (II-15)$$

Where:

N_f = Allowable load applications of constant stress to cause fatigue failure.

T_i = Total layer thickness.

K_r = Fatigue constant.

ϵ_i = Initial tensile strain at the bottom of the HMA layer, in/in.

E_R = HMA modulus, lb/in².

$$C_r = K_r \left[\frac{\text{Log}\epsilon_i(T_1) - \text{Log}\epsilon_i(T_2)}{\text{Log}E_R(T_2) - \text{Log}E_R(T_1)} \right]$$

T_1 = Thickness of layer 1.

T_2 = Thickness of layer 2.

Equations II-16a and 16b give the relationship used to modify the FHWA Cost Allocation fatigue cracking relationship for 10 percent alligator cracks (Equation II-15).

$$\text{Log}N_f(T_i) = \text{Log} \left[C_r \left(\frac{E_R(T_i)}{E_{Rr}(T_r)} \right)^{-K_r} \right] - \left[1.35 - 0.252 \text{Log} \left(C_r \left(\frac{E_R(T_i)}{E_{Rr}(T_r)} \right)^{-K_r} \right) \right] \text{Log}\epsilon_i(T_i) \quad (II-16a)$$

and

$$0.1867[\text{Log}\epsilon_t(T_1) - \text{Log}\epsilon_t(T_2)] = \left[\frac{\text{Log}\epsilon_t(T_1)}{\text{Log}\left(C_r \left(\frac{E_R(T_1)}{E_{Rr}(T_r)}\right)^{-K_r}\right)} - \frac{\text{Log}\epsilon_t(T_2)}{\text{Log}\left(C_r \left(\frac{E_R(T_2)}{E_{Rr}(T_r)}\right)^{-K_r}\right)} \right] \quad (II-16b)$$

Where:

- N_f = Allowable load applications of constant stress to cause fatigue failure.
- T_i = Total layer thickness.
- T_1 = Thickness of layer 1.
- T_2 = Thickness of layer 2.
- T_r = Reference thickness.
- E_R = Resilient modulus.
- E_{Rr} = Reference resilient modulus of the HMA measured at the reference temperature, (500,000 psi was used in the calibration work), psi.
- K_r = Fatigue constant.
- ϵ_t = Tensile strain at the bottom of the HMA layer, in/in.
- $C_r = K_r \left[\frac{\text{Log}\epsilon_t(T_1) - \text{Log}\epsilon_t(T_2)}{\text{Log}E_R(T_2) - \text{Log}E_R(T_1)} \right]$.

Figure II-1 shows relationships between the resilient modulus and tensile strain at failure measured with the indirect tensile strength and repeated load test that was developed by Von Quintus, et al. (1991) for both the FHWA Cost Allocation and PDMAP fatigue equations (10 percent fatigue cracking). These relationships identify the minimum tensile strain at failure for different modulus values (or temperatures) that meet or exceed the fatigue life for these fatigue equations. A larger tensile strain at failure for the same resilient modulus implies a longer fatigue life or a more fatigue resistant mixture. Use of these laboratory test results permits the fatigue relationship to be adjusted for specific HMA mixtures.

Twelve different HMA mixtures and projects were used in the AAMAS project to evaluate the reasonableness of the fatigue equation and Figure II-1. The evaluation process was later used within the LTPP program for comparing the predicted to measured fatigue cracking for many of the LTPP General Pavement Sections (GPS) (Von Quintus and Killingsworth 1998). Adequate correspondence was found between the predictions and observations. However, tensile strain at failure and total resilient modulus values were unavailable for most of the LTPP test sections. The values used in the comparisons were estimated based on volumetric and mixture component properties.

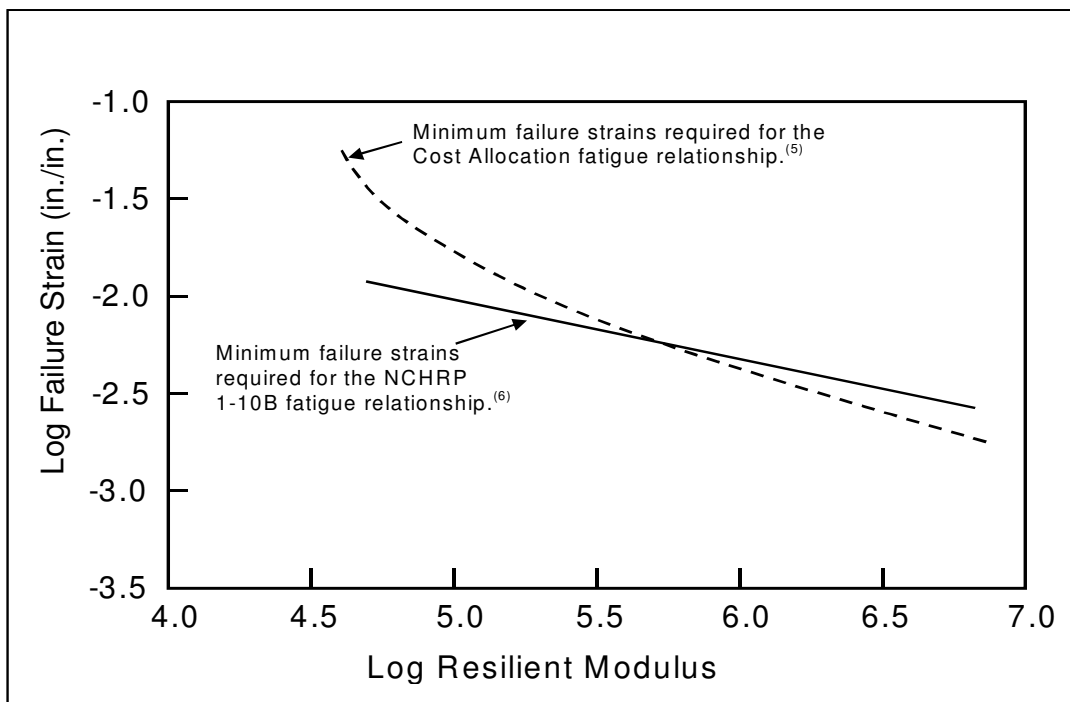


Figure II-1 Relationship between tensile strain at failure and indirect tensile total resilient modulus (Von Quintus et al. 1991).

II-2.3.7 Virginia Research Council

G. W. Maupin, with the Virginia Research Council, developed a fatigue relationship (Equation II-17) from laboratory flexural constant-strain fatigue tests using supported beams, which is given below and is similar to other fatigue strength relationships (Maupin and Freeman 1976).

$$N_f = K_1 (\epsilon_t)^{-n} \quad (II-17)$$

Where:

- N_f = Allowable load applications to cause fatigue failure.
- K_1 = Fatigue constant.
- ϵ_t = Tensile strain at the bottom of HMA layer, in/in.
- n = Actual number of load applications within a specific time period.

Maupin and Freeman (1976) found that the fatigue constants in the above equation were related to the tensile strength measured from the indirect tensile test. The resulting relationships between the fatigue constants (Equation II-17) and indirect tensile strength are given in Equations II-18 and II-19.

$$n = 0.0374(\sigma_t) - 0.744 \quad (II-18)$$

and

$$\text{Log}(K_1) = 7.92 - 1.122(\sigma_f) \quad (II-19)$$

Where:

n = Actual number of load applications within a specific time period.

σ_t = Tensile stress at bottom of layer.

K_1 = Fatigue constant.

σ_f = Indirect tensile strength measured at 70 °F, psi.

II-2.3.8 Transport and Road Research Laboratory

The Transport and Road Research Laboratory (TRRL) developed a fatigue-cracking model that related fatigue cracking to tensile strain at the bottom of the asphalt concrete layer (*Powell et al. 1984*). This model does not consider asphalt concrete material properties because their influences on the predictions were found to be negligible. The TRRL model is shown in Equation II-20.

$$N_f = 1.66 \times 10^{-10} (\epsilon_t)^{-4.32} \quad (II-20)$$

Where:

N_f = Allowable load applications to fatigue failure.

ϵ_t = Tensile strain at the bottom of the HMA layer, in/in.

II-2.3.9 Illinois

The Illinois DOT full-depth asphalt concrete design procedure uses a mechanistic-empirical approach developed at the University of Illinois. Using the previous equation and ILLI-PAVE derived algorithms, Thompson developed a transfer function relating surface deflections of a full-depth asphalt concrete pavement to its fatigue life (*Thompson 1987*). The equations for using tensile strain and number of 18-kip Equivalent Single Axle Loads (ESALs) are shown in Equations II-21 and II-22, respectively.

$$N_f = 5.0 \times 10^{-6} (\epsilon_t)^{-3.0} \quad (II-21)$$

Where:

N_f = Allowable number of strain repetitions (at ϵ_t level) to failure (initiation of a fatigue crack).

ϵ_t = Tensile strain at bottom of HMA layer.

$$N_{18} = 5.6 \times 10^{11} (\Delta)^{-4.6} \quad (II-22)$$

Where:

- N_{18} = Number of 80-kN (18-kip) single axle loads to fatigue failure.
 Δ = Surface deflection for a moving 80-kN (18-kip) single axle load (mils).

II-2.3.10 Michigan

At Michigan State University, Baladi developed an equation (Equation II-23) to predict the fatigue life of HMA based on the observed performance of 10 pavement sections located in Michigan and Indiana (Baladi 1987). The prediction equation was validated using some of the LTPP test sections. The pavement responses calculated with the MICH-PAVE program includes; surface deflection, tensile strain, and vertical strain at the bottom of the HMA layer. The equation is given below.

$$\begin{aligned} \log(ESAL) = & -2.544 + 0.154T_{AC} + 0.0694TB_{EQ} - 2.799 \log \delta_o \\ & -0.261V_a + 0.917 \log E_{base} + 0.0000269M_R - 1.0964 \log \epsilon_t \\ & + 1.173 \log \epsilon_v - 0.001KV + 0.064ANG \end{aligned} \quad (II-23)$$

Where:

$ESAL$ = Number of 80-kN (18-kip) equivalent single axle loads to failure.

T_{AC} = Thickness of the HMA layer, in.

TB_{EQ} = Equivalent thickness of base material, in.

$$TB_{EQ} = T_{base} + T_{subbase} \left(\frac{E_{subbase}}{E_{base}} \right)$$

T_{base} = Actual thickness of base material, in.

$T_{subbase}$ = Actual thickness of subbase material, in.

E_{base} = Resilient modulus of the base material, lbf/in².

$E_{subbase}$ = Resilient modulus of the subbase material, lbf/in².

δ_o = Surface deflection, in.

V_a = Percent air voids in the mix.

M_R = Resilient modulus of the subgrade, lbf/in².

ϵ_t = Tensile strain at the bottom of the HMA layer, in/in.

ϵ_v = Compressive strain at the bottom of the HMA layer, in/in.

KV = Kinematic viscosity at 135 °C (275 °F), CSt.

ANG = Aggregate angularity:

4 for 100 percent crushed material.

2 for 100 percent rounded river-deposited material.

3 for a 50 percent mix of crushed and rounded aggregate.

CHAPTER II-3: RUTTING

II-3.1 RUTTING MECHANISMS

Rutting is a surface depression in the wheel paths, and some amount of rutting occurs in nearly all flexible pavements. The LTPP Distress Identification Manual (*SHRP 1993, FHWA 2003*) defines rutting as:

“A longitudinal surface depression in the wheel path. Rutting may have associated transverse displacement.”

Rutting is caused by inelastic or plastic deformations in any or all of the pavement layers and subgrade. These plastic deformations can be the result of: 1) densification or one-dimensional compression and consolidation and/or 2) lateral movements or plastic flow of materials (HMA, aggregate base, and subgrade soils) from wheel loads. The more severe premature distortion and rutting failures are related to lateral flow and/or loss of shear strength of the HMA mixture, rather than one-dimensional densification. Rutting is categorized into three types and defined by the cause and layers in which the rutting occurs. Each of the different types is summarized below.

- One-dimensional densification or vertical compression. A rut depth caused by material densification is a depression near the center of the wheel path without an accompanying hump on either side of the depression. Densification of materials is generally caused by excessive air voids or inadequate compaction after placement of the HMA mat, thereby allowing the mat or underlying layers to compact when subjected to traffic loads. In other words, a further densification of the mat and or underlying materials caused by traffic. This type of rut depth usually results in a low to moderate severity level of rutting.
- Lateral flow. A rut depth caused by the lateral flow of material is a depression near the center of the wheel path with humps on either side of the depression. This type of rut depth usually results in a moderate to high severity level of rutting. Lateral flow or the plastic movement of materials will occur in those mixtures with inadequate shear strength or by an insufficient amount of total voids in the HMA layer. Voids of an HMA mixture in the range of two percent or less right after construction are susceptible to lateral flow, because the low voids allow the asphalt to act as a lubricant rather than a binder during hot weather. Over-densification of the HMA layer by heavy wheel loads can result in bleeding or flushing on the pavement surface. This type of rutting is the most difficult to predict and measure in the laboratory.
- Mechanical Deformation. A third type of rutting is densification and/or lateral movement of the unbound materials below the HMA surface. This type of rutting has been referred to as mechanical deformation. Mechanical deformation is a result of subsidence in the base, subbase and/or subgrade and is usually accompanied by a longitudinal cracking pattern at the pavement's surface when the HMA surface mixture is stiff (i.e., high elastic modulus) compared to the underlying layers. These longitudinal cracks generally occur in the center and along the outside edges of the ruts.

Most ME based analysis procedures use a combination of two techniques for evaluating the rutting potential of flexible pavements and HMA overlays. One technique is to predict the plastic deformation in each paving layer, and sum the individual layer rut depths for the total rutting measured at the surface. The second technique is based on limiting the elastic strains in the unbound layers. This section of the document is divided into two parts: rut depth or plastic deformation in HMA mixtures and unbound layers.

II-3.2 TYPES OF RUTTING PREDICTION MODELS

II-3.2.1 Layered Permanent Strain Approach

In this approach, the permanent vertical strain is determined in each layer of the pavement structure as a function of the number of repeated load applications. This vertical strain is then multiplied by the layer thickness to obtain the permanent deformation of the layer. The permanent deformations of the various layers are then added up to obtain the total rutting at the surface.

Various models that determine the accumulation of permanent strain with the number of wheel load applications and structural layer have been evaluated by Barenberg and Thompson (1992). The Barenberg/Thompson study concluded that the equations or models relating the log of permanent strain to the log of wheel load repetitions were the most appropriate. These models take the following form (Equation II-24):

$$\text{Log}(\epsilon_p) = a + b[\text{Log}(N)] \quad (\text{II-24})$$

Where:

- ϵ_p = Permanent or plastic strain.
- a, b = Regression coefficients.
- N = Number of repeated axle load applications.

To calculate the permanent deformation from the permanent strains, Huang suggested the following steps (Huang 1993):

- Divide the pavement structure into a number of manageable layers and estimate the vertical and radial stresses at the mid-height of each layer.
- Using the applied vertical load as the vertical stress and the radial load due to the applied load together with the overburden pressure as the confining pressure, conduct repeated load tests to determine the permanent strain in laboratory samples that represent field materials.
- Compute the permanent deformation of each layer by multiplying the permanent strain with the layer thickness.
- Add the permanent deformations over all the layers to obtain the rutting at the surface.

II-3.2.2 Plastic-Elastic Vertical Strain Ratio Approach

Another approach that has been used for predicting the rutting in different layers is termed the plastic-elastic or resilient strain ratio. The constitutive relationship used is based on the statistical analysis of laboratory repeated load permanent deformation tests. The model form is similar to the classical power model, but determines and evaluates the resulting permanent strain as a percentage of the resilient strain, Equation II-25:

$$\frac{\epsilon_p}{\epsilon_r} = a(N)^b \quad (II-25)$$

Where:

- ϵ_p = Accumulated plastic strain at N repetitions of load.
- ϵ_r = Resilient strain of the asphalt material as a function of mixture properties, temperature and time rate of loading.
- N = Number of axle load repetitions.
- a, b = Non-linear regression coefficients.

While statistical relationships for plastic strain can be determined for HMA mixtures from laboratory repeated load tests, a field adjustment or shift factor, β_r , is required to provide reasonable correlations between the predicted rut depths and field observations. As a consequence, Equation II-25 takes the form of Equation II-26 (II-26a or II 26b):

$$\frac{\epsilon_p}{\epsilon_r} = \beta_r a N^b \quad (II-26a)$$

or

$$\epsilon_p = \beta_r \epsilon_r a N^b \quad (II-26b)$$

Where:

- ϵ_p = Accumulated plastic strain at N repetitions of load.
- β_r = Field adjustment or shift factor.
- ϵ_r = Resilient strain of the asphalt material as a function of mixture properties, temperature and time rate of loading.
- N = Number of axle load repetitions.
- a, b = Non-linear regression coefficients.

II-3.2.3 Permanent Strain Rate Approach

An alternative form of the permanent axial strain mathematical model has been used to evaluate the rutting potential of flexible pavements and materials. The mathematical form used to characterize the plastic strain per load repetition, ϵ_{pn} , relationship can be expressed by Equation II-27 (II-27a or II-27b), which is a modified form of the classical power model (refer to Equation II- 38):

$$\frac{\partial \varepsilon_p}{\partial N} = \varepsilon_{pn} = \frac{\partial (aN^b)}{\partial N} \quad (II-27a)$$

or

$$\varepsilon_{pn} = abN^{(b-1)} \quad (II-27b)$$

Where:

- ε_p = Permanent or plastic strain.
- ε_{pn} = Plastic strain per load repetition.
- a, b = Regression coefficients.
- N = Number of repeated axle load applications.

In the plastic strain per load repetition above, the resilient strain, ε_r , generally is assumed to be independent of the load repetitions value, N . The ratio of plastic to resilient strain components of the material in question can be defined by Equation II-28:

$$\frac{\varepsilon_{pn}}{\varepsilon_r} = \left(\frac{ab}{\varepsilon_r} \right) N^{b-1} \quad (II-28)$$

Where:

- ε_{pn} = Plastic strain per load repetition.
- ε_r = Resilient strain of the asphalt material as a function of mixture properties, temperature, and time rate of loading.
- a, b = Regression coefficients.
- N = Number of repeated axle load applications.

The mathematical relationship in Equation II- 29a is further obtained when applying the elements expressed in Equations II-29b and II-29c:

$$\frac{\varepsilon_{pn}}{\varepsilon_r} = \mu N^{-\alpha} \quad (II-29a)$$

Where:

- ε_{pn} = Permanent strain due to a single load application.
- ε_r = Resilient strain of the asphalt material as a function of mixture properties, temperature, and time rate of loading.
- μ = At N th application, μ (μ) is the permanent deformation parameter representing the constant of proportionality between permanent strain and elastic strain (i.e., plastic strain at $N-1$).
- N = Number of repeated axle load applications.
- α = Permanent deformation parameter indicating the rate of decrease in permanent deformation as the number of load applications increase.

When Letting:

$$\mu = \frac{\alpha b}{\epsilon_r} \quad (II-29b)$$

and

When Letting:

$$\alpha = 1 - b \quad (II-29c)$$

Where:

- μ = At Nth application, μ is the permanent deformation parameter representing the constant of proportionality between permanent strain and elastic strain (i.e., plastic strain at N-1).
- α = Permanent deformation parameter indicating the rate of decrease in permanent deformation as the number of load applications increase.
- b = Slope of deformation curve.
- ϵ_r = Resilient strain of the asphalt material as a function of mixture properties, temperature, and time rate of loading.

II-3.3 HMA PERMANENT DEFORMATION MODELS

II-3.3.1 MEPDG: HMA Permanent Deformation

The approach presented in the MEPDG is based upon incremental rut depth. Rutting is estimated for each sub-season at the mid-depth of each sub-layer within the pavement system. The permanent deformation for a given season is the sum of the permanent deformation within each layer. It is expressed mathematically in Equation II-30:

$$PD = \sum_{i=1}^{nsublayers} \epsilon_p^i \times h^i \quad (II-30)$$

Where:

- PD = Pavement permanent or plastic deformation, inches.
- $nsublayers$ = Number of sublayers.
- ϵ_p^i = Total plastic strain in sublayer i .
- h^i = Thickness of sublayer i .

Permanent deformation is calculated for each load level, sub-season, and month in the analysis period. The permanent or plastic deformation prediction models included in the MEPDG is based on work conducted by Leahy (1989), Ayres (1997), and Kaloush (2001). The initial work conducted by Leahy was based on 2,860 permanent strain data points (Leahy1989). Ayres re-analyzed the original Leahy data plus additional laboratory data developed at the University of Maryland (Ayers 1997).

Additional work was conducted at Arizona State University by Kaloush (2001) and Witczak, et al. (2002) under NCHRP Project 9-19 of the Superpave Models contract, which was adopted and included in the MEPDG procedure (Kaloush and Witczak 2002). The HMA mixtures, temperatures, and stress levels investigated by Kaloush greatly expanded the data range of the variables introduced in the statistical modeling. Kaloush examined a combined database using the original Leahy data in combination with the Superpave Models results. This database included a total of 3,476 permanent deformation strain data points being used in the regression analysis. The field calibrated form of the final lab expression selected for use in the MEPDG is given in Equation II-31 below.

$$\frac{\epsilon_p}{\epsilon_r} = \beta_{r1} k_z 10^{k_{r1}} T^{k_{r3} \beta_{r3}} N^{k_{r2} \beta_{r2}} \quad (II-31)$$

Where:

ϵ_p = Accumulated permanent strain, in/in.

ϵ_r = Resilient strain, in/in.

k_z = Depth confinement factor.

$$k_z = (C_1 + C_2 D) 0.328196^D, \text{ when}$$

$$C_1 = -0.1039(h_{HMA})^2 + 2.4868h_{HMA} - 17.342.$$

$$C_2 = 0.0172(h_{HMA})^2 - 1.7331h_{HMA} + 27.428.$$

D = Depth below the surface, in.

h_{HMA} = Total HMA thickness, in.

k_{r1}, k_{r2}, k_{r3} = Global calibration factors from the NCHRP Project 1-37A calibration effort
 $k_{r1} = -3.448, k_{r2} = 0.4791, k_{r3} = 1.5606.$

Global calibration factors from the NCHRP Project 1-40D recalibration effort
 $k_{r1} = -3.35412$ and the other factors remained unchanged.

T = Mixing temperature, °F.

$\beta_{r1}, \beta_{r2}, \beta_{r3}$ = Local or mixture field calibration constants, all set to 1.0 during the calibration efforts under NCHRP Projects 1-37A and 1-40D.

N = Number of load repetitions.

II-3.3.2 WesTrack Permanent Deformation Model

The WesTrack models were developed to determine the importance of different mixture properties and their variance as related to rutting in establishing performance related specifications (Epps et al. 2002). Two models were developed from the study: Level I is an empirical model relating mix properties to rut depth, while Level II is based on ME principles. For Level I, rut depth is a function of ESALs, air voids, asphalt content (percent by weight), and the percent of aggregate finer than the number 200 sieve. The Level II analysis consists of calculating the permanent shear strain (γ) at 50 mm below the surface, shear stress (τ) and compressive strain (ϵ_v) on top of the subgrade.

Total rut depth measured at the surface is expressed as a function of the number of load repetitions by combining the rut depth predicted in the HMA layer and unbound layers. In simple loading, permanent shear strain in the HMA was assumed to accumulate according to Equation II-32, (WesTrack 2000, Monismith et al. 2000).

$$\gamma_p = ae^{b\tau} \gamma_e N^c \quad (II-32)$$

Where:

- γ_p = Plastic or inelastic shear strain at a depth of 2 inches (50 mm) below the surface, in./in.
- γ_e = Elastic shear strain at the same depth noted above, in./in.
- τ = Shear stress computed at a depth of 2 inches from the surface using an elastic response model, psi.
- N = Number of axle load applications.
- a, b, c = Regression constants.

The time-hardening principle is used to estimate the accumulation of the inelastic strains in the HMA under in-situ conditions by Equations II-33a and II-33b. This time-hardening principle is similar to the concept used by Lytton, et al. (1993) for predicting plastic deformation in HMA mixtures during the Strategic Highway Research Program (SHRP).

$$\gamma_{p,1} = a_1 [\Delta N_t]^c \quad (II-33a)$$

and

$$\gamma_{p,t} = a_t \left[\left(\frac{\gamma_{p,t-1}}{a_t} \right)^{\frac{1}{c}} + \Delta N_t \right]^c \quad (II-33b)$$

Where:

- $\gamma_{p,1}$ = Plastic shear strain at the first hour or intercept.
- c = Regression constant.
- a_1 = Regression coefficient.
- ΔN_t = Number of load applications during the t^{th} hour.
- $\gamma_{p,t}$ = Plastic shear strain at the t^{th} hour.
- a_t = $ae^{b\tau} \gamma_{e,t}$.

Where:

- a = Regression constant.
- $b\tau$ = Shear stress.
- $\gamma_{e,t}$ = Elastic shear strain at the t^{th} hour.
- t = The n^{th} hour of traffic applications.

The rutting, estimated in the HMA layer due to the shear deformation, is determined using Equation II-34.

$$RD_{HMA} = K_r \gamma_{p,t} \quad (II-34)$$

Where:

- RD_{HMA} = Rut depth in the HMA.

- K_r = A coefficient relating rut depth to plastic strain and developed from finite element analyses of representative pavement structures (Sousa et al. 1991, SHRP 1994). K_r is related to the thickness of the HMA layer and is given in Table II-2 (WesTrack 2000, Monismith et al. 2000).
- $\gamma_{p,t}$ = Plastic shear strain at the t^{th} hour.

Table II-2 Suggested Values of K_r as Function of HMA Layer Thickness

HMA Thickness, inches	K_r -Value (Equation II-44)
5 to 7	5.5
7 to 9	7.0
9 to 12	8.5
>12	10.0

The total rut depth measured at the surface of the pavement is the estimated rut depth from the HMA layers plus the rut depth from the unbound layers and subgrade soil, as shown by Equation II-30 or Equation II-35.

$$RD = RD_{HMA} + \sum_{i=1}^I RD_i \quad (II-35)$$

Where:

- RD = Total rut depth.
 RD_{HMA} = Rut depth in the HMA.
 I = Rut depth in the i^{th} layer.

II-3.3.3 VESYS Permanent Deformation Model

The VESYS structural response procedure is a layered elastic analysis technique (Kenis 1977, FHWA 1978). The model can be used as a pavement design program, including performance prediction models for rutting, fatigue, low temperature cracking, and serviceability.

The VESYS model uses axial repeated load (creep) test results to predict overall rutting of flexible pavements. The parameters required by the model are the resilient modulus, resilient strain, Alpha (Equation II-36), and Gnu (Equation II-37):

Alpha is defined as:

$$\alpha = I - S \quad (II-36)$$

Where:

- I = Linear intercept with the permanent strain axis.
 S = Slope of the linear portion of the logarithmic relationship.

Gnu is defined as:

$$\mu = \frac{IS}{E_r} \quad (II-37)$$

Where:

- I = Linear intercept with the permanent strain axis.
- S = Slope of the linear portion of the logarithmic relationship.
- E_r = Resilient modulus.

Alpha and Gnu are calculated from their repeated load permanent deformation test (i.e., the slope and intercept of the permanent deformation curve and the resilient strain). The theory assumes that the logarithmic relationship between the number of repeated loads and permanent strain is essentially linear over a range of load applications (the steady state zone) and can be described by the classical power law, Equation II-38:

$$\epsilon_p = IN^s \quad (II-38)$$

Where:

- ϵ_p = Accumulated permanent strain.
- I = Linear intercept with the permanent strain axis.
- N = Number of repeated axle load applications.
- S = Slope of the linear portion of the logarithmic relationship.

The VESYS model employs the deformation properties of each layer in the pavement structure to calculate directly the total rutting at the surface. A detailed discussion of the original model development is provided in other documents (*Moavenzdeh et al. 1974, Brademeyer 1988*).

II.3.3.4 Ohio State University Model

The Ohio State University model predicts total rutting and is described by Equation II-39 (*Majidzadeh et al. 1980*).

$$\frac{\epsilon_p}{N} = A(N)^{-m} \quad (II-39)$$

Where:

- ϵ_p = Permanent strain, in./in.
- N = Number of allowable axle load applications.
- A = Experimental constant dependent on material type and stress state.
- m = Experimental constant dependent on material type.

This equation is valid for describing the progression of rutting in a flexible pavement (i.e., HMA) layer, surface and base courses, granular base and subbase courses, and the subgrade. For cohesive soils, m does not vary greatly. However, A is rather variable and is dependent on material type, repeated stress state, and environmental conditions. For HMA, Khedr found that b (where $b = m + 1$) is 0.22 on average and varies a little with changes in temperature and

stress state (*Khedr 1986*). However, *A* was dependent on the repeated deviator stress and the HMA mixture modulus. Table II-3 provides a summary of typical values for *A* and *m* in the Ohio prediction model for rut depths.

Table II-3 Typical Values of *A* and *m* in the Ohio State Rut Depth Prediction Model

Moisture	Unconfined Strength, kPa (psi)	Repeated Deviator Stress, kPa (psi)	M	A x 10 ⁻⁴
Optimum	159 (23)	34 (5)	0.86	12.4
		69 (10)	0.86	18.2
		103 (15)	0.86	43.7
Optimum + 4%	90 (13)	34 (5)	0.83	17.0
		69 (10)	0.83	42.5
		103 (15)	0.83	138.0

II-3.3.5 Asphalt Institute Model

The Asphalt Institute developed an equation to calculate the permanent strain in HMA layers based on various mixture design factors (*AI 1983, May and Witczak 1992*). This equation is based on 251 specimens, which were compacted from two aggregate types (rounded gravel and crushed stone) and two types of asphalt (AC-5 and AC-20). Equation II-40, employs the DAMA program.

$$\log \varepsilon_p = -14.97 + 0.408 \log N + 6.865 \log T + 1.107 \log \sigma_d - 0.117 \log V + 1.908 \log P_{eff} + 0.971 \log V_v \quad (II-40)$$

Where:

- ε_p = Permanent or plastic strain, in./in.
- N = Number of load repetitions to failure.
- T = Temperature, °F.
- σ_d = Deviator stress, lbf/in².
- V = Viscosity at 21 °C (70 °F), Ps x 10⁶.
- P_{eff} = Percent by volume of effective asphalt.
- V_v = Percent volume of air voids.

II-3.3.6 Leahy, Ayers, and Kaloush and Witczak Models

Several studies conducted by Leahy (1989), Ayers (1997), and Kaloush and Witczak (2002), have related the plastic to elastic strain model to various HMA mixture variables. The Leahy model is found in Equation II-41:

$$\log \left(\frac{\varepsilon_p}{\varepsilon_r} \right) = -6.631 + 0.435 \log N + 2.767 \log T + 0.110 \log \sigma_d + 0.118 \log \eta + 0.930 \log V_{beff} + 0.5011 \log V_a \quad (II-41)$$

The regression correlation coefficient, $R^2=0.76$.

Where:

- ϵ_p = Accumulated plastic strain at N axle load repetitions.
- ϵ_r = Resilient strain of the HMA layer as a function of mixture properties, temperature, and time rate of loading.
- N = Number of axle load repetitions.
- T = Mixing temperature, °F.
- σ_d = Deviatoric stress, psi.
- η = Viscosity at 70 °F (10^6 poise).
- V_{beff} = Effective asphalt content, percent by volume.
- V_a = Air void content, percent.

From a sensitivity analysis performed on the model, Leahy reported that temperature was by far the most important variable. The model was less sensitive to the loading conditions, material type, and mix parameters. The resilient strain, under a dynamic repeated load using axial compression test, was assumed to be reasonably constant and independent of the number of load repetitions. Witczak, et al. (2002) developed several models (e.g., Equations II-42 and II-43) that reflected a fewer number of independent variables used in the above equation, with approximately the same accuracy.

$$\text{Log} \left(\frac{\epsilon_p}{\epsilon_r} \right) = -3.74938 + 2.02755 \log T + 0.4262 \log N \quad (\text{II-42})$$

The regression correlation coefficient, $R^2=0.73$.

Where:

- ϵ_p = Accumulated plastic strain at N axle load repetitions.
- ϵ_r = Resilient strain of the HMA layer as a function of mixture properties, temperature, and time rate of loading.
- T = Mixing temperature, °F.
- N = Number of axle load repetitions.

and

$$\text{Log} \left(\frac{\epsilon_p}{\epsilon_r} \right) = 0.1981 + 0.4041 \log N \quad (\text{II-43})$$

The regression correlation coefficient, $R^2=0.63$.

Where:

- ϵ_p = Accumulated plastic strain at N axle load repetitions.
- ϵ_r = Resilient strain of the HMA layer as a function of mixture properties, temperature, and time rate of loading.
- N = Number of axle load repetitions.

Ayres (1997) suggested two alternative models for the ratio between plastic and resilient strains as a function of two variables: temperature level and number of load repetitions. Leahy's model included six predictor variables: load repetitions, temperature, deviator stress, viscosity, asphalt content, and air voids. Ayres reported that the modification was necessary to avoid spurious

correlation and high inter-correlation between predictor variables. The two models Ayres suggested are shown in Equations II-44 and II-45:

Log Quadratic:

$$\log\left(\frac{\epsilon_p}{\epsilon_r}\right) = [-277161 + 1.451074\log(T)] + [-0.17796 + 0.36640\log(N) - 0.0915x\log(N)^2] \quad (II-44)$$

The regression correlation coefficient, $R^2=0.734$.

Where:

- ϵ_p = Accumulated plastic strain at N axle load repetitions.
- ϵ_r = Resilient strain of the HMA layer as a function of mixture properties, temperature, and time rate of loading.
- T = Mixing temperature, °F.
- N = Number of axle load repetitions.

Log Linear:

$$\log\left(\frac{\epsilon_p}{\epsilon_r}\right) = -4.80661 + 2.58155\log T + 0.429561\log N \quad (II-45)$$

The regression correlation coefficient, $R^2=0.725$.

Where:

- ϵ_p = Accumulated plastic strain at N axle load repetitions.
- ϵ_r = Resilient strain of the HMA layer as a function of mixture properties, temperature, and time rate of loading.
- T = Mixing temperature, °F.
- N = Number of axle load repetitions.

Subsequently, Ayers utilized Equation II-45 in his development of Program AYMA, developed at the University of Maryland, dealing with the probabilistic methodology for flexible pavements (Ayers 1997).

II-3.3.7 Flow Model

It has been observed that most of the models presented above tend to under-predict the (ϵ_p/ϵ_r) ratio at higher numbers of load repetitions. This has been attributed to the occurrence of tertiary flow (or flow point N_F) where the permanent strain begins to increase rapidly with an increase in load repetition. The under-prediction of the rut depth was expected because most of the regression constants were determined from the steady-state zone of creep or repeated load tests. Therefore, to utilize the developed model in a rational range of cycles, it is preferable to predict the N_F value based on the mixture volumetric properties, binder type, test temperature, and/or stress level.

A power model was developed by Witczak, et al. (2002) utilizing data from the University of Maryland to predict the number of cycles at which tertiary flow occurs. The model was based

on the HMA mixture volumetric properties, binder viscosity, test temperature, and stress level. The model is given in Equation II-46:

$$N_{FLOW} = (1.00788 * 10^5) T^{-1.6801} S^{-0.1502} \eta^{0.2179} V_{beff}^{-3.6444} V_a^{-0.9421} \quad (II-46)$$

(Se / Sy = 0.4306, R²=0.8336)

Where:

- N_{FLOW} = Flow point.
- T = Mixing temperature.
- S = Deviator stress, psi.
- η = Viscosity at 70°F (10⁶ poise).
- V_{beff} = Effective asphalt content, percent by volume.
- V_a = Air void content, percent.
- Se = Standard error.
- Sy = Standard deviation.
- R = Regression correlation coefficient.

In addition, histogram plots of the (ϵ_p/ϵ_r) ratio at failure (flow) can be developed from any database. With future refinement of these plots, the (ϵ_p/ϵ_r) ratio at failure can be used as a guide for HMA mixture failure analysis by comparing the ratio predicted for the mixture under consideration with the distribution of the critical ratio at failure.

II-3.3.8 Allen and Deen Model

Allen and Deen (1980) developed rutting prediction models from laboratory testing. The models can predict rutting in the asphalt concrete layers, dense-graded aggregate layers, and subgrade soils. These models, together with a traffic and temperature model, are used to predict rutting and have been incorporated into a computer program called PAVRUT (see Equation II-47).

$$\log \epsilon_p = C_0 + C_1(\log N) + C_2(\log N)^2 + C_3(\log N)^3 \quad (II-47)$$

Where:

- ϵ_p = Permanent strain (axial), in/in.
- N = Number of stress repetitions.
- C_i = Regression coefficient refer to Table II-4 (Allen and Deen 1980).

Table II-4 Regression Coefficients for the Allen and Deen Rutting Prediction Model

Coeff.	HMA	Dense-Graded Aggregate Base	Subgrade
C_0	$- 0.000663 T^2 + 0.1521 T - 13.304 + (1.46 - 0.00572 T) * \log \sigma_1$	$- 4.41 + (0.173 + 0.003 w) * \sigma_1 - (0.00075 + 0.0029 w) * \sigma_3$	$- 6.5 + 0.38w - 1.1 (\log \sigma_3) + 1.86 (\log \sigma_1)$
C_1	0.63974	0.72	$10^{(-1.1 + 0.1 w)}$
C_2	- 0.10392	$- 0.142 + 0.092 (\log w)$	0.018 w
C_3	0.00938	$0.0066 - 0.004 (\log w)$	$0.007 - 0.001 w$
Where:	T = Temperature, °F. σ_1 = Deviator stress, lbf/in ² . W = Moisture content, percent. σ_3 = Confining pressure, lbf/in ² .		

Depending on the type of material being evaluated, the regression constants (C_0 , C_1 , C_2 , and C_3) are calculated based on material and test conditions. For asphalt concrete mixtures, the regression constants are a factor of the temperature and deviator stress. For dense-graded aggregate bases and the subgrade, the regression constants are a factor of the moisture content, the deviator stress, and the confining pressure.

II-3.3.9 Asphalt-Aggregate Mixture Analysis System

The plastic deformation model included in the AAMAS procedure was based on Equation II-24 with the exception that triaxial creep tests were performed to determine the HMA mixture permanent deformation constants, as shown in Equations II-48a and II-48b (*Von Quintus et al. 1991*).

$$\epsilon_p = A(N)^b = a(t_l)^{m_c} - \epsilon_{rt} \quad (II-48a)$$

and

$$\epsilon_p = a(t_l)^{m_c} (1 - X) \quad (II-48b)$$

Where:

- ϵ_p = Permanent strain (axial), in./in.
- A, b, a, m_c = Regression constants for the creep curve in the steady state region.
- N = Number of stress repetitions.
- t_l = Loading time for one cycle of a repeated load permanent deformation test, sec.
- X = Recoverable creep ratio measured during a triaxial creep-recovery test, dimensionless, or $\frac{\epsilon_{rt}}{(\epsilon_{ct})}$, $\epsilon_{ct} = \epsilon_{il} + \epsilon_{cr}$.
- ϵ_{rt} = $\epsilon_{ir} + \epsilon_R$
 - ϵ_{ir} = Instantaneous resilient or recovered strain after load release, in./in.
 - ϵ_R = Recovered strain or relaxation during the rest period of one loading cycle, in./in.
 - ϵ_{il} = Instantaneous strain measured after load application, in./in.
 - ϵ_{cr} = Creep strain measured during one load application or cycle, in./in.

The slope of the triaxial repeated load permanent deformation test (Equation II-24) was found to be correlated to the slope of the triaxial creep-recovery test. The relationship presented and used in the AAMAS procedure is shown in Equation II-49:

$$b = \frac{3.5563m_c + \text{Log}(a) + \text{Log}(1 + X) - \text{Log}[a(0.1)^{m_c} - \epsilon_{rt}]}{4.5563} \quad (II-49)$$

Where:

- b = Regression coefficients.
- a, m_c = Regression constants for the creep curve on the steady state region.
- X = Recoverable creep ratio measured during a triaxial creep – recovery test, dimensionless.
- ϵ_{rt} = Instantaneous resilient or recovered strain after load release, in/in.

II-3.3.10 Michigan State Model

Baladi at Michigan State University developed a model for predicting rut depth in HMA layers of flexible pavements (Baladi 1987). Equation II-50 is the result for predicting rut depth:

$$\begin{aligned} \log RD = & -1.6 + 0.067V_a - 1.4 \log T_{AC} + 0.07T_{avg} - 0.000434KV_a \\ & + 0.15 \log(ESAL) - 0.4 \log M_R - 0.50 \log E_{base} + 0.1 \log \delta_0 \\ & + 0.01 \log \epsilon_v - 0.7 \log TB_{EQ} + 0.09 \log (50 - T_{AC} - TB_{EQ}) \end{aligned} \quad (II-50)$$

Where:

- RD = Rut depth, in.
- T_{avg} = Average annual temperature, °F.
- T_{AC} = Thickness of the HMA layer, inches.
- KV_a = Kinematic viscosity.
- δ_0 = Surface deflection for referenced condition, inches.
- TB_{EQ} = Equivalent thickness of the base, inches.
- $ESAL$ = Number of 80-kN (18-kip) ESALs at which the rut depth is being calculated.
- M_R = Resilient modulus of the HMA.
- E_{base} = Modulus of the base.
- ϵ_v = Average vertical resilient strain.
- V_a = Air voids.

Baladi notes that this equation is based on limited field data and should be used with extreme caution. In addition, Baladi recommends that these models be re-calibrated with additional field data, if used for designing HMA pavements and mixtures.

II-3.3.11 Shell International Model

The Shell International procedure uses the compressive creep test to estimate the reduction in layer thickness or the amount of rutting, a one-dimensional compression test. The generalized equation included in the Shell procedure is given in Equation II-51 (Shell 1978).

$$\Delta h = C_m h_{AC} \left(\frac{\sigma_c}{E_{mix}} \right) \quad (II-51)$$

Where:

- Δh = Thickness reduction in HMA layer, mm.
 C_m = Correction factor for dynamic effect that is a function of mixture type with values ranging from 1 to 2 (Table II-5).
 h_{AC} = Thickness of the HMA layer, mm.
 σ_c = Average vertical compressive stress in the HMA layer, kPa.
 E_{mix} = Modulus of the HMA material, kPa.

Table II-5 Correction Factors, C_m , for the Shell International Procedure to Predict Rutting

HMA Mix Type		C_m
Open  Dense	Sand Sheet & Lean Sand Mixes	1.6-2.0
	Lean Bitumen Macadam	1.5-1.8
	Dense Graded HMA Gravel Sand Asphalt Dense Bitumen Macadam	1.2-1.6
	Mastic Asphalt Types Gussasphalt Hot Rolled Asphalt	1.0-1.3

Repeated unconfined or confined axial permanent deformation tests, however, have been used to determine the permanent deformation characteristics or parameters used for the rutting models previously discussed. For this test, the results are presented in terms of accumulated permanent strain versus number of loading cycles.

II-3.3.12 Verstraeten Plastic Strain Model

Verstraeten, et al. (1982) developed a permanent or plastic strain model similar to the Shell and Asphalt Institute procedures. The generalized equation, Equation II-52, is given below and is based on repeated load unconfined or confined triaxial permanent deformation tests.

$$\epsilon_p = A \left(\frac{\sigma_1 - \sigma_3}{E^*} \right) \left(\frac{N}{1000f} \right)^{b_{HMA}} \quad (II-52)$$

Where:

- ϵ_p = Permanent or plastic strain, in/in.
 E^* = Dynamic modulus of the HMA mix, psi.
 σ_1 = Vertical stress, psi.
 σ_3 = Radial stress, psi.
 N = Number of load cycles.
 f = Frequency of loads, cps.
 A, b_{HMA} = Regression coefficients (for conventional mixes; $A=57.5$ and $b_{HMA}=0.25$).

II-3.4 UNBOUND LAYERS PERMANENT DEFORMATION MODELS

Most ME based rut depth prediction models for unbound materials are based on limiting the unbound pavement responses so that minimal plastic deformations occur within those unbound layers. This section of Chapter II-3 lists and overviews some of the different models for predicting plastic deformation in unbound pavement layers and subgrade soils.

II-3.4.1 MEPDG

Unbound Pavement Layers. Models developed by Tseng and Lytton (1989) are used to estimate the permanent or plastic deformation in granular and subgrade materials. The basic relationship is shown in Equation II-53:

$$\Delta_a(N) = \beta k_{s1} \varepsilon_v h \left(\frac{\varepsilon_0}{\varepsilon_r} \right) e^{-\left(\frac{\rho}{N}\right)^\beta} \quad (II-53)$$

Where:

- Δ_a = Permanent deformation for the layer/sublayer.
- N = Number of axle load applications.
- $\beta, \varepsilon_0, \rho$ = Material properties.
- ε_r = Resilient strain imposed in laboratory test to obtain material properties ε_0 , β , and ρ , in/in.
- ε_v = Average vertical resilient strain in the layer/sublayer as obtained from the primary response model, in/in.
- h = Thickness of the layer/sublayer, in.
- k_{s1} = Global calibration coefficients; $k_{s1}=1.673$ for granular materials and 1.35 for fine-grained materials.

The ratio $\varepsilon_0/\varepsilon_r$ is estimated according to the type of material investigated: granular or subgrade soil. The models developed by Tseng and Lytton are given in Equations II-54, II-55, II-56, II-57, II-58, and II-59, below.

Granular or Coarse-Grained Soils

$$\log \left(\frac{\varepsilon_0}{\varepsilon_r} \right) = 0.80978 - 0.06626 W_c - 0.003077 \sigma_\theta + 0.000003 E_r \quad (II-54)$$

and

$$\log \beta = -0.9190 + 0.03105 W_c + 0.001806 \sigma_\theta - 0.0000015 E_r \quad (II-55)$$

and

$$\log \rho = -1.78667 + 1.45062 W_c + 0.0003784 \sigma_\theta^2 - 0.002074 W_c^2 \sigma_\theta - 0.0000105 E_r \quad (II-56)$$

Where:

- ϵ_0 = Material property.
- ϵ_r = Resilient strain imposed in laboratory test to obtain material properties ϵ_0 , β , and ρ , in/in.
- W_c = Water content, %.
- σ_θ = Bulk stress, psi.
- E_r = Resilient modulus of the layer/sublayer, psi.
- β, ρ = Material properties.

Fine-Grained Soils

$$\log\left(\frac{\epsilon_0}{\epsilon_r}\right) = -1.69867 + 0.09121 W_c - 0.11921 \sigma_d + 0.91219 \log E_r \quad (II-57)$$

and

$$\log \beta = -0.9730 - 0.0000278 W_c^2 \sigma_d + 0.017165 \sigma_d - 0.0000338 W_c^2 \sigma_\theta \quad (II-58)$$

and

$$\log \rho = 11.009 + 0.000681 W_c^2 \sigma_d - 0.40260 \sigma_d + 0.0000545 W_c^2 \sigma_\theta \quad (II-59)$$

Where:

- ϵ_0 = Material property.
- ϵ_r = Resilient strain imposed in laboratory test to obtain material properties ϵ_0 , β , and p , in/in.
- W_c = Water content, %.
- σ_d = Deviator stress, psi.
- σ_θ = Bulk stress, psi.
- E_r = Resilient modulus of the layer/sublayer, psi.
- β, ρ = Material properties.

Subgrade or Embankment Soils. The subgrade is the part of the pavement with very large depths and, sometimes, for practical purposes, is modeled to be a layer with infinite depth. Therefore, it is often not practical to divide it into sublayers and compute plastic strains at the mid-depth of each sublayer because of the huge computational effort required. Ayres (1997) evaluated the plastic strain for an infinite layer and developed an alternative approach. His analysis indicated that the following model structure, Equation II-60 provides a R^2 exceeding 97 percent:

$$\epsilon_p(z) = (\epsilon_{p,z=0}) e^{-k z} \quad (II-60)$$

Where:

- $\epsilon_p(z)$ = Plastic vertical strain at depth z (measured from the top of the subgrade), in/in.
- $\epsilon_{p,z=0}$ = Plastic vertical strain at the top of the subgrade ($z = 0$), in/in.
- z = Depth measured from the top of the subgrade, in.
- k = Constant obtained from regression analysis.

A limiting value for k of 0.000001 is used to prevent the assumption that permanent strain decreases with depth from being violated. This assumption will not cause any significant error in the results because the subgrade is divided into several sub-layers and the contribution for the last sub-layer should be negligible. This approach is only used for the last subgrade layer, which is eight feet below the top of the subgrade. The total permanent deformation in the subgrade is found by solving the integral, Equations II-61a and II-61b:

$$\delta_{soil} = \int_0^{h_{bedrock}} \epsilon_p(z) dz \quad (II-61a)$$

or

$$\delta_{soil} = \epsilon_{p,z=0} \int_0^{h_{bedrock}} e^{-kz} dz = \left(\frac{1 - e^{-kh_{bedrock}}}{k} \right) \epsilon_{p,z=0} \quad (II-61b)$$

Where:

- δ_{soil} = Total plastic deformation of the subgrade, in.
- $h_{bedrock}$ = Depth to bedrock, in.
- $\epsilon_{p,z=0}$ = Plastic vertical strain at depth z (measured from the top of the subgrade), in/in.
- z = Depth measured from the top of the subgrade.
- k = Constant obtained from regression analysis.

II-3.4.2 WesTrack Model

The rut depth contribution from all unbound materials or layers within the pavement structure is calculated by Equation II-62 in the procedure resulting from the WesTrack project (2000).

$$RD_{Unbound} = \frac{0.14}{\left[1.05 \times 10^{-9} (\epsilon_{v(Unbound)})^{-4.484} \right]^{0.372}} (N)^{0.372} \quad (II-62)$$

Where:

- $RD_{Unbound}$ = Rut depth from unbound materials.
- $\epsilon_{v(Unbound)}$ = Vertical resilient strain.
- N = Number of load repetitions to failure.

The WesTrack procedure uses a similar time-hardening principle for the unbound materials, as used for the HMA and in the MEPDG. Rut depth accumulation and can be expressed in Equation II-63.

$$RD_{t(Unbound)} = d_t \left[\left(\frac{RD_{t-1(Unbound)}}{d_t} \right)^{0.372} + \Delta N_t \right]^{0.372} \quad (II-63)$$

Where:

$RD_{t(Unbound)}$ = Rut depth accumulation with time, t .

$$d_t = \frac{0.14}{\left[1.05 \times 10^{-9} (\epsilon_{v(Unbound)})^{-4.484}\right]^{0.372}}$$

Where:

$\epsilon_{v(Unbound)}$ = Vertical compressive strain in an unbound aggregate base/subbase layer or subgrade soil, in/in.

ΔN_t = Number of load repetitions during the t^{th} hour.

II-3.4.3 Limiting Vertical Compressive Strain Approach

The vertical compressive strain models are not used to estimate the amount of rutting over time on the pavement's surface. Rather, these types of models are used to ensure that there is sufficient structure above the subgrade to lower or minimize the plastic deformations in the subgrade so that distortions observed at the surface of the pavement are insignificant. When using these type models, rutting (surface distortion) is considered to occur primarily in the subgrade, and has been related to the vertical compressive strain at the top of the subgrade by the following functional form, Equation II-64.

$$N_f = b_1 \beta (\epsilon_v)^{-b_2} (M_R)^{b_3} \quad (II-64)$$

Where:

N_f = Number of load repetitions for subgrade distortions that cause surface distortions exceeding a specific depth.

b_1, b_2, b_3 = Soil properties from repeated load triaxial tests.

β = Field calibration factor for subgrade distortion based on vertical compressive strain.

ϵ_v = Vertical compressive strain at the top of the subgrade soil or foundation, in/in.

M_R = Design resilient modulus of the subgrade soil or foundation, psi.

This assumption implies that the structural layers above the subgrade or foundation will be constructed so that only negligible rutting will occur within those layers. The soil properties b_1 , b_2 , and b_3 are obtained through triaxial repeated load permanent deformation tests in the laboratory. The regression coefficient b_1 is shifted or adjusted to correlate laboratory results to a specific level of subgrade distortion. This assumes that the materials placed above the foundation will be properly compacted and of sufficient strength so that significant permanent deformation will not occur in those layers.

The Corp of Engineers used this concept in developing a structural design procedure for flexible airfield pavements (*Barker and Brabston 1975*). Rauhut, et al. (*1984b*) modified the original Corp of Engineers relationship to account for resilient modulus differences of the soil to ensure there is a sufficient pavement thickness to protect the subgrade. Equation II-65 is the modified version of the Corp of Engineers limiting vertical strain model for unbound layers.

$$N_f = 1.259 \times 10^{-11} (M_R)^{0.955} (\epsilon_v)^{-4.082} \quad (II-65)$$

Where:

- N_f = Number of load repetitions for subgrade distortions that cause surface distortions exceeding a specific depth.
- M_R = Resilient modulus of the unbound layer or soil, psi.
- ϵ_v = Vertical strain computed at the surface of the unbound layer or soil, in/in.

The Ohio DOT included this concept in their pavement evaluation and design system developed by Ohio State University (Majidzadeh et al. 1978,1980; Khedr 1985). Other examples of rutting prediction models that are based on limiting the vertical compressive strain on top of the subgrade include the Asphalt Institute (1982), Shell International (1978), TRRL (Powell et al. 1984), and the Belgian Road Research Center (Verstraeten et al. 1982) models. These models calculate the allowable number of load repetitions before rutting or surface distortions become unacceptable using the following mathematical form, Equation II-66.

$$N_f = f_4 (\epsilon_v)^{-f_5} \tag{II-66}$$

Where:

- N_f = Number of allowable load applications.
- f_4, f_5 = Constants determined from road tests or field performance studies.
- ϵ_v = Vertical compressive strain on top of the subgrade, in/in.

The above-mentioned four models are based on field studies conducted under different geographic, climatic, and traffic loading conditions and therefore have different field calibration factors. Subsequently, the use of these models to estimate the number of loads to failure for conditions different from those used to develop the models is not recommended. Models of this form assume that the allowable rut depth will not be exceeded if the vertical compressive strain on the subgrade is limited. Table II-6 shows the field calibration factors and subgrade strain criteria used by these four models.

Table II-6 Field Calibration Constants and Subgrade Strain Criteria for Permanent Deformation Models

Organization	Limiting Strain Constants		Allowable Rut Depth	
	f_4	f_5	mm	in
Asphalt Institute	1.365×10^{-9}	4.477	13	0.5
Shell (revised 1985)				
50% Reliability	6.15×10^{-7}	4.0	13	0.5
85% Reliability	1.94×10^{-7}	4.0	13	0.5
95% Reliability	1.05×10^{-7}	4.0	13	0.5
U.K. Transport and Road Research Laboratory (85% Reliability)	6.18×10^{-8}	3.95	10	0.4
Belgian Road Research Center	3.05×10^{-9}	4.35	10	0.4

II-3.4.4 Limiting Modulus Ratio Approach for Unbound Layers

A concept used in some flexible pavement design systems is the limiting layer modulus ratio of adjacent unbound layers. This concept defines the maximum resilient modulus of an unbound

layer based on the resilient modulus of the supporting layers. The hypothesis is that when the layer modulus ratio of adjacent unbound layers exceeds some value (approximately 3), large tensile stresses will occur in the upper unbound layer. Unbound layers have minimal tensile strength and will decompact under this condition, reducing the modulus and tensile stresses in that layer.

The hypothesis of decompaction is debatable, but different flexible pavement methods have included this concept in selecting permissible resilient modulus values for the unbound layers. As an example, the Corp of Engineers structural design procedure developed by Barker and Brabston (1975) employed this limiting layer modulus ratio concept, which is illustrated in Figure II-2.

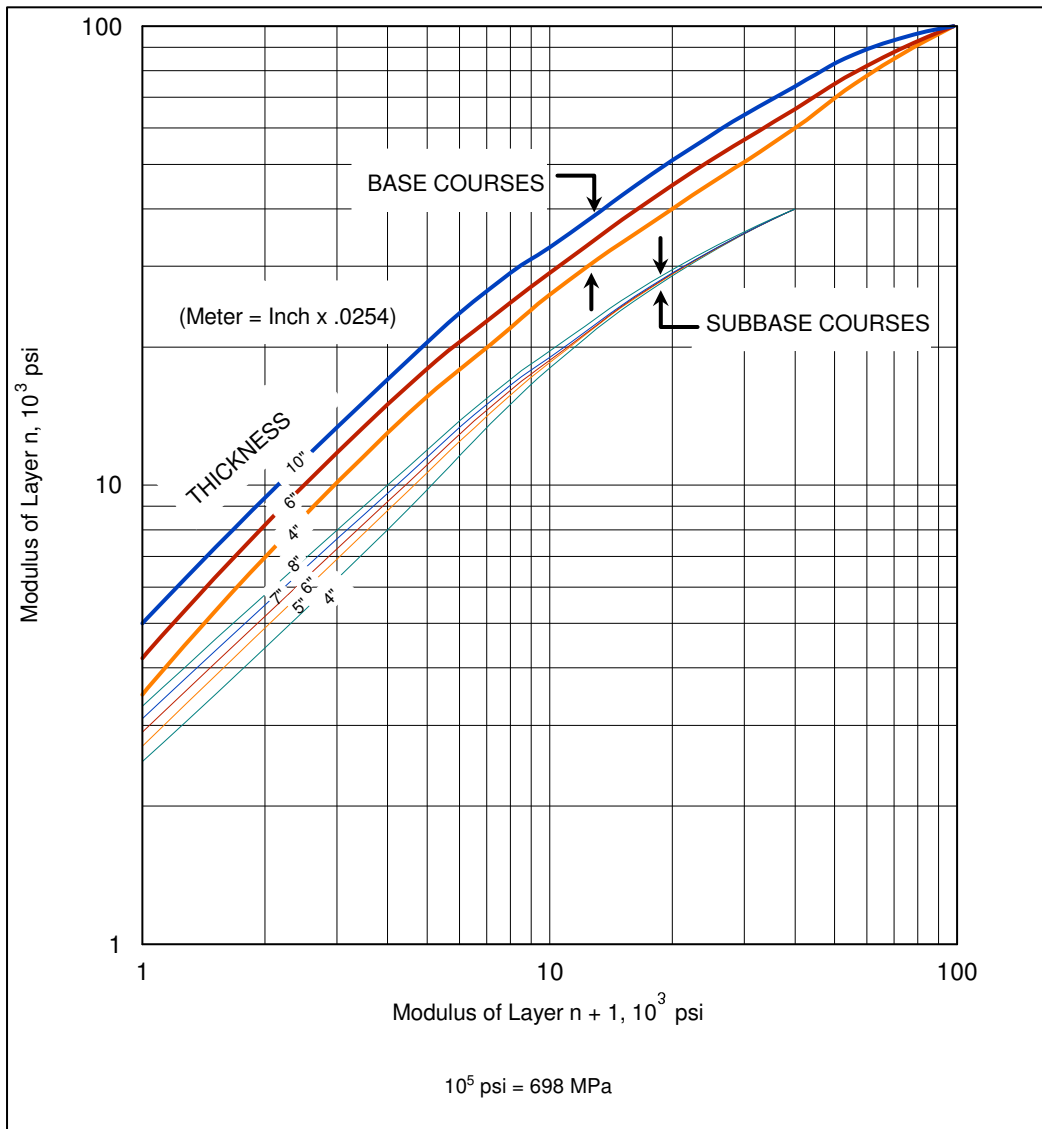


Figure II-2 Limiting modulus criteria of unbound aggregate base and subbase layers.

CHAPTER II-4: TRANSVERSE CRACKS

The structural deterioration of flexible pavements is associated with the occurrence of non-load related linear cracks that are a result of decreases in temperature in the HMA mixture – transverse and longitudinal cracks. Thermal cracking of flexible pavements has long been a problem in nearly all climate areas. The problem occurs not only in colder climates (i.e., Canada or the northern U.S.), but also in warmer climates of the U.S. when the certain conditions of temperature and HMA properties are present.

II-4.1 TRANSVERSE CRACKING MECHANISMS

II-4.1.1 Low Temperature Cracking

Low temperature cracking occurs when a drop in temperature causes the tensile stresses developed in an asphalt concrete pavement that are equal to the tensile strength of the HMA mixtures. When this occurs, a micro crack develops at the surface of the pavement and propagates down through the layer. Figure II-3 graphically illustrates this stress-strength mechanism. The temperature at which the thermal stress and the tensile strength curve intersect is defined as the critical temperature (T_{CR}).

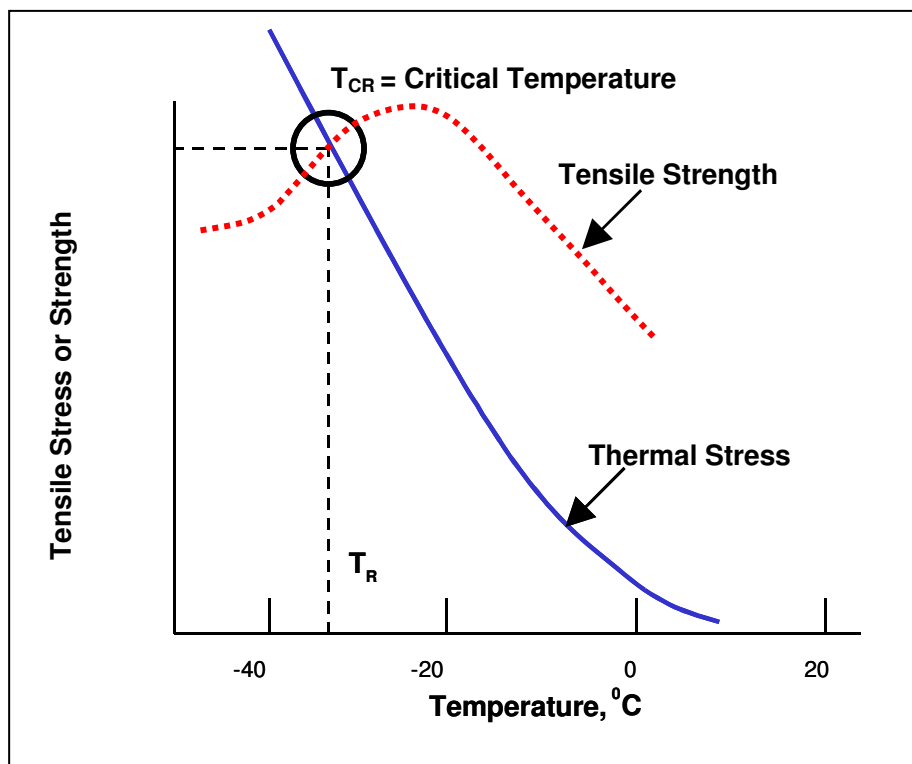


Figure II-3 Example of thermal effects or drops in temperature on the tensile strength and thermal stress development in HMA mixtures.

It is important to note in Figure II-3 that the tensile stress and strength increase with a decrease or drop in temperature. However, the tensile strength increases to a maximum value and then begins to decrease with continued drops in temperature. The reason for this drop in strength is that micro-cracks begin to occur at the interface of the asphalt binder and aggregate. These micro-cracks reduce the tensile strength, but have little to no significant effect on the elastic modulus.

Low temperature cracking is sometimes referred to as transverse cracking because it appears on the surface perpendicular to the directions of travel. Crack spacing can range from 1 to 100 m (3 to 300 ft). If the transverse crack spacing is less than the width of the pavement, longitudinal thermal cracking may occur, and a block pattern of cracks is formed.

As the temperature decreases, the pavement tries to shrink but is restrained. This restraint causes a gradual tensile stress build up. Due to the viscoelastic nature of the HMA mixture, the tensile stress that builds up dissipates through stress relaxation. This relaxation occurs very rapidly at temperatures above 70°F. Below this temperature, the relaxation times increase and stresses develop in the mixture. The rate at which thermal cracks occur depends upon the magnitude of the temperature drop, the asphalt rheological properties, the HMA mixture properties, and other environmental factors.

II-4.1.2 Thermal Fatigue Cracking

Thermal fatigue cracking is associated with thermal cycling at moderate temperatures. During the night, tensile stresses are greater due to the drop in temperature. During the day, these stresses drop due to warmer temperatures. While the induced stresses are lower than the tensile strength of the HMA and do not cause cracks immediately, cracks do occur eventually due to thermal fatigue – similar to load-related fatigue cracks.

The same general considerations apply to thermal fatigue cracking that apply to the development of low temperature cracking. The daily drop in temperatures causes thermal stress to develop that are much smaller than those that occur during the worst part of the winter, but they occur more frequently. The number of cycles required to produce a crack depends on the magnitude of the tensile stress. The larger the stress the fewer cycles required to produce a crack – consistent with the load related fatigue cracks.

II-4.2 TRANSVERSE CRACKING PREDICTION MODELS

II-4.2.1 MEPDG: Transverse Cracking

The thermal cracking model that is embedded in the MEPDG is an enhanced version of the approach originally developed under the SHRP A-005 research contract by Dr. Roque and Dr. Hiltunen of the Pennsylvania Transportation Institute (*Lytton et al. 1993, Roque et al. 2000*). In summary, fourteen Canadian SHRP, and five MnRoad sections were added to the 22 SHRP General Pavement Studies (GPS) sections (originally used in the initial TCMODEL calibration) to re-calibrate the TCMODEL used in the MEPDG. The MEPDG software predicts the total length of transverse cracks – the combined length of low temperature cracks and thermal fatigue cracks.

The Enhanced Integrated Climatic Model (EICM) is used as the climatic algorithm to determine the temperature-depth profile within the asphalt layer at hourly time intervals over the analysis period. Using viscoelastic transformation theory, the compliance, $D(t)$, can be related to the Relaxation modulus, E_r , of the HMA mix. Knowledge of this parameter, coupled with the temperature data obtained from the EICM model, allows for the prediction of thermal stress at any given depth and time within the HMA layer. Fracture mechanics (Paris law) is then used to compute the growth of the thermal crack length within the HMA layer.

The viscoelastic properties of the HMA mixture control the level of stress development during cooling. More specifically, the time and temperature-dependent relaxation modulus of the mixture is the property needed to compute thermal stresses in the pavement according to Equation II-67, the constitutive equation.

$$\sigma(\xi) = \int_0^{\xi} E(\xi - \xi') \frac{d\varepsilon}{d\xi} d\xi' \quad (II-67)$$

Where:

- $\sigma(\xi)$ = Stress at reduced time ξ .
- ξ' = Variable of integration.
- $E(\xi - \xi')$ = Relaxation modulus at reduced time $\xi - \xi'$.
- ε = Strain at reduced time $\xi (= \alpha(T(\xi') - T_0))$.
- $T(\xi')$ = Pavement temperature at reduced time ξ' .
- T_0 = Pavement temperature when $\sigma = 0$.
- α = Linear coefficient of thermal contraction.

A generalized Maxwell model was selected to represent the viscoelastic properties of the HMA mixture. Mathematically, the generalized Maxwell model is expressed according to the following Prony Series expansion, Equation II-68.

$$E(\xi) = \sum_{i=1}^{N+1} E_i e^{-\frac{\xi}{\lambda_i}} \quad (II-68)$$

Where:

- ξ = Reduced time = t/a_T , when:
 t = Real time.
 a_T = Temperature shift factor.
- $E(\xi)$ = Relaxation modulus at reduced time.
- N = Number of time intervals.
- E_i, λ_i = Prony Series parameters.

The relaxation modulus function is obtained by transforming the following time-dependent creep compliance function, Equation II-69, which is determined by performing creep tests at multiple temperatures.

$$D(\xi) = D(0) + \sum_{i=1}^N D_i \left(1 - e^{-\frac{\xi}{\tau_i}} \right) + \frac{\xi}{\eta_v} \quad (II-69)$$

Where:

- $D(\xi)$ = Creep compliance at reduced time ξ
- ξ = Reduced time = t/a_T , when:
 a_T = Temperature shift factor.
- $D(0), D_i, \tau_i, \eta_v$ = Prony Series parameters.

Prony Series parameters and shift factors are obtained by performing creep compliance tests at multiple temperatures and mathematically shifting data from the different temperatures to establish one smooth, continuous curve. This process is illustrated conceptually in Figure II-4. The resulting curve is called the master creep compliance curve.

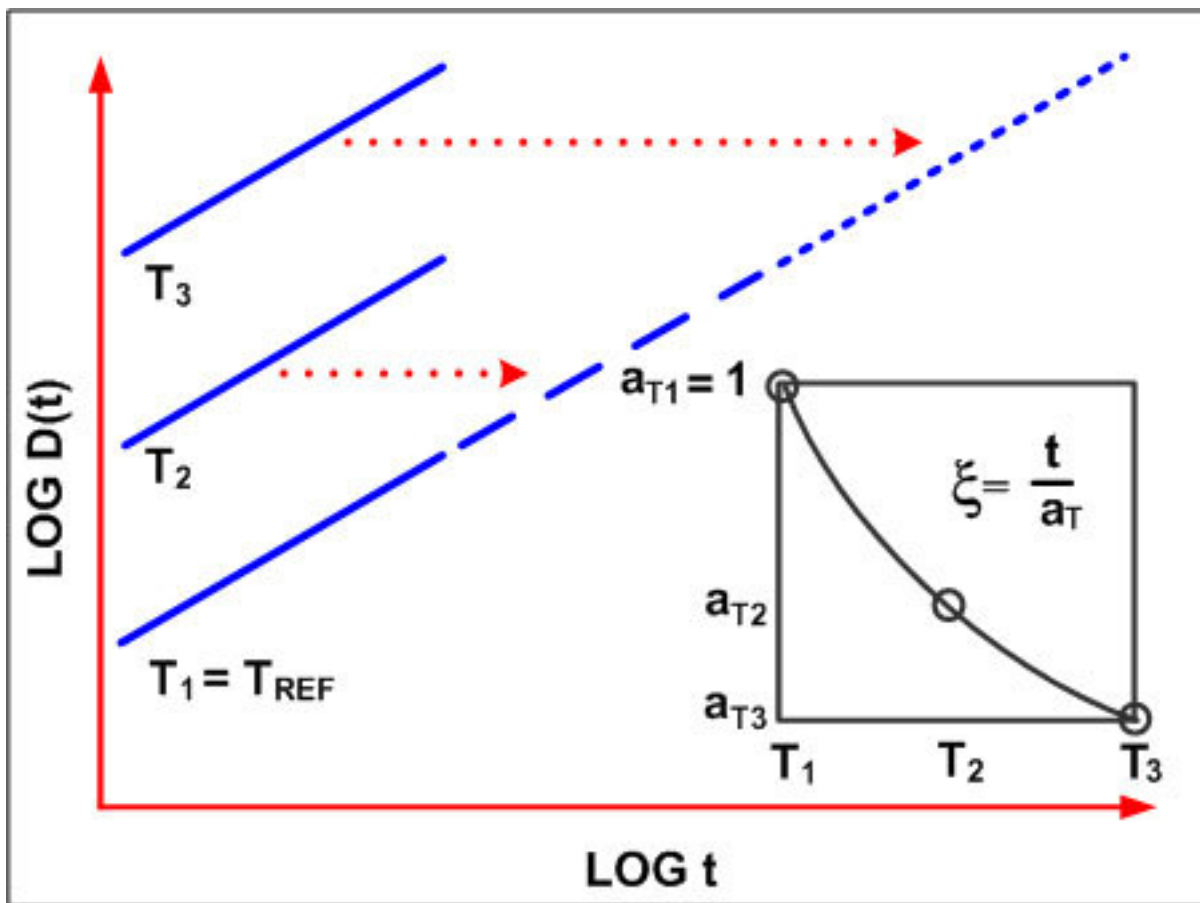


Figure II-4 Illustration of the formation of a master creep compliance curve.

The amount of crack propagation induced by a given thermal cooling cycle can be predicted using the Paris law of crack propagation, Equation II-70, which is the same type of mechanism for fatigue cracking discussed in Chapter II-2.

$$\Delta C = A(\Delta K)^n \quad (II-70)$$

Where:

- ΔC = Change in the crack depth due to a cooling cycle.
 A, n = Fracture parameters for the HMA mixture.
 A = Fracture parameter.
 $n = 0.8 \left[1 + \frac{1}{m} \right]$, where:
 m = Slope of the linear portion of the log compliance-log time relationship.
 ΔK = Change in the stress intensity factor due to a cooling cycle.

Determination of the fracture energy density requires moderately complex testing. However, experimental results indicate that reasonable estimates of A and n can be obtained from the m value and the strength of the material. Experiments by Molenaar (1983) led to the development of a relationship between A and tensile strength. Because the meaning of mixture stiffness included in Molenaar's relationship is load related, the particular relationship may not be directly applicable when considering variable temperature conditions during thermal stress development. Therefore, a calibration coefficient was applied resulting in Equation II-71.

$$A = 10^{k_t \beta_i (4.389 - 2.52 \text{Log}(E\sigma_m^n))} \quad (II-71)$$

Where:

- A = Fracture parameter.
 $n = 0.8 \left[1 + \frac{1}{m} \right]$, where:
 m = Slope of the linear portion of the log compliance-log time relationship.
 k_t = Coefficient determined through field calibration for each input level (for the NCHRP Project 1-37A (ARA 2004a,b) global calibration effort Level 1 = 3.0, Level 2 = 1.5, Level 3 = 5.0; while for the updated NCHRP Project 1-40D (NCHRP 2006) global calibration effort Level 1 = 1.0, Level 2 = 0.5, Level 3 = 6.0).
 β_i = Local or mixture calibration factor.
 σ_m = Mixture tensile strength, psi.
 E = Moisture modulus.

This equation is used to determine the fracture parameter A . The parameter n is determined as a function of m using the equation developed by Lytton and presented above (Lytton et al. 1983). Therefore, the two measured properties used to obtain the fracture parameters are:

- The m -value, which is the slope of the linear portion of the log compliance-log time relationship determined from creep tests.
- The tensile strength of the mixture.

The stress intensity factor, K , has been incorporated in the MEPDG through the use of a simplified equation developed from theoretical finite element studies (Equation II-72).

$$K = \sigma_{tip} \left(0.45 + 1.99(C_o)^{0.56} \right) \quad (II-72)$$

Where:

- K = Stress intensity factor.
- σ_{tip} = Far-field stress from pavement response model at depth of crack tip, psi.
- C_o = Current crack length, feet.

Given that the coefficients of thermal contraction of asphalt cement and aggregate are not measured as part of routine mixture design, an average value of volumetric coefficient of thermal contraction of $3.45 \times 10^{-4}/^{\circ}\text{C}$ is recommended for asphalt cements. A nonlinear regression routine is used to determine the master creep compliance curve from the creep compliance curves measured at multiple temperatures. The regression is performed in two basic steps.

Step 1. A regression is performed to determine simultaneously the temperature shift factors, a_T , and the parameters for the following Prony Series (Maxwell Model) representation of the master creep compliance curve, Equation II- 73:

$$D(\xi) = D(0) + \sum_{i=1}^N D_i \left(1 - e^{-\xi/\tau_i} \right) + \frac{\xi}{\eta_v} \quad (II-73)$$

Where:

- $D(\xi)$ = Creep compliance at reduced time ξ .
- ξ = Reduced time $=t/a_T$, when:
 t = Real time.
 a_T = Temperature shift factor.
- $D(0), D_i, \tau_i, \eta_v$ = Prony Series parameters.

In essence, the regression finds the best shift factors and Prony Series parameters to fit the measured data based upon a least-squares criterion. One of the temperatures is selected as the reference temperature for the master curve and thus the creep compliance curve at this temperature is fixed in time, $a_T=1$. The regression determines the amount of time (horizontal) shift required for the curves at the remaining temperatures to result in a smooth master curve. Each of these remaining creep compliance curves will have a shift factor, a_t , associated with it.

In conjunction with the determination of the shift factors, the regression determines the coefficients for the Prony Series. Four Maxwell elements, $N=4$, were found to be sufficient to fit the data accurately when creep compliance curves at three temperatures (-20, -10, and 0°C) are used to construct the master curve.

The shift factor-temperature relationship is modeled as a piecewise linear relationship between shift factors determined at the specified test temperatures. In other words, shift factors at arbitrary temperatures are determined by linear interpolation between the shift factors determined from the regression. Linear extrapolation is performed to obtain shift factors at temperatures outside the range of measurements.

Step 2. The second step in the regression routine is to fit a second functional form to the master creep compliance information. This second functional form is the following power law, Equation II-74:

$$D(\xi) = D_0 + D_1 \xi^m \quad (II-74)$$

Where:

$$\begin{aligned} D(\xi) &= \text{Creep compliance at reduced time } \xi \\ \xi &= \text{Reduced time } = t/a_T \end{aligned}$$

Where:

$$t = \text{Time.}$$

$$a_T = \text{Temperature shift factor.}$$

$$D_0, D_1, m = \text{Coefficients of the functional form.}$$

The primary purpose for fitting this functional form is to determine the parameter m . This parameter is essentially the slope of the linear portion of the master creep compliance curve on a log-log plot. It is an important parameter in distinguishing between the thermal cracking performance of different materials and is a direct input into the crack depth (fracture) or crack propagation model. The degree of cracking is predicted using an assumed relationship between the probability distribution of the log of the crack depth to HMA layer thickness ratio and the percent of cracking. Equation II-75 shows the expression used to determine the extent of thermal cracking.

$$TC = \beta_{t1} N \left[\frac{1}{\sigma} \text{Log} \left(\frac{C}{h_{HMA}} \right) \right] \quad (II-75)$$

Where:

$$TC = \text{Observed amount of thermal cracking, ft/mi.}$$

$$\beta_{t1} = \text{Regression coefficient determined through field validation.}$$

$$N(z) = \text{Standard normal distribution evaluated at } (z).$$

$$\sigma = \text{Standard deviation of the log of the depth of cracks in the pavement.}$$

$$C = \text{Crack depth, in.}$$

$$h_{HMA} = \text{Thickness of surface layer, in.}$$

It should be noted that the maximum amount of thermal cracking assumed in the approach is 400 feet per 500-ft pavement length. While this is the assumed maximum value, the model cannot predict more than fifty percent of this maximum value because failure occurs when the average crack depth reaches the thickness of the HMA layer.

The following sections provide two critical properties or data needed in support of the transverse cracking prediction model.

II-4.2.1.1 Temperature and Thermal Gradient Prediction Model

The other piece of critical data is the prediction of pavement temperatures with time and depth through the pavement structure. The Environmental Effects Model (EEM) can be used to predict the temperature conditions within the pavement system using environmental data and material

thermal properties. The model is based upon the program developed at the Texas Transportation Institute for FHWA (*Lytton et al. 1990*). This program has been subsequently updated and expanded for use in supporting the Superpave mixture design technology. The most recent version is referred to as the EICM. This enhanced model was developed at the University of Illinois by Larson and Dempsey (*1997*). It simulates climatic conditions that control both temperature and moisture in the pavement layers and subgrade.

The EICM is used as the climatic algorithm to determine the temperature-depth profile within the asphalt layer at hourly time intervals over the analysis period. The EICM model (Equation II-76) uses a one-dimensional, forward finite difference, heat transfer model to determine frost penetration and temperature distribution in the pavement system. While the model considers radiation, convection, conduction, and the effects of latent heat, it does not consider transpiration, condensation, evaporation, and sublimation. The effects not considered were omitted because of the uncertainty in their calculation and the insignificance of their contribution to the model.

$$T_{(i,t+\Delta t)} = T_{(i,t)} + \left(\frac{k\Delta t}{\gamma_d C \Delta z^2} \right) [T_{(i+1,t)} + T_{(i-1,t)} - 2T_{(i,t)}] \quad (II-76)$$

Where:

- T = Temperature in °F.
- t = Time.
- k = Thermal conductivity in BTU/(hr-ft²-°F).
- Δt = Time increment.
- γ_d = Dry density.
- C = Mass specific heat in BTU/(hr-°F).
- Δz = Depth increment.
- z = Vertical coordinate.

Using viscoelastic transformation theory, the compliance, $D(t)$, can be related to the relaxation modulus, E_r , of the HMA mix. Knowledge of this parameter, coupled with the temperature data obtained from the EICM model, allows for the prediction of thermal stress at any given depth and time within the HMA layer. Fracture Mechanics (Paris law) is then used to compute the growth of the thermal crack length within the HMA layer.

II-4.2.1.2 Coefficient of Thermal Contraction

The coefficient of thermal contraction is an extremely important property for predicting thermal cracks. However, the thermal coefficient usually is not measured, but estimated from previous test results reported in the literature. Only limited laboratory data are available on the measured coefficient of thermal length change for HMA mixtures.

Jones, Darter, Littlefield, Ellis, and Tuckett conducted studies on thermally induced length changes and densification of HMA at the University of Utah (*Littlefield 1967, Jones et al. 1986, Ellis et al. 1969, Tuckett et al. 1970*). The measurements from these studies for linear thermal coefficients varied from 1.17 to 2.05 x 10⁻⁵/°F (2.11 to 3.69 x 10⁻⁵/°C) for low temperature measurements of HMA of varying asphalt contents and percent air voids (*Jones et al. 1986*). In

development of the models to predict thermal cracking during the SHRP program, Lytton and Roque used this information and data to estimate the thermal coefficient of HMA mixtures based on the HMA volumetric properties (Lytton et al. 1993, Roque et al. 2000). The linear coefficient of thermal contraction for an HMA mixture can be computed using Equation II-77, which is a modified version of the relationship proposed by Jones, et al. (1986):

$$B_{MIX} = \frac{VMA \times B_{AC} + V_{AGG} \times B_{AGG}}{3 \times V_{TOTAL}} \quad (II-77)$$

Where:

- B_{MIX} = Linear coefficient of thermal contraction of the HMA mixture (1/°C).
- VMA = Percent volume of voids in the mineral aggregate (equals percent volume of air voids plus percent volume of asphalt cement minus percent volume of absorbed asphalt cement).
- B_{AC} = Volumetric coefficient of thermal contraction of the asphalt cement in the solid state (1/°C).
- V_{AGG} = Percent volume of aggregate in mixture.
- B_{AGG} = Volumetric coefficient of thermal contraction of the aggregate (1/°C).
- V_{TOTAL} = 100 percent.

II-4.2.2 Other Models

Several thermal cracking prediction models are currently available and include models developed by Finn, et al. (1973), Ruth, et al. (1982), Lytton, et al. (1983), and Shahin and McCullough (1973). Hajek and Haas (1972) developed a model to predict the cracking index due to low-temperature cracking. Equation II-78 shows the cracking index predictive relationship:

$$I = 30.3974 + (6.7966 - 0.8741h + 1.3388a) \log(0.1S_{bit}) - 2.15165d - 1.2496m + 0.06026S_{bit} \log d \quad (II-78)$$

Where:

- I = Cracking index (≥ 0) in terms of the number of full cracks plus one-half of the half-transverse cracks per 500-ft section of two-lane road, cracks shorter than half-width are not due to low temperature cracking and are not considered in the regression.
- h = Total thickness of HMA layer in inches.
- a = Pavement age in years.
- S_{bit} = Stiffness modulus of the original asphalt in kg/cm², as determined from the Van der Poel nomograph (1954) using a loading time of 20,000 s and the winter design temperature; however, values of PI and $T_{R\&B}$ of bitumen should be determined from penetration at 77 °F (25 °C) and kinematic viscosity at 275 °F (135 °C) as suggested by McLeod (1987).
- m = Winter design temperature in -°C, neglect the negative sign and use positive value only.
- d = Subgrade type in terms of a dimensionless code with 5 for sand, 3 for loam, and 2 for clay.

Haas et al. (1987) published a regression equation to predict the average transverse crack spacing based on a study of twenty-six airfields in Canada. The prediction Equation II-79 is shown below.

$$TCRACK = 218 + 1.28 ACTH^{2.52} MTEMP + 30 PVN - 60 COFX \quad (II-79)$$

Where:

- TCRACK* = Transverse crack average spacing in meters.
- ACTH* = Thickness of the HMA layer in centimeters.
- MTEMP* = Minimum temperature recorded on site in °C.
- PVN* = McLeod (1987) dimensionless Pen-Vis Number (PVN).
- COFX* = Coefficient of thermal contraction in mm/100 mm/°C.

CHAPTER II-5: HMA DISINTEGRATION – RAVELING

HMA surface mixtures, like all other paving materials, are subject to a variety of distresses. Those distresses that can be predicted with ME models have been previously discussed. These distresses included various forms of fatigue cracking, distortion, and thermal cracking. Unfortunately, there are other structural, materials, and functional related distresses or surface defects that can significantly reduce flexible pavement life. Most of these other distresses fall into a distress category defined as surface disintegration.

Disintegration is the breakup or change in the characteristics of the pavement surface. Disintegration distresses are just as important as the ones previously discussed, but it is generally assumed during design that materials selection, mixture design, and construction operations will prevent their occurrence.

Disintegration usually involves the loss of individual pieces or the separation of the individual components of the HMA from each other. Disintegration type distresses are primarily related to environmental and/or material factors, but their severity is dependent on the magnitude and number of wheel load applications. Disintegration typically takes the forms of raveling, potholes, and stripping. However, loss of skid resistance, bleeding, and flushing are included in this category. None of these disintegration type distresses are predicted by any ME based procedure reviewed in the literature.

Stripping is identified in many publications as a distress type in flexible pavements. However, stripping is not a distress but a mechanism that can significantly accelerate the occurrence of other material, structural, and functional related distresses (e.g., raveling, fatigue cracking, and distortion). Stripping is a form of moisture damage in the HMA mixture and has a significant effect on the adhesion, tensile strength, and modulus of the HMA mixture. When stripping occurs, the HMA mixture is susceptible to raveling and cracking.

Raveling is related to a combination of asphalt consistency and film thickness, aggregate characteristics, air void content, and adhesion between the asphalt and aggregate. Asphalt contents should be selected to reduce air voids and increase film thickness to prevent extensive raveling. As note above, there are no known ME based models for predicting the area and severity of raveling. The AAMAS procedure, however, does include a measure of raveling or mixture disintegration potential using results from the indirect tensile strength test (*Von Quintus et al. 1991*).

The AAMAS procedure assumed that raveling is related to the loss of bond or adhesion between the asphalt and aggregate, and the loss of adhesion can be estimated using the tensile strain at failure from the indirect tensile strength test. The bonding loss is determined in accordance with Equation II-80.

$$BondingLoss = 100 \left[1 - \frac{\mathcal{E}_{f-cond}}{\mathcal{E}_{f-uncond}} \right] \quad (II-80)$$

Where:

ϵ_{f-cond} = *Tensile strain at failure after mixture conditioning – moisture or age-hardening.*

$\epsilon_{f-uncond}$ = *Tensile strain at failure before any conditioning.*

Specifically, the procedure used the expected bonding loss and tensile strain at failure to determine whether the HMA mixture was susceptible to raveling and other weathering types of distress. The criteria included in the AAMAS procedure for judging the adequacy of HMA mixtures was that the bonding loss should be less than 50 percent and that the tensile strain at failure should be greater than 2 mils per inch at 41°F after moisture conditioning or accelerated aging simulations in the laboratory.

CHAPTER II-6: SMOOTHNESS / RIDE QUALITY MODELS

Roughness or loss of ride quality is considered to be more of a true measure of pavement performance because the public feels rough pavements. Indication of roughness is a key element in many pavement management programs to determine when to rehabilitate a pavement surface. Roughness is a functional failure of the pavement surface, and included within this study, because of its overall importance to performance. In addition, many agencies are now using some type of smoothness measurement for accepting flexible pavement construction and deciding on when to rehabilitate pavement structures (*AASHTO 1987*).

Several research studies have successfully modeled serviceability (which is highly correlated to smoothness) using key pavement distress types for both original and overlaid pavements. These previous studies have found that flexible pavement smoothness can be significantly affected by rutting, rut depth variance, and fatigue cracking. Some of the distresses that have been correlated to smoothness are load related and can be predicted by ME modeling techniques. However, other distresses such as potholes and depressions/swells caused by soil movements and other climatic factors (represented by mechanistic clusters based on pavement and climatic properties) have been shown to affect roughness, but are not predicted with ME models.

Some studies have developed prediction equations for roughness based on mechanistic response parameters with limited success (*Perera et al. 1998*). These mathematical relationships are still highly empirical and heavily dependent on pavement and soil type. This structure-material dependency suggests that the prediction equations and mechanistic response parameters do not adequately capture or explain, mechanistically, the increase in roughness with time and truck traffic.

II-6.1 SITE VARIABLES AND DISTRESSES THAT INFLUENCE FLEXIBLE PAVEMENT SMOOTHNESS

Empirical and mechanistic analyses have identified several pavement design features and site conditions that affect smoothness. The identified variables can be used as the basis for developing mechanistic clusters or enhancing existing clusters for use in model development. Some of the design features and site condition variables that affect smoothness are presented in Table II-7. The site condition variables listed relate to the pavement's temperature, moisture, and axle load cycles, while the design features relate to pavement strength. A summary of distress variables that have been shown to influence significantly user-rated serviceability or smoothness is presented in Table II-8.

**Table II-7 Design Features and Site Condition Variables
 Affecting Flexible Pavement Roughness**

Design Features and Site Conditions	Cost Allocation Model, Owusu-Antwi et al.(1997)	Kayner et al.* (1990)	Sebaaly et al. (1995)
Initial smoothness	√	√	
ESAL	√	√	√
Age	√	√	√
Base thickness	√		
Freezing index	√		
Initial IRI/serviceability		√	
Subgrade type		√	
Overlay thickness		√	
Maximum temperature			√
Minimum temperature			√
Annual number of wet days			√

*HMA-overlaid pavement

**Table II-8 Distress Variables Affecting Flexible Pavement
 Smoothness/Serviceability**

Distress	Al-Omari & Darter (1992)	Anderson & Peterson (1979)	Paterson (HDM-III) (1989)	Carey & Irick (AASHO Eq.) (1960)	Darter and Barenberg (1976)
Rut depth	√	√		√	√
Potholes	√		√		
Depression and swells	√				
Transverse cracking	√	√		√	√
Standard deviation or Variance of rut depth	√		√		√
Patching		√	√	√	√
Fatigue cracking			√		√

II-6.2 ROUGHNESS PREDICTION MODELS

II-6.2.1 MEPDG – Smoothness Prediction Models

From work completed under NCHRP Projects 1-37A and 1-40D the LTPP data were used to confirm the results from previous studies and develop a more in-depth regression model to predict roughness or the IRI from surface distress. The general smoothness prediction model form related IRI to the four main contributing factors to IRI that have been documented from previous studies. The model form is shown in Equation II-81:

$$IRI = IRI_O + \Delta IRI_D + \Delta IRI_F + \Delta IRI_S \quad (II-81)$$

Where:

- IRI = International roughness index.
- IRI_O = Initial IRI.
- ΔIRI_D = Increase in IRI due to distress.
- ΔIRI_F = Increase in IRI due to frost heave potential of the subgrade.
- ΔIRI_S = Increase in IRI due to swell potential of the subgrade.

Initially, IRI_F and IRI_S of Equation II-81 were assumed to be zero or have no effect on the measured IRI over time. Only the initial IRI (IRI_o), age, and the effect of surface distresses (IRI_D) were considered in the final analysis. The initial analysis included the relative effect of the other non-distress-specific variables. Five equations were initially developed under NCHRP Project 1-37A for predicting the IRI over time using LTPP data. These five equations were collapsed into two basic equations (Equations II-82 and II-83) under NCHRP Project 1-40D:

1. New Flexible Pavements and HMA Overlays of Flexible Pavements

$$IRI = IRI_o + 0.0150(SF) + 0.400(FC) + 0.0080(TC) + 40.0(RD) \quad (II-82)$$

Where:

IRI = International roughness index.

IRI_o = Initial IRI after construction, in/mi.

SF = Site factor.

$$SF = Age(0.02003(PI + 1) + 0.007947(Rain + 1) + 0.000636(FI + 1))$$

Where:

Age = Pavement age, years.

PI = Percent plasticity index of the soil.

FI = Average annual freezing index, °F days.

$Rain$ = Average annual rainfall, in.

FC = Area of fatigue cracking (combined alligator and longitudinal cracking in the wheel path), percent of total lane area.

TC = Length of transverse cracking, ft/mi.

RD = Average rut depth, in.

2. HMA Overlays of Rigid Pavements

$$IRI = IRI_o + 0.00825(SF) + 0.575(FC) + 0.0014(TC) + 40.8(RD) \quad (II-83)$$

Where:

IRI = International roughness index.

IRI_o = Initial IRI after construction, in/mi.

SF = Site factor.

FC = Area of fatigue cracking (combined alligator and longitudinal cracking in the wheel path), percent of total lane area.

TC = Length of transverse cracking, ft/mi.

RD = Average rut depth, in.

II-6.2.2 LTPP Smoothness Prediction Models

Original HMA Surfaces

The initial model suggested for use in predicting IRI for the original HMA surfaced pavements within the LTPP program was base type dependent and is shown in Equations II-84 through II-88.

Unbound Aggregate Bases and Subbases

$$IRI = IRI_o + 0.03670(SF)[e^{age/20} - 1] + 0.00325(FC) + 0.4092(COV_{RD}/100) + 0.00106(TC) + 0.00704(BC) + 0.00156(SLCNWP_{MH}) \quad (II-84)$$

Where:

- IRI* = International roughness index.
IRI_o = Initial IRI after construction, in/mi.
SF = Site factor:

$$SF = \left(\frac{(R_{SD})(P_{.075} + 1)(PI)}{2 \times 10^4} \right) + \left(\frac{\ln(FI + 1)(P_{0.2} + 1)[\ln(R_m + 1)]}{10} \right)$$

Where:

- R_{SD}* = Standard deviation of the monthly rainfall, mm.
P_{.075} = Percent passing the 0.075 mm sieve.
PI = Percent plasticity index of the soil.
FI = Average annual freezing index.
P_{0.2} = Percent passing the 0.02 mm sieve.
R_m = Average annual rainfall, mm.
Age = Age after HMA placement, years.
FC = Area of fatigue cracking (combined alligator and longitudinal cracking in the wheel path), percent of total lane area.
COV_{RD} = Coefficient of variation of the rut depth, %.
TC = Length of transverse cracking, ft/mi.
BC = Area of block cracking, sq ft.
SLCNWP_{MH} = Medium and high severity sealed longitudinal cracks located outside the wheel path area, ft.

Asphalt Treated Bases

$$IRI = IRI_o + 0.00552(FC) + 33.59[1/(TCS_H + 1)] + 0.9529(P_H) \quad (II-85)$$

Where:

- IRI* = International roughness index.
IRI_o = Initial IRI after construction, in/mi.
FC = Area of fatigue cracking (combined alligator and longitudinal cracking in the wheel path), percent of total lane area.
TCS_H = High severity transverse crack spacing, ft.
P_H = Area of high severity patches, square ft.

Cement or Pozzolonic Treated Bases

$$IRI = IRI_o + 0.00732(FC) + 0.07647(SD_{RD}) + 0.0001449(TC) + 0.00842(BC) + 0.0002115(LCNWP_{MH}) \quad (II-86)$$

Where:

- IRI* = International roughness index.

- IRI_o = Initial IRI after construction, in/mi.
 FC = Area of fatigue cracking (combined alligator and longitudinal cracking in the wheel path), percent of total lane area.
 SD_{RD} = Standard deviation of the rut depths, in.
 TC = Length of transverse cracking, ft/mi.
 BC = Area of block cracking, square ft.
 $LCNWP_{MH}$ = Medium and high severity longitudinal cracking outside the wheel path area, ft.

HMA Overlays

HMA Overlays Placed on Flexible Pavements:

$$IRI = IRI_o + 0.04283[\ln(\text{Age}+1)] + 0.00880(FC) + 0.00129(TC_{MH}) + 2.9065(BC_H) + 8.7702(P_H) + 0.00100(SLCNWP) \quad (II-87)$$

Where:

- IRI = International roughness index.
 IRI_o = Initial IRI after construction, in/mi.
 Age = Pavement age, years.
 FC = Area of fatigue cracking (combined alligator and longitudinal cracking in the wheel path), percent of total lane area.
 TC_{MH} = High severity transverse crack spacing, ft.
 BC_H = Area of high severity block cracking, sq ft.
 P_H = Area of high severity patches, square ft.
 $SLCNWP$ = Sealed longitudinal cracks located outside the wheel path, area/ft.

HMA Overlays Placed on Rigid Pavements:

$$IRI = IRI_o + 0.02069(RD) + 8.396 [1/(TCS_{MH}+1)] + 13.122(P_{MH}) \quad (II-88)$$

Where:

- IRI = International roughness index.
 IRI_o = Initial IRI after construction, in/mi.
 RD = Rut depth, in.
 TCS_{MH} = Medium and high severity transverse crack spacing, ft.
 P_{MH} = Medium and high severity patches.

II-6.2.3 AASHO Serviceability Equation

One of the most well-known and used performance or serviceability equations for flexible pavements was developed from the AASHO Road Test (Carey and Irick 1960, AASHTO 1993). The Present Serviceability Rating (PSR) was found to be significantly affected by the average rut depth, slope variance, and the amount of cracking and patching (Equation II-89).

$$PSR = 5.03 - 1.91 \log(1 + SV) - 0.01(C + P)^{0.5} - 1.38 RD^2 \quad (II-89)$$

Where:

- PSR = Present serviceability rating (panel mean rating).
 SV = Slope variance.
 C = Major cracking in ft per 1,000 sq ft area.

- P = Bituminous patching in sq ft per 1,000 sq ft area.
 RD = Average rut depth of both wheel paths in inches measured at the center of a 4-ft. span in the most deeply rutted part of the wheel path.

Slope variance is defined by Equation II-90.

$$SV = \frac{\sum Y^2 - \frac{1}{n}(\sum Y)^2}{n - 1} \quad (II-90)$$

Where:

- SV = Slope variance.
 Y = Difference between two elevations 9 in. apart.
 n = Number of elevation readings.

The accuracy of the models can be judged by the following statistics:

- R^2 = 84 percent.
 SEE = 0.38 PSR points.

II-6.2.4 FHWA Zero-Maintenance Pavements Study

The model in Equation II-91 was developed using data from the AASHO Road Test and relates serviceability to distress (*Darter and Barenberg 1976*).

$$PSR = 4.5 - 0.49RD - 1.16RDV^{0.5}(1 - 0.087RDV^{0.5}) - 0.13\log(1 + TC) - 0.0344(AC + P)^{0.5} \quad (II-91)$$

Where:

- PSR = Pavement serviceability rating.
 RD = Rut depth in both wheel paths of the pavement, in.
 RDV = Rut depth variance, sq in*100.
 TC = Transverse and longitudinal cracking, sq ft/1,000 sq ft.
 AC = Class 2 or Class 3 alligator or fatigue cracking, sq ft/1,000 sq ft.
 P = Patching, sq ft/1,000 sq ft..

The accuracy of the model can be judged by the following statistics:

- R^2 = 0.76.
 SEE = 0.455 points.
 N = 95.

II-6.2.5 World Bank HDM-III

The World Bank HDM-III flexible pavement smoothness model (*Paterson 1989*) combines both distress and mechanistic variables related to pavement strength and site conditions to predict smoothness loss. The model is shown in Equation II-92.

$$\Delta RI = 134(e^{mi})(MSNK)^{-5.0}(\Delta NE4) + 0.114(\Delta RDS) + 0.0066(\Delta CRX) + 0.003h(\Delta PAT) + 0.16(\Delta POT) + mRI_t(\Delta t) \quad (II-92)$$

Where:

ΔRI	=	Increase in roughness over time period Δt , m/km.
$MSNK$	=	A factor related to pavement thickness, structural number, and cracking.
$\Delta NE4$	=	Incremental Number of ESALs in period Δt .
ΔRDS	=	Increase in rut depth, mm.
ΔCRX	=	Percent increase in area of cracking.
ΔPAT	=	Percent increase in surface patching.
ΔPOT	=	Increase in total volume of potholes, $m^3/\text{lane km}$.
m	=	Environmental factor.
RI_t	=	Roughness at time t , years.
Δt	=	Incremental time period for analysis, years.
t	=	Average age of pavement or overlay, years.
h	=	Average deviation of patch from original pavement profile, mm.

The accuracy of the model can be judged by the following statistics:

R^2	=	0.59.
SEE	=	0.51 points.
N	=	36.1

II-6.2.6 FHWA/Illinois Department of Transportation Study

The following flexible pavement smoothness prediction model (*IL DOT 1989*) was developed using “manufactured” profile data. The International Roughness Index (IRI) was computed from the manufactured profile, Equation II-93.

$$PSR = 4.95 - 0.685D - 0.334P - 0.051C - 0.211RD \quad (II-93)$$

Where:

PSR	=	Pavement serviceability rating.
D	=	Number of high-severity depressions (number per 50 m).
P	=	Number of high-severity potholes (number per 50 m).
C	=	Number of high-severity cracks (number per 50 m).
RD	=	Average rut depth, mm.

The accuracy of the model can be judged by the following statistics:

R^2	=	0.92.
SEE	=	0.226 points.
N	=	81.

CHAPTER II-7: SUMMARY AND CONCLUSIONS – SELECTION OF DISTRESS PREDICTION MODELS SUMMARY

Part II of Volume II has provided a review of ME based distress prediction models for those distresses included in Montana's Pavement Management System and those generally considered in pavement design and analysis procedures. The following provides a listing of the distress prediction models that will be considered for calibration to assist Montana decision makers in designing and managing their highway network.

- Load Related Fatigue Cracks – The MEPDG prediction model for alligator cracks has been found to be acceptable from other studies and is recommended for use in Montana (Equations II-1, II-3, II-5, and II-6). This includes the bottom-up cracking model for HMA mixtures and the fatigue cracking model for CTB layers.

The top-down cracking model was found to have a high error term from the calibration work completed under NCHRP Projects 1-37A (*ARA 2004a,b*) and 1-40D (*NCRHP 2006*). In addition, Von Quintus, et al., recommended that this model not be used until it is further refined based on work completed under NCHRP Projects 9-30 (*Von Quintus et al. 2004*), 9-30(001) (*Von Quintus et al. 2005a*), and 1-40B (*Von Quintus et al. 2005b*). No other fatigue cracking model predicts surface initiated cracks that can be reasonably embedded into a practical pavement design procedure. As a result, the MEPDG prediction model for surface initiated cracks will be used to evaluate the LTPP and non-LTPP test sections placed in Montana to build confidence in its use and accuracy.

- Rut Depth: The MEPDG prediction model for rutting in the HMA layers has been found to be acceptable from other studies relating the predicted to measured values, and is recommended for use in Montana (Equations II-30 and II-31).

The model used to predict the plastic deformations in the unbound layers was found to over predict the rut depths in those layers, especially the foundation or subgrade soil. The positive bias found from other studies, however, is relatively linear across the range of soils and total predicted rutting. Local calibration should be able to easily eliminate this bias. Therefore, the MEPDG prediction model for rutting in the unbound layers is recommended for use in Montana.

It is recommended that the limiting strain criteria in accordance with the modified Corp of Engineers model (Equation II-64) be used to ensure that there is sufficient cover above any unbound pavement layer and soil.

- Transverse Cracks: The MEPDG prediction model has been found to be acceptable for flexible pavements in northern climates, and is recommended for use in Montana (Equation II-75). The critical factor is to obtain a reasonable estimate of the coefficient of thermal contraction for different HMA mixtures used in Montana. The equation embedded in the MEPDG (Equation II-77) is the only regression equation found that can be used to calculate this mix property from volumetric mix data – without extensive

testing. Therefore, the MEPDG default values are initially recommended for use in Montana.

- Smoothness: The MEPDG prediction model for smoothness or increasing roughness is recommended for use in Montana, because it is based on hundreds of test sections placed around the U.S. and was found to have a reasonable error term (Equation II-82). No other model was found to provide the accuracy considering the diverse pavements and site conditions within the LTPP database.
- Raveling: The MEPDG does not predict any HMA disintegration type distresses. The procedure developed and used within the AAMAS procedure will be considered for use in Montana for managing and predicting the performance of their HMA mixtures (Equation II-80).

It is recommended that the limiting layer modulus ratio between two adjacent layers (Figure II-2) be used within the local calibration procedure and for future flexible pavement designs in Montana.

PART III: TRAFFIC CHARACTERIZATION AND ANALYSES

CHAPTER III-1: INTRODUCTION

This report describes the results of a review of 15 months of Montana truck volume and weight data. The purpose of this review was to develop recommendations and traffic load data sets for use with the NCHRP Project 1-37A pavement design software (*Von Quintus et al. 2005b*).

The 15 months of data (May 2000 through July 2001) were collected at 21 Montana Weigh-in-Motion (WIM) sites and provided to the project team by MDT (*Von Quintus and Moulthrop 2007a*). Weight data were available for all 21 sites. Extensive data on volume by vehicle classification were provided for 19 of those sites. These two types of data were used to determine general pavement loading patterns in the State of Montana.

Patterns were developed for seasonal variation in both truck volumes and weights. Conclusions were then drawn about how Montana should apply its knowledge of these patterns within its pavement design process through an analysis of the truck traffic data. This analysis was limited in scope because of the restricted timeframe with sufficient WIM data. To confirm the reliability of the patterns and identify potential changes in those patterns over time requires WIM data measured at standard sites over longer periods of time. The analysis used to develop the truck traffic default values included in the MEPDG software required a minimum of three years of WIM data with more than 150 consecutive days of weight data for each year at each WIM site.

No significant data quality review was performed on the truck traffic data provided by MDT for use within this study. Any concerns about data accuracy that arose during the analysis process are identified and described in the appropriate chapters of this part of Volume II. Most of the concerns centered on the validity of WIM scale calibration. It is distinctly possible that some of the outlier values for seasonal truck volume trends resulted from data quality problems.

Conclusions have been made about the traffic patterns observed. These conclusions should be carefully reviewed by MDT regarding the State's weight laws, enforcement program, and economic activity patterns. The traffic analyst did not have knowledge of local Montana truck travel patterns, which could lead to different conclusions about traffic loading patterns in Montana (and/or about the likelihood that data used were, in fact, erroneous). Accurate local knowledge is necessary to expand application of the general load patterns described in this part of Volume II to all roads within Montana. The vast majority of Montana roads were not covered by the limited data set provided by MDT for use within this study, which will be the case for most State agencies.

CHAPTER III-2: GENERAL LOADING PATTERNS

Traffic loading is a function of the number of trucks (by type / class of truck) and the axle weights of each of those trucks. The damage caused by traffic increases with both the volume of heavy trucks and the weight of those trucks. Therefore, to design a pavement requires that the analyst understand how many trucks of each type use a particular road, and the load distribution of each of those types of trucks.

A strong, project-specific counting program provides the basic truck volume data necessary for each pavement design. An adequate count program consists of vehicle classification counts done at or near each pavement project location specifically to collect data on the volume and classification of trucks using the roadway, and how the truck traffic volume distribution changes over season and time. What the general Montana count program needs to provide for pavement design purposes is an understanding of how those truck volumes vary over time, and what type of loads are carried by each kind of truck.

This project reviewed the loading patterns and truck volumes at 21 Montana WIM sites to determine the variability of truck volumes and loading patterns across the State. The intent was to create a limited number of “groups” that describe the variation in truck volumes that can be expected at any given project location, as well as the types of loads that can be expected.

In creating these groups, the analyst emphasized FHWA truck Classes 9 and 13. This decision was based on the fact that at the vast majority of Montana test sites, most load (accounting for both volumes and weights) is applied by a combination of Class 9 and Class 13 vehicles. Class 9 trucks generally contribute the vast majority of traffic load, with Class 13 vehicles supplying a significant but secondary load.

The exception to this rule of thumb was found at the two sites with the lowest volumes (Site 102 on S-314 near Decker, and Site 109 on S-273 near Galen) where Class 6 vehicles made up a significant portion of the traffic load. Interestingly, these two sites were the only “county” roads in the data set. (All other roads were Interstates, US-signed highways, or Montana State highways.) This suggests that roads that serve primarily local truck traffic can expect a greater proportion of load to be supplied by Class 6 trucks, and therefore, for pavement design purposes, they may need to be treated somewhat differently than larger routes.

In a few cases, vehicles from truck Classes 5 and 10 contributed slightly more than 10 percent of the total traffic load, but in most cases these trucks contributed only modestly in terms of load. Class 5 trucks were ignored for this effort because they tend to be quite light and, therefore, contribute relatively minor amounts of pavement damage, even when they are a large portion of total volume. Class 10 trucks may be of more significance. Class 10 trucks are tractor-semi-trailers with six- or more axles. This usually means a conventional, heavy duty, three-axle tractor pulling a single trailer with a tridem or quad axle. These trucks can be quite heavy, and therefore, their presence, while relatively low in number, may be of interest for specific routes.

Table II-9 shows the three most significant vehicle classes in terms of load for each of the data collection sites for which volume by class and truck weight information were present. For this table, the percentage of load applied by the primary truck classes was calculated using a

traditional AASHTO ESAL calculation for flexible pavements. This is a simple method for judging the relative damage caused by different types of trucks.

Table II-9 Percentage of Load Caused by Primary Truck Classes

Site	Vehicle Class	Percentage of Load Applied by Noted Class	Total Percentage Each Site
101: US 12 Townsend	9	43	82
	13	32	
	10	8	
102: S 314 Decker	13	33	76
	9	24	
	6	19	
103: I-94 Bad Route	9	82	93
	13	9	
	10	2	
104: I-90 Manhattan	9	79	92
	13	9	
	10	4	
105: US 93 Arlee	9	41	87
	13	37	
	10	9	
106: US 191 Four Corners	9	63	85
	13	16	
	5	7	
107: US 191 Gallatin	9	69	85
	13	10	
	5	6	
108: I-90 Big Timber	9	80	92
	13	8	
	5	4	
109: S 273 Galen	6	41	88
	9	32	
	5	18	
110: MT 3 Broadview	9	69	94
	13	13	
	10	12	
111: US 12 Miles City East	9	62	91
	13	21	
	10	8	
112: I-15 Ulm	9	65	91
	13	19	
	10	7	
113: US 12 Ryegate	9	67	93
	13	15	
	10	11	
114: US 87 Stanford	9	64	92
	13	19	
	10	9	
115: US 87 Fort Benton	9	37	77
	13	32	
	10	8	

Table II-9 Percentage of Load Caused by Primary Truck Classes, Continued

Site	Vehicle Class	Percentage of Load Applied by Noted Class	Total Percentage Each Site
116: US 2 Havre	9	45	81
	13	24	
	5	12	
118: MT 200 Paradise	9	49	83
	13	23	
	10	11	
202: I-15 Lima	9	70	93
	13	18	
	10	5	
203: I-90 Mossmain Pre-pass	9	74	92
	13	14	
	5	4	

Concentrating on these classes created some minor biases in the traffic load estimate, but those biases were very small because they were produced by truck classes that cause very little pavement damage.

CHAPTER III-3: TRUCK VOLUME PATTERNS

Because significant numbers of double-bottom trailers use Montana highways, these trucks need to be tracked separately from combination trucks. As a result, it is recommended that Montana use three truck categories to create and apply seasonal adjustment factors for truck volumes when using the MEPDG software. Following are the three recommended truck classes:

- Single Unit Trucks (SU).
- Combination Trucks (Comb).
- Multi-Trailer trucks (Multi).

The category of single unit trucks should contain all trucks in FHWA Classes 5, 6, and 7. Combination trucks should include all vehicles in Classes 8, 9, and 10. Multi-trailer trucks should include all trucks in FHWA Classes 11, 12, and 13.

Only three truck classes are recommended for seasonal factoring because at many Montana road sites the number of trucks in many of the FHWA vehicle categories was quite small. When small volumes of vehicles are present, seasonal and day-of-week adjustment factors become unstable, and unstable factors do not improve the accuracy of pavement loading estimates. By aggregating FHWA truck classes into three broader categories, Montana should be able to apply seasonal patterns to its design process, while limiting the work involved in that effort and the effects that truck classes with low volumes would have on the accuracy of those factors.

In most cases, one specific FHWA vehicle class will contribute the vast majority of trucks within each of these aggregated truck categories. For example, in the data set reviewed, the vast majority of the trucks included in the “combination” category comprised FHWA Class 9 vehicles. Most multi-trailer trucks were from FHWA Class 13, and the single unit category was primarily made up of Class 5 trucks. In the case of the single unit trucks, however, it is important to note that while Class 5 trucks made up the majority of vehicles, Class 6 vehicles provides the majority of pavement loading and damage.

The seasonal patterns in the data provided by MDT vary by type of truck. Figure II-5 shows the mean seasonal patterns for all sites combined, and represents “*Montana’s basic seasonal truck pattern.*” Table II-10 shows the numerical factors and the standard deviation for each factor.

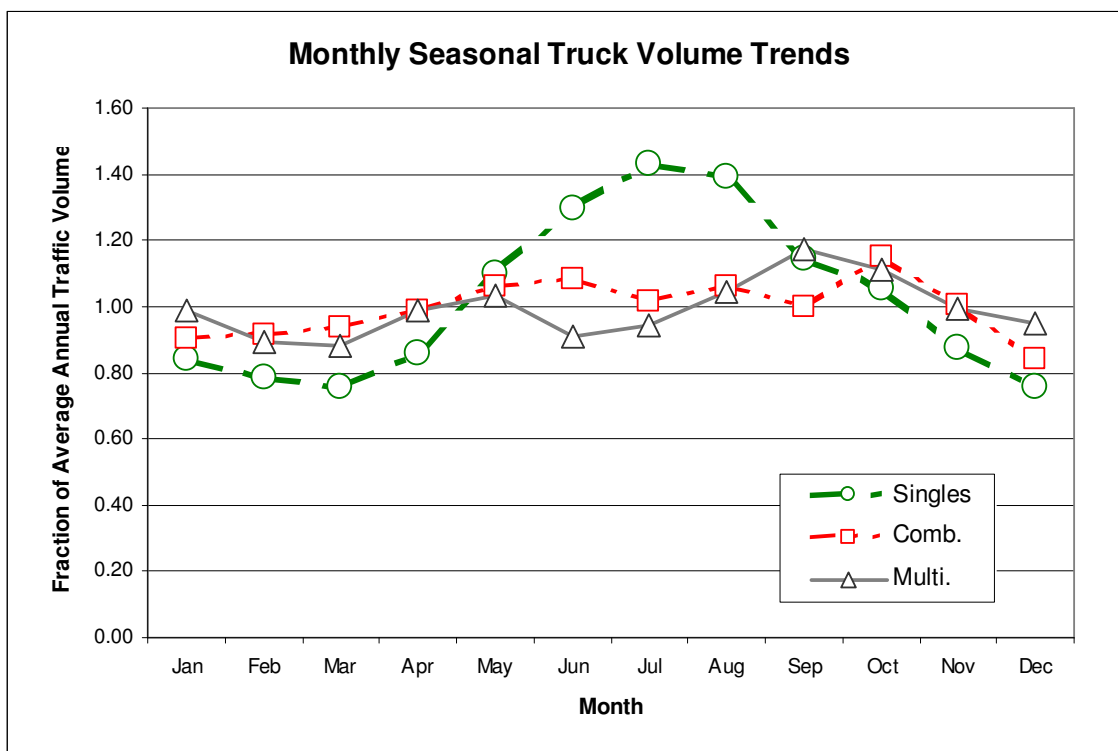


Figure II-5 Truck Seasonal Patterns for All Sites Combined

Table II-10 Monthly Volume Factors

Month	Single Units		Combinations		Multi-Trailer	
	Monthly Factor	Standard Deviation	Monthly Factor	Standard Deviation	Monthly Factor	Standard Deviation
January	0.84	0.16	0.91	0.06	0.99	0.19
February	0.79	0.17	0.92	0.06	0.89	0.18
March	0.76	0.14	0.94	0.12	0.88	0.19
April	0.86	0.12	0.99	0.07	0.99	0.20
May	1.10	0.18	1.06	0.08	1.03	0.37
June	1.30	0.31	1.09	0.08	0.96	0.35
July	1.43	0.29	1.02	0.10	0.92	0.25
August	1.39	0.29	1.06	0.09	1.11	0.26
September	1.14	0.16	1.00	0.14	1.09	0.24
October	1.06	0.14	1.15	0.12	1.12	0.10
November	0.87	0.13	1.00	0.10	1.00	0.11
December	0.76	0.15	0.84	0.07	0.87	0.17

NOTE: Monthly Volume Factors are computed by dividing Average Monthly Truck Volume by Average Annual Truck Volumes

Generally, combination trucks (Classes 8, 9, and 10) had the least seasonal variation, while single unit trucks (Classes 5, 6, and 7) had the greatest seasonal variation. Multi-trailer trucks (Classes 11, 12, and 13) showed a seasonal pattern that was reasonably similar to that of combination trucks. Both showed an increase in volume in late summer and early fall (shippers sending their products to stores before the start of the holiday shopping period). Multi-trailer trucks, however, experienced a decline in truck volumes in the summer that was not seen in combination trucks and started their “holiday increase” earlier than combination trucks. Conversely, single unit trucks showed a substantial volume increase in summer with significantly lower volumes during the winter and spring.

Individual data collection sites may frequently have volume patterns that differ, sometimes significantly, from these average patterns. In the data supplied by MDT there was considerable diversity in both the single unit truck and multi-trailer truck patterns. Diversity in truck volume patterns is caused in part by differences in the timing of seasonal commodity movements and in part by changes in the volume of commodities carried as changes in both the national and local economy affect the number of truck trips.

On some truck routes, local economic conditions and shipping patterns tend to dominate truck travel patterns. On other roads (particularly Interstates dominated by through-truck traffic), national economic trends and shipping patterns may overshadow local effects. Without direct knowledge of the nature of local commodities and their flows, it is not possible to comment accurately on the relative causes of the diversity in truck volume patterns observed at specific sites.

Some of the variation observed in the computed average monthly truck volumes at specific Montana sites appeared to be caused by short duration economic activity. For example, a major construction project may have created a substantial increase in heavy truck traffic on a road that served that construction site. This temporary increase in truck volumes may have significantly skewed the average monthly truck volumes for the month when natural resources were moved into or out of the construction site. Some of these dramatic seasonal peaks may have been caused by minor problems in the data collection hardware (for example, misclassification of recreational vehicles pulling cars behind them as a combination truck).

Some of the diversity in observed truck volume patterns is explored in the following sections. A far more substantial analysis is required before definitive statements about truck travel patterns within Montana can be made. What is obvious from the available data is that truck volumes can vary considerably from site to site, and from year to year at individual sites. Until a more detailed analysis (including input from MDT personnel familiar with commodity flows within the State and the basic shipping patterns associated with those key commodities) can be performed to create a more definitive approach to seasonal factoring, it is recommended that MDT adopt a moderately simple approach to seasonal truck volume adjustments.

III-3.1 SEASONAL PATTERNS FOR SINGLE UNIT TRUCKS

As noted above, single unit trucks had the most seasonal variation of the three truck classes. In addition, site-specific travel patterns for single unit trucks were not very consistent across sites. The average standard deviation associated with the mean monthly factors, illustrated in Figure

II-5 and shown in Table II-10, averaged just under 0.18, which corresponds to a coefficient of variation of about 18 percent.

Figure II-6 illustrates the diversity of seasonal adjustment factors computed from the 15 months of 2000 and 2001 data provided by the MDT. Note that these factors are computed from 15 consecutive months of data, but those 15 months do not include a complete calendar year. All 15 months are illustrated in Figure II-6 to show the truck volume changes that can occur at sites from year to year. Peak monthly factors for single unit trucks were often greater than 1.50 or less than 0.7. In other words, the average-day-of-month single unit truck volume ranged between 50 percent more than the average annual day to 30 percent less than the average annual day. To estimate average annual conditions from a short duration count, the short duration count would be divided by these factors.

It is apparent from Figure II-6 that the basic shape of the seasonal distribution of single unit truck volumes was reasonably consistent across the 18 sites for which data were provided. However, the actual seasonal adjustment factor for a given month at a given site varied considerably from the average statistic for all sites. The standard deviation of each monthly factor was generally equal to the size of the adjustment being made for that month. This means that while use of the factors would improve the accuracy of traffic load estimates, the adjusted load volumes were not precise.

An attempt was made to group the 18 stations into “regional” travel time patterns. Unfortunately, the variation both from month to month and from site to site was so large that the resulting “regional monthly factors” did not provide a significantly better estimation of seasonal trends than use of the average condition for all pavement loading analyses not located near a road with a permanent vehicle classification counter.

Because the single unit truck volume patterns were primarily influenced by Class 5 trucks, which cause relatively little pavement damage, a test was performed to ensure that the single unit monthly factors were applicable to Class 6 trucks.

Figure II-7 shows that Class 5 and Class 6 volume patterns were similar. The standard deviations for each of the monthly factors for both classes were reasonably similar in size, averaging around 0.2. Class 6 factors were slightly more variable than those of Class 5 because Class 6 volumes were lower and therefore, less stable than Class 5 volumes.

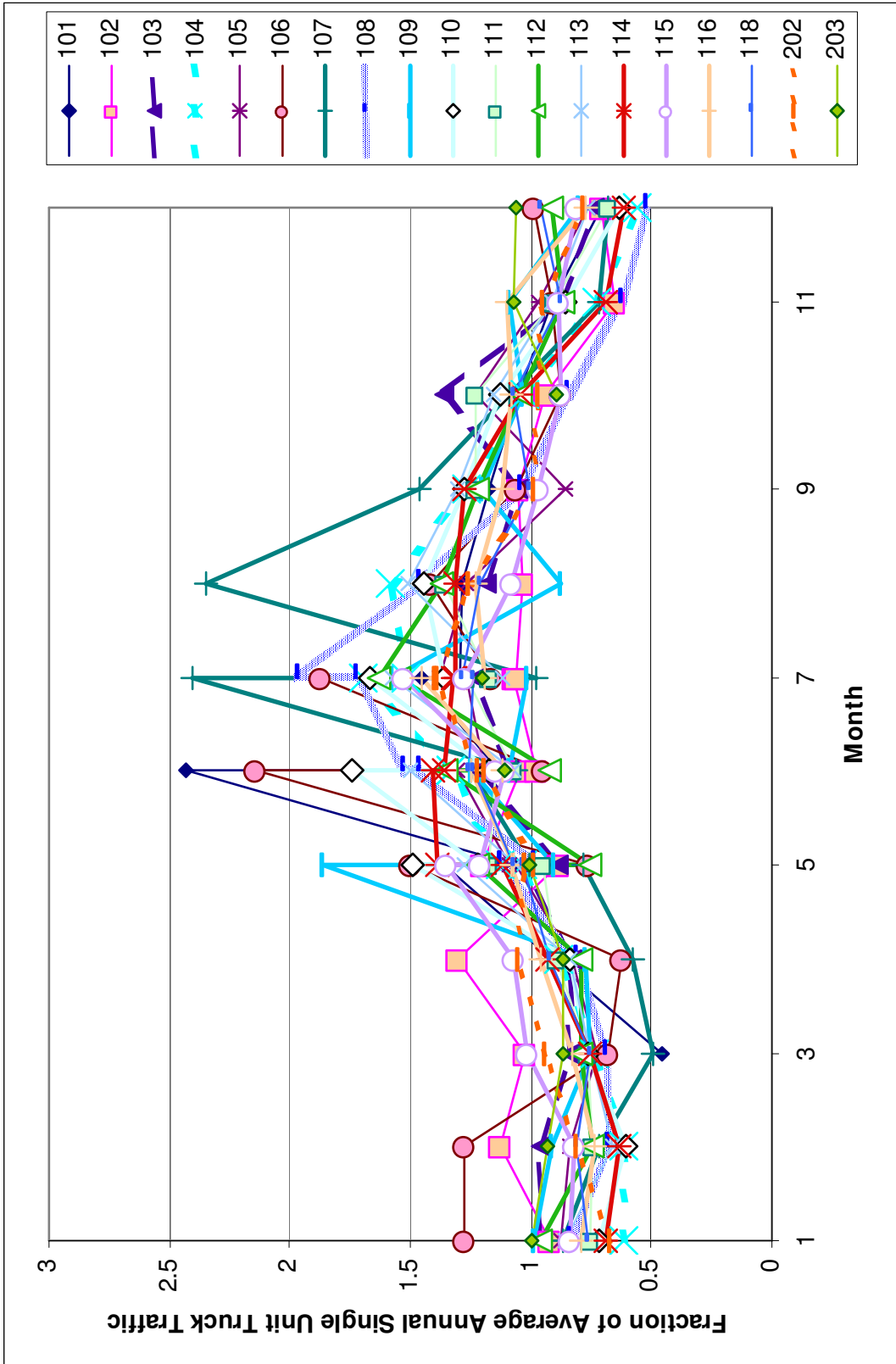


Figure II-6 Seasonal Traffic Patterns for Single Unit Trucks

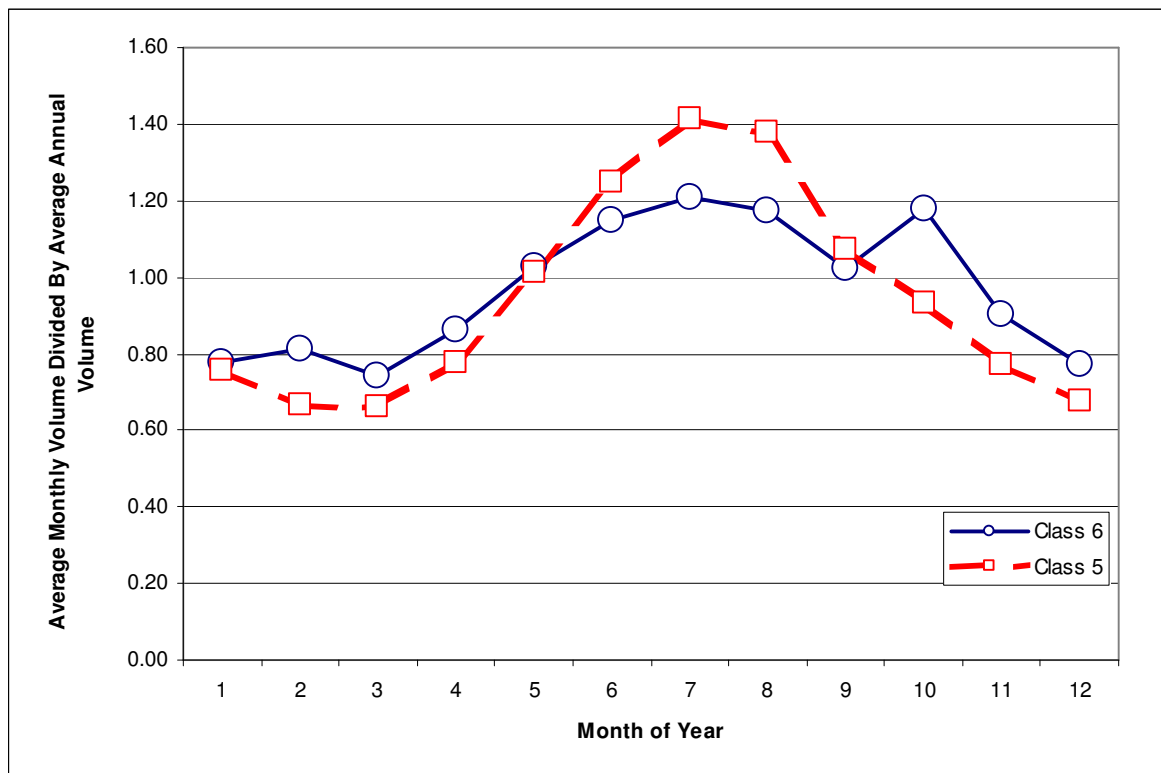


Figure II-7 FHWA Class 5 and Class 6 Monthly Volume Patterns

Because low volumes are inherently unstable and because the two patterns were similar, it is recommended that seasonality for Class 6 trucks remain within the combined single unit truck factor. Furthermore, it is recommended that for Montana’s truck seasonality computations, only one single unit truck seasonal or monthly distribution factor group be used. In other words, the monthly volume distribution factors should be the same for all single unit trucks.

III-3.2 SEASONAL PATTERNS FOR MULTI-TRAILER TRUCKS

The multi-trailer truck classification is predominately made up of FHWA Class 13 vehicles. On Montana’s high volume roadways, between 10 to 15 percent of all multi-trailer trucks may have been from FHWA Classes 11 or 12, but the remaining 85 to 90 percent were FHWA Class 13.

For all sites combined, multi-trailer trucks had the most flat seasonal pattern of the three truck classes. As with the single unit truck factors, however, individual sites frequently exhibited seasonal fluctuations that were substantial. These large fluctuations were caused by a combination of small volumes of very large trucks and changes in local conditions. From the data provided by MDT, it is impossible to determine whether the significant volume fluctuations observed at specific sites were part of a consistent trend (agricultural harvests), or whether they were caused by unusual or one-time occurrences such as construction projects.

A review of the seasonal patterns for multi-trailer trucks at each site showed that three WIM sites (102, 111, and 109) had multi-trailer truck volumes that were too low to produce stable seasonal adjustment factors. Site 109 had less than 1 per day. Site 111 averaged just over 11 multi-trailer trucks per day, and although Site 102 averaged just under 20 multi-trailer trucks per day on an annual basis, without the four high volume months between September and December, it too averaged 11 trucks per day. Because of the low average annual truck volume, all three of these sites had relatively unstable seasonal factors for multi-trailer trucks and were removed from most truck volume seasonal analyses.

Site 102, however, provides an excellent illustration of both the importance and difficulty of using seasonal factors for truck volumes in pavement design. During the four-month period from September to December, this site averaged almost 30 multi-trailer trucks per day, with a seasonal peak in September of over 45 trucks per day. During the rest of the year, the site experienced just over 11, while in the summer monthly multi-trailer truck volumes fell to 5 or 6. So an unadjusted vehicle classification count taken in the middle of the summer (June / July) would underestimate the average annual daily load applied by multi-trailer trucks on this road by a factor of roughly three to four. That same count would underestimate average annual combination truck volumes by roughly 50 percent. A count taken in September would overestimate average annual load by a factor of roughly two.

Although most sites did not have this extreme level of seasonality for multi-trailer trucks (refer to Figure II-8), data for many of the sites showed monthly surges in heavy truck traffic. The result of these periodic fluctuations in multi-trailer truck volumes was that the standard deviation of the seasonal factors was high. Unfortunately, attempts to create factor groups based on geographic location and/or roadway type were unsuccessful. This observation was made from analyzing over 250 WIM sites within the LTPP program in determining the global default values (*ARA 2004a*). Most of these 250 WIM sites, however, were located along Interstate or primary roadways where the geographic location would be expected to have a minimal effect of the monthly distribution factors.

For example, a review of the January and February factors showed that most of the sites exhibited January multi-trailer truck volumes that exceeded annual conditions were located towards the eastern portion of the State (Sites 103 and 111) or at least are farther east than most of the other WIM sites (Sites 108 and 203). Creating a factor group of these four sites resulted in a marginally better factor group than a group consisting of all valid sites for the State. The mean standard deviation for a monthly factor of the “east” factor group was 0.20, while the “all sites in the State” factor group had a mean standard deviation of just under 0.22. The “non-eastern” group of sites had an average monthly factor standard deviation of 0.20. The remaining sites in the State were then grouped together.

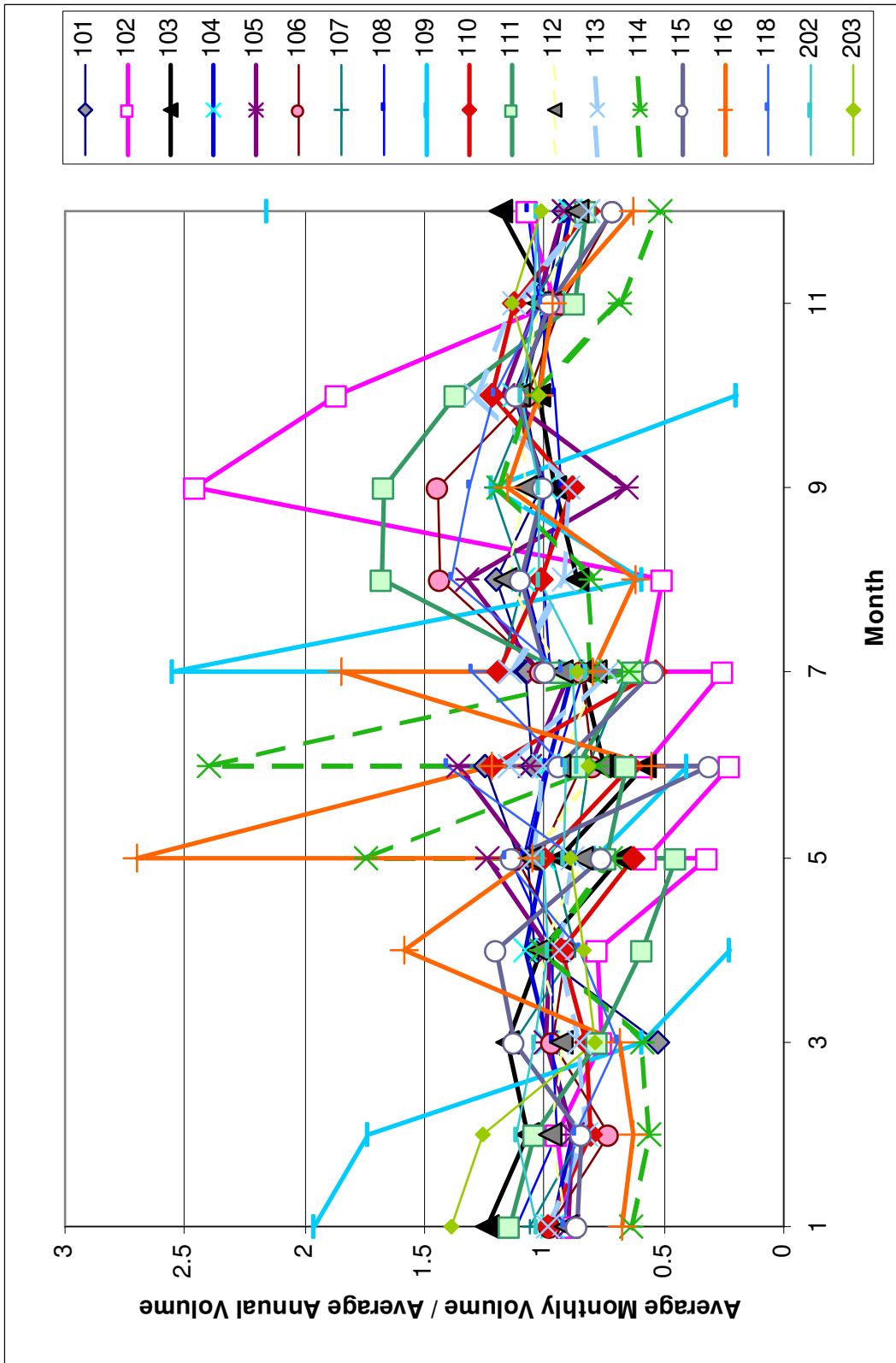


Figure II-8 Monthly Multi-Trailer Truck Volume Patterns by Site

The result was one pattern with a minor volume peak between December and February, and a second with a minor peak between April and May (see Figure II-9). Both patterns showed increased volumes during September and October, when shipping picked up to meet holiday season demands. In addition, both patterns were marginally more homogeneous than the “average for the State pattern.” However, creating two patterns would mean that MDT would need a mechanism for determining which roadways in the State fell into which of these two patterns. For example, at what point would a milepost on I-90 stop being in the “eastern” factor group and start belonging to the “other parts of the State” group?

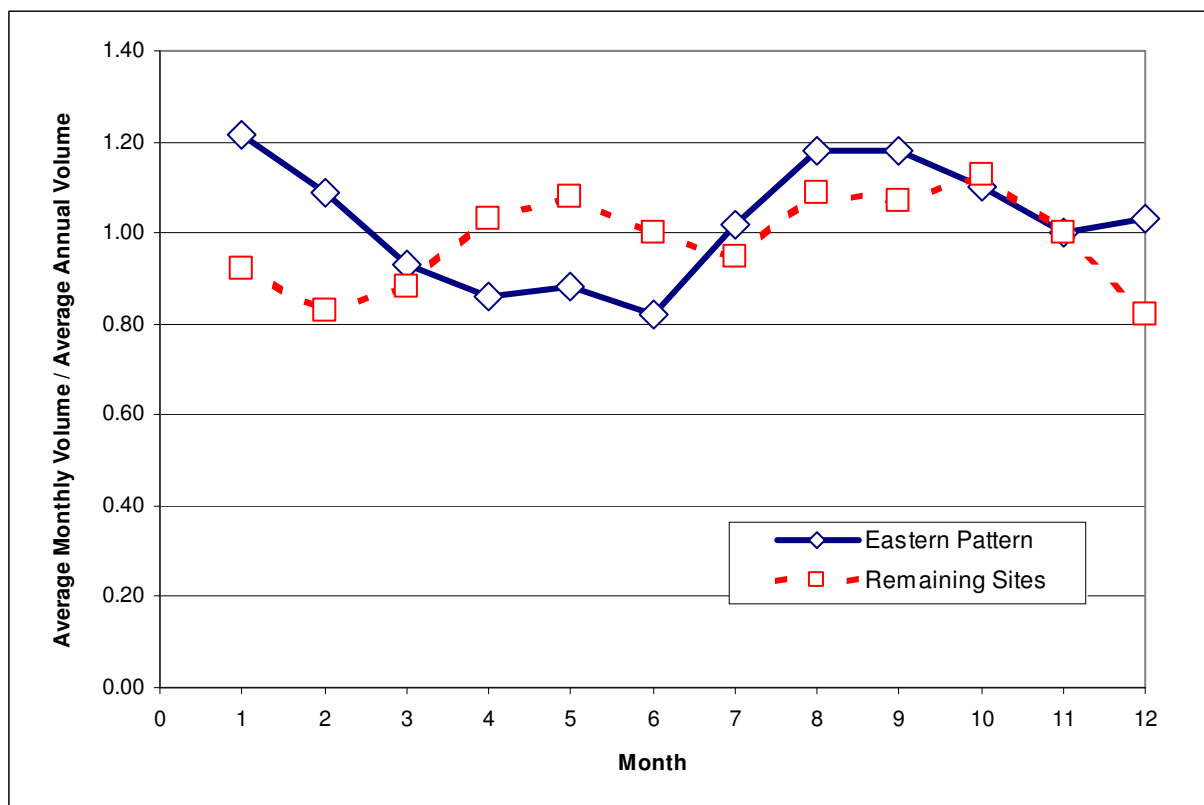


Figure II-9 Comparison of Eastern and Non-Eastern Monthly Seasonal Patterns for Multi-Trailer Trucks

Without detailed knowledge of the commodity flows occurring on Montana’s highways, it is not possible for this analysis to determine which of these approaches is truly better. If freeze thaw damage due to loads were a concern in either February or April, then the difference in seasonal adjustments produced by using these two groups, instead of a single group, might justify the additional effort of determining which factor group each Montana road should belong to. If freeze thaw were not an issue, then the benefit might not exceed the cost of the more complex procedures necessary to apply seasonal adjustments with more than one pattern.

III-3.3 MONTHLY SEASONAL FACTORS FOR COMBINATION TRUCKS

The seasonal patterns for combination trucks were dominated by the travel patterns of FHWA Class 9 trucks. Class 9 trucks (tractor semi-trailers) generally make up between 70 and 90 percent of all combination trucks and generally account for 40 to 70 percent of all pavement loadings or damage.

The average combination truck seasonal pattern was quite similar to the average pattern for multi-trailer trucks. It was reasonably flat, with modest increases in volume during the winter months. However, unlike multi-trailer trucks, the combination truck volume patterns were reasonably stable from site to site and from month to month. Figure II-10 illustrates the range of seasonal factors at all sites for which data were provided.

While a large number of Montana sites had monthly multi-trailer factors of less than 0.5 or greater than 1.5, relatively few sites had monthly factors for combination trucks that were less than 0.8 or greater than 1.3. In addition, when taken as a single statewide factor group, the average standard deviation for monthly combination factors (0.09) was less than half that of the corresponding value for either single unit or multitrailer trucks. The majority of the exceptionally high or low points seen in Figure II-10 are believed to be the result of problems with the data collection equipment, rather than the result of real changes in truck travel behavior.

One set of high seasonality factors that did appear to be real was the relatively high peak in truck volumes at about one-third of the sites in October. These data collection sites (Sites 105, 110, 111, 113, 114, and 116) experienced combination truck volumes in October that were more than 20 percent above average annual conditions. A single factor group from these sites was established to try to capture these heavy seasonal volumes.

If these sites were combined into a group and all remaining sites with good data were grouped in a second seasonal factor group, the average standard deviation for monthly factors would decline slightly for both groups (from 0.9 for the statewide group to 0.8 for both new groups). Dividing these sites into groups would provide a slightly more homogeneous set of monthly distribution factors.

However, this group would be completely different from the seasonal factor group that was discussed for multi-trailer trucks. A review of the sites with high October volumes showed that they were geographically spread throughout the State of Montana. Interestingly, every one of the sites was located on a US-signed route (e.g., Site 105 was located on US-93). In fact, all but three of the data collection sites located on US-signed routes in Montana were in the above list, and those three sites (Sites 106, 107, and 115) all had October seasonal factors above 1.10 and, therefore, could be added to this seasonal grouping without significantly changing the homogeneity of the factor group. Such an approach would allow any US-signed route to be associated with that seasonal factor group. All other roads in the State would be associated with the rest of the State group.

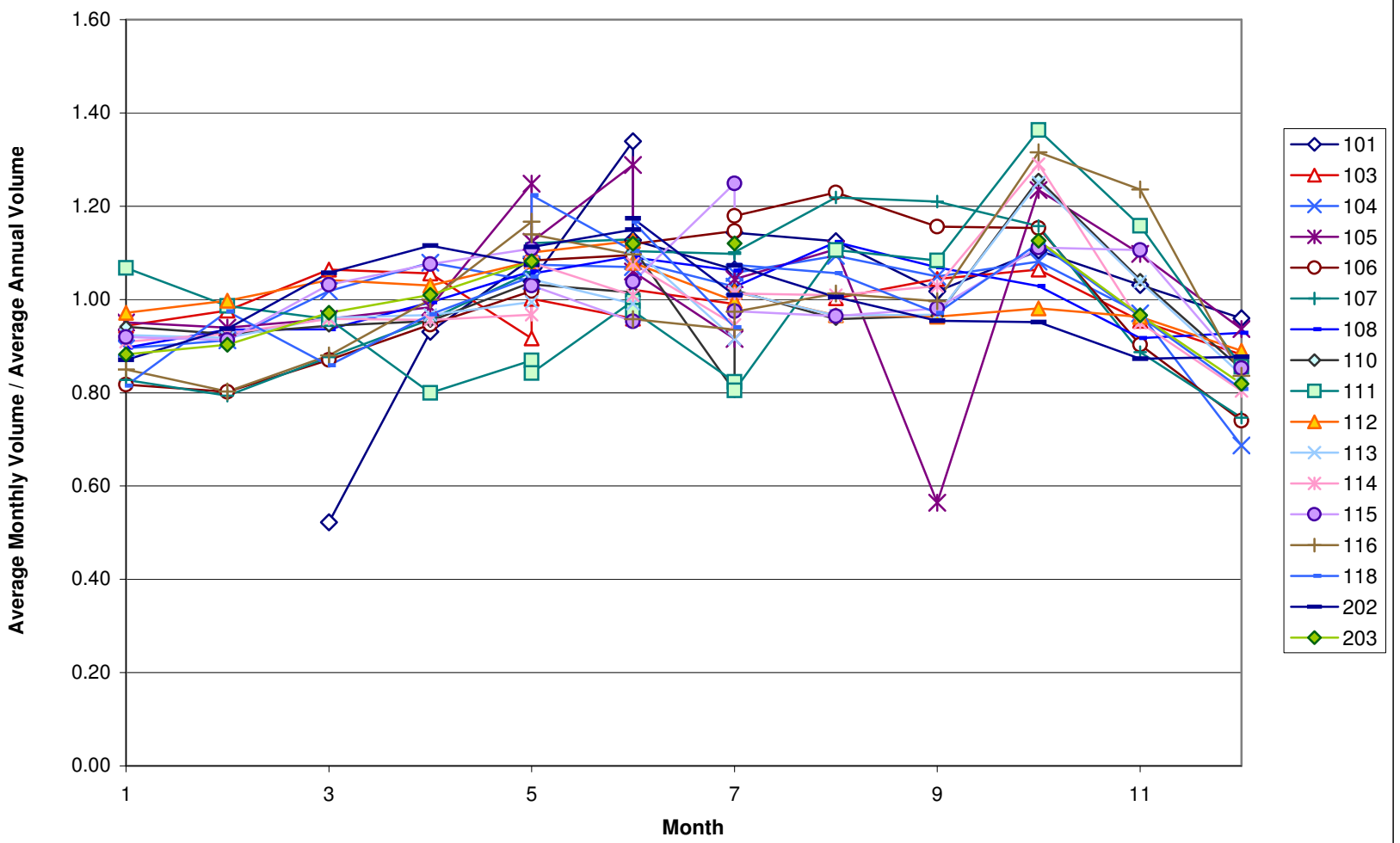


Figure II-10 Monthly Seasonal Factors for Combination Trucks

As with the multi-trailer truck factors, it is not clear whether use of this “split” factor group would actually be better than using a single statewide group. Unlike the two multi-trailer truck factor groups, the seasonal patterns for these two groups were minor except for the months immediately surrounding October. Better knowledge of the economic activity and commodity movements taking place within Montana is needed to judge the merits of the split factor approach to combination factors.

III-3.4 RECOMMENDATIONS FOR SEASONAL TRUCK VOLUME FACTORING

For the initial calibration of the MEPDG in Montana, it is recommended that either statewide average seasonal factors be used or factors for site-specific WIM locations (see Volume I, Figure I-6) (*Von Quintus and Moulthrop 2007a*). While minor improvement in the accuracy of truck volume estimates might be gained by using multiple seasonal factor groups, the complexity that such an approach would bring to the traffic load estimation process does not appear to be warranted at this time.

To apply multiple seasonal truck factor groups, Montana would have to track and apply more than one set of factor groups for each pavement design. This would likely be a complex process to develop, implement, and maintain. The truck volume variability observed in the data is a result of day-to-day volume fluctuations in truck volumes by class. It would be a difficult task for defining the road segments that should be associated with specific seasonal patterns observed at the WIM sites. Given the high level of truck volume variability already present and the difficulty in defining appropriate roadway segments, the benefits in accuracy that would result from the application of multiple factor groups do not appear to be substantial.

Consequently, it is recommended that MDT continue to analyze its growing archive of truck volume data. In addition to the mathematical analysis of those data, the MDT should consult experts who understand the economic activity patterns of the State and can provide explanations of what is occurring in the observed patterns and help develop more rational and easier to apply factor groups.

CHAPTER III-4: TRUCK WEIGHT PATTERNS

The same 15 months of WIM data that were used to analyze seasonal volume factors were reviewed for truck weight information. However, multiple cases of possible WIM scale calibration drift were noted, and are discussed briefly in this chapter of Part III of Volume II. Except in extreme cases, no data were removed or adjusted during this analysis. As an example, suspected calibration drift at Site 113 made it impossible to classify this site into a truck weight group. Consequently, this site was removed from the data. Essentially, the majority of the analysis performed for this project assumed that the data supplied by MDT were valid.

It is distinctly possible that axle weight will vary by lane and by direction. Lighter trucks may be more likely to use the passing lane, whereas heavier trucks may be more likely to use the right or slow lane. Similarly, experience with data submitted to the LTPP program indicates that directional loading (trucks are loaded in one direction, but empty in the reverse direction) can occur at many sites. MDT may wish to expand this research by collecting more WIM data and performing an analysis of that data as MDT progresses through the implementation process of the new MEPDG.

For this analysis, truck weight records, or W-card records, were obtained from MDT. The data were run through a Beta version of the NCHRP Project 1-39 software (*Cambridge 2005*). Monthly load distributions were then examined for tandem and single axles. The majority of effort was spent examining load distributions for FHWA Class 9 trucks because those trucks were responsible for far more traffic loading and pavement damage in Montana than any other classification of vehicle.

It was determined that in many, but not all cases, sites with similar Class 9 tandem load axle distributions had similar Class 13 tandem axle load distributions, and that Class 6 tandem axle load distributions for those sites were reasonably similar. In other words, if Site 1 and Site 2 had Class 9 tandem axle loads with similar shapes, then the Class 13 tandem axle load distributions at those two sites would have similar shapes. As a result of this observation in the WIM data, the grouping of Montana WIM sites was based on the observed loading patterns of Class 9 tandem axle loads. The axle load distribution histograms were based on the input axle weights categories used by the MEPDG software. The axle weight boundaries associated with these categories are given in Appendix II-A. The groups were named after the shape of the load distribution patterns, and only a minor amount of analysis was given to the axle load distributions of the other vehicle types.

One other observation from the analysis of multiple vehicle classes was that sites that tended to have heavy axle load distributions relative to other sites in their group for one class of vehicles tended to have heavy axle load distributions for all classes of trucks. This observation led to the speculation that these trends were primarily the result of minor WIM scale calibration problems, rather than truly different truck loading characteristics. This speculation is based on the analyst's experience in analyzing WIM data from LTPP and other agencies where drift in the WIM scales was found. It is recommended that MDT check all portions of the WIM scale calibration process to confirm or reject this speculation.

III-4.1 GENERAL AXLE LOAD DISTRIBUTION FINDINGS

Five basic patterns of truck axle weight distributions (Truck Weight Road Groups [TWRG]) were observed in Montana's data for FHWA Class 9 trucks. For pavement design, individual roadway segments would be assigned to one of these groups based on the nature of truck travel on that road segment, and the axle load distribution for that group would then be used, along with the number of trucks for each truck class, to determine the expected pavement load on that roadway. These five TWRGs were based on the shape of the tandem axle load distribution found for Class 9 trucks.

The five TWRG groups with homogeneous loading patterns are defined below and discussed in more detail in the following sections of this chapter.

- Primarily Loaded – Significant Load.
- Bimodal Loaded – Primarily Heavy Load (greater number of heavyweight than lightweight trucks).
- Bimodal Loaded – Primarily Even Load (distribution between loaded and unloaded trucks).
- Lightly Loaded – Primarily Empty.
- Flat Distribution – Even Load.

A brief review of monthly changes in axle load distributions was conducted for each of the WIM sites for which data were provided. That review indicated that WIM scale calibration drift (a consistent increase or decrease in the measured axle loads) might have significantly affected the loading rates described in this chapter. A thorough investigation of those concerns was beyond the scope of the analysis effort. MDT is encouraged to perform such an analysis, as the MEPDG uses monthly axle load distributions, and the variation observed in the data at many WIM sites would be large enough to affect pavement design decisions.

Four Excel files were created for the analysis effort. Those files contain the loading patterns, by month, for both individual sites and the TWRGs. MDT may include these data in the pavement design and performance analysis processes to evaluate if there is a continued shift in the axle load spectra or distribution measured over time.

III-4.2 PRIMARILY LOADED – SIGNIFICANT LOAD

The first TWRG identified in this study is called Primarily Loaded. It represents sites where the vast majority of Class 9 trucks operating on that roadway carried a significant load. For Class 9 trucks at these sites, only one obvious peak was observed in the tandem axle load distribution. Figure II-11 shows the average of the 12 monthly load distributions for each of the seven sites grouped into this TWRG.

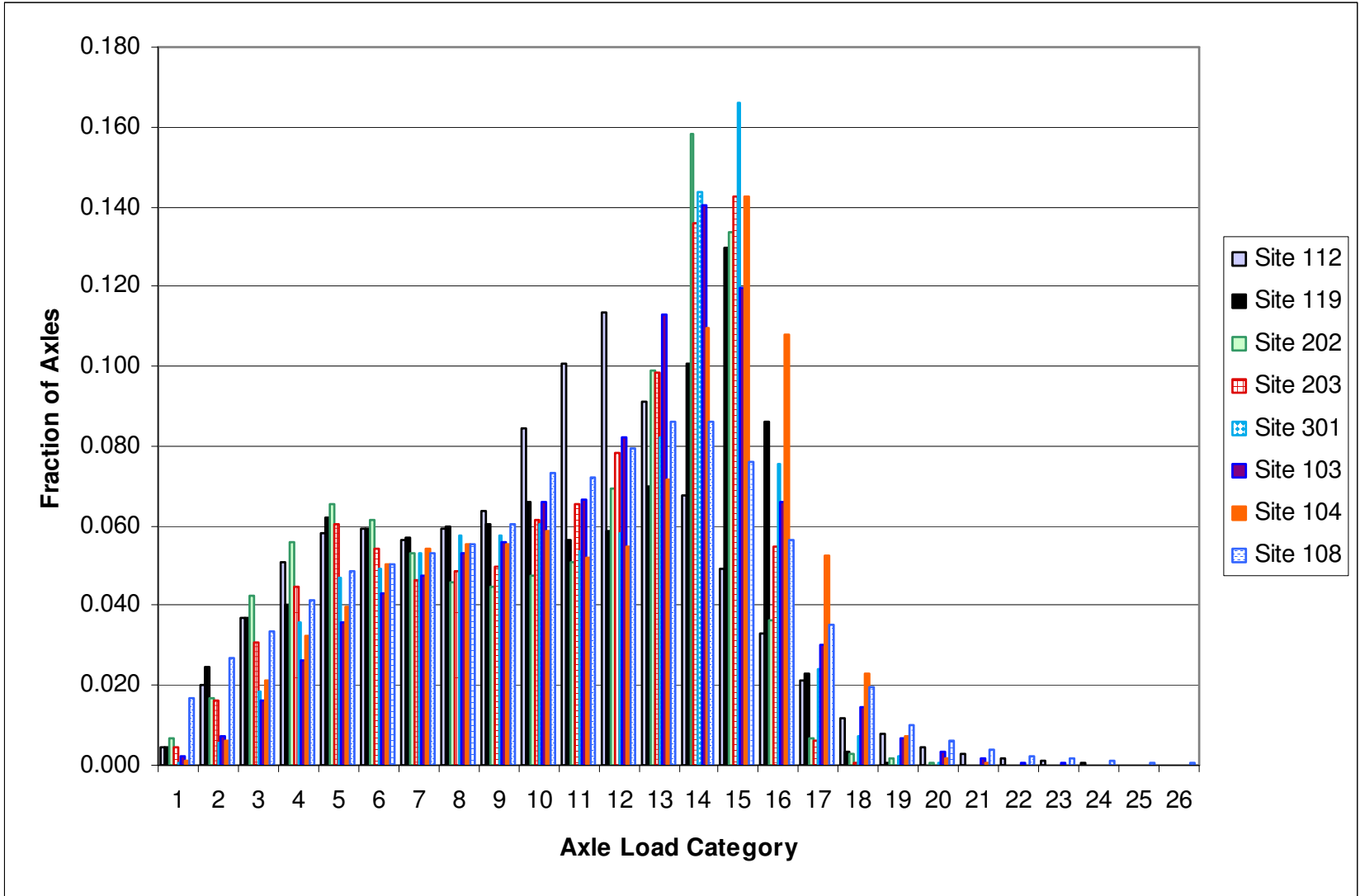


Figure II-11 Average Annual Tandem Axle Load Distribution for Class 9 Trucks, Primarily Loaded Truck Weight Road Group

The only significant peak in the tandem axle load distribution shown in Figure II-11 corresponds to tandem axle loads near the legal limit. The axles weigh roughly 30,000 to 32,000 pounds and are associated with fully loaded, 5-axle, tractor semi-trailers. See Appendix II-A for the weights associated with each category of axle loads.

An axle load distribution of this type indicates that heavy trucks on these roads are loaded to near their legal limits, and that the majority of Class 9 trucks using these roads are fully loaded. This pattern is common to Interstate highways in rural areas that serve significant long-haul truck movements. Not surprisingly, all except one of the Montana WIM sites associated with this truck weight group are located on rural Interstates. Site 301 is located on US-2 (not an Interstate highway) near Malta in the north central portion of Montana, and is a portable WIM site, which could have different axle load distributions because the measurement equipment is different. This site was included in the analysis because it is the only site with data provided by MDT along a rural non-Interstate roadway. All WIM sites located on Montana's Interstate system were classified within this group, although Sites 119, 202, and 112 had enough of an unloaded peak that they might have been included in the bimodal-heavy group.

The Class 13 tandem axle load distributions for the different sites in this TWRG were not nearly as uniform as those for Class 9 trucks (compare Figure II-12 with Figure II-11). Unlike Class 9 trucks, Class 13 trucks weighed at five of the eight sites in this group had both loaded and unloaded peaks. For example, Sites 108 and 119 had very substantial peaks in the first two histogram ranges, which corresponded to tandem axles below 6,000 pounds and between 6,000 and 8,000 pounds. However, the size and relative position of the unloaded peaks differed from site to site. Sites 103, 104, and 203 had no substantially unloaded peak in the Class 13 tandem axle distribution for this group.

The fact that there were unloaded peaks in the tandem axle distribution indicates that a significant portion of these trucks were most likely operating with trip origins and destinations within roughly four hours or less of each other. Therefore, a significant portion of the Class 13 trips at these sites were likely not long distance hauls. Long distant hauls are uneconomical and not probable if the reverse haul must be made empty, whereas the majority of the Class 9 trucks were probably in long haul service.

The variability seen in the axle load distribution for Class 13 trucks means that the group's average axle load distribution would not be as accurate a load estimate for any one site associated with this group as it would be for the Class 9 load distribution. For some of these sites (e.g., Site 108), the group average would over-estimate loads applied by Class 13 trucks, while at other sites (e.g., Site 203) the group average would underestimate actual loads. Because the Class 9 load estimates were much more similar when compared between sites, these errors would be much less common and/or pronounced for Class 9 trucks.

Figure II-13 shows the tandem axle weight distribution for Class 6 trucks for this site. The axle load distribution for Class 6 trucks was more uniform than that for Class 13, but less uniform than that for Class 9. The biggest discrepancy in the uniformity of this axle load distribution group was the unusually large number of very lightly loaded axles for Sites 108 and 203, as well as the very light loaded peak for Site 202.

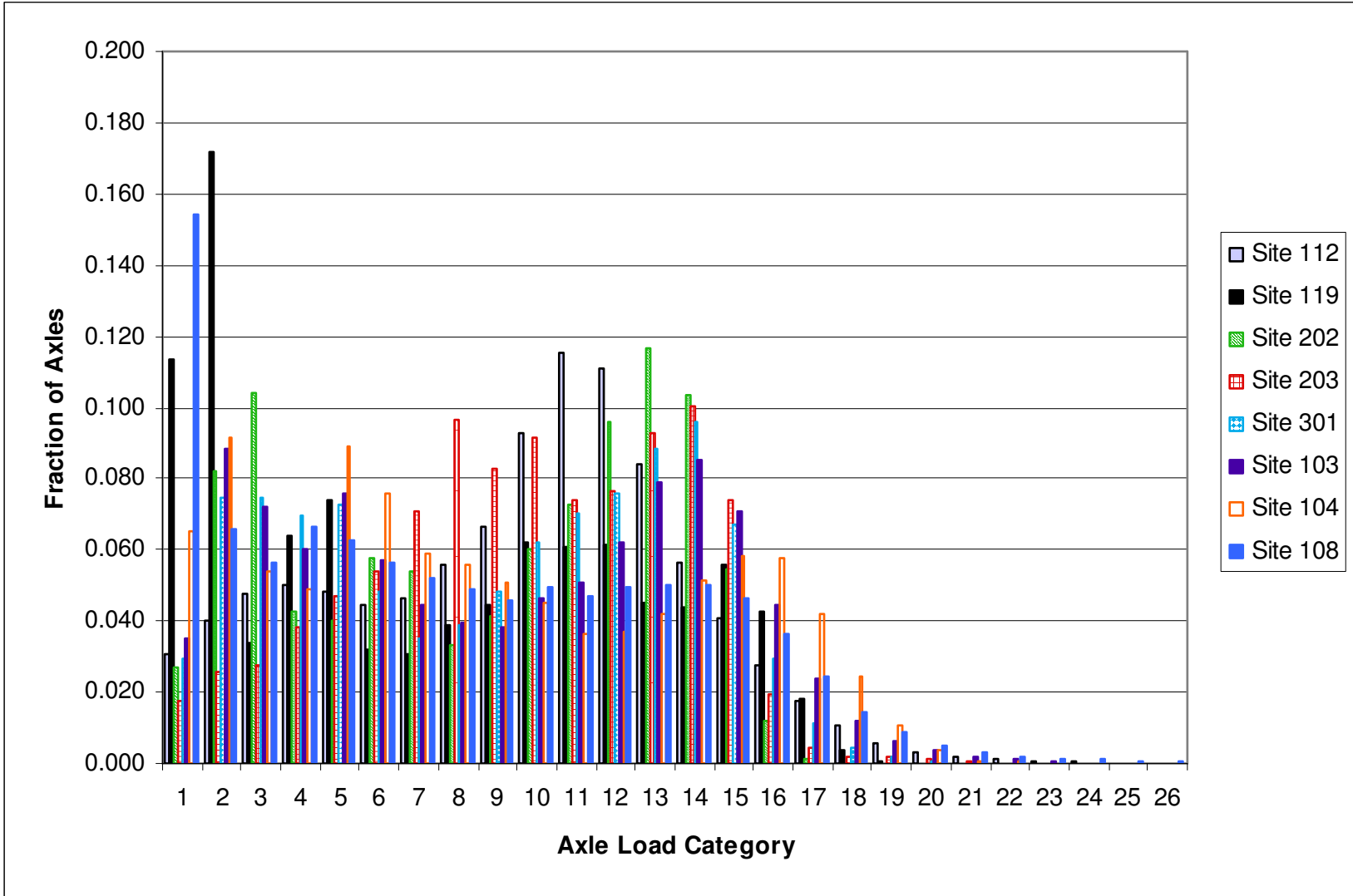


Figure II-12 Average Annual Tandem Axle Load Distribution for Class 13 Trucks, Primarily Loaded Truck Weight Road Group

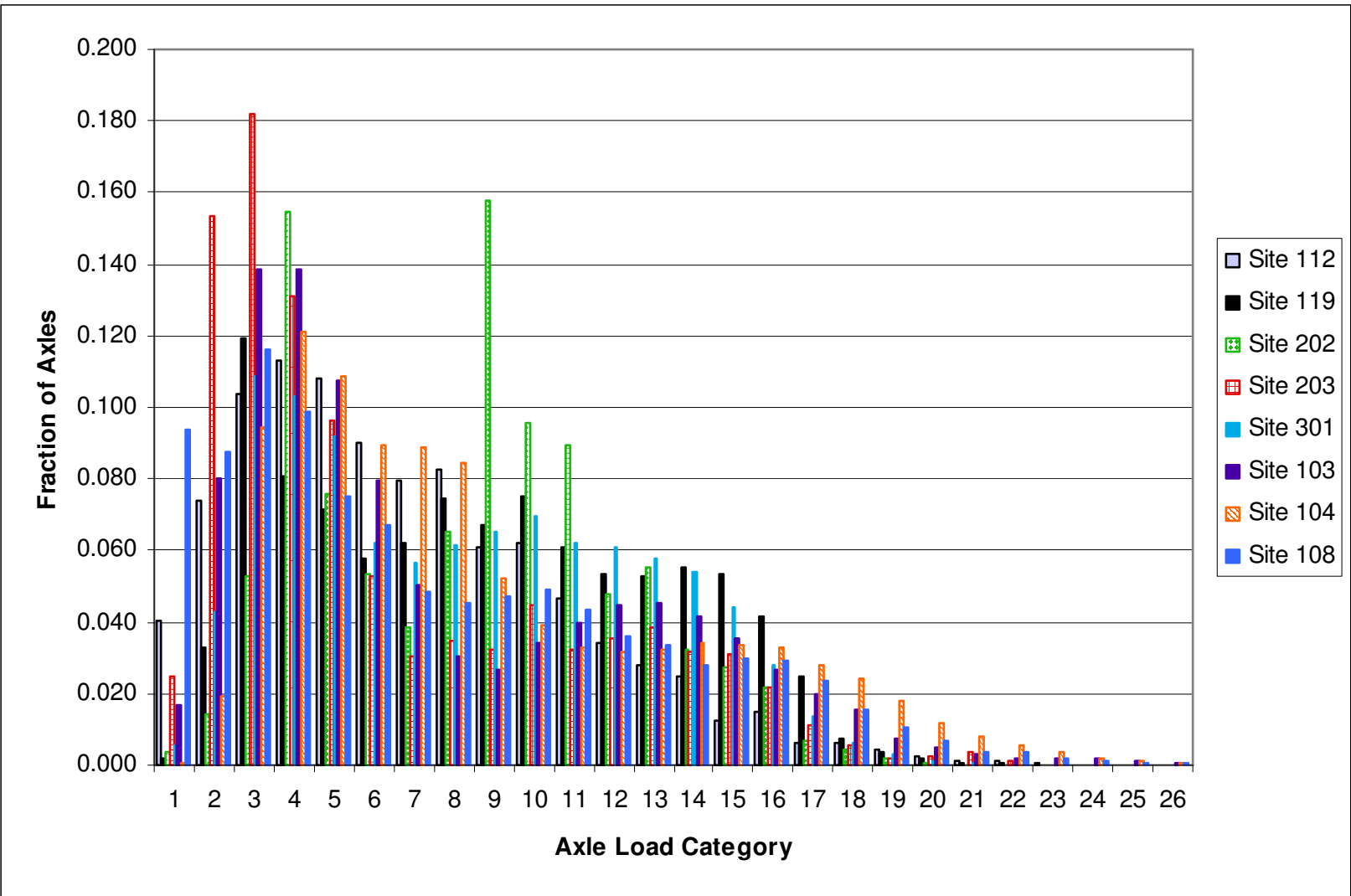


Figure II-13 Average Annual Tandem Axle Load Distribution for Class 6 Trucks, Primarily Loaded Truck Weight Road Group

Also of interest in the Class 6 graphic (Figure II-13) is the fact that roughly 1 percent of tandem axles at Sites 103, 104, and 108 were 40,000 pounds or greater (histogram categories 19 and up). These very heavy axles were not nearly as prevalent in the other five sites in this group. These very heavy axles would be likely to have a substantial impact on pavement life and, consequently, pavement design.

When Figures II-11, II-12, and II-13 are taken together, they do suggest some scale calibration concerns. For example, the locations of both loaded and unloaded peaks in the tandem axle distributions for Site 202 were generally lighter than those of the other six sites. Conversely, Sites 103 and 104 had heavier loaded and unloaded peaks (more heavy axles) than the other six sites. These consistent differences may have been caused by minor differences in scale calibration at the different sites.

Site 108 tended to have both relatively high numbers of very heavy axles and very light axles in comparison to the other sites. This could indicate that truck dynamic motion was higher at this site than at the other sites in the group, which normally means that the pavement near the scale is not smooth, causing high levels of dynamic vehicle motion. This in turn leads to abnormally high numbers of very light and very heavy axles being reported. It means that the pavement loading estimate based on axle distributions from this site may overestimate actual traffic loading, because very heavy axles have a disproportionate effect on pavement design than very light axles.

Using an average axle load distribution for the entire group of sites, rather than the load spectra for a single site, would dampen the effects of these potential scale problems. It is therefore recommended that MDT use an average load spectrum for the group as a whole for all pavement design and calibration efforts using the MEPDG.

III-4.3 BIMODAL LOADED – PRIMARILY HEAVY LOAD

The second distribution group examined was very similar to the first in that there was a significant loaded peak in the tandem axle load distribution for Class 9 trucks. The primary difference between this group and the last one is that sites in this group had a higher level of unloaded Class 9 truck traffic. This resulted in a more noticeable unloaded peak in the axle load distribution (see Figure II-14). As with all grouping efforts, however, the boundaries between this group and the Primarily Loaded group were somewhat arbitrary. None of these sites was an Interstate: four were US-signed routes, and one was a Montana State route. They were not geographically related, although Sites 106 and 107 were only 8 miles apart on US-191. They appear to represent sites with heavy truck movements, but with a modest number of empty trucks mixed in with the heavily loaded trucks.

Of particular interest in Figure II-14 is the significant number of very heavy tandem axles at Sites 106 and 107. It is not clear whether this resulted from scale calibration problems or is an indication of over-loaded axles at these two sites (they were only 8 miles apart). Very heavy tandem axles were present at these two sites for both Class 13 and Class 6 trucks (see Figures II-15 and II-16). Very heavy axles were also present in Class 6 trucks at Site 114, but only to a modest extent for Class 13 trucks at that site.

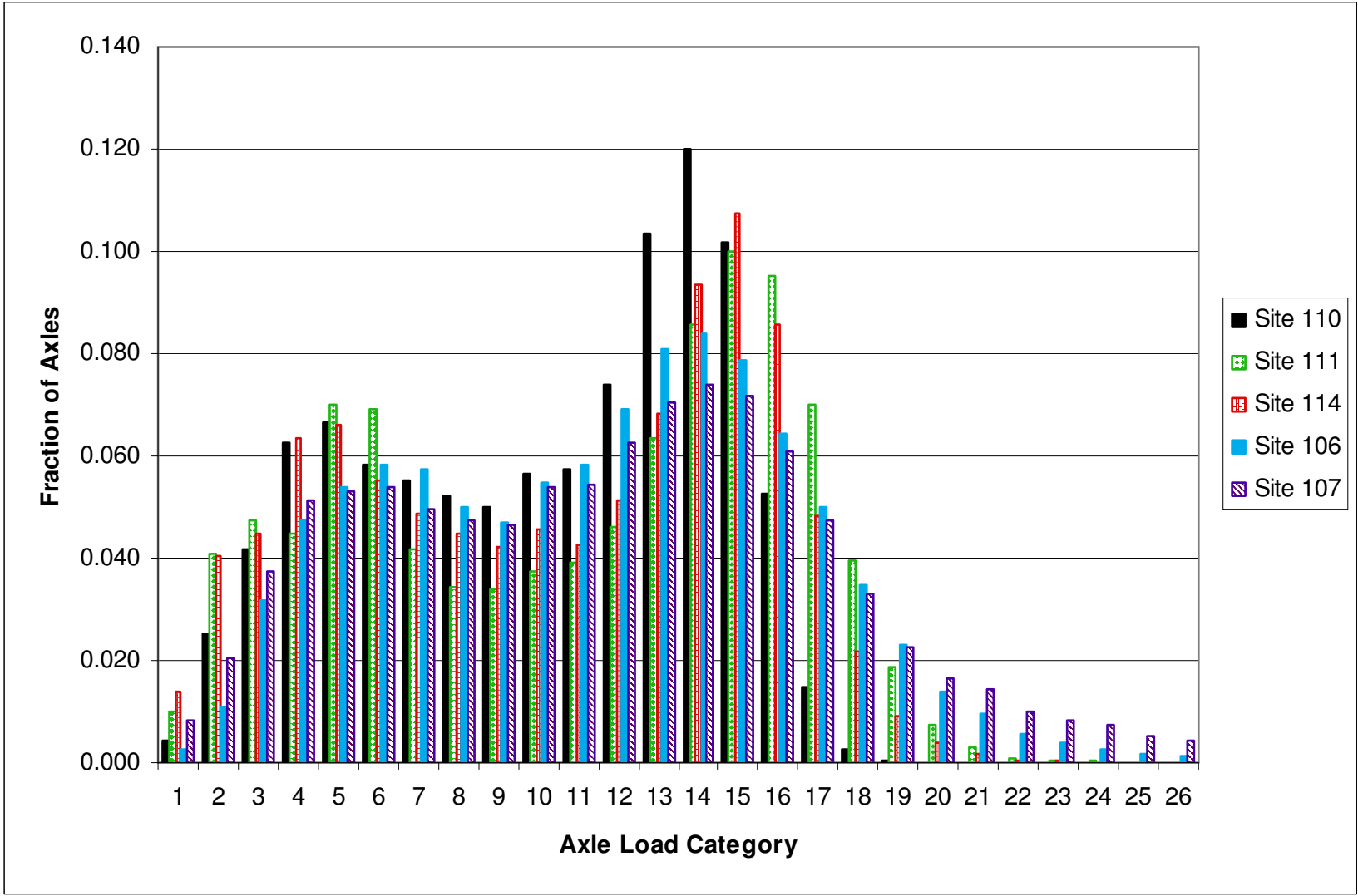


Figure II-14 Average Annual Tandem Axle Load Distribution for Class 9 Trucks, Heavy-Bimodal Truck Weight Road Group

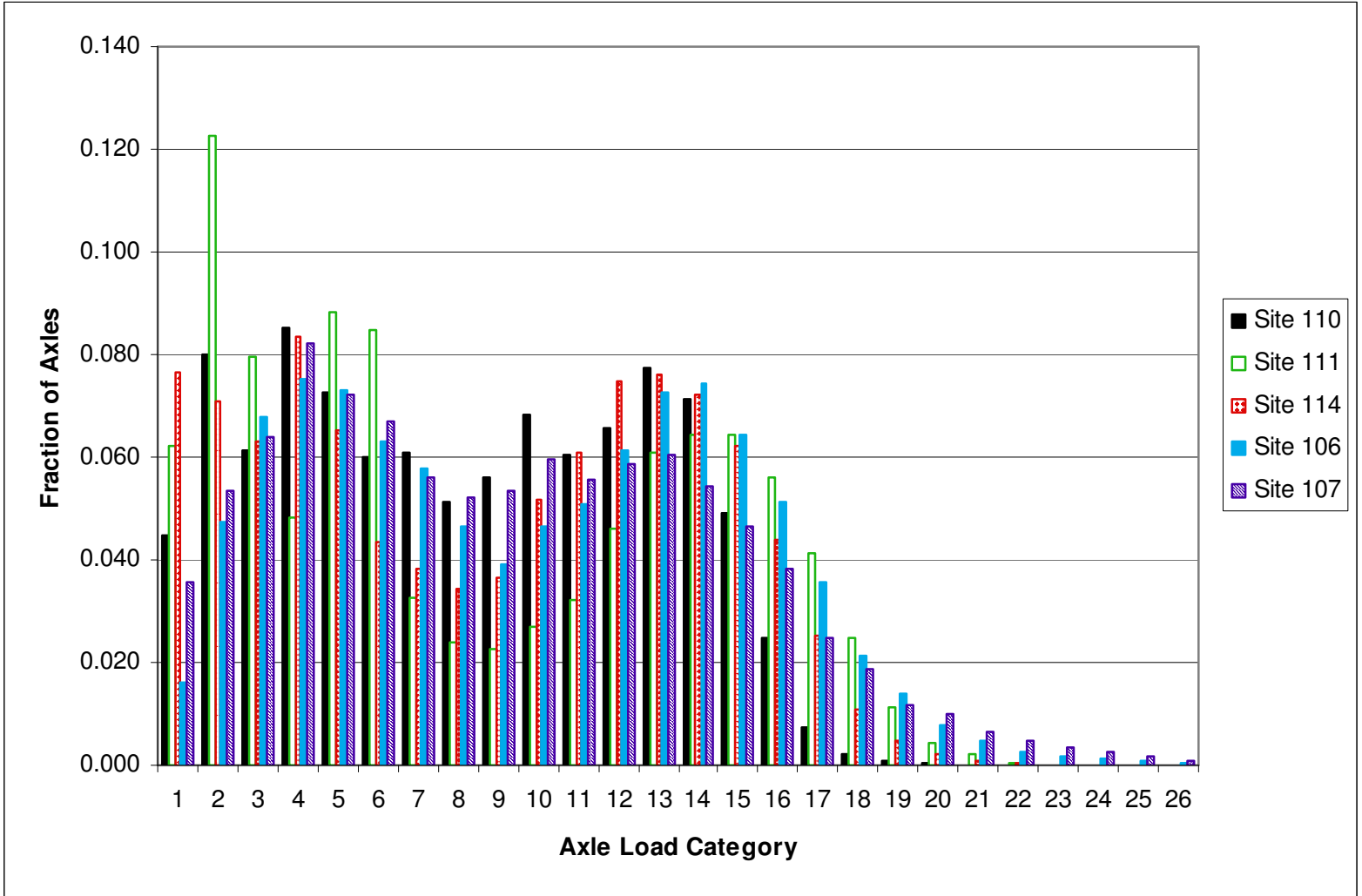


Figure II-15 Average Annual Tandem Axle Load Distribution for Class 13 Trucks, Heavy-Bimodal Truck Weight Road Group

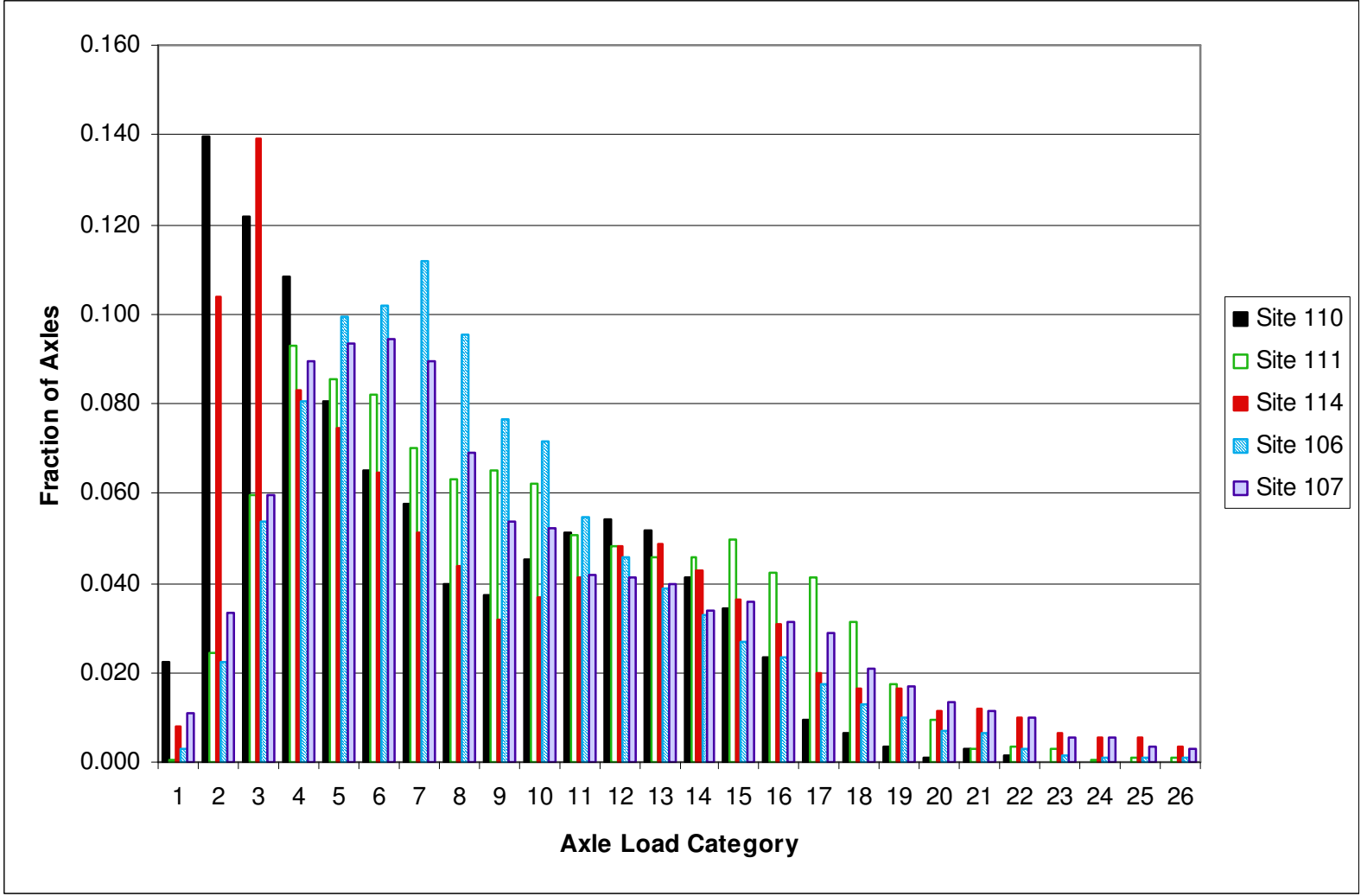


Figure II-16 Average Annual Tandem Axle Load Distribution for Class 6 Trucks, Heavy-Bimodal Truck Weight Road Group

Other than the differences in the extent of overloaded axles observed, the tandem axle distributions measured at the sites within this heavy bimodal group tended to be more homogeneous for most classes of trucks than those observed in the Primarily Loaded group of Interstate sites. The group averages are generally an excellent descriptor of the loads carried at sites within these groups.

The two difficulties associated with this TWRG are: 1) the group itself may be hard to define (which roads within Montana should be associated with this group), and 2) the fact that the presence of overloaded axles in some but not all sites would result in different pavement loading rates for those sites, even though the shape of the two distributions are similar. Overloaded axles can be so important to pavement design that if overloading is as prevalent as suggested by these data, Montana might want to consider developing a TWRG specifically to handle roads with this level of overloading. The only issue then would be to determine which road segments are applicable to the frequent overload truck weight group. This statement assumes, of course, that these data do not have measurement errors, exclude measurements being influenced by pavement roughness at the WIM site, and the WIM equipment has no drift or calibration errors.

Without having better local knowledge of the prevalence of overloads, it is initially recommended that this be treated as a single group. Averaging of the axle load distribution patterns for the five sites will dilute the effect of the overloaded axles somewhat, but it will also result in a conservative loading design for non-Interstate Montana roadways that are carrying loaded heavy trucks.

III-4.4 BIMODAL LOADED – PRIMARILY EVEN LOAD

The third TWRG had a very balanced tandem axle load distribution. For sites in this group, the loaded and unloaded peaks were roughly equal in height, as shown in Figure II-17. This signifies that the numbers of loaded and unloaded trucks on these roads were roughly equal. As with the heavy bimodal group, the WIM sites allocated to this group were all US or Montana State routes. Site 102 was on SR-314, where it carried only 10 to 25 Class 9 trucks per day. These sites were spread geographically around the State.

Of significant interest for this group is what appears to be an overloaded condition for Site 102. All three major truck categories (Classes 6, 9, and 13) showed very heavy tandem axles at this site, but not at the other four sites in this group (see Figures II-18 and II-19). It is unknown whether the large number of overloaded axles was the result of a high percentage of overloaded vehicles or poor scale calibration at this low volume WIM scale.

There were very few lightly loaded tandem axles for Class 6 trucks at this site, which might indicate over-calibration of the scale. However, the number of light tandem axles was reasonable for both Classes 9 and 13, which might suggest a problem with overloaded trucks at the site.

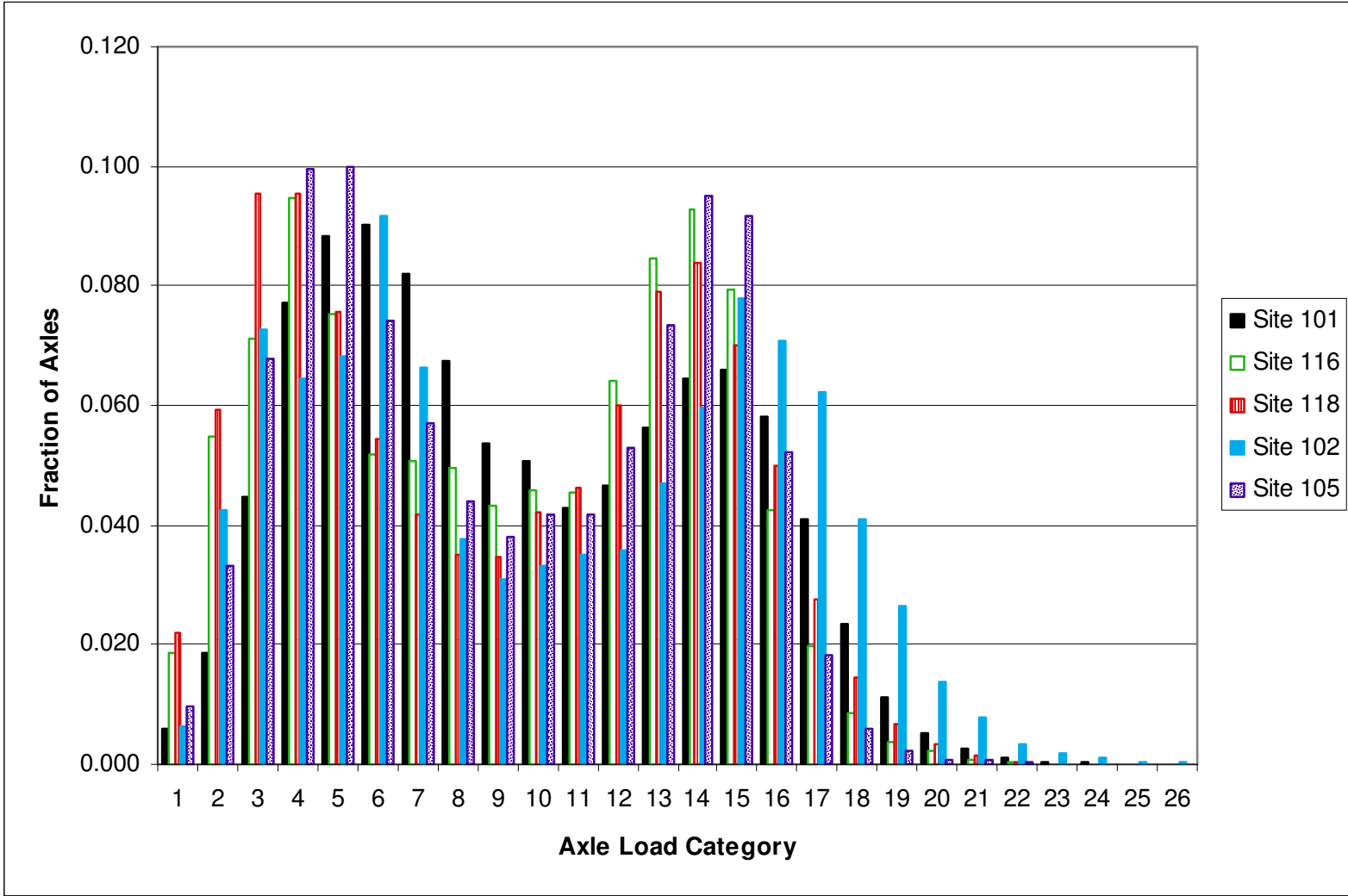


Figure II-17 Average Annual Tandem Axle Load Distribution for Class 9 Trucks, Bimodal Truck Weight Road Group

II-91

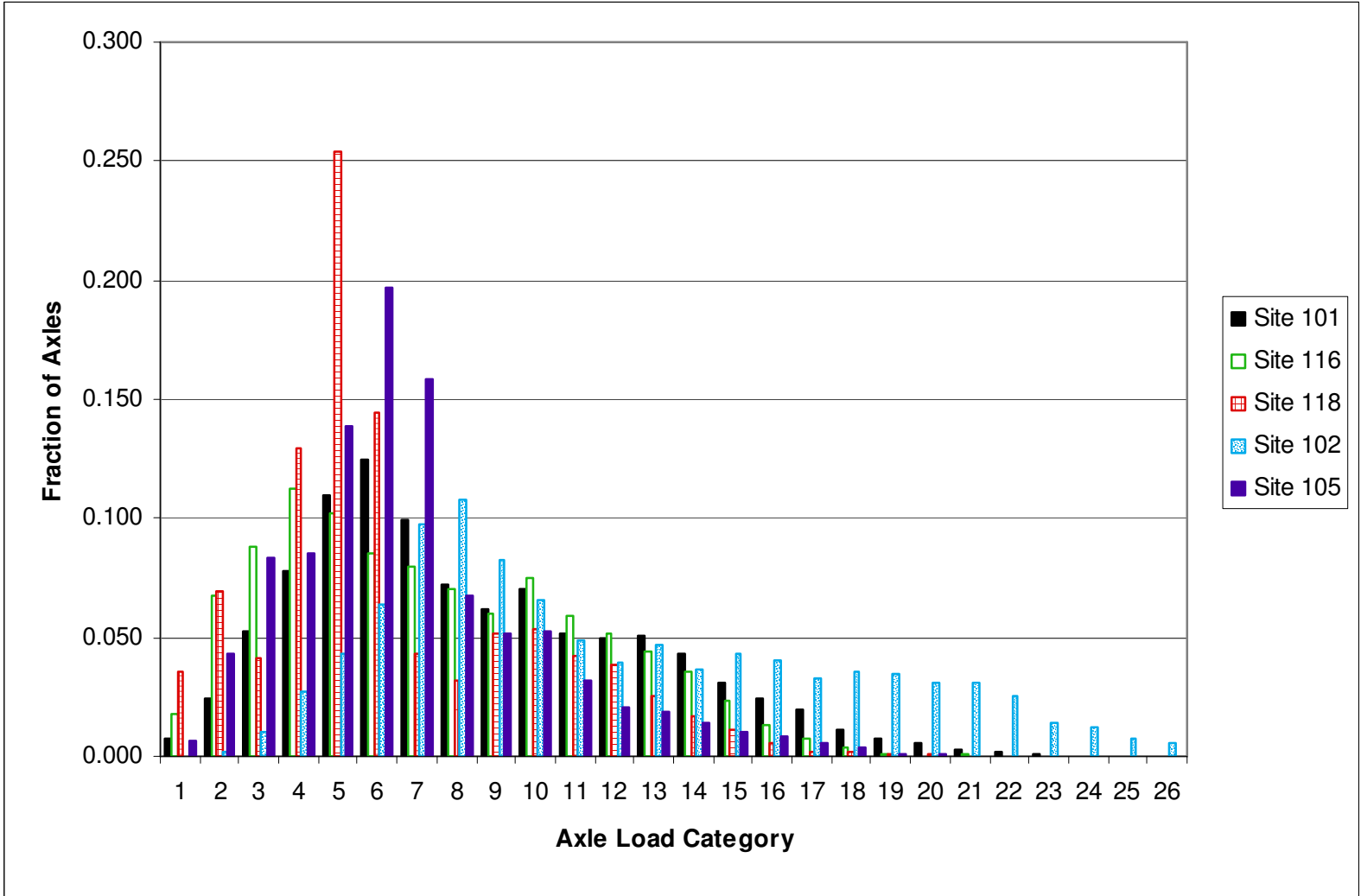


Figure II-18 Average Annual Tandem Axle Load Distribution for Class 6 Trucks, Bimodal Truck Weight Road Group

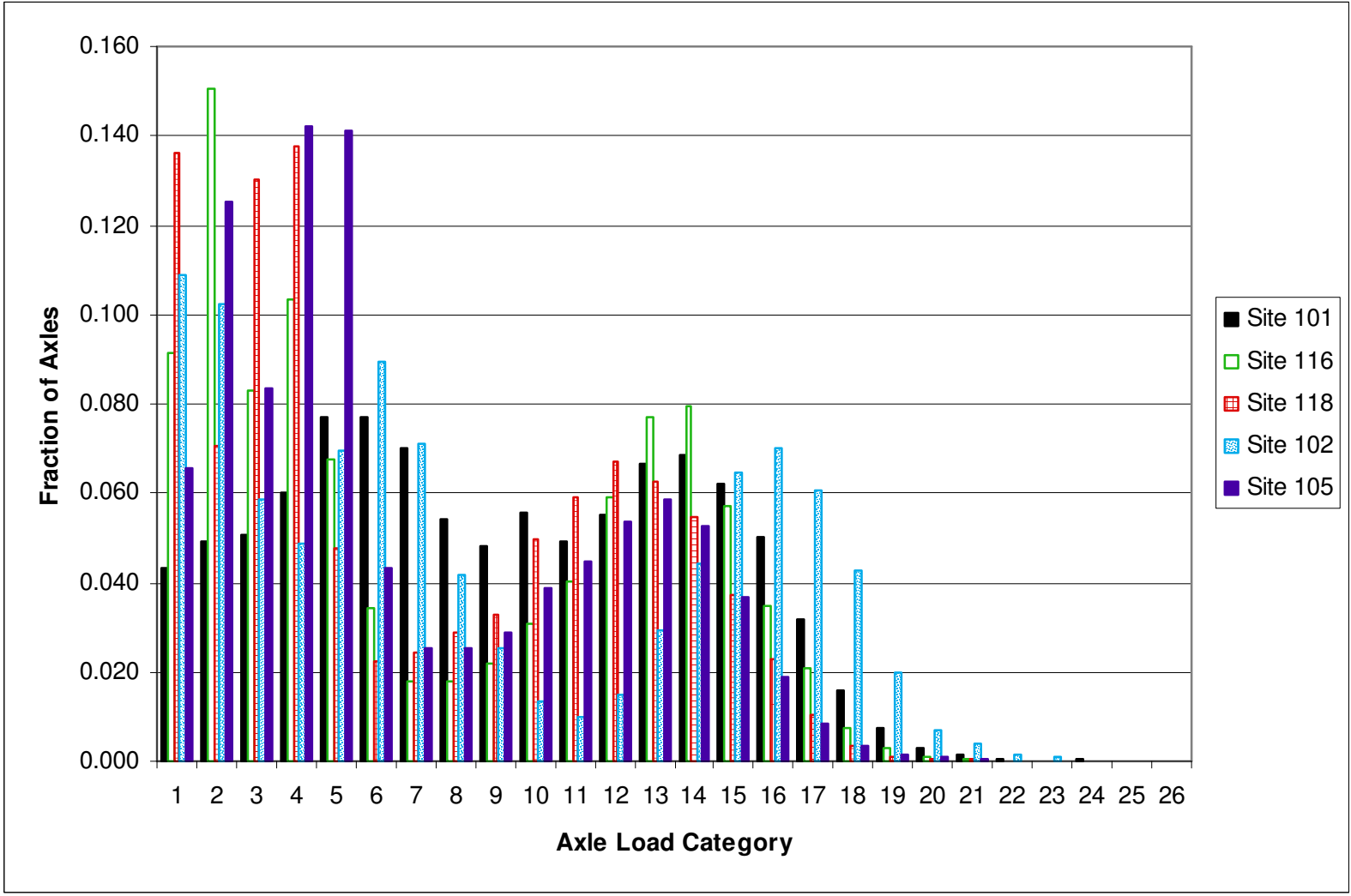


Figure II-19 Average Annual Tandem Axle Load Distribution for Class 13 Trucks, Bimodal Truck Weight Road Group

To look for further insight into the status of the Site 102 scale calibration a review of the 12 monthly single axle load distributions for Class 9 trucks is shown in Figure II-20. For a consistently calibrated site, this distribution should be stable throughout the year. Figure II-20 indicates that the scale calibration for this site may not have been stable throughout much of the year. Without local knowledge of expected changes in the commodities being carried at this site to contradict this conclusion, the recommendation is to remove this site from the group average. If additional analysis shows that a significant overload condition exists at Site 102, that site may need to be treated as a unique traffic loading pattern.

III-4.5 LIGHTLY LOADED – PRIMARILY EMPTY

The fourth TWRG represents road segments where unloaded trucks dominated the truck loading pattern. Figure II-21 illustrates the tandem axles load distribution pattern common to these sites. A significant peak exists for very lightly loaded tandem axles, with little or no peak in the loaded axle weight ranges.

This pattern is relatively common in the national LTPP database, but only two sites in the Montana data supplied for this effort illustrated this trend. One of those two sites, Site 109 was on a low truck volume road (SR-273, near Galen). It averaged less than five Class 9 trucks per day during the year and essentially no multi-trailer trucks. The other site in this group, Site 115, was on US-87 near Fort Benton. It carried substantial truck traffic (over 75 combination trucks per day).

A review of Figures II-21 and II-22 suggests that Site 109 was over-calibrated relative to Site 115. Site 109 had a large percentage of heavy tandem axle weights for both Class 9 and Class 6 trucks relative to what was measured at Site 115. These axles were heavy in comparison to most other tandem axles measured at other sites in the Montana data set. Finally, the loaded peak for Class 9 trucks was located in load category 17, which corresponds to 36,000 to 38,000 pounds, a value that exceeds the legal limits. However, given the small number of trucks included in the Site 109 data set and without on-site calibration, it is uncertain whether this site had an overload or scale calibration problem. Site-specific calibration checks are needed to answer this question.

The initial assumption for the development of traffic load inputs for using the MEPDG in Montana is that Site 109 is somewhat over-calibrated. As a result, it is suggested that the Lightly Loaded TWRG use only the weights from Site 115 until the calibration of Site 109 can be confirmed.

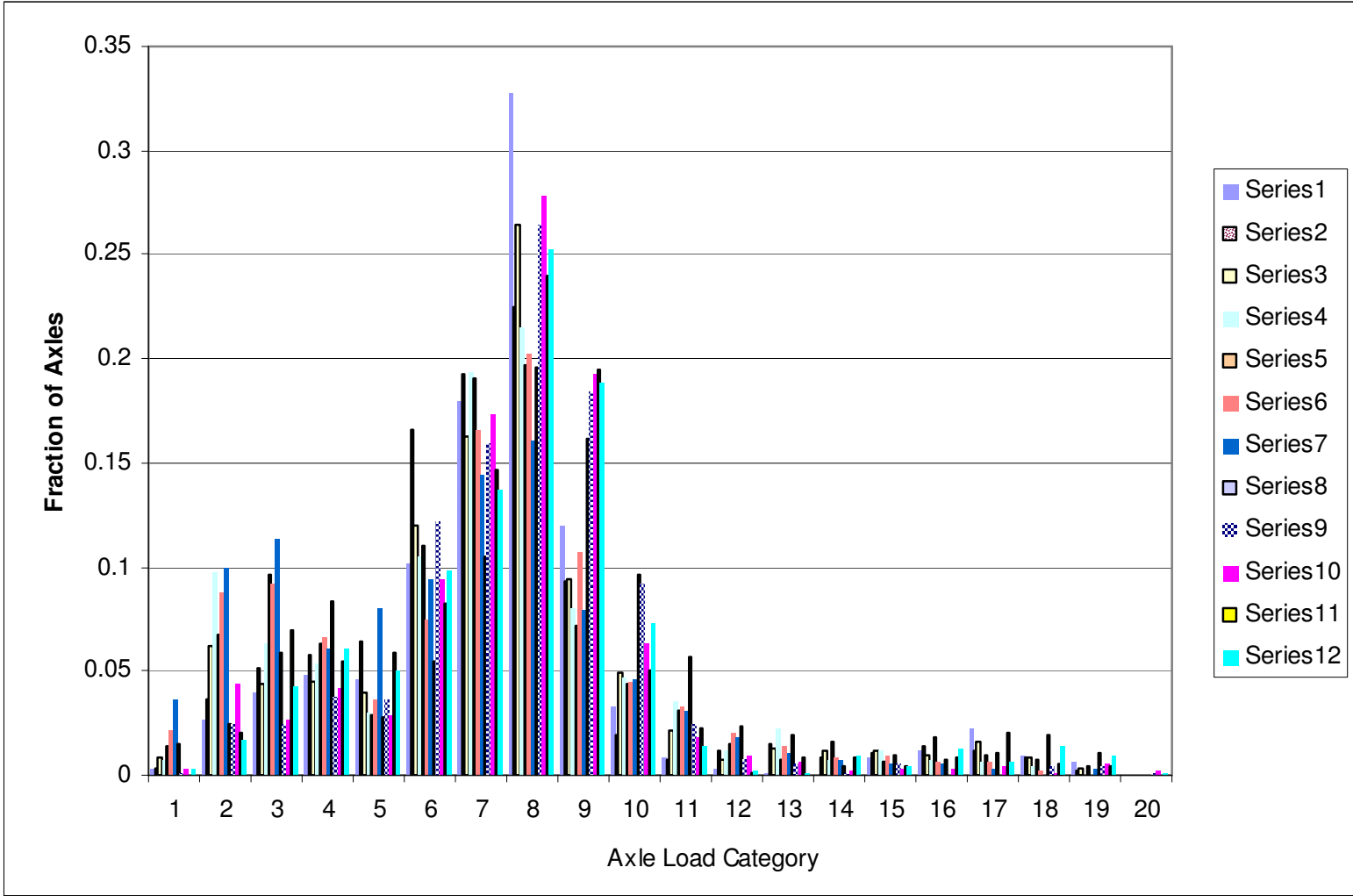


Figure II-20 Monthly Single Axle Load Distribution for Class 9 Trucks, at Site 102

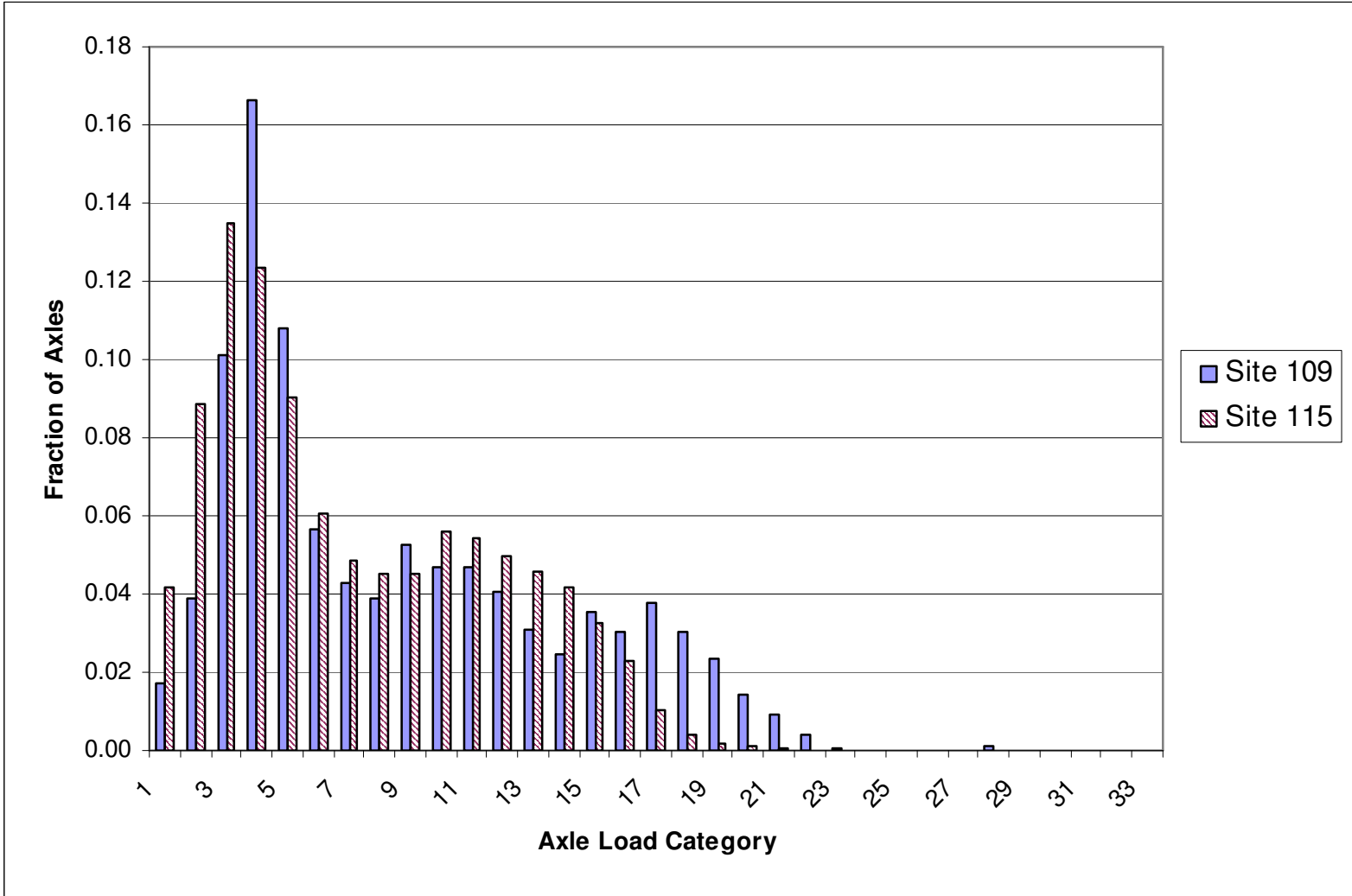


Figure II-21 Average Annual Tandem Axle Load Distribution for Class 9 Trucks, Lightly Loaded Truck Weight Road Group

II-96

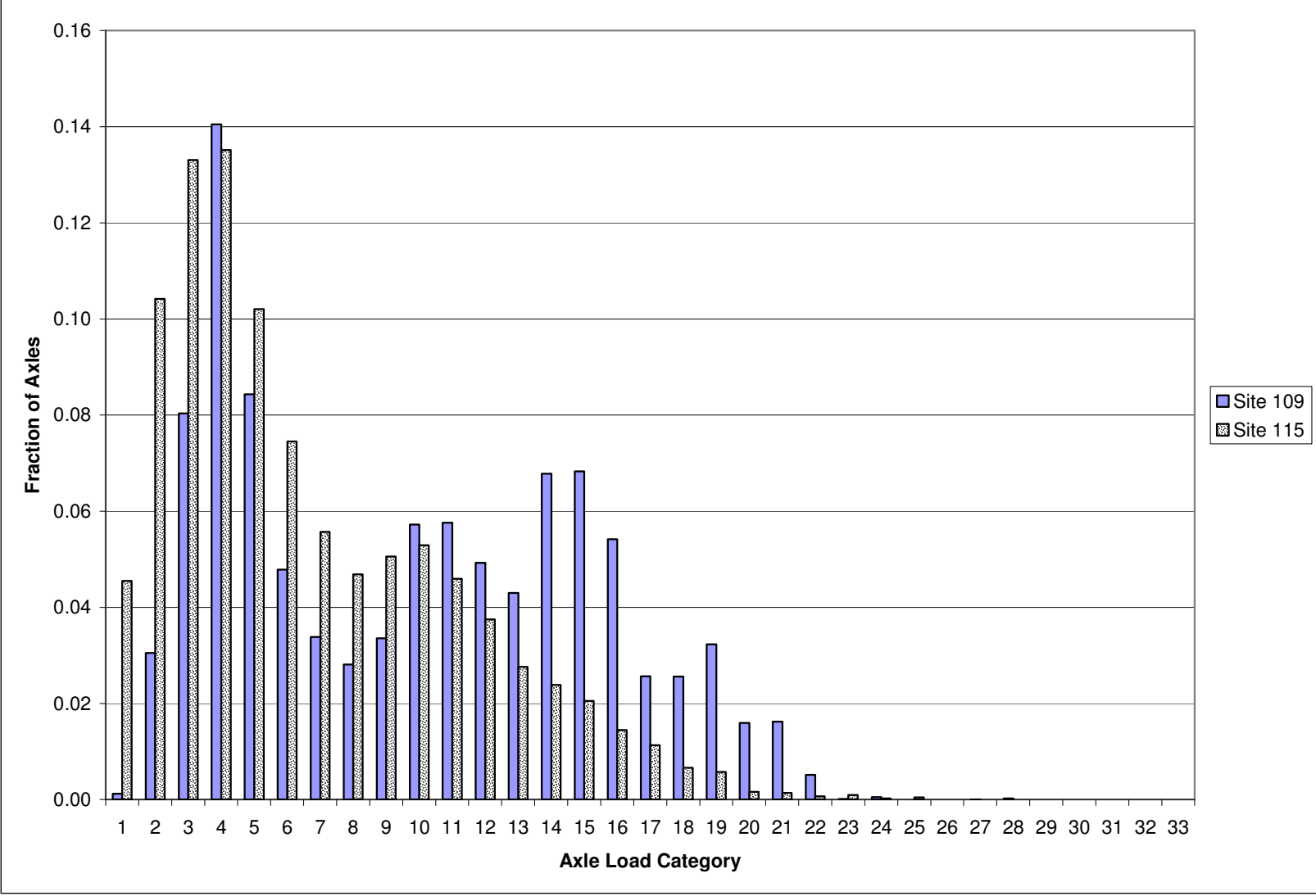


Figure II-22 Average Annual Tandem Axle Load Distribution for Class 6 Trucks, Lightly Loaded Truck Weight Road Group

III-4.6 FLAT DISTRIBUTION – EVEN LOAD

The last tandem axle weight distribution pattern observed was apparent at Site 113. This WIM site had a tandem axle load distribution curve for Class 9 trucks that was essentially flat between axle load category 5 (12,000 to 14,000 lbs) and category 16 (34,000 to 26,000 lbs) (see Figure II-23). This was the only site with such an even distribution. The even distribution was a sign that either many trucks at this site carried partial loads or the scale had significant calibration difficulties.

A review of the graph that depicts the 12 monthly tandem axle load distributions (see Figure II-24) and the graph for monthly average distribution of front axle weights for Class 9 trucks (see Figure II-25) indicates that this site probably had significant calibration difficulties. The distribution of axle weights changed from one exhibiting very light axles for April through July 2000, to one with very heavy axles in November 2000 through January 2001. Note that the weight data supplied by MDT ran from May 2000 through July 2001, so the axle load distributions shown in these figures for May, June, and July include data from two different time periods. This may disguise some of the possible drift in WIM scale calibration. When combined these very different patterns yield an evenly distributed pattern unlike what is likely being experienced at this site.

Unlike Site 109, which exhibited signs of significant scale calibration drift, Site 113 had large Class 9 truck volumes (approximately 170 Class 9 trucks per day), so a lack of Class 9 truck volume is unlikely to be the cause of an inability to maintain scale calibration. According to the information included on MDT station records, however, the scale used a piezo-electric sensor. These sensors are known to periodically experience calibration drift problems associated with an inability to control changes in the weight sensor's sensitivity to temperature fluctuations.

A month-by-month review of the tandem axle load distribution for Class 9 trucks indicates that if calibration were held constant, this site might belong in the Heavy Bimodal axle distribution TWRG. However, without considerably more information on scale calibration at this site or local knowledge about trucking activities on this road, it is inappropriate at this time to assign this site to a specific TWRG.

It is recommended that Montana consider not using this particular truck weight group for pavement design until additional work confirms that the data observed accurately describe actual axle loading conditions.

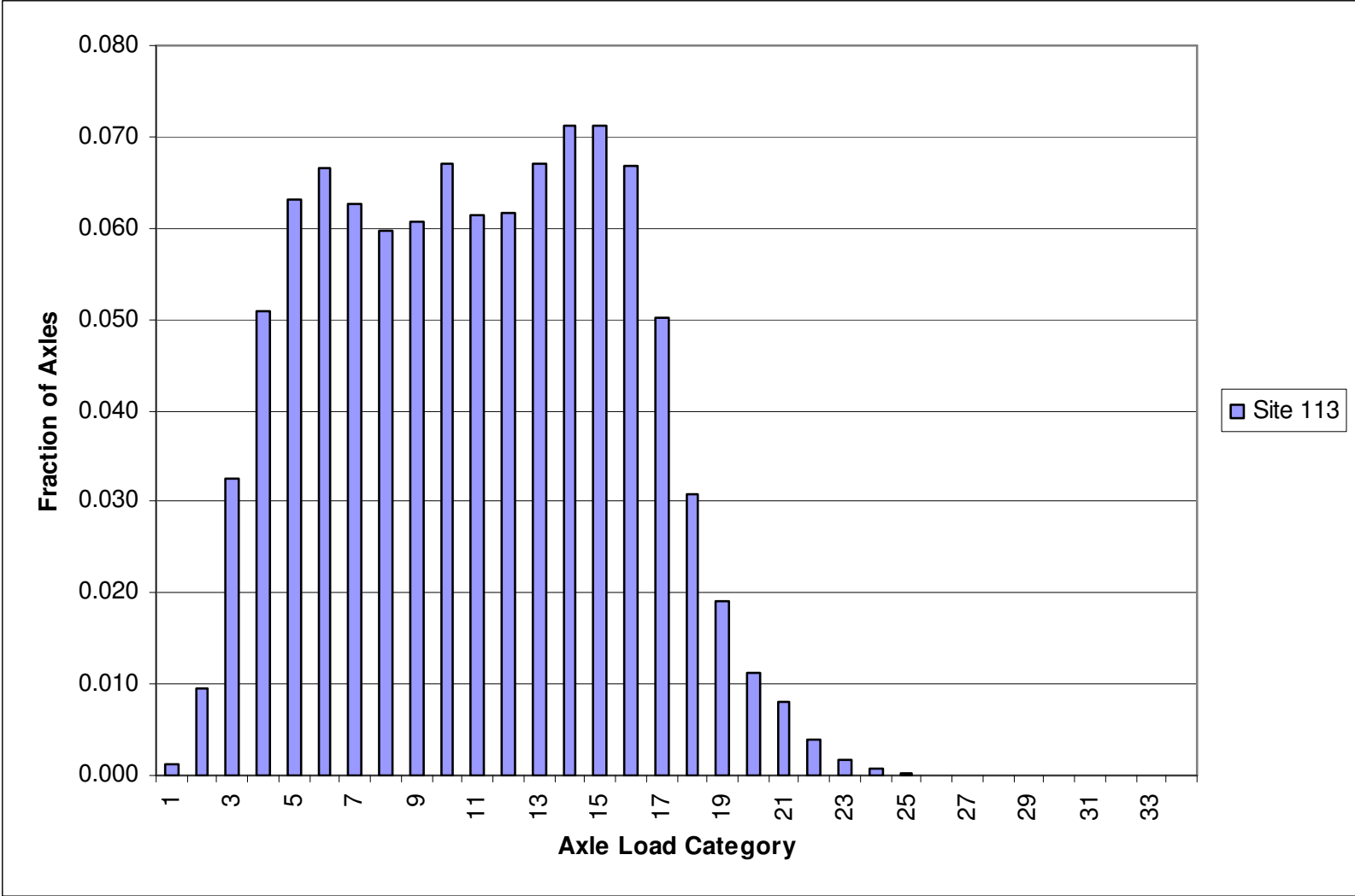


Figure II-23 Average Annual Tandem Axle Load Distribution for Class 9 Trucks, Flat Truck Weight Road Group

II-99

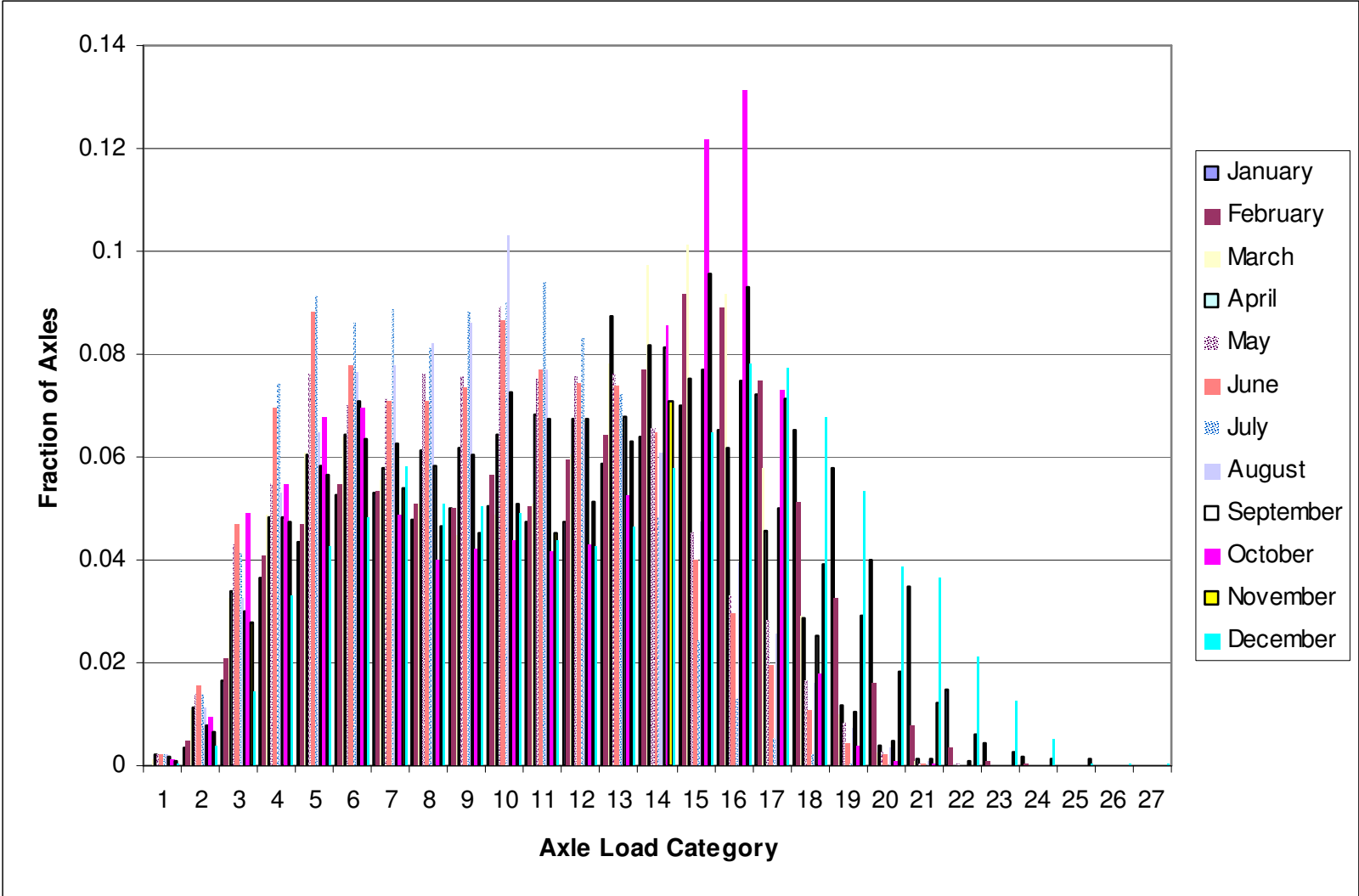


Figure II-24 Average Monthly Tandem Axle Load Distribution for Class 9 Trucks, Site 113

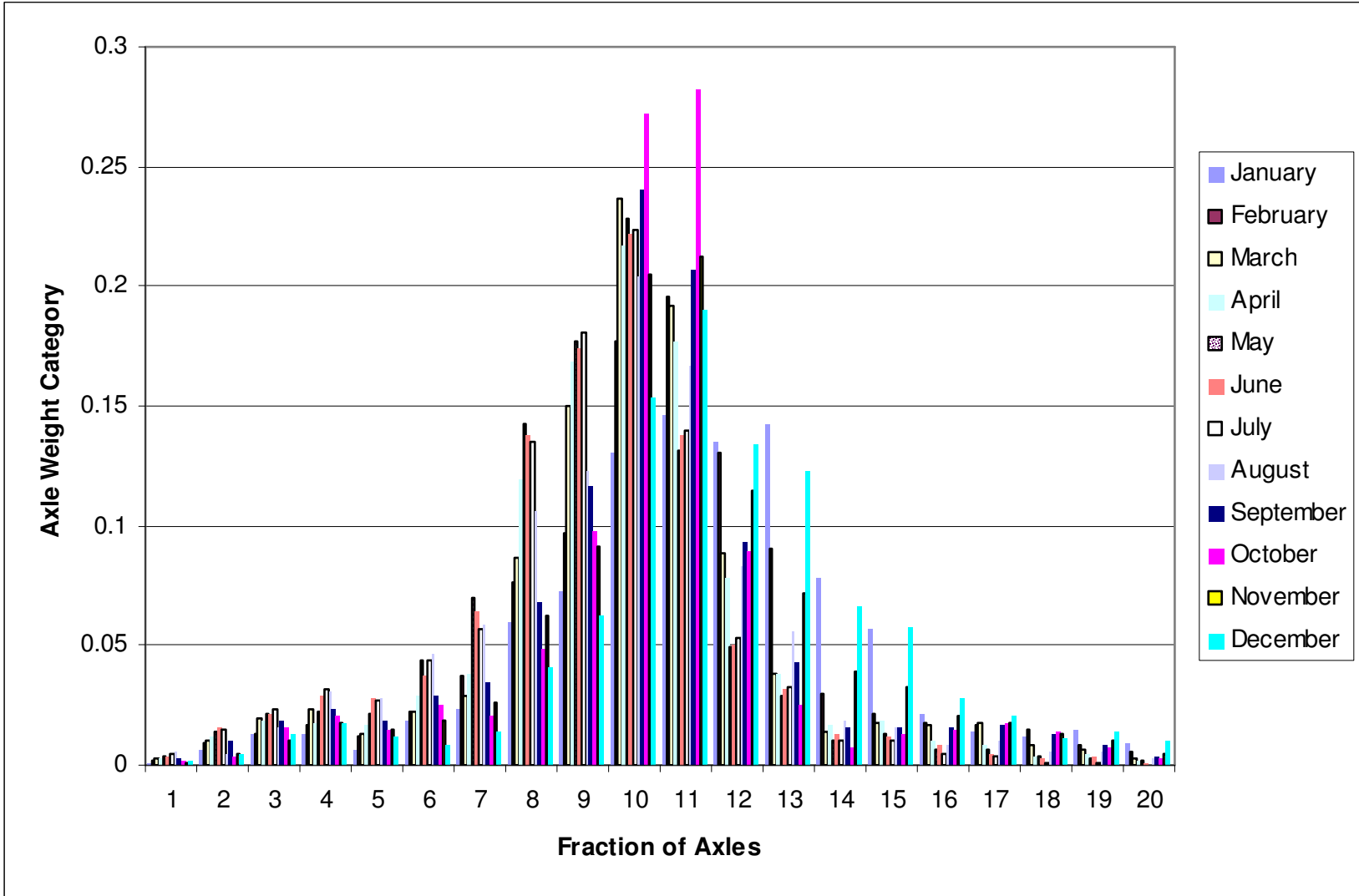


Figure II-25 Average Monthly Tandem Axle Load Distribution for Class 9 Trucks, Site 113

CHAPTER III-5: SUMMARY AND CONCLUSIONS – TRAFFIC

III-5.1 SEASONAL FACTORING OF VEHICLE VOLUMES BY CLASSIFICATION

For the initial calibration of the MEPDG in Montana, it is recommended that MDT develop and apply seasonal adjustment factors for three categories of trucks: single units, combinations, and multi-trailer trucks. When these factors are applied for pavement design, MDT should use either statewide average factors or factors for site-specific, permanent data collection sites that are located on roads for which a pavement design is being developed. To use a site-specific seasonal factor, a major truck trip generator (e.g., a major urban area, a large industrial facility such as a mine, or the intersection of the route in question with another major roadway) should not be located between the continuous data collection site from which the seasonal factors have been developed and the roadway section for which the pavement is being designed.

For all other sites, the statewide average should be used for now. While a minor improvement in the accuracy of truck volume estimates might be gained by using multiple seasonal factor groups instead of a single statewide average, the complexity that such an approach brings to the traffic load estimation process does not appear to be warranted at this time.

It is recommended, however, that Montana continue to analyze its growing archive of truck volume data to determine whether a more appropriate factoring group process can be developed. In addition to the mathematical analysis of its data, the MDT should consult experts who understand the economic activity patterns of the State and can help provide explanations of what is occurring in the observed patterns. This will help determine if use of regional or functional stratifications of Montana's roads would allow a more accurate application of truck volume seasonal factors (the association of specific road sections to those groups), thus improving the accuracy of truck loading estimates used in pavement design.

III-5.2 TRUCK WEIGHT ROAD GROUPS – TWRG'S

The review of truck axle load distributions showed that the basic shape of the axle load distributions does not appear to change dramatically during the year at any given site. However, individual sites do have different axle load distribution patterns. In addition, the data analyzed for this report indicated that many Montana WIM sites experience seasonal calibration changes that can affect the accuracy of the load estimates used for pavement design.

The differences observed in the shape of axle load distributions lead to the recommendation that Montana DOT maintain four different TWRGs. TWRGs are groups of roads for which a common axle load distribution is maintained. The four recommended groups are named after the shape of the tandem axle load distribution for Class 9 trucks. The recommended road condition groups are listed below and Table II-11 identifies the WIM sites associated with each of these groups.

- Primarily Loaded – Significant Load (including all Interstates).
- Bimodal Loaded – Heavy Load (greater number of heavyweight than lightweight trucks).
- Bimodal Loaded – Even Load (even distribution between loaded and unloaded trucks).
- Lightly Loaded – Empty (primarily empty trucks).
- Flat Distribution – Even Load (**questionable data – do not use for pavement design**).

Table II-11 Assignment of WIM Sites to Truck Weight Road Groups

Truck Weight Road Groups	WIM Sites Belonging to That Group
Primarily Loaded – Significant Load	103, 104, 108, 112, 119, 202, 203, 301
Bimodal Loaded – Primarily Heavy Distribution	106, 107, 110, 111, 114
Bimodal Loaded – Primarily Even Distribution	101, 102, 105, 116, 118
Lightly Loaded – Primarily Empty	109, 115
Flat Distribution – Even Load (do not use for pavement design)	113

MDT should compute average monthly axle load distributions for each classification of trucks at each WIM site. TWRG averages can then be computed by averaging the axle load distributions for all of the sites contained in a given TWRG. This analytical process can be performed by using the software developed in NCHRP Project 1-39 (*Cambridge 2005*).

There appears to be considerable drift in the weights reported in the 2000–2001 data for a number of the Montana WIM scales. This can result in substantial shifts in estimated pavement damage computed for a given number of trucks. It is unclear whether these reported weights are correct or the data provided to the consultant team had scale calibration problems; in several cases, there were strong indications that scale calibration was drifting.

If MDT has not already developed an ongoing calibration process that confirms the accuracy and reliability of axle weight data collected by its WIM scales, such a program should be developed and implemented. At a minimum, seasonal calibration checks of several WIM stations should be performed to determine whether the observed changes in load spectrum are caused by changes in the performance of the scale, or in fact considerably heavier loads are being carried by trucks at some times of the year (usually winter).

Finally, MDT will need to perform additional work to assign individual roadway segments from around the State to the four recommended TWRGs. This assignment should be based on the relative percentage of Class 9 trucks that are operated fully, or nearly fully loaded. If no knowledge of the truck loading distribution is available, and the road in question is not an Interstate highway, it is recommended that MDT assign the road to the Bimodal-Heavy distribution. The reason for this recommendation is that most non-Interstate roads carry a reasonable number of unloaded or lightly loaded trucks, and the Bimodal-Heavy axle load distribution is the most conservative load distribution for pavement design purposes.

PART IV: DATABASE FOR CALIBRATION OF MECHANISTIC-EMPIRICAL PAVEMENT DISTRESS PREDICTION MODELS

CHAPTER IV-1: INTRODUCTION

IV-1.1 BACKGROUND

Model calibration requires the assembly and analysis of large quantities of data for many test sections. A well-designed and easy-to-use relational database can greatly ease the management and access of this information. Consequently, the design of an appropriate database structure and the population of that database is an important product for calibrating ME based distress prediction models.

The Montana ME database was structured to focus on the calibration and confirmation of ME distress prediction models. The database was developed to permit future data entries and the collective storage of test results (e.g., performance observations, material tests and properties, layer structure, traffic loads) from existing and future projects and distress surveys. This database allows for future calibration updates to enhance and refine MDT local calibration factors for use in pavement design and management.

IV-1.2 DATABASE OBJECTIVE

Stated simply, the purpose of the MDT ME database is to provide an organized data storehouse for use in improving ME distress prediction models. Improvement is defined as eliminating any bias and reducing the residual errors between the distress observations and predictions. The following lists the capabilities considered mandatory to achieve the above objective of the database.

- The MDT ME database must support calibration efforts for both present and future ME based distress prediction models for those distresses considered in managing their highway network. This database must be as practical as possible to facilitate its use and implementation.
- The MDT ME database must have the capability to store and maintain the data needed for future local calibration updates. In other words, the database must be adaptable to future projects built in Montana and allow the collective storage of test results (e.g., performance observations, material tests and properties, layer structure, traffic loads) from those future projects. In this way, MDT can draw upon results from future forensic investigations, and use the performance of pavements built within the past five years and those that will be built in the near future to enhance and refine model calibration factors.

CHAPTER IV-2: OVERVIEW OF DATABASE

As noted above, the purpose of the MDT ME database is to store appropriate flexible and composite pavement data from test sections for the continued improvement of ME distress prediction models used to design pavements and manage the MDT highway network. The minimum database elements were the inputs needed for the MEPDG prediction models, developed under NCHRP Project 1-37A (*ARA 2004a,b*) and re-calibrated under NCHRP Project 1-40D (*NCHRP 2006*). This database, however, must be flexible enough to encompass other performance-based design procedures and specifications. The ME-based distress prediction models that the database will support are summarized and referred to in Part II of this report, Selection of Distress Prediction Models.

The MDT ME database is based on Microsoft Access 2000, similar to the standard data releases for the FHWA-LTPP databases. Microsoft Access is a powerful and versatile tool for developing and populating the calibration database. It is widely available as part of the Microsoft Office suite of programs. It provides an easy-to-use interface for , among other things, querying data and generating reports that can be augmented by custom-designed data entry/reporting forms and by powerful macros (written using Visual Basic for Applications). This ME database should be perceived as a living source of data to be used in the future, similar to the LTPP database, DataPave 3.0.

IV-2.1 DATABASE DESIGN

The design of the ME database is based on tables for general project information, traffic data, climate information, pavement structure (layer) data, material property data, deflection data, and pavement performance data. The initial implementation includes only those material properties required for the MEPDG and other similar models. However, the design for the material property tables permits incorporation of other material properties that might be needed in the future. Flexibility is a key feature designed into the MDT ME database to permit the addition of future distress observations measured on existing projects and projects that will be built in the near future. The additional performance data can be used to check and update the calibration factors or coefficients with time.

The starting point for developing the MDT ME database design was the LTPP DataPave 3.0 database. The LTPP database is very good for storing climate, traffic, and measured performance data. It is less practical for storing the detailed material property data for each layer that are required for the MEPDG and other models. It was perceived desirable to retain as much of the familiar LTPP database structure as possible. Consequently, the original design of the ME database was based on similar tables for general project information, pavement structure (layer) data, and material property data combined with links to the climate, traffic, and performance tables from the LTPP DataPave 3.0 databases. Many of the definitions included in the LTPP database were adopted for the MDT ME database to ensure consistency of data elements.

The LTPP tables are not structured in an optimal way for the purposes of performance model calibration. A reason for this impractical structure is that the LTPP database must accommodate much more complicated pavement scenarios than needed for the MDT ME database objective, which is calibration. For example, LTPP sections can change over time as a consequence of construction; this is tracked by the CONSTRUCTION_NO field for each LTPP section. Calibration test sections in the database, on the other hand, must have a constant section over the analysis period; any construction-related changes to the pavement section are treated by defining a new section in the database.

The more complicated LTPP database design is not needed for the much smaller and more sharply focused calibration database, and complicates the storage and retrieval of data for performance model calibration purposes. The primary goal or design was to streamline the organization of all information required for the calibration of ME distress prediction models. Appendix II-B shows the flow chart for the relational ME database structure used to calibrate selected distress prediction models for climatic conditions in Montana, pavement design strategies, and materials.

IV-2.2 DATABASE ELEMENTS

The MEPDG software uses a hierarchical approach for defining the inputs. This hierarchical approach was envisioned and developed to facilitate the implementation process of the method. The MEPDG suggests that the best available data (the highest level of inputs) should be used and does not require the use of a specific level for all inputs. This approach allows agencies without advanced materials test equipment or with minimal axle weight data to use the program with a relatively low investment cost – a definite advantage. This hierarchical approach, however, complicates the calibration process and definitely increases the number of data elements needed to refine the ME based calibration factors and design procedures.

All inputs required for the MEPDG were included in the MDT ME database. These inputs are grouped into six basic types including general section information, layered structure information, traffic, climate, material properties, pavement responses or deflection basins, and measures of performance. Appendix II-C provides a tabular listing of the database elements included within each data category.

IV-2.3 DATABASE STRUCTURE

The basic structure and organization of Montana's ME database is conceptually shown in Appendices II-B and II-C. Appendix II-B includes a flow chart for the MDT ME database and the organization of that data for use in calibration studies. Appendix II-C includes a tabular listing of the data elements and format included in the database. Both appendices provide a quick overview of the available information and data in ME database.

IV-2.4 DATABASE OPERATION AND UPGRADES

Appendix II-D contains a process that MDT can use to populate and upgrade the database. Part 1 gives a general review of the population process. Part 2 presents the steps necessary to append (upgrade) the MDT database with the latest LTPP release. Part 3 indicates how to update the database with data from non-LTPP test sections.

CHAPTER IV-3: DATABASE POPULATION

Tables II-12 and II-13 list the projects and test sections that were used to initially populate the MDT ME database. A total of 107 test sections are currently included in the MDT ME database. The test sections consist of both LTPP and non-LTPP test sections located in Montana and in States adjacent to Montana, most of which were used in the calibration refinement study for this project. Table II-12 lists the test sections located in Montana – thirteen are non-LTPP projects and thirty-nine are included in the LTPP program. Table II-13 lists the test sections that are located in adjacent States. All of these test sections are included in the LTPP program.

Table II-12 Data from the LTPP and Non-LTPP Test Sections Located in Montana Included in the MDT ME Database

ID Number	Section/LTPP ID Number	ID Number	Section/LTPP ID Number
358	30-0113	384	30-0903
359	30-0114	385	30-1001
360	30-0115	386	30-6004
361	30-0116	387	30-7066
362	30-0117	388	30-7075
363	30-0118	389	30-7076
364	30-0119	390	30-7088
365	30-0120	391	30-8129
366	30-0121	392	30-A310
367	30-0122	393	30-A320
368	30-0123	394	30-A330
369	30-0124	395	30-A350
370	30-0502	440	30-Geyser E
371	30-0503	442	30-Silver City W
372	30-0504	443	30-Deerlodge/Beckhill
373	30-0505	444	30-Perma
374	30-0506	445	30-Condon N
375	30-0507	446	30-Hammond NW
376	30-0508	447	30-Wolf Point S
377	30-0509	448	30-Fort Belknap
378	30-0560	449	30-Roundup E
379	30-0561	450	30-Lavina W
380	30-0805	452	30-Lothair E
381	30-0806	453	30-Baum Road
382	30-0901	454	30-Vaughn N
383	30-0902		

**Table II-13 Data from the LTPP Test Sections Located in States Adjacent to
 Montana Included in the MDT ME Database**

ID Number	State	Section/LTPP ID Number	ID Number	State	Section/LTPP ID Number
347	Idaho	16-1001	413	Wyoming	56-7772
348	Idaho	16-1005	412	Wyoming	56-7773
349	Idaho	16-1007	414	Wyoming	56-7775
350	Idaho	16-1009	416	Alberta	81-0501
351	Idaho	16-101	417	Alberta	81-0502
352	Idaho	16-1020	418	Alberta	81-0503
353	Idaho	16-1021	419	Alberta	81-0504
354	Idaho	16-5025	420	Alberta	81-0505
355	Idaho	16-6027	421	Alberta	81-0506
356	Idaho	16-9032	422	Alberta	81-0507
357	Idaho	16-9034	423	Alberta	81-0508
396	North Dakota	38-2001	424	Alberta	81-0509
397	South Dakota	46-0803	425	Alberta	81-1803
398	South Dakota	46-0804	426	Alberta	81-1804
399	South Dakota	46-7049	427	Alberta	81-1805
400	South Dakota	46-9106	428	Alberta	81-2812
401	South Dakota	46-9187	429	Alberta	81-8529
402	South Dakota	46-9197	430	Alberta	81-A901
403	Wyoming	56-1007	431	Alberta	81-A902
404	Wyoming	56-2015	432	Alberta	81-A903
405	Wyoming	56-2017	433	Saskatchewan	90-1802
406	Wyoming	56-2018	434	Saskatchewan	90-6400
407	Wyoming	56-2019	435	Saskatchewan	90-6405
408	Wyoming	56-2020	436	Saskatchewan	90-6410
409	Wyoming	56-2037	437	Saskatchewan	90-6412
410	Wyoming	56-6029	438	Saskatchewan	90-6420
411	Wyoming	56-6031	439	Saskatchewan	90-6801
412	Wyoming	56-6032			

PART V: REFERENCES

- Al-Omari, B. and Darter, M.I. (1992) *Relationships Between IRI and PSR*. Report No. UILU-ENG-92-2013. Illinois Department of Transportation. Springfield, IL.
- Allen, D.L. and Deen, R.C. (1980) "Rutting Models for Asphaltic Concrete and Dense-Grade Aggregate from Repeated-Load Tests." *Proceedings Vol. 49*. Association of Asphalt Paving Technologists. Louisville, KY.
- American Association of State Highway and Transportation Officials (AASHTO). (1987) *Summary of Results of 1987 AASHTO Rideability Survey*. Washington, DC.
- American Association of State Highway and Transportation Officials (AASHTO). (1993) *AASHTO Guide of Pavement Structures*. Washington, DC.
- Anderson, D.I. and Peterson, D.E. (1979) *Pavement Rehabilitation Design Strategies*. Final Report No. FHWA-UT-79/6. Utah Department of Transportation. Salt Lake City, UT.
- Applied Research Associates, Inc. (ARA). ERES Consultants Division. (2004a) *Guide for Mechanistic-Empirical Design of New and Rehabilitated Pavement Structures: Part 1-Introduction and Part 2-Design Inputs*. Final Report. NCHRP Project 1-37A. National Cooperative Highway Research Program. Transportation Research Board. National Research Council. Washington, DC.
- Applied Research Associates, Inc. (ARA). ERES Consultants Division. (2004b) *Guide for Mechanistic-Empirical Design of New and Rehabilitated Pavement Structures: Part 3-Design Analysis and Part 4-Low Volume Roads*. Final Report. NCHRP Project 1-37A. National Cooperative Highway Research Program. Transportation Research Board, National Research Council. Washington, DC.
- Asphalt Institute (AI). (1982) *Research and Development of The Asphalt Institute's Thickness Design Manual (MS-1)*. Ninth Edition. Research Report 82-1. College Park, MD.
- Asphalt Institute (AI). (1983) *Computer Program DAMA-User's Manual*. CP-1. Lexington, KY.
- Asphalt Institute (AI). (1991) "Thickness Design – Asphalt Pavements for Highways and Streets." *Manual Series No.1 (MS-1)*. Lexington, KY.
- Ayres, M. (1997) *Development of a Rational Probabilistic Approach for Flexible Pavement Analysis*. Ph.D. Dissertation. University of Maryland, College Park, MD.
- Baladi, G. (1987) *Fatigue Life and Permanent Deformation Characteristics of Asphalt Concrete Mixes. Transportation Research Record 1227*. Transportation Research Board. National Research Council. Washington, DC.
- Barenberg, E.J. and Thompson, M.R. (1992) "Calibrated Mechanistic Structural Analysis Procedures for Pavements, Phase 2." Draft Final Report. NCHRP Project 1-26. National

- Cooperative Highway Research Program. Transportation Research Board. National Research Council. Washington, DC.
- Barker, W.R. and Brabston, W.N. (1975) *Development of a Structural Design Procedure for Flexible Airport Pavements*. FAA Report No. FAA-RD-74-199. U.S. Army Engineer Waterways Experiment Station. Federal Aviation Administration. Washington, DC.
- Brademeyer, B. (1988) *VESYS Modification*. Final Report. FHWA Work Order DTFH61-87-P-00441. Federal Highway Administration. Washington, DC.
- Cambridge Systematics, Inc. (Cambridge). (2005) *Traffic Data Collection, Analysis, and Forecasting for Mechanistic Pavement Design*. NCHRP Report 538. National Cooperative Highway Research Program. Transportation Research Board. National Research Council. Washington, DC.
- Carey, W.N. and Irick, P.E. (1960) *The Serviceability-Performance Concept*. Highway Research Bulletin No. 250. Highway Research Board. Washington, DC.
- Darter, M.I. and Barenberg, E.J. (1976) *Zero-Maintenance Pavements: Results of Field Studies on the Performance Requirements and Capabilities of Conventional Pavements*. Report No. FHWA-RD-76-015. Federal Highway Administration. Washington, DC.
- Ellis, D.S.; Jones, G.M.; and Littlefield, G. (1969) "Thermally Induced Densification of Asphaltic Concrete." *Proceedings Vol. 38*. Association of Asphalt Paving Technologists. Los Angeles, CA.
- Epps, J.A.; Hand, A.; Seeds, S.; Schulz, T.; Alavi, S.; Ashmore, C.; Monismith, C.; Deacon, J.; Harvey J.; and Leahy, R. (2002) *Recommended Performance-Related Specification for Hot-Mix Asphalt Construction: Results of the WesTrack Project*. NCHRP Report No. 455. National Cooperative Highway Research Program. Transportation Research Board. National Research Council. Washington, DC.
- Federal Highway Administration (FHWA). (1978) *Predictive Design Procedures – VESYS Users Manual*. Report No. FHWA-RD-77-154. Washington, DC.
- Federal Highway Administration (FHWA). (2003) *Distress Identification Manual for Long Term Pavement Performance Program (Fourth Revised Edition)*. Publication No. FHWA-RD-03-031. Washington, DC.
- Finn, F.N.; Nair, K.; and Hilliard, C. (1973) *Minimizing Premature Cracking of Asphalt Concrete Pavements*. NCHRP Report 195. National Cooperative Highway Research Program. National Research Council. Washington, DC.
- Finn, F.N.; Saraf, C.L.; Kulkarni, R.; Nair, K.; Smith, W.; and Abdullah, A. (1986) *Development of Pavement Structural Subsystems*. NCHRP Report 291. National Cooperative Highway Research Program. Transportation Research Board. National Research Council. Washington, DC.

- Haas, R.; Meyer, F.; Assaf, G.; and Lee, H. (1987) "A Comprehensive Study of Cold Climate Airfield Pavement Cracking." *Proceedings Vol. 56*. Association of Asphalt Paving Technologists. Reno, NV.
- Hajek, J.J. and Haas, R.C.G. (1972) *Predicting Low-Temperature Cracking Frequency of Asphalt Concrete Pavement. Transportation Research Record 407*. Transportation Research Board. National Research Council. Washington, DC.
- Huang, Y.H. (1993) *Pavement Analysis and Design*. Prentice Hall. Englewood Cliffs, NJ.
- Illinois Department of Transportation (IL DOT). (1989) *Mechanistic Pavement Design, Supplement to Section 7 of the Illinois Department of Transportation Design Manual*. Springfield, IL.
- Jones, G.M.; Darter, M.I.; and Littlefield, G. (1986) "Thermal Expansion-Contraction of Asphaltic Concrete." *Proceedings Vol. 37*. Association of Asphalt Paving Technologists. Atlanta, GA.
- Kaloush, K.E. (2001) *Simple Performance Test for Permanent Deformation of Asphalt Mixes*. Ph.D. Dissertation. Arizona State University. Tempe, AZ.
- Kaloush, K.E. and Witczak, M.W. (2002) "Development of a Permanent to Elastic Strain Ratio Model for Asphalt Mixtures." *Inter-Team Technical Report*. NCHRP Project 1-37A. National Cooperative Highway Research Program. University of Maryland. College Park, MD.
- Kayner, L.; Kirlanda, M.; and Sparks, G. (1990) *Development of Bayesian Regression Model to Predict Hot-Mix Asphalt Concrete Overlay Roughness*. Transportation Research Record No. 1539. Transportation Research Board. National Research Council. Washington, DC.
- Kenis, W.J. (1977) "Predictive Design Procedures – A Design Method for Flexible Pavements Using the VESYS Structural Subsystem." *Proceedings Vol. 1*. Fourth International Conference on the Structural Design of Asphalt Pavements. The University of Michigan. Ann Arbor, MI.
- Khedr, S.A. (1985) *Deformation Characteristics of Granular Base Course in Flexible Pavements. Transportation Research Record 1043*. Transportation Research Board. National Research Council. Washington, DC.
- Khedr, S.A. (1986) "Deformation Mechanism in Asphaltic Concrete." *Journal of Transportation Engineering*. American Society of Civil Engineers. Volume 12 No.1. Reston, VA.
- Larson, G. and Dempsey, B.J. (1997) *Enhanced Integrated Climatic Model (Version 2.0)*. Report No. DTFA MN/DOT 72114. University of Illinois at Urbana-Champaign. Urbana, IL.
- Leahy, R.B. (1989) *Permanent Deformation Characteristics of Asphalt Concrete*. Ph.D. Dissertation. University of Maryland. College Park, MD.
- Littlefield, G. (1967) "Thermal Expansion-Contraction of Utah Asphalt Concretes." *Proceedings Vol. 36*. Association of Asphalt Paving Technologists. Denver, CO.

- Lytton, R.L.; Pufahl, D.E.; Michalak, C.H.; Liang, H.S. and Dempsey, B.J. (1990) *An Integrated Model of the Climatic Effects on Pavements*. Report No. FHWA-RD-90-03. Federal Highway Administration. Washington, DC.
- Lytton, R.L.; Shanmugham, U.; and Garrett, B.D. (1983) *Design of Asphalt Pavements for Thermal Cracking*. Report No. 284-4. Texas Transportation Institute. Texas A&M University. College Station, TX.
- Lytton, R.L.; Uzan, J.; Fernando, E.G.; Roque, R.; Hiltunen, D.; and Stoffels, S.M. (1993) *Development and Validation of Performance Prediction Models and Specifications for Asphalt Binders and Paving Mixes*. Report No. SHRP-A-357. Strategic Highway Research Program. National Research Council. Washington, DC.
- Majidzadeh, K.; Aly, M.; Bayomy, F.; and El-Laithy, A. (1980) *Implementation of a Pavement Design System Volumes 1 and 2 of the Final Report*. Research Project EES 579. Ohio State University. Columbus, OH.
- Majidzadeh, K.; Bayomy, F.; and Khedr, S. (1978) *Rutting Evaluation of Subgrade Soils in Ohio*. *Transportation Research Record 671*. Transportation Research Board. National Research Council. Washington, DC.
- Maupin, G.W., Jr.; and Freeman, J.R., Jr. (1976) *Sample Procedure for Fatigue Characterization of Bituminous Concrete*. Report No. FHWA-RD-76-102. Federal Highway Administration. Washington, DC.
- May, R. W. and Witczak, M.W. (1992) "An Automated Asphalt Concrete Mix Analysis System." *Proceedings Vol. 61*. Association of Asphalt Paving Technologists. Charleston, SC.
- McLeod, N.W. (1987). "Pen-Vis Number (PVN) as a Measure of Paving Asphalt Temperature Susceptibility and its Application to Pavement Design." *Proceedings. Paving in Cold Areas Workshop*. Volume 1.
- Moavenzdeh, F.; Soussou, J.E.; Findakly, H.K.; and Brademeyer, B. (1974) *Synthesis for Rational Design of Flexible Pavements, Part 3: Operating Instructions and VESYS Program Documentation*. Final Report. FHWA Contract FH 11-776. Federal Highway Administration. Washington, DC.
- Molenaar, A.A.A. (1983) *Structural Performance and Design of Flexible Road Construction and Asphalt Concrete Overlay*. Ph.D. Dissertation. Delft University of Technology. Netherlands.
- Monismith, C.L.; Deacon, J.A.; and Harvey, J.T. (2000) *WesTrack: Performance Models for Permanent Deformation and Fatigue*. Pavement Research Center. Institute of Transportation Studies. University of California at Berkeley. Berkeley, CA.
- Monismith, C.L.; Epps, J.A.; Kasianchuk, D.A.; and McLean, D.B. (1972) *Asphalt Mixture Behavior in Repeated Flexure*. Report No. TE 70-5. Institute of Transportation and Traffic Engineering. University of California at Berkeley. Berkeley, CA.

- Montana Department of Transportation (MDT). (2000) *Montana Pavement Management System – Manual of Rating Instructions, 2000 Edition*. Pavement Analysis and Research Section. Helena, MT.
- National Cooperative Highway Research Program (NCHRP). (2006) *Changes to the Mechanistic-Empirical Pavement Design Guide Software Through Version 0.900*. NCHRP Research Results Digest 308. NCHRP Project 1-40D. Transportation Research Board. National Research Council. Washington, DC.
- National Highway Institute (NHI). (2002) *Introduction to Mechanistic-Empirical Pavement Design. NHI Course No. 131064*. Publication No. NHI-02-043. Federal Highway Administration. Washington, DC.
- Owusu-Antwi, E.B.; Titus-Glover, L.; Khazanovich, L.; and Roessler, J.R. (1997) *Development and Calibration of Mechanistic-Empirical Distress Models for Cost Allocation*. Final Report. Federal Highway Administration. Washington, DC.
- Paterson, W.D.O. (1989) *A Transferable Causal Model for Predicting Roughness Progression in Flexible Pavements. Transportation Research Record No. 1215*. Transportation Research Board. National Research Council. Washington, DC.
- Perera, R.W.; Byrum, C.; and Kohn, S.D. (1998) *Investigation of Development of Pavement Roughness*. Report No. FHWA-RD-97-147. Federal Highway Administration. Washington, DC.
- Powell, W.D.; Potter, J.F.; Mayhew, H.C.; and Nunn, M.E. (1984) *The Structural Design of Bituminous Pavements*. TRRL Laboratory Report 1132. Transportation and Road Research Laboratory. United Kingdom.
- Rauhut, J.B.; Lytton, R.L.; and Darter, M.I. (1984a) *Pavement Damage Functions and Load Equivalence Factors. Vol. 1*. Report No. FHWA/RD-84/018. Federal Highway Administration. Washington, DC.
- Rauhut, J.B.; Lytton, R.L.; and Darter, M.I. (1984b) *Pavement Damage Functions for Cost Allocation, Vol. 2 – Description of Detailed Studies*. Report No. FHWA/RD-84/019. Federal Highway Administration. Washington, DC.
- Roque, R.; Hiltunen, D.R.; and Buttlar, W.G. (2000) "Modification and Re-Calibration of Superpave Thermal Cracking Model." Inter-Team Draft Final Report. NCHRP Project 1-37A. National Cooperative Highway Research Program. National Research Council. Washington, DC.
- Ruth, B.E.; Bloy, L.A.K.; and Avital, A.A. (1982) "Prediction of Pavement Cracking at Low Temperatures." *Proceedings Vol. 51*. Association of Asphalt Paving Technologists. Louisville, KY.
- Sebaaly, P.; Law, S.; and Hand, A. (1995) *Performance Models for Flexible Pavement Maintenance Treatments. Transportation Research Record No. 11508*. Transportation Research Board. National Research Council. Washington, DC.

- Shahin, M.Y. and McCullough, B.F. (1973) *Prediction of Low-Temperature and Thermal-Fatigue Cracking in Flexible Pavements*. Report CFHR 1-8-69-123-14. University of Texas at Austin. Austin, TX.
- Shell International Petroleum (Shell). (1978) *Shell Pavement Design Manual – Asphalt Pavements and Overlays for Road Traffic*. London, England. United Kingdom.
- Sousa, J.; Craus, J.; and Monismith, C.L. (1991) *Summary Report on Permanent Deformation in Asphalt Concrete*. Report No. SHRP-A/IR-91-104. Strategic Highway Research Program. Washington, DC.
- Strategic Highway Research Program (SHRP). (1993) *Distress Identification Manual for the Long Term Pavement Performance Project*. Report No. SHRP-P-338. National Research Council. Washington, DC.
- Strategic Highway Research Program (SHRP). (1994) *Permanent Deformation Response of Asphalt-Aggregate Mixes*. Report No. SHRP-A-414. National Research Council. Washington, DC.
- Thompson, M.R. (1987) “ILLI-PAVE Based Full-Depth Asphalt Concrete Pavement Design Procedure.” *Proceedings*. 6th International Conference on Structural Design of Asphalt Pavements. University of Michigan. Ann Arbor, MI.
- Tseng, K. and Lytton, R. (1989) “Prediction of Permanent Deformation in Flexible Pavement Materials.” *Implication of Aggregates in the Design, Construction and Performance of Flexible Pavements*. ASTM STP 1016. American Society for Testing and Materials. West Conshocken, PA.
- Tuckett, G.M.; Jones, G.M.; and Littlefield, G. (1970) “The Effects of Mixture Variables on Thermally Induced Stresses in Asphaltic Concrete.” *Proceedings Vol. 39*. Association of Asphalt Paving Technologists. Kansas City, MO.
- Van der Poel, C.J. (1954) “A General System Describing the Visco-Elastic Properties of Bitumens and its Relation to Routine Test Data.” *Journal of Applied Chemistry*. Volume 4.
- Verstraeten, J.; Veverka, V.; and Francken, L. (1982) “Rational and Practical Designs of Asphalt Pavements to Avoid Cracking and Rutting.” *Proceedings*. Fifth International Conference on the Structural Design of Asphalt Pavements. University of Michigan. Ann Arbor, MI.
- Von Quintus, H.L. and Killingsworth, B.M. (1998) *Analyses Relating to Pavement Material Characterizations and Their Effects on Pavement Performance*. Publication No. FHWA-RD-97-085. Federal Highway Administration. Washington, DC.
- Von Quintus, H.L. and Moulthrop, J.S. (2007a) *Performance Prediction Models: Volume I Executive Research Summary*. No. FHWA/MT-07-008/8158-1. Montana Department of Transportation. Research Programs. Helena, MT.

- Von Quintus, H.L. and Moulthrop, J.S. (2007b) *Performance Prediction Models: Volume III Field Guide – Calibration and User’s Guide for the Mechanistic-Empirical Pavement Design Guide*. No. FHWA/MT-07-008/8158-3. Montana Department of Transportation. Research Programs. Helena, MT.
- Von Quintus, H.L.; Andrei, D.; and Schwartz, C. (2005a) *Expand Population of M-E_DPM Database and Conduct Two Pre-Implementation Studies*. Final Report. NCHRP 9-30(001). Fugro Consultants LP and ARA Inc. ERES Consultants Division. National Cooperative Highway Research Program. Transportation Research Board. National Research Council. Washington, DC.
- Von Quintus, H.L.; Darter, M.I.; and Mallela, J. (2005b) “Phase I – Local Calibration Adjustments for the HMA Distress Prediction Models in the M-E Pavement Design Guide Software.” *Interim Report*. NCHRP Project 1-40B. National Cooperative Highway Research Program. National Research Council. Washington, DC.
- Von Quintus, H.L.; Scherocman, J.A.; Hughes, C.S.; and Kennedy, T.W. (1991) *Asphalt-Aggregate Mixture Analysis System (AAMAS)*. NCHRP Project No. 338. National Cooperative Highway Research Program. Transportation Research Board. National Research Council. Washington, DC.
- Von Quintus, H.L.; Swartz, C.; McCuen, R.H.; and Andrei, D. (2004) *Experimental Plan for Calibration and Validation of Hot Mix Asphalt Performance Models for Mix and Structural Design*. Final Report, NCHRP Project 9-30. National Cooperative Highway Research Program. Transportation Research Board. National Research Council. Washington, DC.
- WesTrack. (2000) “Part II: Performance-Related Specification.” Draft Final Report. Federal Highway Administration. Washington, DC.
- Witczak, M.W.; Kaloush, K.; Pellinen, T.; El-Basyouny, M.; and Von Quintus, H.L. (2002) *Simple Performance Test for Superpave Mix Design*. NCHRP Report No. 465. NCHRP Project 9-19. National Cooperative Highway Research Program. Transportation Research Board. National Research Council. National Academy Press. Washington, DC.

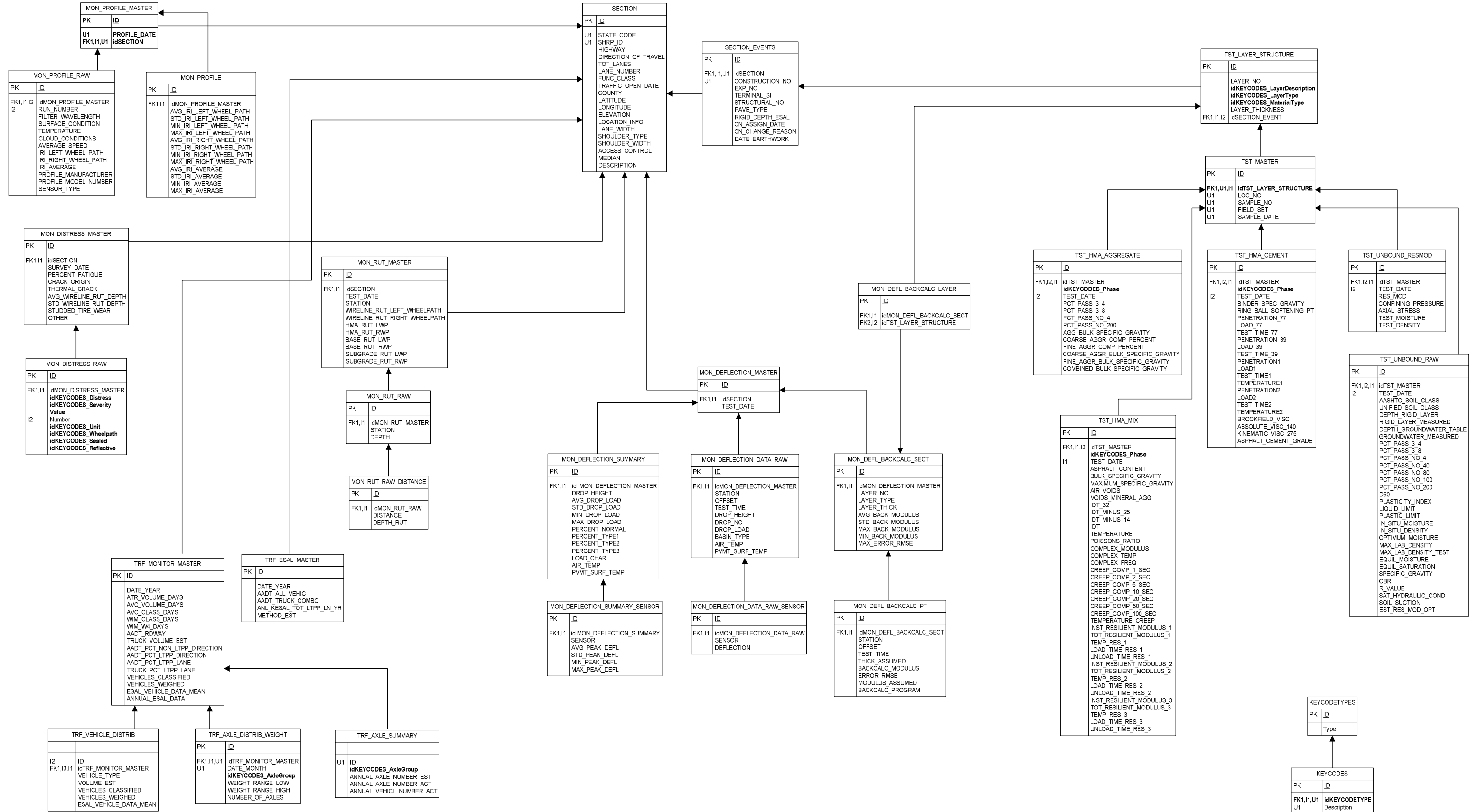
APPENDIX II-A LOAD RANGES USED FOR NCHRP PROJECT 1-37A LOAD SPECTRA

Table II-A-1 shows the upper bounds associated with the load range categories used to create the axle load distributions that are inputs to the NCHRP Project 1-37A pavement design procedures. All weights shown in this table are given in “kips” (1,000s of pounds). For example, Load Range 1 for Single Axles contains the single axles that weigh less than 3,000 pounds. Load Range 20 for tandem axles contains the axles with weights equal to or greater than 42,000 pounds but less than 44,000 pounds.

Table II-A-1 Load Ranges Used for Load Spectra Upper Limit of Load Ranges (kips) by Type of Axle Group

Load Range	Single	Tandem	Tridem	Quad
1	3	6	12	12
2	4	8	15	15
3	5	10	18	18
4	6	12	21	21
5	7	14	24	24
6	8	16	27	27
7	9	18	30	30
8	10	20	33	33
9	11	22	36	36
10	12	24	39	39
11	13	26	42	42
12	14	28	45	45
13	15	30	48	48
14	16	32	51	51
15	17	34	54	54
16	18	36	57	57
17	19	38	60	60
18	20	40	63	63
19	21	42	66	66
20	22	44	69	69
21	23	46	72	72
22	24	48	75	75
23	25	50	78	78
24	26	52	81	81
25	27	54	84	84
26	28	56	87	87
27	29	58	90	90
28	30	60	93	93
29	31	62	96	96
30	32	64	99	99
31	33	66	102	102
32	34	68		
33	35	70		
34	36	72		
35	37	74		
36	38	76		
37	39	78		
38	40	80		
39	41	82		

APPENDIX II-B: MONTANA DATABASE SCHEMA



APPENDIX II-C: TABLES DESCRIBING THE DATA ELEMENTS INCLUDED IN MONTANA'S ME DATABASE

Table Name: SECTION_INFO

Description: Provides general information about the test section.

SECTION_INFO			
Field Name	Units	Field Type	Description
MT_SECTION_ID		CHARACTER	Test section identification number.
LTPP_SECTION_ID		CHARACTER(6)	LTPP test section identification.
LTPP_EXP_NO		CHARACTER(5)	The experiment number of the test section based on the LTPP program guidelines.
HIGHWAY		CHARACTER(5)	The highway or route that the section is located on.
DIRECTION_OF_TRAVEL		CHARACTER(1)	E for East, W for West, N for North, S for South base on the direction of travel within the lane for which data is being collected.
TOT_LANES		NUMBER(1,0)	Total number of lanes in one direction.
LANE_NUMBER		NUMBER(1,0)	The number of the lane on which data is being collected. 1 is the outside lane. The others are numbered consecutively as you move to the inside edge of the pavement.
FUNC_CLASS		CHARACTER	Functional class of roadway on which section is located.
DATE_EARTHWORK		DATE	Date the earthwork was completed in the construction of the project.
DATE_HMA_PLACED		DATE	Date the hot-mix asphalt was placed in the construction of the project.
TRAFFIC_OPEN_DATE		DATE	Date the test section was opened to traffic.
COUNTY		CHARACTER	County in which the test section is located.
LATITUDE	Degrees	NUMBER(5,3)	Latitude of the test section in degrees.
LONGITUDE	Degrees	NUMBER(5,3)	Longitude of the test section in degrees.
ELEVATION	Ft	NUMBER(4,0)	Estimate of the elevation of the test section relative to sea level.
LOCATION_INFO		CHARACTER(100)	Description of the location of the test section.
LANE_WIDTH	Ft	NUMBER(2,0)	Width of the lane the test section occupies.
SHOULDER_TYPE		CHARACTER(7)	Indication of whether the shoulder is "paved," "unpaved," or "none."
SHOULDER_WIDTH	Ft	NUMBER(2,0)	The width of the shoulder in feet.
ACCESS_CONTROL		CHARACTER(1)	Y or N indicating that the roadway does or does not have controlled access.
MEDIAN		CHARACTER(1)	Y or N indicating that the roadway does or does not have a median.

Table Name: MON_DEFLECTION_DATA
Description: Peak deflections obtained from deflection testing

MON_DEFLECTION_DATA			
Field Name	Units	Field Type	Description
MT_SECTION_ID		CHARACTER	Test section identification number.
LTPP_SECTION_ID		CHARACTER(6)	LTPP test section identification.
TEST_DATE		DATE	Date of deflection test.
DROP_HEIGHT		NUMBER(1,0)	An integer code for the height from which the weight was dropped.
AVG_DROP_LOAD	Lbs	NUMBER(5,1)	The average peak drop load for the given drop height.
STD_DROP_LOAD	Lbs	NUMBER(5,1)	The standard deviation of the peak drop load for the given drop height.
MIN_DROP_LOAD	Lbs	NUMBER(5,1)	The minimum peak drop load for the given drop height.
MAX_DROP_LOAD	Lbs	NUMBER(5,1)	The maximum peak drop load for the given drop height.
AVG_PEAK_DEFL_1	Microns	NUMBER(3,0)	The average peak deflection at sensor 1.
STD_PEAK_DEFL_1	Microns	NUMBER(3,0)	The standard deviation of the peak deflection at sensor 1.
MIN_PEAK_DEFL_1	Microns	NUMBER(3,0)	The minimum peak deflection at sensor 1.
MAX_PEAK_DEFL_1	Microns	NUMBER(3,0)	The maximum peak deflection at sensor 1.
AVG_PEAK_DEFL_2	Microns	NUMBER(3,0)	The average peak deflection at sensor 2.
STD_PEAK_DEFL_2	Microns	NUMBER(3,0)	The standard deviation of the peak deflection at sensor 2.
MIN_PEAK_DEFL_2	Microns	NUMBER(3,0)	The minimum peak deflection at sensor 2.
MAX_PEAK_DEFL_2	Microns	NUMBER(3,0)	The maximum peak deflection at sensor 2.
AVG_PEAK_DEFL_3	Microns	NUMBER(3,0)	The average peak deflection at sensor 3.
STD_PEAK_DEFL_3	Microns	NUMBER(3,0)	The standard deviation of the peak deflection at sensor 3.
MIN_PEAK_DEFL_3	Microns	NUMBER(3,0)	The minimum peak deflection at sensor 3.
MAX_PEAK_DEFL_3	Microns	NUMBER(3,0)	The maximum peak deflection at sensor 3.
AVG_PEAK_DEFL_4	Microns	NUMBER(3,0)	The average peak deflection at sensor 4.
STD_PEAK_DEFL_4	Microns	NUMBER(3,0)	The standard deviation of the peak deflection at sensor 4.
MIN_PEAK_DEFL_4	Microns	NUMBER(3,0)	The minimum peak deflection at sensor 4.
MAX_PEAK_DEFL_4	Microns	NUMBER(3,0)	The maximum peak deflection at sensor 4.
AVG_PEAK_DEFL_5	Microns	NUMBER(3,0)	The average peak deflection at sensor 5.
STD_PEAK_DEFL_5	Microns	NUMBER(3,0)	The standard deviation of the peak deflection at sensor 5.
MIN_PEAK_DEFL_5	Microns	NUMBER(3,0)	The minimum peak deflection at sensor 5.
MAX_PEAK_DEFL_5	Microns	NUMBER(3,0)	The maximum peak deflection at sensor 5.
AVG_PEAK_DEFL_6	Microns	NUMBER(3,0)	The average peak deflection at sensor 6.
STD_PEAK_DEFL_6	Microns	NUMBER(3,0)	The standard deviation of the peak deflection at sensor 6.
MIN_PEAK_DEFL_6	Microns	NUMBER(3,0)	The minimum peak deflection at sensor 6.
MAX_PEAK_DEFL_6	Microns	NUMBER(3,0)	The maximum peak deflection at sensor 6.
AVG_PEAK_DEFL_7	Microns	NUMBER(3,0)	The average peak deflection at sensor 7.
STD_PEAK_DEFL_7	Microns	NUMBER(3,0)	The standard deviation of the peak deflection at sensor 7.
MIN_PEAK_DEFL_7	Microns	NUMBER(3,0)	The minimum peak deflection at sensor 7.
MAX_PEAK_DEFL_7	Microns	NUMBER(3,0)	The maximum peak deflection at sensor 7.
PERCENT_NORMAL	%	CHARACTER(6)	The percentage of basins included in the average that have normal curvature.
PERCENT_TYPE1	%	CHARACTER(6)	The percentage of basins included in the average that are a Type 1 basin.
PERCENT_TYPE2	%	CHARACTER(6)	The percentage of basins included in the average that are a Type 2 basin.
PERCENT_TYPE3	%	CHARACTER(6)	The percentage of basins included in the average that are a Type 3 basin.

LOAD_CHAR		CHARACTER(9)	The load response characterization for the given test date.
AIR_TEMP	°F	NUMBER(3,0)	Air temperature inside FWD enclosure at the start of the test sequence at this location.
PVMT_SURF_TEMP	°F	NUMBER(3,0)	The pavement surface temperature measured by the FWD automatic temperature sensor.

Table Name: MON_DEFLECTION_DATA_RAW
Description: Peak deflections obtained from deflection testing

MON DEFLECTION DATA RAW			
Field Name	Units	Field Type	Description
MT_SECTION_ID		CHARACTER	Test section identification number.
LTPP_SECTION_ID		CHARACTER(6)	LTPP test section identification.
TEST_DATE		DATE	Date of deflection test.
STATION		NUMBER(5,1)	Location of test, relative to the beginning of the test section.
OFFSET		NUMBER(3,1)	Offset of test from inside edge of shoulder stripe.
TEST_TIME		NUMBER(4,0)	Time deflection testing was initiated at this location.
DROP_HEIGHT		NUMBER(1,0)	An integer code for the height from which the weight was dropped.
DROP_NO		NUMBER(2,0)	A sequential number indicating the order of the drop in the series.
DROP_LOAD	Lbs	NUMBER(5,1)	The peak drop load.
PEAK_DEFL_1	Microns	NUMBER(3,0)	The peak deflection at sensor 1.
PEAK_DEFL_2	Microns	NUMBER(3,0)	The peak deflection at sensor 2.
PEAK_DEFL_3	Microns	NUMBER(3,0)	The peak deflection at sensor 3.
PEAK_DEFL_4	Microns	NUMBER(3,0)	The peak deflection at sensor 4.
PEAK_DEFL_5	Microns	NUMBER(3,0)	The peak deflection at sensor 5.
PEAK_DEFL_6	Microns	NUMBER(3,0)	The peak deflection at sensor 6.
PEAK_DEFL_7	Microns	NUMBER(3,0)	The peak deflection at sensor 7.
BASIN_TYPE		CHARACTER(6)	The type of deflection basin curvature that exists based on BR95-1 reports.
AIR_TEMP	°F	NUMBER(3,0)	Air temperature inside FWD enclosure at the start of the test sequence at this location.
PVMT_SURF_TEMP	°F	NUMBER(3,0)	The pavement surface temperature measured by the FWD automatic temperature sensor.

Table Name: MON_DEFL_BACKCALC_PT

Description: Results from backcalculation of FWD data at each location

MON_DEFL_BACKCALC_PT			
Field Name	Units	Field Type	Description
MT_SECTION_ID		CHARACTER	Test section identification number.
LTPP_SECTION_ID		CHARACTER(6)	LTPP test section identification.
TEST_DATE		DATE	Date of deflection test.
STATION		NUMBER(5,1)	Location of test, relative to the beginning of the test section.
OFFSET		NUMBER(3,1)	Offset of test from inside edge of shoulder stripe.
TEST_TIME		NUMBER(4,0)	Time deflection testing was initiated at this location.
LAYER_NO		NUMBER(1,0)	Unique sequential number assigned to pavement layers, starting with layer 1 as the deepest layer (subgrade).
LAYER_TYPE		CHARACTER(2)	Indication of the type of material used in the layer.
LAYER_THICK	Inches	NUMBER(3,2)	The thickness of the layer.
THICK_ASSUMED		CHARACTER(1)	Y or N indicating whether or not the thickness was assumed.
BACKCALC_MODULUS	psi	NUMBER(6,0)	The backcalculated modulus for that location.
ERROR_RMSE	%	NUMBER(4,1)	The percent error resulting from the backcalculation process.
MODULUS_ASSUMED		CHARACTER(1)	Y or N indicating whether or not the modulus was an assumed value.
BACKCALC_PROGRAM		CHARACTER(15)	The name and version of the program used to perform the backcalculation.

Table Name: MON_DEFL_BACKCALC_SECT

Description: Section statistics of the results from backcalculation of FWD data

MON_DEFL_BACKCALC_SECT			
Field Name	Units	Field Type	Description
MT_SECTION_ID		CHARACTER	Test section identification number.
LTPP_SECTION_ID		CHARACTER(6)	LTPP test section identification.
TEST_DATE		DATE	Date of deflection test.
LAYER_NO		NUMBER(1,0)	Unique sequential number assigned to pavement layers, starting with layer 1 as the deepest layer (subgrade).
LAYER_TYPE		CHARACTER(2)	Indication of the type of material used in the layer.
LAYER_THICK	Inches	NUMBER(3,1)	The thickness of the layer.
AVG_BACK_MODULUS	psi	NUMBER(6,0)	The average backcalculated modulus for the test section.
STD_BACK_MODULUS	psi	NUMBER(6,0)	The standard deviation of the moduli for that layer for the test section.
MAX_BACK_MODULUS	psi	NUMBER(6,0)	The maximum of the moduli for that layer for the test section.
MIN_BACK_MODULUS	psi	NUMBER(6,0)	The minimum of the moduli for that layer for the test section.
MAX_ERROR_RMSE	%	NUMBER(4,1)	The maximum percent error resulting from the backcalculation process for that test date.

Table Name: MON_DISTRESS

Description: Table providing cracking and rutting data for the section. This is the data used in the calibration.

MON_DISTRESS			
Field Name	Units	Field Type	Description
MT_SECTION_ID		CHARACTER	Test section identification number.
LTPP_SECTION_ID		CHARACTER(6)	LTPP test section identification.
SURVEY_DATE		DATE	Date of distress survey.
PERCENT_FATIGUE	%	NUMBER(3,1)	Percentage of wheel path area that has experienced fatigue.
CRACK_ORIGIN		CHARACTER(9)	Indication of the origination of the cracking, i.e., top-down or bottom-up.
THERMAL_CRACK	ft/mi	NUMBER(4,1)	Total length of thermal cracking per lane-mile.
AVG_WIRELINE_RUT_DEPTH	in	NUMBER(3,2)	Average rut depth for the 500-ft test section.
STD_WIRELINE_RUT_DEPTH	in	NUMBER(3,2)	Standard deviation of rut depth measurements taken on the test section.
STUDDDED_TIRE_WEAR	in	NUMBER(3,2)	Portion of rut depth due to wearing of the surface from studded tires.

Table Name: MON_DISTRESS_RAW

Description: Table providing results from LTPP-type distress survey

MON_DISTRESS_RAW			
Field Name	Units	Field Type	Description
MT_SECTION_ID		CHARACTER	Test section identification number.
LTPP_SECTION_ID		CHARACTER(6)	LTPP test section identification.
SURVEY_DATE		DATE	Date of distress survey.
GATOR_CRACK_A_L	ft ²	NUMBER(5,1)	Area of alligator (fatigue) cracking of low severity (no or few connecting cracks, not spalled or sealed, no pumping evident).
GATOR_CRACK_A_M	ft ²	NUMBER(5,1)	Area of alligator (fatigue) cracking of moderate severity (interconnected cracks possibly slightly spalled, may be sealed, pumping may be evident).
GATOR_CRACK_A_H	ft ²	NUMBER(5,1)	Area of alligator (fatigue) cracking of high severity (moderately or severely spalled interconnected cracks, may be sealed, pumping may be evident).
BLK_CRACK_A_L	ft ²	NUMBER(5,1)	Area of low severity block cracking (cracks of unknown width well sealed or with mean width of 6 mm or less).
BLK_CRACK_A_M	ft ²	NUMBER(5,1)	Area of moderate severity block cracking (mean crack width from 6 to 19 mm or under 19 mm with adjacent low severity random cracking).
BLK_CRACK_A_H	ft ²	NUMBER(5,1)	Area of high severity block cracking (mean crack width greater than 19 mm or under 19 mm with moderate to high severity random cracking).
EDGE_CRACK_L_L	ft	NUMBER(4,1)	Length of low severity edge cracking (cracks without break up or loss of material).
EDGE_CRACK_L_M	ft	NUMBER(4,1)	Length of moderate severity edge cracking (cracks with some break up and loss of material for up to 10 percent of the affected length).
EDGE_CRACK_L_H	ft	NUMBER(4,1)	Length of high severity edge cracking (considerable break up and loss of material for more than 10 percent of the affected length).

LONG_CRACK_WP_L_L	ft	NUMBER(4,1)	Length of low severity, longitudinal cracking in wheel path (cracks of unknown width well sealed or with mean width of 6 mm or less).
LONG_CRACK_WP_L_M	ft	NUMBER(4,1)	Length of moderate severity, longitudinal cracking in wheel path (mean crack width from 6 to 19 mm or under 19 mm with adjacent low severity random cracking).
LONG_CRACK_WP_L_H	ft	NUMBER(4,1)	Length of high severity, longitudinal cracking in wheel path (mean crack width greater than 19 mm or under 19 mm with adjacent moderate to high severity random cracking).
LONG_CRACK_WP_SEAL_L_L	ft	NUMBER(4,1)	Length of low severity, well sealed longitudinal cracking in wheel path (cracks of unknown width or with mean width of 6 mm or less).
LONG_CRACK_WP_SEAL_L_M	ft	NUMBER(4,1)	Length of moderate severity, well sealed longitudinal cracking in wheel path (mean crack width from 6 to 19 mm or under 19 mm with adjacent low severity random cracking).
LONG_CRACK_WP_SEAL_L_H	ft	NUMBER(4,1)	Length of high severity, well sealed longitudinal cracking in wheel path (crack mean width greater than 19 mm or under 19 mm with adjacent moderate to high severity random cracking).
LONG_CRACK_NWP_L_L	ft	NUMBER(4,1)	Length of low severity, non-wheel path longitudinal cracking (cracks of unknown width well sealed or with mean width of 6 mm or less).
LONG_CRACK_NWP_L_M	ft	NUMBER(4,1)	Length of moderate severity, non-wheel path longitudinal cracking (mean crack width from 6 to 19 mm or under 19 mm with adjacent low severity random cracking).
LONG_CRACK_NWP_L_H	ft	NUMBER(4,1)	Length of high severity, non-wheel path longitudinal cracking (mean crack width greater than 19 mm or under 19 mm with adjacent moderate to high severity random cracking).
LONG_CRACK_NWP_SEAL_L_L	ft	NUMBER(4,1)	Length of low severity, well sealed non-wheel path longitudinal cracking (cracks of unknown width or with mean width of 6 mm or less).
LONG_CRACK_NWP_SEAL_L_M	ft	NUMBER(4,1)	Length of moderate severity, well sealed non-wheel path longitudinal cracking (mean crack width from 6 to 19 mm or under 19 mm with adjacent low severity random cracking).
LONG_CRACK_NWP_SEAL_L_H	ft	NUMBER(4,1)	Length of high severity, well sealed non-wheel path longitudinal cracking (mean crack width greater than 19 mm or under 19 mm with adjacent moderate to high severity random cracking).
REFL_CRACK_TRANS_NO_L		NUMBER(3,0)	Number of low severity, transverse reflection cracks (cracks of unknown width well sealed or with mean width of 6 mm or less).
REFL_CRACK_TRANS_NO_M		NUMBER(3,0)	Number of moderate severity, transverse reflection cracks (mean crack width of 6 to 19 mm or under 19 mm with adjacent low severity random cracking).
REFL_CRACK_TRANS_NO_H		NUMBER(3,0)	Number of high severity, transverse reflection cracks (mean crack width greater than 19 mm or under 19 mm with adjacent moderate to high severity random cracking).

REFL_CRACK_TRANS_L_L	ft	NUMBER(5,1)	Length of low severity, transverse reflection cracking at joints (cracks of unknown width well sealed or with mean width of 6 mm or less).
REFL_CRACK_TRANS_L_M	ft	NUMBER(5,1)	Length of moderate severity, transverse reflection cracking at joints (mean crack width of 6 to 19 mm or under 19 mm with adjacent low severity random cracking).
REFL_CRACK_TRANS_L_H	ft	NUMBER(5,1)	Length of high severity, transverse reflection cracking at joints (mean crack width greater than 19 mm or under 19 mm with adjacent moderate to high severity random cracking).
REFL_CRACK_TRANS_SEAL_L_L	ft	NUMBER(5,1)	Length of well sealed, low severity transverse cracking (cracks of unknown width or with mean width of 6 mm or less).
REFL_CRACK_TRANS_SEAL_L_M	ft	NUMBER(5,1)	Length of well sealed, moderate severity transverse cracking (mean crack width from 6 to 19 mm or under 19 mm with adjacent low severity random cracking).
REFL_CRACK_TRANS_SEAL_L_H	ft	NUMBER(5,1)	Length of well sealed, high severity transverse cracking (mean crack width greater than 19 mm or under 19 mm with adjacent moderate to high severity random cracking).
REFL_CRACK_LONG_L_L	ft	NUMBER(4,1)	Length of low severity, longitudinal reflection cracking at joints (cracks of unknown width well sealed or with mean width of 6 mm or less).
REFL_CRACK_LONG_L_M	ft	NUMBER(4,1)	Length of moderate severity, longitudinal reflection cracking at joints (mean crack width from 6 to 19 mm or under 19 mm with adjacent low severity random cracking).
REFL_CRACK_LONG_L_H	ft	NUMBER(4,1)	Length of high severity, longitudinal reflection cracking at joints (mean crack width greater than 19 mm or under 19 mm with adjacent moderate to high severity random cracking).
REFL_CRACK_LONG_SEAL_L_L	ft	NUMBER(4,1)	The length of well sealed, low severity longitudinal reflection cracking at joints (cracks of unknown width or with mean width of 6 mm or less).
REFL_CRACK_LONG_SEAL_L_M	ft	NUMBER(4,1)	The length of well sealed, moderate severity longitudinal reflection cracking at joints (mean crack width from 6 to 19 mm or under 19 mm with adjacent low severity random cracking).
REFL_CRACK_LONG_SEAL_L_H	ft	NUMBER(4,1)	The length of well sealed, high severity longitudinal reflection cracking at joints (mean crack width greater than 19 mm or under 19 mm with adjacent moderate to high severity random cracking).
TRANS_CRACK_NO_L		NUMBER(3,0)	Number of low severity transverse cracks (cracks of unknown width well sealed or with mean width of 6 mm or less).
TRANS_CRACK_NO_M		NUMBER(3,0)	Number of moderate severity transverse cracks (mean crack width from 6 to 19 mm or under 19 mm with adjacent low severity random cracking).
TRANS_CRACK_NO_H		NUMBER(3,0)	Number of high severity transverse cracks (mean crack width greater than 19 mm or under 19 mm with adjacent moderate to high severity random cracking).

TRANS_CRACK_L_L	ft	NUMBER(5,1)	Length of low severity transverse cracking (cracks of unknown width well sealed or with mean width of 6 mm or less).
TRANS_CRACK_L_M	ft	NUMBER(5,1)	Length of moderate severity transverse cracking (crack mean width from 6 to 19 mm or under 19 mm with adjacent low severity random cracking).
TRANS_CRACK_L_H	ft	NUMBER(5,1)	Length of high severity transverse cracking (mean crack width greater than 19 mm or under 19 mm with adjacent moderate to high severity random cracking).
TRANS_CRACK_SEAL_L_L	ft	NUMBER(5,1)	The length of well sealed, low severity transverse cracking (cracks of unknown width or with mean width of 6 mm or less).
TRANS_CRACK_SEAL_L_M	ft	NUMBER(5,1)	The length of well sealed, moderate severity transverse cracking (mean crack width from 6 to 19 mm or under 19 mm with adjacent low severity random cracking).
TRANS_CRACK_SEAL_L_H	ft	NUMBER(5,1)	The length of well sealed, high severity transverse cracking (mean crack width greater than 19 mm or under 19 mm with adjacent moderate to high severity random cracking).
PATCH_NO_L		NUMBER(3,0)	Number of patches/patch deteriorations with low severity distress of any type.
PATCH_NO_M		NUMBER(3,0)	Number of patches/patch deteriorations with moderate severity distress type.
PATCH_NO_H		NUMBER(3,0)	Number of patches/patch deteriorations with high severity distress of any type.
PATCH_A_L	ft ²	NUMBER(5,1)	Area of patching with low severity distress or patch deterioration.
PATCH_A_M	ft ²	NUMBER(5,1)	Area of patching with moderate severity distress or patch deterioration.
PATCH_A_H	ft ²	NUMBER(5,1)	Area of patching with high severity distress or patch deterioration.
POTHOLES_NO_L		NUMBER(3,0)	Number of low severity potholes (less than 25 mm deep).
POTHOLES_NO_M		NUMBER(3,0)	Number of moderate severity potholes (from 25 to 50 mm deep).
POTHOLES_NO_H		NUMBER(3,0)	Number of high severity potholes (more than 50 mm deep).
POTHOLES_A_L	ft ²	NUMBER(5,1)	Area of low severity potholes (less than 25 mm deep).
POTHOLES_A_M	ft ²	NUMBER(5,1)	Area of moderate severity potholes (from 25 to 50 mm deep).
POTHOLES_A_H	ft ²	NUMBER(5,1)	Area of high severity potholes (more than 50 mm deep).
SHOVING_NO		NUMBER(3,0)	Number of areas where shoving exists.
SHOVING_A	ft ²	NUMBER(5,1)	The area of shoving, localized longitudinal displacement of the pavement surface.
BLEEDING	ft ²	NUMBER(5,1)	Presence of excess asphalt on the pavement surface, which may create a shiny, glass-like reflective surface.
POLISH_AGG_A	ft ²	NUMBER(5,1)	Area of polished aggregate (binder worn away to expose coarse aggregate).
RAVELING	ft ²	NUMBER(5,1)	Wearing away of the pavement surface caused by the dislodging of aggregate particles and loss of asphalt binder.
PUMPING_NO		NUMBER(3,0)	Number of occurrences of water bleeding and pumping.

PUMPING_L	ft	NUMBER(4,1)	Length of pavement affected by water bleeding and pumping.
OTHER		CHARACTER(80)	A description of other surface distress.

Table Name: MON_PROFILE_RAW

Description: Roughness data collected on the test section.

MON_PROFILE_RAW			
Field Name	Units	Field Type	Description
MT_SECTION_ID		CHARACTER	Test section identification number.
LTPP_SECTION_ID		CHARACTER(6)	LTPP test section identification.
TEST_DATE		DATE	Date of profile collection.
RUN_NUMBER		NUMBER(1,0)	A number indicating the position of the run in the series.
FILTER_WAVELENGTH	ft	NUMBER(5,2)	Index filter wavelength.
SURFACE_CONDITION		CHARACTER(10)	Description of the surface condition.
TEMPERATURE	°F	NUMBER(4,1)	The ambient temperature at the time of the test.
CLOUD_CONDITIONS		CHARACTER(10)	Description of the cloud conditions.
AVERAGE_SPEED	mph	NUMBER(3,1)	The average speed of the profilometer during the test.
IRI_LEFT_WHEEL_PATH	in/mi	NUMBER(4,1)	IRI value for the left wheel path.
IRI_RIGHT_WHEEL_PATH	in/mi	NUMBER(4,1)	IRI value for the right wheel path.
IRI_AVERAGE	in/mi	NUMBER(4,1)	Average of the left and right wheel path IRIs.
PROFILE_MANUFACTURER		CHARACTER(25)	Identification of the profilometer manufacturer.
PROFILE_MODEL_NUMBER		CHARACTER(10)	Manufacturer's model number for the profilometer.
SENSOR_TYPE		CHARACTER(5)	The type of sensor used in the profilometer.

Table Name: MON_PROFILE

Description: Roughness data collected on the test section.

MON_PROFILE			
Field Name	Units	Field Type	Description
MT_SECTION_ID		CHARACTER	Test section identification number.
LTPP_SECTION_ID		CHARACTER(6)	LTPP test section identification.
TEST_DATE		DATE	Date of profile collection.
AVG_IRI_LEFT_WHEEL_PATH	in/mi	NUMBER(4,1)	Average IRI value for the left wheel path.
STD_IRI_LEFT_WHEEL_PATH	in/mi	NUMBER(4,1)	Standard deviation of the IRIs measured in the left wheel path.
MIN_IRI_LEFT_WHEEL_PATH	in/mi	NUMBER(4,1)	Minimum of the IRIs measured in the left wheel path.
MAX_IRI_LEFT_WHEEL_PATH	in/mi	NUMBER(4,1)	Maximum of the IRIs measured in the left wheel path.
AVG_IRI_RIGHT_WHEEL_PATH	in/mi	NUMBER(4,1)	Average IRI value for the right wheel path.
STD_IRI_RIGHT_WHEEL_PATH	in/mi	NUMBER(4,1)	Standard deviation of the IRIs measured in the right wheel path.
MIN_IRI_RIGHT_WHEEL_PATH	in/mi	NUMBER(4,1)	Minimum of the IRIs measured in the right wheel path.
MAX_IRI_RIGHT_WHEEL_PATH	in/mi		Maximum of the IRIs measured in the right wheel path.
AVG_IRI_AVERAGE	in/mi	NUMBER(4,1)	Average of the average of the left and right wheel path IRIs.
STD_IRI_AVERAGE	in/mi	NUMBER(4,1)	Standard deviation of the average IRIs.
MIN_IRI_AVERAGE	in/mi	NUMBER(4,1)	Minimum of the average IRIs.
MAX_IRI_AVERAGE	in/mi	NUMBER(4,1)	Maximum of the average IRIs.

Table Name: MON_RUT

Description: Rut depths collected from the test section

MON_RUT			
Field Name	Units	Field Type	Description
MT_SECTION_ID		CHARACTER	Test section identification number.
LTPP_SECTION_ID		CHARACTER(6)	LTPP test section identification.
TEST_DATE		DATE	Date of rut data collection.
STATION		NUMBER(5,1)	Location of test, relative to the beginning of the test section.
WIRELINE_RUT_LEFT_WHEEL PATH	in	NUMBER(3,2)	Rut depth measured in the left wheel path.
WIRELINE_RUT_RIGHT_WHEEL PATH	in	NUMBER(3,2)	Rut depth measured in the right wheel path.
HMA_RUT_LWP	in	NUMBER(3,2)	Rut depth measured in the HMA layer in the left wheel path.
HMA_RUT_RWP	in	NUMBER(3,2)	Rut depth measured in the HMA layer in the right wheel path.
BASE_RUT_LWP	in	NUMBER(3,2)	Rut depth measured in the base layer in the left wheel path.
BASE_RUT_RWP	in	NUMBER(3,2)	Rut depth measured in the base layer in the right wheel path.
SUBGRADE_RUT_LWP	in	NUMBER(3,2)	Rut depth measured in the subgrade layer in the left wheel path.
SUBGRADE_RUT_RWP	in	NUMBER(3,2)	Rut depth measured in the subgrade layer in the right wheel path.

Table Name: MON_RUT_RAW

Description: Rut depths collected from the test section

MON_RUT_RAW			
Field Name	Units	Field Type	Description
MT_SECTION_ID		CHARACTER	Test section identification number.
LTPP_SECTION_ID		CHARACTER(6)	LTPP test section identification.
TEST_DATE		DATE	Date of rut data collection.
STATION		NUMBER(5,1)	Location of test, relative to the beginning of the test section.
DEPTH	in	NUMBER(3,1)	Depth below the surface that the transverse profile is measured.
X1	in	NUMBER(4,1)	Distance of the point from the control point on the shoulder side along the reference base line.
X2	in	NUMBER(4,1)	Distance of the point from the control point on the shoulder side along the reference base line.
X3	in	NUMBER(4,1)	Distance of the point from the control point on the shoulder side along the reference base line.
X4	in	NUMBER(4,1)	Distance of the point from the control point on the shoulder side along the reference base line.
X5	in	NUMBER(4,1)	Distance of the point from the control point on the shoulder side along the reference base line.
X6	in	NUMBER(4,1)	Distance of the point from the control point on the shoulder side along the reference base line.
X7	in	NUMBER(4,1)	Distance of the point from the control point on the shoulder side along the reference base line.
X8	in	NUMBER(4,1)	Distance of the point from the control point on the shoulder side along the reference base line.
X9	in	NUMBER(4,1)	Distance of the point from the control point on the shoulder side along the reference base line.
X10	in	NUMBER(4,1)	Distance of the point from the control point on the shoulder side along the reference base line.

X11	in	NUMBER(4,1)	Distance of the point from the control point on the shoulder side along the reference base line.
X12	in	NUMBER(4,1)	Distance of the point from the control point on the shoulder side along the reference base line.
X13	in	NUMBER(4,1)	Distance of the point from the control point on the shoulder side along the reference base line.
X14	in	NUMBER(4,1)	Distance of the point from the control point on the shoulder side along the reference base line.
X15	in	NUMBER(4,1)	Distance of the point from the control point on the shoulder side along the reference base line.
X16	in	NUMBER(4,1)	Distance of the point from the control point on the shoulder side along the reference base line.
X17	in	NUMBER(4,1)	Distance of the point from the control point on the shoulder side along the reference base line.
X18	in	NUMBER(4,1)	Distance of the point from the control point on the shoulder side along the reference base line.
X19	in	NUMBER(4,1)	Distance of the point from the control point on the shoulder side along the reference base line.
X20	in	NUMBER(4,1)	Distance of the point from the control point on the shoulder side along the reference base line.
X21	in	NUMBER(4,1)	Distance of the point from the control point on the shoulder side along the reference base line.
X22	in	NUMBER(4,1)	Distance of the point from the control point on the shoulder side along the reference base line.
X23	in	NUMBER(4,1)	Distance of the point from the control point on the shoulder side along the reference base line.
X24	in	NUMBER(4,1)	Distance of the point from the control point on the shoulder side along the reference base line.
X25	in	NUMBER(4,1)	Distance of the point from the control point on the shoulder side along the reference base line.
X26	in	NUMBER(4,1)	Distance of the point from the control point on the shoulder side along the reference base line.
X27	in	NUMBER(4,1)	Distance of the point from the control point on the shoulder side along the reference base line.
X28	in	NUMBER(4,1)	Distance of the point from the control point on the shoulder side along the reference base line.
X29	in	NUMBER(4,1)	Distance of the point from the control point on the shoulder side along the reference base line.
X30	in	NUMBER(4,1)	Distance of the point from the control point on the shoulder side along the reference base line.
Y1	in	NUMBER(4,2)	Distance of the point from the reference base line.
Y2	in	NUMBER(4,2)	Distance of the point from the reference base line.
Y3	in	NUMBER(4,2)	Distance of the point from the reference base line.
Y4	in	NUMBER(4,2)	Distance of the point from the reference base line.
Y5	in	NUMBER(4,2)	Distance of the point from the reference base line.
Y6	in	NUMBER(4,2)	Distance of the point from the reference base line.
Y7	in	NUMBER(4,2)	Distance of the point from the reference base line.
Y8	in	NUMBER(4,2)	Distance of the point from the reference base line.
Y9	in	NUMBER(4,2)	Distance of the point from the reference base line.
Y10	in	NUMBER(4,2)	Distance of the point from the reference base line.
Y11	in	NUMBER(4,2)	Distance of the point from the reference base line.
Y12	in	NUMBER(4,2)	Distance of the point from the reference base line.
Y13	in	NUMBER(4,2)	Distance of the point from the reference base line.
Y14	in	NUMBER(4,2)	Distance of the point from the reference base line.
Y15	in	NUMBER(4,2)	Distance of the point from the reference base line.
Y16	in	NUMBER(4,2)	Distance of the point from the reference base line.
Y17	in	NUMBER(4,2)	Distance of the point from the reference base line.
Y18	in	NUMBER(4,2)	Distance of the point from the reference base line.

Y19	in	NUMBER(4,2)	Distance of the point from the reference base line.
Y20	in	NUMBER(4,2)	Distance of the point from the reference base line.
Y21	in	NUMBER(4,2)	Distance of the point from the reference base line.
Y22	in	NUMBER(4,2)	Distance of the point from the reference base line.
Y23	in	NUMBER(4,2)	Distance of the point from the reference base line.
Y24	in	NUMBER(4,2)	Distance of the point from the reference base line.
Y25	in	NUMBER(4,2)	Distance of the point from the reference base line.
Y26	in	NUMBER(4,2)	Distance of the point from the reference base line.
Y27	in	NUMBER(4,2)	Distance of the point from the reference base line.
Y28	in	NUMBER(4,2)	Distance of the point from the reference base line.
Y29	in	NUMBER(4,2)	Distance of the point from the reference base line.
Y30	in	NUMBER(4,2)	Distance of the point from the reference base line.

Table Name: TRF_AXLE_DISTRI
Description: Axle load spectra data

MON PROFILE			
Field Name	Units	Field Type	Description
MT_SECTION_ID		CHARACTER	Test section identification number.
LTPP_SECTION_ID		CHARACTER(6)	LTPP test section identification.
DATE_YEAR		NUMBER(4,0)	Year for which traffic data are reported.
DATE_MONTH		NUMBER(2,0)	Month for which traffic data are reported.
SINGLE_0		NUMBER(8,0)	Number of single axles ranging from 0 to 2999 lbs.
SINGLE_3000		NUMBER(8,0)	Number of single axles ranging from 3000 to 3999 lbs.
SINGLE_4000		NUMBER(8,0)	Number of single axles ranging from 4000 to 4999 lbs.
SINGLE_5000		NUMBER(8,0)	Number of single axles ranging from 5000 to 5999 lbs.
SINGLE_6000		NUMBER(8,0)	Number of single axles ranging from 6000 to 6999 lbs.
SINGLE_7000		NUMBER(8,0)	Number of single axles ranging from 7000 to 7999 lbs.
SINGLE_8000		NUMBER(8,0)	Number of single axles ranging from 8000 to 8999 lbs.
SINGLE_9000		NUMBER(8,0)	Number of single axles ranging from 9000 to 9999 lbs.
SINGLE_10000		NUMBER(8,0)	Number of single axles ranging from 10,000 to 10,999 lbs.
SINGLE_11000		NUMBER(8,0)	Number of single axles ranging from 11,000 to 11,999 lbs.
SINGLE_12000		NUMBER(8,0)	Number of single axles ranging from 12,000 to 12,999 lbs.
SINGLE_13000		NUMBER(8,0)	Number of single axles ranging from 13,000 to 13,999 lbs.
SINGLE_14000		NUMBER(8,0)	Number of single axles ranging from 14,000 to 14,999 lbs.
SINGLE_15000		NUMBER(8,0)	Number of single axles ranging from 15,000 to 15,999 lbs.
SINGLE_16000		NUMBER(8,0)	Number of single axles ranging from 16,000 to 16,999 lbs.
SINGLE_17000		NUMBER(8,0)	Number of single axles ranging from 17,000 to 17,999 lbs.
SINGLE_18000		NUMBER(8,0)	Number of single axles ranging from 18,000 to 18,999 lbs.
SINGLE_19000		NUMBER(8,0)	Number of single axles ranging from 19,000 to 19,999 lbs.
SINGLE_20000		NUMBER(8,0)	Number of single axles ranging from 20,000 to 20,999 lbs.
SINGLE_21000		NUMBER(8,0)	Number of single axles ranging from 21,000 to 21,999 lbs.
SINGLE_22000		NUMBER(8,0)	Number of single axles ranging from 22,000 to 22,999 lbs.
SINGLE_23000		NUMBER(8,0)	Number of single axles ranging from 23,000 to 23,999 lbs.
SINGLE_24000		NUMBER(8,0)	Number of single axles ranging from 24,000 to 24,999 lbs.
SINGLE_25000		NUMBER(8,0)	Number of single axles ranging from 25,000 to 25,999 lbs.
SINGLE_26000		NUMBER(8,0)	Number of single axles ranging from 26,000 to 26,999 lbs.
SINGLE_27000		NUMBER(8,0)	Number of single axles ranging from 27,000 to 27,999 lbs.
SINGLE_28000		NUMBER(8,0)	Number of single axles ranging from 28,000 to 28,999 lbs.
SINGLE_29000		NUMBER(8,0)	Number of single axles ranging from 29,000 to 29,999 lbs.
SINGLE_30000		NUMBER(8,0)	Number of single axles ranging from 30,000 to 30,999 lbs.
SINGLE_31000		NUMBER(8,0)	Number of single axles ranging from 31,000 to 31,999 lbs.
SINGLE_32000		NUMBER(8,0)	Number of single axles ranging from 32,000 to 32,999 lbs.
SINGLE_33000		NUMBER(8,0)	Number of single axles ranging from 33,000 to 33,999 lbs.
SINGLE_34000		NUMBER(8,0)	Number of single axles ranging from 34,000 to 34,999 lbs.
SINGLE_35000		NUMBER(8,0)	Number of single axles ranging from 35,000 to 35,999 lbs.
SINGLE_36000		NUMBER(8,0)	Number of single axles ranging from 36,000 to 36,999 lbs.

SINGLE_37000		NUMBER(8,0)	Number of single axles ranging from 37,000 to 37,999 lbs.
SINGLE_38000		NUMBER(8,0)	Number of single axles ranging from 38,000 to 38,999 lbs.
SINGLE_39000		NUMBER(8,0)	Number of single axles ranging from 39,000 to 39,999 lbs.
SINGLE_40000		NUMBER(8,0)	Number of single axles ranging from 40,000 to 40,999 lbs.
TANDEM_0		NUMBER(8,0)	Number of tandem axles ranging from 0 to 5,999 lbs.
TANDEM_6000		NUMBER(8,0)	Number of tandem axles ranging from 6,000 to 7,999 lbs.
TANDEM_8000		NUMBER(8,0)	Number of tandem axles ranging from 8,000 to 9,999 lbs.
TANDEM_10000		NUMBER(8,0)	Number of tandem axles ranging from 10,000 to 11,999 lbs.
TANDEM_12000		NUMBER(8,0)	Number of tandem axles ranging from 12,000 to 13,999 lbs.
TANDEM_14000		NUMBER(8,0)	Number of tandem axles ranging from 14,000 to 15,999 lbs.
TANDEM_16000		NUMBER(8,0)	Number of tandem axles ranging from 16,000 to 17,999 lbs.
TANDEM_18000		NUMBER(8,0)	Number of tandem axles ranging from 18,000 to 19,999 lbs.
TANDEM_20000		NUMBER(8,0)	Number of tandem axles ranging from 20,000 to 21,999 lbs.
TANDEM_22000		NUMBER(8,0)	Number of tandem axles ranging from 22,000 to 23,999 lbs.
TANDEM_24000		NUMBER(8,0)	Number of tandem axles ranging from 24,000 to 25,999 lbs.
TANDEM_26000		NUMBER(8,0)	Number of tandem axles ranging from 26,000 to 27,999 lbs.
TANDEM_28000		NUMBER(8,0)	Number of tandem axles ranging from 28,000 to 29,999 lbs.
TANDEM_30000		NUMBER(8,0)	Number of tandem axles ranging from 30,000 to 31,999 lbs.
TANDEM_32000		NUMBER(8,0)	Number of tandem axles ranging from 32,000 to 33,999 lbs.
TANDEM_34000		NUMBER(8,0)	Number of tandem axles ranging from 34,000 to 35,999 lbs.
TANDEM_36000		NUMBER(8,0)	Number of tandem axles ranging from 36,000 to 37,999 lbs.
TANDEM_38000		NUMBER(8,0)	Number of tandem axles ranging from 38,000 to 39,999 lbs.
TANDEM_40000		NUMBER(8,0)	Number of tandem axles ranging from 40,000 to 41,999 lbs.
TANDEM_42000		NUMBER(8,0)	Number of tandem axles ranging from 42,000 to 43,999 lbs.
TANDEM_44000		NUMBER(8,0)	Number of tandem axles ranging from 44,000 to 45,999 lbs.
TANDEM_46000		NUMBER(8,0)	Number of tandem axles ranging from 46,000 to 47,999 lbs.
TANDEM_48000		NUMBER(8,0)	Number of tandem axles ranging from 48,000 to 49,999 lbs.
TANDEM_50000		NUMBER(8,0)	Number of tandem axles ranging from 50,000 to 51,999 lbs.
TANDEM_52000		NUMBER(8,0)	Number of tandem axles ranging from 52,000 to 53,999 lbs.
TANDEM_54000		NUMBER(8,0)	Number of tandem axles ranging from 54,000 to 55,999 lbs.
TANDEM_56000		NUMBER(8,0)	Number of tandem axles ranging from 56,000 to 57,999 lbs.
TANDEM_58000		NUMBER(8,0)	Number of tandem axles ranging from 58,000 to 59,999 lbs.
TANDEM_60000		NUMBER(8,0)	Number of tandem axles ranging from 60,000 to 61,999 lbs.
TANDEM_62000		NUMBER(8,0)	Number of tandem axles ranging from 62,000 to 63,999 lbs.
TANDEM_64000		NUMBER(8,0)	Number of tandem axles ranging from 64,000 to 65,999 lbs.
TANDEM_66000		NUMBER(8,0)	Number of tandem axles ranging from 66,000 to 67,999 lbs.
TANDEM_68000		NUMBER(8,0)	Number of tandem axles ranging from 68,000 to 69,999 lbs.
TANDEM_70000		NUMBER(8,0)	Number of tandem axles ranging from 70,000 to 71,999 lbs.
TANDEM_72000		NUMBER(8,0)	Number of tandem axles ranging from 72,000 to 73,999 lbs.
TANDEM_74000		NUMBER(8,0)	Number of tandem axles ranging from 74,000 to 75,999 lbs.
TANDEM_76000		NUMBER(8,0)	Number of tandem axles ranging from 76,000 to 77,999 lbs.
TANDEM_78000		NUMBER(8,0)	Number of tandem axles ranging from 78,000 to 79,999 lbs.
TANDEM_80000		NUMBER(8,0)	Number of tandem axles ranging from 80,000 to 81,999 lbs.
TRIDEM_0		NUMBER(8,0)	Number of tridem axles ranging from 0 to 11,999 lbs.
TRIDEM_12000		NUMBER(8,0)	Number of tridem axles ranging from 12,000 to 14,999 lbs.
TRIDEM_15000		NUMBER(8,0)	Number of tridem axles ranging from 15,000 to 17,999 lbs.
TRIDEM_18000		NUMBER(8,0)	Number of tridem axles ranging from 18,000 to 20,999 lbs.
TRIDEM_21000		NUMBER(8,0)	Number of tridem axles ranging from 21,000 to 23,999 lbs.
TRIDEM_24000		NUMBER(8,0)	Number of tridem axles ranging from 24,000 to 26,999 lbs.
TRIDEM_27000		NUMBER(8,0)	Number of tridem axles ranging from 27,000 to 29,999 lbs.
TRIDEM_30000		NUMBER(8,0)	Number of tridem axles ranging from 30,000 to 32,999 lbs.
TRIDEM_33000		NUMBER(8,0)	Number of tridem axles ranging from 33,000 to 35,999 lbs.
TRIDEM_36000		NUMBER(8,0)	Number of tridem axles ranging from 36,000 to 38,999 lbs.
TRIDEM_39000		NUMBER(8,0)	Number of tridem axles ranging from 39,000 to 41,999 lbs.
TRIDEM_42000		NUMBER(8,0)	Number of tridem axles ranging from 42,000 to 44,999 lbs.
TRIDEM_45000		NUMBER(8,0)	Number of tridem axles ranging from 45,000 to 47,999 lbs.
TRIDEM_48000		NUMBER(8,0)	Number of tridem axles ranging from 48,000 to 50,999 lbs.
TRIDEM_51000		NUMBER(8,0)	Number of tridem axles ranging from 51,000 to 53,999 lbs.

TRIDEM_54000		NUMBER(8,0)	Number of tridem axles ranging from 54,000 to 56,999 lbs.
TRIDEM_57000		NUMBER(8,0)	Number of tridem axles ranging from 57,000 to 59,999 lbs.
TRIDEM_60000		NUMBER(8,0)	Number of tridem axles ranging from 60,000 to 62,999 lbs.
TRIDEM_63000		NUMBER(8,0)	Number of tridem axles ranging from 63,000 to 65,999 lbs.
TRIDEM_66000		NUMBER(8,0)	Number of tridem axles ranging from 66,000 to 68,999 lbs.
TRIDEM_69000		NUMBER(8,0)	Number of tridem axles ranging from 69,000 to 71,999 lbs.
TRIDEM_72000		NUMBER(8,0)	Number of tridem axles ranging from 72,000 to 74,999 lbs.
TRIDEM_75000		NUMBER(8,0)	Number of tridem axles ranging from 75,000 to 77,999 lbs.
TRIDEM_78000		NUMBER(8,0)	Number of tridem axles ranging from 78,000 to 80,999 lbs.
TRIDEM_81000		NUMBER(8,0)	Number of tridem axles ranging from 81,000 to 83,999 lbs.
TRIDEM_84000		NUMBER(8,0)	Number of tridem axles ranging from 84,000 to 86,999 lbs.
TRIDEM_87000		NUMBER(8,0)	Number of tridem axles ranging from 87,000 to 89,999 lbs.
TRIDEM_90000		NUMBER(8,0)	Number of tridem axles ranging from 90,000 to 92,999 lbs.
TRIDEM_93000		NUMBER(8,0)	Number of tridem axles ranging from 93,000 to 95,999 lbs.
TRIDEM_96000		NUMBER(8,0)	Number of tridem axles ranging from 96,000 to 98,999 lbs.
TRIDEM_99000		NUMBER(8,0)	Number of tridem axles ranging from 99,000 to 101,999 lbs.
QUAD_0		NUMBER(8,0)	Number of quadruple axles ranging from 0 to 11,999 lbs.
QUAD_12000		NUMBER(8,0)	Number of quadruple axles ranging from 12,000 to 14,999 lbs.
QUAD_15000		NUMBER(8,0)	Number of quadruple axles ranging from 15,000 to 17,999 lbs.
QUAD_18000		NUMBER(8,0)	Number of quadruple axles ranging from 18,000 to 20,999 lbs.
QUAD_21000		NUMBER(8,0)	Number of quadruple axles ranging from 21,000 to 23,999 lbs.
QUAD_24000		NUMBER(8,0)	Number of quadruple axles ranging from 24,000 to 26,999 lbs.
QUAD_27000		NUMBER(8,0)	Number of quadruple axles ranging from 27,000 to 29,999 lbs.
QUAD_30000		NUMBER(8,0)	Number of quadruple axles ranging from 30,000 to 32,999 lbs.
QUAD_33000		NUMBER(8,0)	Number of quadruple axles ranging from 33,000 to 35,999 lbs.
QUAD_36000		NUMBER(8,0)	Number of quadruple axles ranging from 36,000 to 38,999 lbs.
QUAD_39000		NUMBER(8,0)	Number of quadruple axles ranging from 39,000 to 41,999 lbs.
QUAD_42000		NUMBER(8,0)	Number of quadruple axles ranging from 42,000 to 44,999 lbs.
QUAD_45000		NUMBER(8,0)	Number of quadruple axles ranging from 45,000 to 47,999 lbs.
QUAD_48000		NUMBER(8,0)	Number of quadruple axles ranging from 48,000 to 50,999 lbs.
QUAD_51000		NUMBER(8,0)	Number of quadruple axles ranging from 51,000 to 53,999 lbs.
QUAD_54000		NUMBER(8,0)	Number of quadruple axles ranging from 54,000 to 56,999 lbs.
QUAD_57000		NUMBER(8,0)	Number of quadruple axles ranging from 57,000 to 59,999 lbs.
QUAD_60000		NUMBER(8,0)	Number of quadruple axles ranging from 60,000 to 62,999 lbs.
QUAD_63000		NUMBER(8,0)	Number of quadruple axles ranging from 63,000 to 65,999 lbs.
QUAD_66000		NUMBER(8,0)	Number of quadruple axles ranging from 66,000 to 68,999 lbs.
QUAD_69000		NUMBER(8,0)	Number of quadruple axles ranging from 69,000 to 71,999 lbs.

QUAD_72000		NUMBER(8,0)	Number of quadruple axles ranging from 72,000 to 74,999 lbs.
QUAD_75000		NUMBER(8,0)	Number of quadruple axles ranging from 75,000 to 77,999 lbs.
QUAD_78000		NUMBER(8,0)	Number of quadruple axles ranging from 78,000 to 80,999 lbs.
QUAD_81000		NUMBER(8,0)	Number of quadruple axles ranging from 81,000 to 83,999 lbs.
QUAD_84000		NUMBER(8,0)	Number of quadruple axles ranging from 84,000 to 86,999 lbs.
QUAD_87000		NUMBER(8,0)	Number of quadruple axles ranging from 87,000 to 89,999 lbs.
QUAD_90000		NUMBER(8,0)	Number of quadruple axles ranging from 90,000 to 92,999 lbs.
QUAD_93000		NUMBER(8,0)	Number of quadruple axles ranging from 93,000 to 95,999 lbs.
QUAD_96000		NUMBER(8,0)	Number of quadruple axles ranging from 96,000 to 98,999 lbs.
QUAD_99000		NUMBER(8,0)	Number of quadruple axles ranging from 99,000 to 101,999 lbs.

Table Name: TRF_AXLE_DISTRIB_ORIG

Description: Axle load spectra data from LTPP data

MON_PROFILE			
Field Name	Units	Field Type	Description
MT_SECTION_ID		CHARACTER	Test section identification number.
LTPP_SECTION_ID		CHARACTER(6)	LTPP test section identification.
DATE_YEAR		NUMBER(4,0)	Year for which traffic data are reported.
AXLE_GROUP		NUMBER(1,0)	Number of axles in this group.
WEIGHT_RANGE_LOW		NUMBER(5,0)	Lower limit of weight range.
WEIGHT_RANGE_HIGH		NUMBER(6,0)	Upper limit of weight range.
NUMBER_AXLES		NUMBER(8,0)	Number of axles belonging to this weight range.

Table Name: TRF_AXLE_SUMMARY

Description: Annual number of axles in each axle group

MON_PROFILE			
Field Name	Units	Field Type	Description
MT_SECTION_ID		CHARACTER	Test section identification number.
LTPP_SECTION_ID		CHARACTER(6)	LTPP test section identification.
DATE_YEAR		NUMBER(4,0)	Year for which traffic data are reported.
AXLE_GROUP		NUMBER(1,0)	Number of axles in this group.
ANNUAL_AXLE_NUMBER_EST		NUMBER(8,0)	Estimated number of axles belonging to this axle group in the LTPP lane.
ANNUAL_AXLE_NUMBER_ACT		NUMBER(8,0)	Actual number of axles from the WIM data that contributed to the estimates in the W-4 table for this axle group.
ANNUAL_VEHICL_NUMBER_ACT		NUMBER(8,0)	Actual number of vehicles from the WIM data that contributed at least one axle to the W-4 axle distribution for this axle group.

Table Name: TRF_VEHICLE_DISTRIB
Description: Annual vehicle type distribution information

MON_PROFILE			
Field Name	Units	Field Type	Description
MT_SECTION_ID		CHARACTER	Test section identification number.
LTPP_SECTION_ID		CHARACTER(6)	LTPP test section identification.
DATE_YEAR		NUMBER(4,0)	Year for which traffic data are reported.
VEHICLE_TYPE		NUMBER(2,0)	FHWA vehicle class code from the traffic monitoring guide.
VOLUME_EST		NUMBER(7,0)	Annual total truck volume estimate in LTPP lane.
VEHICLES_CLASSIFIED		NUMBER(7,0)	Actual number of vehicles used in the calculations of vehicles by class that come from classification data.
VEHICLES_WEIGHED		NUMBER(7,0)	Actual number of vehicles used in the ESAL calculations from WIM data.
ESAL_VEHICLE_DATA_MEAN		NUMBER(5,3)	Average ESALs per vehicle for this vehicle type in the LTPP lane calculated using WIM data.

Table Name: TRF_EST_ESAL
Description: Estimated annual ESALs and truck volumes

MON_PROFILE			
Field Name	Units	Field Type	Description
MT_SECTION_ID		CHARACTER	Test section identification number.
LTPP_SECTION_ID		CHARACTER(6)	LTPP test section identification.
DATE_YEAR		NUMBER(4,0)	Year for which traffic data are reported.
AADT_ALL_VEHIC		NUMBER(8,0)	Estimated annual average daily traffic for the LTPP lane.
AADT_TRUCK_COMBO		NUMBER(8,0)	Estimated annual average daily number of trucks in the LTPP lane.
ANL_KESAL_LTPP_LN_YR		NUMBER(5,0)	Annual ESALs in the thousands in the LTPP lane.
METHOD_EST		CHARACTER(1)	H or M indicating that the data was obtained from historical or monitored information.

Table Name: TRF_SHRP_DAT
Description: Data used in ESAL calculation

MON_PROFILE			
Field Name	Units	Field Type	Description
MT_SECTION_ID		CHARACTER	Test section identification number.
LTPP_SECTION_ID		CHARACTER(6)	LTPP test section identification.
EFFECTIVE_YEAR		NUMBER(4,0)	Year of construction event from which pavement parameters become effective.
EFFECTIVE_MONTH		NUMBER(2,0)	Month of construction event from which pavement parameters become effective.
EFFECTIVE_DAY		NUMBER(2,0)	Day of construction event from which pavement parameters become effective.
TERMINAL_SI		NUMBER(3,2)	Terminal serviceability index used in ESAL calculations.
STRUCTURAL_NO		NUMBER(4,2)	Structural number for flexible pavements used in ESAL calculations.
DEPTH		NUMBER(4,2)	Depth of rigid pavement used in ESAL calculations.
PAVE_TYPE		CHARACTER(1)	Type of pavement, flexible (F) or rigid (R), used in ESAL calculations.

Table Name: TRF_MONITOR_BASIC_INFO

Description: Summary information concerning data collection and site characteristics on a yearly basis

MON_PROFILE			
Field Name	Units	Field Type	Description
MT_SECTION_ID		CHARACTER	Test section identification number.
LTPP_SECTION_ID		CHARACTER(6)	LTPP test section identification.
DATE_YEAR		NUMBER(4,0)	Year for which traffic data are reported.
ATR_VOLUME_DAYS		NUMBER(3,0)	Number of days of volume data used in the calculation of AADT from an ATR device.
AVC_VOLUME_DAYS		NUMBER(3,0)	Number of days of volume data used in the calculations of AADT from an AVC device.
AVC_CLASS_DAYS		NUMBER(3,0)	Number of days of vehicle class data used in the calculations of vehicles by class from an AVC device.
WIM_CLASS_DAYS		NUMBER(3,0)	Number of days of vehicle class data used in the calculations of vehicles by class from a WIM device.
WIM_W4_DAYS		NUMBER(3,0)	Number of days of W-4 data used in the ESAL calculations from a WIM device.
AADT_RDWAY		NUMBER(6,0)	Annual average daily traffic (AADT) for the entire roadway.
TRUCK_VOLUME_EST		NUMBER(7,0)	Annual total truck volume (classes 4-15) estimate in LTPP lane only.
AADT_PCT_NON_LTPP_DIRECTION		NUMBER(3,1)	Percent of AADT flowing in the direction opposite of the flow of traffic in the LTPP lane.
AADT_PCT_LTPP_DIRECTION		NUMBER(4,1)	Percent of AADT flowing in the same direction as the flow of traffic in the LTPP lane.
AADT_PCT_LTPP_LANE		NUMBER(3,1)	Percent of AADT flowing in the LTPP lane.
TRUCK_PCT_LTPP_LANE		NUMBER(3,1)	Percent of traffic that are classified as being in classes 4-15 of the LTPP lane volume.
VEHICLES_CLASSIFIED		NUMBER(7,0)	Actual number of vehicles (classes 4-15) used in the calculations that come from classification data.
VEHICLES_WEIGHED		NUMBER(7,0)	Actual number of vehicles (classes 4-15) used in the calculations that come from WIM data.
ESAL_VEHICLE_DATA_MEAN		NUMBER(4,3)	Average ESALs per vehicle in the LTPP lane for classes 4-15 calculated using actual WIM data.
ANNUAL_ESAL_DATA		NUMBER(8,0)	Annual ESAL estimate in the LTPP lane calculated as a product of ESAL_VEHICLE_DATA_MEAN and TRUCK_VOLUME_EST.

Table Name: TST_LAYER_STRUCTURE

Description: Layer structure information on each test section

TST_LAYER_STRUCTURE			
Field Name	Units	Field Type	Description
SECTION_ID		CHARACTER	Test section identification number.
LAYER_NO		NUMBER(2,0)	Unique sequential number assigned to pavement layers, starting with layer 1 as the deepest layer (subgrade).
DESCRIPTION		NUMBER(1,0)	Code indicating general type of layer.
LAYER_TYPE		CHARACTER(3)	A character code indicating the type of layer.
LAYER_THICKNESS	in	NUMBER(3,1)	Thickness of the layer.
MATERIAL		NUMBER(3,0)	Code indicating the material used in the layer.

Table Name: TST_HMA_AGGREGATE_DESIGN

Description: Data on aggregate used in mix design

TST_HMA_AGGREGATE_DESIGN			
Field Name	Units	Field Type	Description
MT_SECTION_ID		CHARACTER	Test section identification number.
LTPP_SECTION_ID		CHARACTER(6)	LTPP test section identification.
LAYER_NO		NUMBER(2,0)	Unique sequential number assigned to pavement layers, starting with layer 1 as the deepest layer (subgrade).
PCT_PASS_3_4	%	NUMBER(3,0)	Percent passing on the 3/4-in sieve.
PCT_PASS_3_8	%	NUMBER(3,0)	Percent passing on the 3/8-in sieve.
PCT_PASS_NO_4	%	NUMBER(3,0)	Percent passing the number 4 sieve.
PCT_PASS_200	%	NUMBER(3,0)	Percent passing the number 200 sieve.
AGG_BULK_SPECIFIC_GRAVITY		NUMBER(4,3)	Bulk specific gravity of the aggregate in the HMA.

Table Name: TST_HMA_AGGREGATE_CONSTRUCTION

Description: Data on aggregate collected at the time of construction

TST_HMA_AGGREGATE_CONSTRUCTION			
Field Name	Units	Field Type	Description
MT_SECTION_ID		CHARACTER	Test section identification number.
LTPP_SECTION_ID		CHARACTER(6)	LTPP test section identification.
LAYER_NO		NUMBER(2,0)	Unique sequential number assigned to pavement layers, starting with layer 1 as the deepest layer (subgrade).
PCT_PASS_3_4	%	NUMBER(3,0)	Percent passing on the 3/4-in sieve.
PCT_PASS_3_8	%	NUMBER(3,0)	Percent passing on the 3/8-in sieve.
PCT_PASS_NO_4	%	NUMBER(3,0)	Percent passing the number 4 sieve.
PCT_PASS_200	%	NUMBER(3,0)	Percent passing the number 200 sieve.
AGG_BULK_SPECIFIC_GRAVITY		NUMBER(4,3)	Bulk specific gravity of the aggregate in the HMA.

Table Name: TST_HMA_AGGREGATE_INSITU

Description: Data on aggregate used in the HMA mix collected sometime after construction

TST_HMA_AGGREGATE_INSITU			
Field Name	Units	Field Type	Description
MT_SECTION_ID		CHARACTER	Test section identification number.
LTPP_SECTION_ID		CHARACTER(6)	LTPP test section identification.
LAYER_NO		NUMBER(2,0)	Unique sequential number assigned to pavement layers, starting with layer 1 as the deepest layer (subgrade).
PCT_PASS_3_4	%	NUMBER(3,0)	Percent passing on the 3/4-in sieve.
PCT_PASS_3_8	%	NUMBER(3,0)	Percent passing on the 3/8-in sieve.
PCT_PASS_NO_4	%	NUMBER(3,0)	Percent passing the number 4 sieve.
PCT_PASS_200	%	NUMBER(3,0)	Percent passing the number 200 sieve.
AGG_BULK_SPECIFIC_GRAVITY		NUMBER(4,3)	Bulk specific gravity of the aggregate in the HMA.
AGE_AT_SAMPLING	Years	NUMBER(3,1)	Age of pavement at time of sampling.
AGE_AT_TESTING	Months	NUMBER(3,0)	Age of sample at time of testing.

Table Name: TST_HMA_CEMENT_DESIGN

Description: Data on asphalt cement used in mix design

TST_HMA_CEMENT_DESIGN			
Field Name	Units	Field Type	Description
MT_SECTION_ID		CHARACTER	Test section identification number.
LTPP_SECTION_ID		CHARACTER(6)	LTPP test section identification.
LAYER_NO		NUMBER(2,0)	Unique sequential number assigned to pavement layers, starting with layer 1 as the deepest layer (subgrade).
BINDER_SPEC_GRAVITY		NUMBER(4,3)	Specific gravity of the asphalt cement.
RING_BALL_SOFTENING_PT	°F	NUMBER(3,0)	Ring and ball softening point of the asphalt cement.
PENETRATION_77	0.01 in	NUMBER(3,0)	Penetration of the asphalt cement at 77°F.
LOAD_77	G	NUMBER(2,0)	Load applied for penetration test at 77°F.
TEST_TIME_77	Seconds	NUMBER(2,0)	Length of time that the load is applied.
PENETRATION_39	0.01 in	NUMBER(3,0)	Penetration of the asphalt cement at 39°F.
LOAD_39	G	NUMBER(2,0)	Load applied for penetration test.
TEST_TIME_39	Seconds	NUMBER(2,0)	Length of time that the load is applied.
PENETRATION1	0.01 in	NUMBER(3,0)	Penetration of asphalt cement.
LOAD1	g	NUMBER(2,0)	Load applied for the penetration test.
TEST_TIME1	Seconds	NUMBER(2,0)	Length of time that the load is applied.
TEMPERATURE1	°F	NUMBER(3,1)	Temperature at which the test is performed.
PENETRATION2	0.01 in	NUMBER(3,0)	Penetration of asphalt cement.
LOAD2	g	NUMBER(2,0)	Load applied for the penetration test.
TEST_TIME2	Seconds	NUMBER(2,0)	Length of time that the load is applied.
TEMPERATURE2	°F	NUMBER(3,0)	Temperature at which the test is performed.
BROOKFIELD_VISC			
ABSOLUTE_VISC_140	Poise	NUMBER(6,0)	Viscosity of asphalt cement at 140°F.
KINEMATIC_VISC_275	Centistokes	NUMBER(6,2)	Viscosity of asphalt cement at 275°F.
ASPHALT_CEMENT_GRADE		CHARACTER(6)	Grade of the asphalt cement.

Table Name: TST_HMA_CEMENT_CONSTRUCTION

Description: Data on asphalt cement collected at the time of construction

TST_HMA_CEMENT_CONSTRUCTION			
Field Name	Units	Field Type	Description
MT_SECTION_ID		CHARACTER	Test section identification number.
LTPP_SECTION_ID		CHARACTER(6)	LTPP test section identification.
LAYER_NO		NUMBER(2,0)	Unique sequential number assigned to pavement layers, starting with layer 1 as the deepest layer (subgrade).
BINDER_SPEC_GRAVITY		NUMBER(4,3)	Specific gravity of the asphalt cement.
RING_BALL_SOFTENING_PT	°F	NUMBER(3,0)	Ring and ball softening point of the asphalt cement.
PENETRATION_77	0.01 in	NUMBER(3,0)	Penetration of the asphalt cement at 77°F.
LOAD_77	g	NUMBER(2,0)	Load applied for penetration test at 77°F.
TEST_TIME_77	Seconds	NUMBER(2,0)	Length of time that the load is applied.
PENETRATION_39	0.01 in	NUMBER(3,0)	Penetration of the asphalt cement at 39°F.
LOAD_39	g	NUMBER(2,0)	Load applied for penetration test.
TEST_TIME_39	Seconds	NUMBER(2,0)	Length of time that the load is applied.
PENETRATION1	0.01 in	NUMBER(3,0)	Penetration of asphalt cement.
LOAD1	g	NUMBER(2,0)	Load applied for the penetration test.
TEST_TIME1	Seconds	NUMBER(2,0)	Length of time that the load is applied.
TEMPERATURE1	°F	NUMBER(3,1)	Temperature at which the test is performed.
PENETRATION2	0.01 in	NUMBER(3,0)	Penetration of asphalt cement.
LOAD2	g	NUMBER(2,0)	Load applied for the penetration test.
TEST_TIME2	Seconds	NUMBER(2,0)	Length of time that the load is applied.
TEMPERATURE2	°F	NUMBER(3,0)	Temperature at which the test is performed.
BROOKFIELD_VISC			
ABSOLUTE_VISC_140	Poise	NUMBER(6,0)	Viscosity of asphalt cement at 140°F.
KINEMATIC_VISC_275	Centistokes	NUMBER(6,2)	Viscosity of asphalt cement at 275°F.
ASPHALT_CEMENT_GRADE		CHARACTER(6)	Grade of the asphalt cement.

Table Name: TST_HMA_CEMENT_INSITU

Description: Data on asphalt cement collected sometime after construction

TST_HMA_CEMENT_INSITU			
Field Name	Units	Field Type	Description
MT_SECTION_ID		CHARACTER	Test section identification number.
LTPP_SECTION_ID		CHARACTER(6)	LTPP test section identification.
LAYER_NO		NUMBER(2,0)	Unique sequential number assigned to pavement layers, starting with layer 1 as the deepest layer (subgrade).
BINDER_SPEC_GRAVITY		NUMBER(4,3)	Specific gravity of the asphalt cement.
RING_BALL_SOFTENING_PT	°F	NUMBER(3,0)	Ring and ball softening point of the asphalt cement.
PENETRATION_77	0.01 in	NUMBER(3,0)	Penetration of the asphalt cement at 77°F.
LOAD_77	G	NUMBER(2,0)	Load applied for penetration test at 77°F.
TEST_TIME_77	Seconds	NUMBER(2,0)	Length of time that the load is applied.
PENETRATION_39	0.01 in	NUMBER(3,0)	Penetration of the asphalt cement at 39°F.
LOAD_39	G	NUMBER(2,0)	Load applied for penetration test.
TEST_TIME_39	Seconds	NUMBER(2,0)	Length of time that the load is applied.
PENETRATION1	0.01 in	NUMBER(3,0)	Penetration of asphalt cement.
LOAD1	G	NUMBER(2,0)	Load applied for the penetration test.
TEST_TIME1	Seconds	NUMBER(2,0)	Length of time that the load is applied.
TEMPERATURE1	°F	NUMBER(3,1)	Temperature at which the test is performed.
PENETRATION2	0.01 in	NUMBER(3,0)	Penetration of asphalt cement.
LOAD2	g	NUMBER(2,0)	Load applied for the penetration test.

TEST_TIME2	Seconds	NUMBER(2,0)	Length of time that the load is applied.
TEMPERATURE2	°F	NUMBER(3,0)	Temperature at which the test is performed.
BROOKFIELD_VISC			
ABSOLUTE_VISC_140	Poise	NUMBER(6,0)	Viscosity of asphalt cement at 140°F.
KINEMATIC_VISC_275	Centistokes	NUMBER(6,2)	Viscosity of asphalt cement at 275°F.
ASPHALT_CEMENT_GRADE		CHARACTER(6)	Grade of the asphalt cement.
AGE_AT_SAMPLING	Years	NUMBER(3,1)	Age of pavement at time of sampling.
AGE_AT_TESTING	Months	NUMBER(3,0)	Age of sample at time of testing.

Table Name: TST_HMA_MIX_DESIGN

Description: Materials information for HMA layers of each test section collected from the mix design

TST_HMA_MIX_DESIGN			
Field Name	Units	Field Type	Description
MT_SECTION_ID		CHARACTER	Test section identification number.
LTPP_SECTION_ID		CHARACTER(6)	LTPP test section identification.
LAYER_NO		NUMBER(2,0)	Unique sequential number assigned to pavement layers, starting with layer 1 as the deepest layer (subgrade).
ASPHALT_CONTENT	%	NUMBER(3,1)	Asphalt content of the HMA mix, by total wt. of mix.
BULK_SPECIFIC_GRAVITY		NUMBER(4,3)	Bulk specific gravity of the HMA mix.
MAXIMUM_SPECIFIC_GRAVITY		NUMBER(4,3)	Theoretical maximum specific gravity of the HMA mix.
AIR_VOIDS	%	NUMBER(3,1)	Air void content of HMA mix.
VOIDS_MINERAL_AGG	%	NUMBER(3,1)	Voids in mineral aggregate.
IDT_32	Psi	NUMBER(5,1)	Indirect diametral tensile strength for the HMA mix measured at 32°F.
IDT_MINUS_25	Psi	NUMBER(5,1)	Indirect diametral tensile strength for the HMA mix measured at 25°F.
IDT_MINUS_14	Psi	NUMBER(5,1)	Indirect diametral tensile strength for the HMA mix measured at 14°F.
IDT_1	Psi	NUMBER(5,1)	Indirect diametral tensile strength at specified temperature.
TEMPERATURE_1	°F	NUMBER(4,1)	Temperature at which the tensile strength test was performed.
IDT_2	Psi	NUMBER(5,1)	Indirect diametral tensile strength at specified temperature.
TEMPERATURE_2	°F	NUMBER(4,1)	Temperature at which tensile strength test was performed.
POISSONS_RATIO		NUMBER(3,2)	Poisson's ratio calculated from testing data.
COMPLEX_MODULUS	Psi	NUMBER(6,0)	
COMPLEX_TEMP	°F	NUMBER(4,1)	Temperature at which complex modulus testing was performed.
COMPLEX_FREQ	1/sec	NUMBER(4,0)	Frequency at which complex modulus testing was performed.
CREEP_COMP_1_SEC	1/psi	NUMBER(5,3)	Creep compliance value at 1 second.
CREEP_COMP_2_SEC	1/psi	NUMBER(5,3)	Creep compliance value at 2 seconds.
CREEP_COMP_5_SEC	1/psi	NUMBER(5,3)	Creep compliance value at 5 seconds.
CREEP_COMP_10_SEC	1/psi	NUMBER(5,3)	Creep compliance value at 10 seconds.
CREEP_COMP_20_SEC	1/psi	NUMBER(5,3)	Creep compliance value at 20 seconds.
CREEP_COMP_50_SEC	1/psi	NUMBER(5,3)	Creep compliance value at 50 seconds.
CREEP_COMP_100_SEC	1/psi	NUMBER(5,3)	Creep compliance value at 100 seconds.
TEMPERATURE_CREEP	°F	NUMBER(4,1)	Temperature at which creep compliance testing was performed.
INST_RESILIENT_MODULUS_1	Psi	NUMBER(7,0)	Instantaneous resilient modulus.

TOT_RESILIENT_MODULUS_1	Psi	NUMBER(7,0)	Total resilient modulus.
TEMP_RES_1	°F	NUMBER(4,1)	Temperature at which test was performed.
LOAD_TIME_RES_1	Seconds	NUMBER(3,2)	Loading time for testing.
UNLOAD_TIME_RES_1	Seconds	NUMBER(3,2)	Unloading time for test.
INST_RESILIENT_MODULUS_2	Psi	NUMBER(7,0)	Instantaneous resilient modulus.
TOT_RESILIENT_MODULUS_2	Psi	NUMBER(7,0)	Total resilient modulus.
TEMP_RES_2	°F	NUMBER(4,1)	Temperature at which test was performed.
LOAD_TIME_RES_2	Seconds	NUMBER(3,2)	Loading time for testing.
UNLOAD_TIME_RES_2	Seconds	NUMBER(3,2)	Unloading time for test.
INST_RESILIENT_MODULUS_3	Psi	NUMBER(7,0)	Instantaneous resilient modulus.
TOT_RESILIENT_MODULUS_3	Psi	NUMBER(7,0)	Total resilient modulus.
TEMP_RES_3	°F	NUMBER(4,1)	Temperature at which test was performed.
LOAD_TIME_RES_3	Seconds	NUMBER(3,2)	Loading time for testing.
UNLOAD_TIME_RES_3	Seconds	NUMBER(3,2)	Unloading time for test.

Table Name: TST_HMA_MIX_CONSTRUCTION

Description: Materials information on the HMA layers of each test section collected from the mix design

TST_HMA_MIX_CONSTRUCTION			
Field Name	Units	Field Type	Description
MT_SECTION_ID		CHARACTER	Test section identification number.
LTPP_SECTION_ID		CHARACTER(6)	LTPP test section identification.
LAYER_NO		NUMBER(2,0)	Unique sequential number assigned to pavement layers, starting with layer 1 as the deepest layer (subgrade).
ASPHALT_CONTENT	%	NUMBER(3,1)	Asphalt content of the HMA mix, by total wt. of mix.
BULK_SPECIFIC_GRAVITY		NUMBER(4,3)	Bulk specific gravity of the HMA mix.
MAXIMUM_SPECIFIC_GRAVITY		NUMBER(4,3)	Theoretical maximum specific gravity of the HMA mix.
AIR_VOIDS	%	NUMBER(3,1)	Air void content of HMA mix.
VOIDS_MINERAL_AGG	%	NUMBER(3,1)	Voids in mineral aggregate.
IDT_32	psi	NUMBER(5,1)	Indirect diametral tensile strength for the HMA mix measured at 32°F.
IDT_MINUS_25	psi	NUMBER(5,1)	Indirect diametral tensile strength for the HMA mix measured at 25°F.
IDT_MINUS_14	psi	NUMBER(5,1)	Indirect diametral tensile strength for the HMA mix measured at 14°F.
IDT_1	psi	NUMBER(5,1)	Indirect diametral tensile strength at specified temperature.
TEMPERATURE_1	°F	NUMBER(4,1)	Temperature at which the tensile strength test was performed.
IDT_2	psi	NUMBER(5,1)	Indirect diametral tensile strength at specified temperature.
TEMPERATURE_2	°F	NUMBER(4,1)	Temperature at which tensile strength test was performed.
POISSONS_RATIO		NUMBER(3,2)	Poisson's ratio calculated from testing data.
COMPLEX_MODULUS	psi	NUMBER(6,0)	
COMPLEX_TEMP	°F	NUMBER(4,1)	Temperature at which complex modulus testing was performed.
COMPLEX_FREQ	1/sec	NUMBER(4,0)	Frequency at which complex modulus testing was performed.
CREEP_COMP_1_SEC	1/psi	NUMBER(5,3)	Creep compliance value at 1 second.
CREEP_COMP_2_SEC	1/psi	NUMBER(5,3)	Creep compliance value at 2 seconds.
CREEP_COMP_5_SEC	1/psi	NUMBER(5,3)	Creep compliance value at 5 seconds.
CREEP_COMP_10_SEC	1/psi	NUMBER(5,3)	Creep compliance value at 10 seconds.

CREEP_COMP_20_SEC	1/psi	NUMBER(5,3)	Creep compliance value at 20 seconds.
CREEP_COMP_50_SEC	1/psi	NUMBER(5,3)	Creep compliance value at 50 seconds.
CREEP_COMP_100_SEC	1/psi	NUMBER(5,3)	Creep compliance value at 100 seconds.
TEMPERATURE_CREEP	°F	NUMBER(4,1)	Temperature at which creep compliance testing was performed.
INST_RESILIENT_MODULUS_1	psi	NUMBER(7,0)	Instantaneous resilient modulus.
TOT_RESILIENT_MODULUS_1	psi	NUMBER(7,0)	Total resilient modulus.
TEMP_RES_1	°F	NUMBER(4,1)	Temperature at which test was performed.
LOAD_TIME_RES_1	Seconds	NUMBER(3,2)	Loading time for testing.
UNLOAD_TIME_RES_1	Seconds	NUMBER(3,2)	Unloading time for test.
INST_RESILIENT_MODULUS_2	psi	NUMBER(7,0)	Instantaneous resilient modulus.
TOT_RESILIENT_MODULUS_2	psi	NUMBER(7,0)	Total resilient modulus.
TEMP_RES_2	°F	NUMBER(4,1)	Temperature at which test was performed.
LOAD_TIME_RES_2	Seconds	NUMBER(3,2)	Loading time for testing.
UNLOAD_TIME_RES_2	Seconds	NUMBER(3,2)	Unloading time for test.
INST_RESILIENT_MODULUS_3	psi	NUMBER(7,0)	Instantaneous resilient modulus.
TOT_RESILIENT_MODULUS_3	psi	NUMBER(7,0)	Total resilient modulus.
TEMP_RES_3	°F	NUMBER(4,1)	Temperature at which test was performed.
LOAD_TIME_RES_3	Seconds	NUMBER(3,2)	Loading time for testing.
UNLOAD_TIME_RES_3	Seconds	NUMBER(3,2)	Unloading time for test.

Table Name: TST_HMA_MIX_INSITU

Description: Materials information for HMA layers of each test section collected from the mix design

TST_HMA_MIX_INSITU			
Field Name	Units	Field Type	Description
MT_SECTION_ID		CHARACTER	Test section identification number.
LTPP_SECTION_ID		CHARACTER(6)	LTPP test section identification.
LAYER_NO		NUMBER(2,0)	Unique sequential number assigned to pavement layers, starting with layer 1 as the deepest layer (subgrade).
ASPHALT_CONTENT	%	NUMBER(3,1)	Asphalt content of the HMA mix, by total wt. of mix.
BULK_SPECIFIC_GRAVITY		NUMBER(4,3)	Bulk specific gravity of the HMA mix.
MAXIMUM_SPECIFIC_GRAVITY		NUMBER(4,3)	Theoretical maximum specific gravity of the HMA mix.
AIR_VOIDS	%	NUMBER(3,1)	Air void content of HMA mix.
VOIDS_MINERAL_AGG	%	NUMBER(3,1)	Voids in mineral aggregate.
IDT_32	Psi	NUMBER(5,1)	Indirect diametral tensile strength for the HMA mix measured at 32°F.
IDT_MINUS_25	Psi	NUMBER(5,1)	Indirect diametral tensile strength for the HMA mix measured at 25°F.
IDT_MINUS_14	Psi	NUMBER(5,1)	Indirect diametral tensile strength for the HMA mix measured at 14°F.
IDT_1	Psi	NUMBER(5,1)	Indirect diametral tensile strength at specified temperature.
TEMPERATURE_1	°F	NUMBER(4,1)	Temperature at which the tensile strength test was performed.
IDT_2	Psi	NUMBER(5,1)	Indirect diametral tensile strength at specified temperature.
TEMPERATURE_2	°F	NUMBER(4,1)	Temperature at which tensile strength test was performed.
POISSONS_RATIO		NUMBER(3,2)	Poisson's ratio calculated from testing data.
COMPLEX_MODULUS	Psi	NUMBER(6,0)	
COMPLEX_TEMP	°F	NUMBER(4,1)	Temperature at which complex modulus testing was performed.

COMPLEX_FREQ	1/sec	NUMBER(4,0)	Frequency at which complex modulus testing was performed.
CREEP_COMP_1_SEC	1/psi	NUMBER(5,3)	Creep compliance value at 1 second.
CREEP_COMP_2_SEC	1/psi	NUMBER(5,3)	Creep compliance value at 2 seconds.
CREEP_COMP_5_SEC	1/psi	NUMBER(5,3)	Creep compliance value at 5 seconds.
CREEP_COMP_10_SEC	1/psi	NUMBER(5,3)	Creep compliance value at 10 seconds.
CREEP_COMP_20_SEC	1/psi	NUMBER(5,3)	Creep compliance value at 20 seconds.
CREEP_COMP_50_SEC	1/psi	NUMBER(5,3)	Creep compliance value at 50 seconds.
CREEP_COMP_100_SEC	1/psi	NUMBER(5,3)	Creep compliance value at 100 seconds.
TEMPERATURE_CREEP	°F	NUMBER(4,1)	Temperature at which creep compliance testing was performed.
INST_RESILIENT_MODULUS_1	Psi	NUMBER(7,0)	Instantaneous resilient modulus.
TOT_RESILIENT_MODULUS_1	Psi	NUMBER(7,0)	Total resilient modulus.
TEMP_RES_1	°F	NUMBER(4,1)	Temperature at which test was performed.
LOAD_TIME_RES_1	Seconds	NUMBER(3,2)	Loading time for testing.
UNLOAD_TIME_RES_1	Seconds	NUMBER(3,2)	Unloading time for test.
INST_RESILIENT_MODULUS_2	Psi	NUMBER(7,0)	Instantaneous resilient modulus.
TOT_RESILIENT_MODULUS_2	Psi	NUMBER(7,0)	Total resilient modulus.
TEMP_RES_2	°F	NUMBER(4,1)	Temperature at which test was performed.
LOAD_TIME_RES_2	Seconds	NUMBER(3,2)	Loading time for testing.
UNLOAD_TIME_RES_2	Seconds	NUMBER(3,2)	Unloading time for test.
INST_RESILIENT_MODULUS_3	Psi	NUMBER(7,0)	Instantaneous resilient modulus.
TOT_RESILIENT_MODULUS_3	Psi	NUMBER(7,0)	Total resilient modulus.
TEMP_RES_3	°F	NUMBER(4,1)	Temperature at which test was performed.
LOAD_TIME_RES_3	Seconds	NUMBER(3,2)	Loading time for testing.
UNLOAD_TIME_RES_3	Seconds	NUMBER(3,2)	Unloading time for test.
AGE_AT_SAMPLING	Years	NUMBER(3,1)	Age of pavement at time of sampling.
AGE_AT_TESTING	Months	NUMBER(3,0)	Age of sample at time of testing.

Table Name: TST_UNBOUND_RAW

Description: Materials information on the HMA layers of each test section

TST_UNBOUND_RAW			
Field Name	Units	Field Type	Description
MT_SECTION_ID		CHARACTER	Test section identification number.
LTPP_SECTION_ID		CHARACTER(6)	LTPP test section identification.
LAYER_NO		NUMBER(2,0)	Unique sequential number assigned to pavement layers, starting with layer 1 as the deepest layer (subgrade).
AASHTO_SOIL_CLASS		CHARACTER(5)	Soil classification based on the AASHTO system.
UNIFIED_SOIL_CLASS		CHARACTER(20)	Soil classification based on the unified soil classification system.
DEPTH_RIGID_LAYER	ft	NUMBER(3,1)	Depth to rigid layer.
RIGID_LAYER_MEASURED		CHARACTER(1)	Y or N indicating whether the depth to rigid layer is a measured value.
DEPTH_GROUNDWATER_TABLE	ft	NUMBER(3,1)	Depth to groundwater table.
GROUNDWATER_MEASURED		CHARACTER(1)	Y or N indicating whether the depth to the groundwater table is a measured value.
PCT_PASS_3_4	%	NUMBER(3,0)	Percent retained on the ¾-in sieve.
PCT_PASS_3_8	%	NUMBER(3,0)	Percent retained on the 3/8-in sieve.
PCT_PASS_NO_4	%	NUMBER(3,0)	Percent passing the number 4 sieve.
PCT_PASS_NO_40	%	NUMBER(3,0)	Percent passing the number 40 sieve.
PCT_PASS_NO_80	%	NUMBER(3,0)	Percent passing the number 80 sieve.
PCT_PASS_NO_100	%	NUMBER(3,0)	Percent passing the number 100 sieve.
PCT_PASS_NO_200	%	NUMBER(3,1)	Percent passing the number 200 sieve.
D60	in	NUMBER(4,3)	Diameter so that 60% by weight is finer.

PLASTICITY_INDEX	%	NUMBER(2,0)	Plasticity index of the material.
LIQUID_LIMIT	%	NUMBER(3,0)	Liquid limit of the unbound material.
PLASTIC_LIMIT	%	NUMBER(3,0)	Plastic limit of the material.
IN_SITU_MOISTURE	%	NUMBER(3,1)	In-place moisture content of the unbound material.
IN_SITU_DENSITY	pcf	NUMBER(4,1)	In-place density of the unbound material.
OPTIMUM_MOISTURE	%	NUMBER(2,0)	Optimum moisture content.
MAX_LAB_DENSITY	pcf	NUMBER(4,1)	Maximum dry density of the unbound material.
MAX_LAB_DENSITY_TEST		CHARACTER(4)	Test type used in performing max density test.
EQUIL_MOISTURE	%	NUMBER(3,1)	Equilibrium volumetric water content which is consistent with depth to groundwater table.
EQUIL_SATURATION	%	NUMBER(3,1)	A stable "before freezing" degree of saturation, %.
SPECIFIC_GRAVITY		NUMBER(4,3)	Specific gravity of unbound material, G_s .
CBR	%	NUMBER(3,0)	California bearing ratio.
R_VALUE	%	NUMBER(3,0)	Resistance.
SAT_HYDRAULIC_COND		NUMBER(3,1)	Saturated hydraulic conductivity, Darcy's law constant under saturated conditions.
SOIL_SUCTION	psi	NUMBER	Difference between pore air pressure and pore water pressure.
EST_RES_MOD_OPT	psi	NUMBER(6,0)	Estimated Resilient Modulus at optimum based on $M_R = 2555(\text{CBR})^{0.64}$.

Table Name: TST_UNBOUND_RESMOD

Description: Materials information on the HMA layers of each test section

TST_UNBOUND_RESMOD			
Field Name	Units	Field Type	Description
MT_SECTION_ID		CHARACTER	Test section identification number.
LTPP_SECTION_ID		CHARACTER(6)	LTPP test section identification.
LAYER_NO		NUMBER(2,0)	Unique sequential number assigned to pavement layers, starting with layer 1 as the deepest layer (subgrade).
TEST_MOISTURE	%	NUMBER(3,1)	Moisture content at which resilient modulus test was conducted.
TEST_DENSITY	pcf	NUMBER(4,1)	Density at which resilient modulus test was conducted.
RES_MOD_3_3	psi	NUMBER(6,0)	Resilient modulus with confining pressure of 3 psi and axial stress of 3 psi.
RES_MOD_3_6	psi	NUMBER(6,0)	Resilient modulus with confining pressure of 3 psi and axial stress of 6 psi.
RES_MOD_3_9	psi	NUMBER(6,0)	Resilient modulus with confining pressure of 3 psi and axial stress of 9 psi.
RES_MOD_5_5	psi	NUMBER(6,0)	Resilient modulus with confining pressure of 5 psi and axial stress of 5 psi.
RES_MOD_5_10	psi	NUMBER(6,0)	Resilient modulus with confining pressure of 5 psi and axial stress of 10 psi.
RES_MOD_5_15	psi	NUMBER(6,0)	Resilient modulus with confining pressure of 5 psi and axial stress of 15 psi.
RES_MOD_10_10	psi	NUMBER(6,0)	Resilient modulus with confining pressure of 10 psi and axial stress of 10 psi.
RES_MOD_10_20	psi	NUMBER(6,0)	Resilient modulus with confining pressure of 10 psi and axial stress of 20 psi.
RES_MOD_10_30	psi	NUMBER(6,0)	Resilient modulus with confining pressure of 10 psi and axial stress of 30 psi.
RES_MOD_15_10	psi	NUMBER(6,0)	Resilient modulus with confining pressure of 15 psi and axial stress of 10 psi.

RES_MOD_15_15	psi	NUMBER(6,0)	Resilient modulus with confining pressure of 15 psi and axial stress of 15 psi.
RES_MOD_15_30	psi	NUMBER(6,0)	Resilient modulus with confining pressure of 15 psi and axial stress of 30 psi.
RES_MOD_20_15	psi	NUMBER(6,0)	Resilient modulus with confining pressure of 20 psi and axial stress of 15 psi.
RES_MOD_20_20	psi	NUMBER(6,0)	Resilient modulus with confining pressure of 20 psi and axial stress of 20 psi.
RES_MOD_20_40	psi	NUMBER(6,0)	Resilient modulus with confining pressure of 20 psi and axial stress of 40 psi.
RES_MOD_6_2	psi	NUMBER(6,0)	Resilient modulus with confining pressure of 6 psi and axial stress of 2 psi.
RES_MOD_6_4	psi	NUMBER(6,0)	Resilient modulus with confining pressure of 6 psi and axial stress of 4 psi.
RES_MOD_6_6	psi	NUMBER(6,0)	Resilient modulus with confining pressure of 6 psi and axial stress of 6 psi.
RES_MOD_6_8	psi	NUMBER(6,0)	Resilient modulus with confining pressure of 6 psi and axial stress of 8 psi.
RES_MOD_6_10	psi	NUMBER(6,0)	Resilient modulus with confining pressure of 6 psi and axial stress of 10 psi.
RES_MOD_4_2	psi	NUMBER(6,0)	Resilient modulus with confining pressure of 4 psi and axial stress of 2 psi.
RES_MOD_4_4	psi	NUMBER(6,0)	Resilient modulus with confining pressure of 4 psi and axial stress of 4 psi.
RES_MOD_4_6	psi	NUMBER(6,0)	Resilient modulus with confining pressure of 4 psi and axial stress of 6 psi.
RES_MOD_4_8	psi	NUMBER(6,0)	Resilient modulus with confining pressure of 4 psi and axial stress of 8 psi.
RES_MOD_4_10	psi	NUMBER(6,0)	Resilient modulus with confining pressure of 4 psi and axial stress of 10 psi.
RES_MOD_2_2	psi	NUMBER(6,0)	Resilient modulus with confining pressure of 2 psi and axial stress of 2 psi.
RES_MOD_2_4	psi	NUMBER(6,0)	Resilient modulus with confining pressure of 2 psi and axial stress of 4 psi.
RES_MOD_2_6	psi	NUMBER(6,0)	Resilient modulus with confining pressure of 2 psi and axial stress of 6 psi.
RES_MOD_2_8	psi	NUMBER(6,0)	Resilient modulus with confining pressure of 2 psi and axial stress of 8 psi.
RES_MOD_2_10	psi	NUMBER(6,0)	Resilient modulus with confining pressure of 2 psi and axial stress of 10 psi.
RES_MOD_1	psi	NUMBER(6,0)	Resilient modulus conducted at selected confining stress and axial stress.
CONF_PRESS_1	psi	NUMBER(3,1)	Confining pressure of resilient modulus test.
AXIAL_STRESS_1	psi	NUMBER(3,1)	Axial stress of resilient modulus test.
RES_MOD_2	psi	NUMBER(6,0)	Resilient modulus conducted at selected confining stress and axial stress.
CONF_PRESS_2	psi	NUMBER(3,1)	Confining pressure of resilient modulus test.
AXIAL_STRESS_2	psi	NUMBER(3,1)	Axial stress of resilient modulus test.

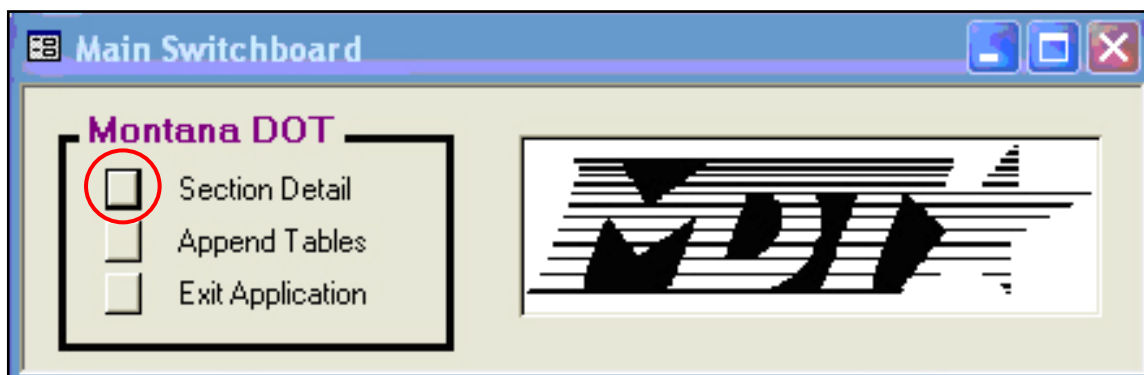
APPENDIX II-D LTPP TABLES DOCUMENTATION – DATABASE OPERATION AND UPGRADES

Part 1: General Review: Population of the Database

A set of queries were designed to populate the database with LTPP data. These queries enable deletions and re-population of the tables with future LTPP data releases. Part 2 presents instructions for deleting and re-populating the database with LTPP data. Part 3 presents instructions for populating the database with data for non-LTPP sections.

Part 2: Appending the Data Tables with Latest LTPP Data Release

It is important to populate the Section Details (see “Main Switchboard” Inventory, Construction Events, and Layers) prior to entering testing and monitoring information for a given site.



Access Database \ Main Switchboard \ Section Detail

BACKUP OF MDT DATABASE:

Make a backup copy of the MontanaDOT.mdb database before proceeding.
Re-link LTPP tables.

Current links are similar in folder structure to the LTPP release.

- Primary Data Set_A
 - \Administrative.mdb
 - \Backcalculation.mdb
 - \Inventory.mdb
 - \Maint_Rehab.mdb
 - \Material_Test.mdb
 - \Monitoring.mdb
 - \Seasonal_Monitoring.mdb
 - \Specific_Pavement_Studies.mdb
 - \Traffic.mdb
- FWD Measurement
 - \FWD_Data_Without_Drop_Data.mdb
 - \FWD_Drop_Data_States_AL_ID.mdb
 - \FWD_Drop_Data_States_MT_TN.mdb
 - \FWD_Drop_Data_States_TX_SK.mdb

Open the MontanaDOT.mdb in Access2000, choose Tools->Database Utilities->Linked Table Manager; locate each specific LTPP table and reset the link.

Make sure ALL links are corrected before performing the Append.
Click the Append Tables button on the Switchboard. Click Start Append., Click YES to continue.

The following is performed:

DELETE OLD DATA:

SECTION_EVENTS

qrySECTION_EVENTS_Delete

delete deflection data

MON_DEFLECTION_MASTER

qryMON_DEFLECTION_MASTER_Delete
MON_DEFLECTION_DATA_RAW
MON_DEFLECTION_DATA_RAW_SENSOR
MON_DEFL_BACKCALC_SECT
MON_DEFL_BACKCALC_PT

delete traffic data

TRF_MONITOR_MASTER

qryTRF_MONITOR_MASTER_Delete
TRF_VEHICLE_DISTRIB
TRF_AXLE_DISTRIB_WEIGHT
TRF_AXLE_SUMMARY

delete esal data

TRF_ESAL_MASTER

qryTRF_ESAL_MASTER_Delete

delete profile data

MON_PROFILE_MASTER

qryMON_PROFILE_MASTER_Delete
MON_PROFILE
MON_PROFILE_RAW

delete distress data

MON_DISTRESS_MASTER

qryMON_DISTRESS_MASTER_Delete
MON_DISTRESS_RAW

delete rut data

MON_RUT_MASTER

qryMON_RUT_MASTER_Delete
MON_RUT_RAW_DISTANCE

delete layer structure data for all LTPP sections

TST_LAYER_STRUCTURE

qryTST_LAYER_STRUCTURE_Delete
TST_MASTER
TST_HMA_AGGREGATE
TST_HMA_CEMENT

TST_UNBOUND_RESMOD
TST_HMA_MIX
TST_UNBOUND_RAW
MON_DEFL_BACKCALC_LAYER

TST_WATERTAB_DEPTH_MAN
qryTST_WATERTAB_DEPTH_MAN_Delete

ADD NEW DATA:

SECTION EVENTS

qrySECTION_EVENTS_Append

PROFILE

MON_PROFILE_MASTER; MON_PROFILE MASTER (LTPP) & SECTION
qryMON_PROFILE_MASTER_Append

MON_PROFILE; MON_PROFILE MASTER (LTPP), MON_PROFILE_MASTER, SECTION
qryMON_PROFILE_Append

MON_PROFILE_RAW; MON_PROFILE MASTER (LTPP), MON_PROFILE_MASTER, SECTION
qryMON_PROFILE_RAW_Append

TRAFFIC

TRF_ESAL_MASTER; TRF_MON_EST_ESAL & SECTION
qryTRF_ESAL_MASTER_MONITORED_Append

TRF_ESAL_MASTER
qryTRF_ESAL_MASTER_Update_M

TRF_ESAL_MASTER; TRF_HIST_EST_ESAL & SECTION
qryTRF_ESAL_MASTER_HISTORICAL_Append

TRF_ESAL_MASTER
qryTRF_ESAL_MASTER_Update_H

TRF_MONITOR_MASTER; qryTRF_MONITOR_MASTER_Union,
qryTRF_Sectons_TRF_MONITOR_MASTER_Select, SECTIONS
qryTRF_MONITOR_MASTER_Append

TRF_MONITOR_LTPP_LN, qryTRF_VEHICLE_DISTRIB_Select, SECTION,
TRF_MONITOR_MASTER
qryTRF_VEHICLE_DISTRIB_Append

TRF_MONITOR_AXLE_DISTRIB,
qryTRF_AXLE_DISTRIB_TRF_MONITOR_BASIC_INFO_Select, SECTIONS,
TRF_MONITOR_MASTER
qryTRF_AXLE_DISTRIB_Append

TRF_MONITOR_LTPP_LN, qryTRF_AXLE_SUMMARY_Union, SECTION,
TRF_MONITOR_MASTER
qryTRF_AXLE_SUMMARY_Append

RUTTING

MON_RUT_MASTER;MON_T_PROF_INDEX_POINT, SECTION
qryMON_RUT_MASTER_Append

MON_RUT_RAW_DISTANCE;MON_T_PROF_PROFILE, SECTION, MON_RUT_MASTER,
qryMON_RUT_RAW_DISTANCE, tbl_MON_T_PROF_PROFILE_Index
qryMON_RUT_RAW_DISTANCE_Append

DISTRESS

MON_DISTRESS_MASTER;qryMON_DISTRESS_SURVEY_DATE_Union,
qryMON_DISTRESS_PERCENT_FATIGUE_THERMAL_CRACK_Union,
qryMON_DISTRESS_WIRELINE_RUT_DEPTH_Avg_Stdev_Select
qryMON_DISTRESS_Append

MON_DISTRESS_RAW;MON_DISTRESS_MASTER, qryMON_DISTRESS_RAW_1_Union,
qryKEYCODEScartesian
qryMON_DISTRESS_RAW_1_Append

MON_DISTRESS_RAWMON_DISTRESS_MASTER, qryMON_DISTRESS_RAW_2_Union,
qryKEYCODEScartesian
qryMON_DISTRESS_RAW_2_Append

TESTING

TST_LAYER_STRUCTURE;SECTION, SECTION_EVENTS, qryTST_L05B_LayerStructure,
SRODBA_CODES, KeyCodes
qryTST_LAYER_STRUCTURE_Append

TST_MASTER;qryTST_MASTER_AddSampleDate, SECTION, SECTION_EVENTS,
TST_LAYER_STRUCTURE
qryTST_MASTER_Append

TST_UNBOUND_RAW;

TST_UNBOUND_RAW;QRY_TST_SS04_UG08_AASHTO,
qrySECT_SECT_EVNT_LAYER_STRUC_TST_MASTER_Select, KEYCODES
qryTST_UNBOUND_RAW_AASHTO_CLASS_Append

TST_UNBOUND_RAW;TST_HOLE_LOG,
qrySECT_SECT_EVNT_LAYER_STRUC_TST_MASTER_Select, KEYCODES
qryTST_UNBOUND_RAW_TST_HOLE_LOG_Append

TST_UNBOUND_RAW;TST_SS01_UG01_UG02,
qrySECT_SECT_EVNT_LAYER_STRUC_TST_MASTER_Select, KEYCODES
qryTST_UNBOUND_RAW_TST_SS01_UG01_UG02_Append

TST_UNBOUND_RAW;TST_SS02_UG03,
qrySECT_SECT_EVNT_LAYER_STRUC_TST_MASTER_Select, KEYCODES
qryTST_UNBOUND_RAW_TST_SS02_UG03_Append

TST_UNBOUND_RAW;TST_UG04_SS03,
qrySECT_SECT_EVNT_LAYER_STRUC_TST_MASTER_Select, KEYCODES
qryTST_UNBOUND_RAW_TST_UG04_SS03_Append

TST_UNBOUND_RAW;TST_UG05_SS05,
qrySECT_SECT_EVNT_LAYER_STRUC_TST_MASTER_Select, KEYCODES

qryTST_UNBOUND_RAW_TST_UG05_SS05_Append

TST_UNBOUND_RAW;INV_SUBGRADE,
qrySECT_SECT_EVNT_LAYER_STRUC_TST_MASTER_Select, KEYCODES
qryTST_UNBOUND_RAW_CBR_SUBGRADE_Append

TST_UNBOUND_RAW;INV_SUBGRADE,
qrySECT_SECT_EVNT_LAYER_STRUC_TST_MASTER_Select, KEYCODES
qryTST_UNBOUND_RAW_CBR_UNBOUND_Append

TST_UNBOUND_RAW;INV_SUBGRADE,
qrySECT_SECT_EVNT_LAYER_STRUC_TST_MASTER_Select, KEYCODES
qryTST_UNBOUND_RAW_R_SUBGRADE_Append

TST_UNBOUND_RAW;INV_SUBGRADE,
qrySECT_SECT_EVNT_LAYER_STRUC_TST_MASTER_Select, KEYCODES
qryTST_UNBOUND_RAW_R_UNBOUND_Append

TST_UNBOUND_RAW;TST_SS11,
qrySECT_SECT_EVNT_LAYER_STRUC_TST_MASTER_Select, KEYCODES
qryTST_UNBOUND_RAW_TST_SS11_Append

TST_UNBOUND_RAW;TST_UG09,
qrySECT_SECT_EVNT_LAYER_STRUC_TST_MASTER_Select, KEYCODES
qryTST_UNBOUND_RAW_TST_UG09_Append

TST_WATERTAB_DEPTH_MAN;

TST_WATERTAB_DEPTH_MAN;qrySECT_SECT_EVNT_Select,
SMP_WATERTAB_DEPTH_MAN, KEYCODES
qryTST_WATERTAB_DEPTH_MAN_Append

TST_UNBOUND_RESMOD;

TST_UNBOUND_RESMOD;QRY_RES_MOD_AVG_FINAL,
qrySECT_SECT_EVNT_LAYER_STRUC_TST_MASTER_Select, KEYCODES
qryTST_UNBOUND_RESMOD_Append

TST_HMA_CEMENT;

TST_HMA_CEMENT;QRY_TST_AE02,
qrySECT_SECT_EVNT_LAYER_STRUC_TST_MASTER_Select, KEYCODES
qryTST_HMA_CEMENT_AE02_Append

TST_HMA_CEMENT;QRY_TST_AE02S,
qrySECT_SECT_EVNT_LAYER_STRUC_TST_MASTER_Select, KEYCODES
qryTST_HMA_CEMENT_AE02S_Append

TST_HMA_CEMENT;QRY_TST_AE03,
qrySECT_SECT_EVNT_LAYER_STRUC_TST_MASTER_Select, KEYCODES
qryTST_HMA_CEMENT_AE03_Append

TST_HMA_CEMENT;QRY_TST_AE05,
qrySECT_SECT_EVNT_LAYER_STRUC_TST_MASTER_Select, KEYCODES
qryTST_HMA_CEMENT_AE05_Append

TST_HMA_CEMENT;QRY_RHB_ACO_PROP,
qrySECT_SECT_EVNT_LAYER_STRUC_TST_MASTER_Select, KEYCODES
qryTST_HMA_CEMENT_RHB_ACO_PROP_Append

TST_HMA_CEMENT;QRY_RHB_CM RAP_COMBINE_AC,
qrySECT_SECT_EVNT_LAYER_STRUC_TST_MASTER_Select, KEYCODES
qryTST_HMA_CEMENT_RHB_CM RAP_COMBINE_AC_Append

TST_HMA_CEMENT;QRY_RHB_HMRAP_COMBINE_AC,
qrySECT_SECT_EVNT_LAYER_STRUC_TST_MASTER_Select, KEYCODES
qryTST_HMA_CEMENT_RHB_HMRAP_COMBINE_AC_Append

TST_HMA_CEMENT;QRY_SPS1_PMA_AC_PROP,
qrySECT_SECT_EVNT_LAYER_STRUC_TST_MASTER_Select, KEYCODES
qryTST_HMA_CEMENT_SPS1_PMA_AC_PROP_Append

TST_HMA_CEMENT;QRY_SPS8_PMA_AC_PROP,
qrySECT_SECT_EVNT_LAYER_STRUC_TST_MASTER_Select, KEYCODES
qryTST_HMA_CEMENT_SPS8_PMA_AC_PROP_Append

TST_HMA_CEMENT;QRY_SPS9_PMA_AC_PROP,
qrySECT_SECT_EVNT_LAYER_STRUC_TST_MASTER_Select, KEYCODES
qryTST_HMA_CEMENT_SPS9_PMA_AC_PROP_Append

TST_HMA_CEMENT;QRY_SPS9_SP_PMA_AC_PROP,
qrySECT_SECT_EVNT_LAYER_STRUC_TST_MASTER_Select, KEYCODES
qryTST_HMA_CEMENT_SPS9_SP_PMA_AC_PROP_Append

TST_HMA_AGGREGATE;

TST_HMA_AGG_LIST_TABLE; temporary table to be deleted
QRY_TST_HMA_AGG_MAKE_LIST_TABLE

TST_HMA_AGGREGATE;QRY_TST_HMA_AGG_DATA_Select,
qrySECT_SECT_EVNT_LAYER_STRUC_TST_MASTER_Select, KEYCODES
qryTST_HMA_AGGREGATE_TST_HMA_AGG_DATA_Append

TST_HMA_AGGREGATE;RHB_HMRAP_COMB_AGG,
qrySECT_SECT_EVNT_LAYER_STRUC_TST_MASTER_Select, KEYCODES
qryTST_HMA_AGGREGATE_RHB_HMRAP_COMB_AGG_Append

TST_HMA_AGGREGATE;RHB_ACO_AGR_PROP,
qrySECT_SECT_EVNT_LAYER_STRUC_TST_MASTER_Select, KEYCODES
qryTST_HMA_AGGREGATE_RHB_ACO_AGR_PROP_Append

TST_HMA_AGGREGATE;SPS1_PMA_AGGREGATE_PROP,
qrySECT_SECT_EVNT_LAYER_STRUC_TST_MASTER_Select, KEYCODES
qryTST_HMA_AGGREGATE_SPS1_PMA_AGG_PROP_Append

TST_HMA_AGGREGATE;SPS8_PMA_AGGREGATE_PROP,
qrySECT_SECT_EVNT_LAYER_STRUC_TST_MASTER_Select, KEYCODES
qryTST_HMA_AGGREGATE_SPS8_PMA_AGG_PROP_Append

TST_HMA_AGGREGATE;SPS9_PMA_AGGREGATE_PROP,
qrySECT_SECT_EVNT_LAYER_STRUC_TST_MASTER_Select, KEYCODES

qryTST_HMA_AGGREGATE_SPS9_PMA_AGG_PROP_Append

TST_HMA_AGGREGATE;SPS9_SP_PMA_AGGREGATE_PROP,
qrySECT_SECT_EVNT_LAYER_STRUC_TST_MASTER_Select, KEYCODES
qryTST_HMA_AGGREGATE_SPS9_SP_PMA_AGG_PROP_Append

TST_HMA_AGG_LIST_TABLE; deleted
DoCmd.DeleteObject acTable, TST_HMA_AGG_LIST_TABLE

TST_HMA_MIX;

TST_HMA_MIX;qryTST_HMA_MIX_Select_AC07_IDT_INFO,
qrySECT_SECT_EVNT_LAYER_STRUC_TST_MASTER_Select, KEYCODES
qryTST_HMA_MIX_AC07_IDT_INFO_Append

TST_HMA_MIX;qryTST_HMA_MIX_Select_AC02_AC03_AC04_SP02,
qrySECT_SECT_EVNT_LAYER_STRUC_TST_MASTER_Select, KEYCODES
qryTST_HMA_MIX_AC02_AC03_AC04_SP02_Append

TST_HMA_MIX;QRY_MODIFY_AC07_MR_DATA,
qrySECT_SECT_EVNT_LAYER_STRUC_TST_MASTER_Select, KEYCODES
qryTST_HMA_MIX_AC07_MR_DATA_Append

TST_HMA_MIX;qryTST_HMA_MIX_Select_AC07_V2_CREEP_COMP_SUM,
qrySECT_SECT_EVNT_LAYER_STRUC_TST_MASTER_Select, KEYCODES
qryTST_HMA_MIX_AC07_V2_CREEP_COMP_SUM_Append

TST_HMA_MIX;QRY_HMA_MIX_CONST_UNION,
qrySECT_SECT_EVNT_LAYER_STRUC_TST_MASTER_Select, KEYCODES
qryTST_HMA_MIX_HMA_MIX_CONST_DATA_Append

DEFLECTION

MON_DEFLECTION_MASTER;MON_DEFL_BACKCALC_SECT, SECTION
qryMON_DEFLECTION_MASTER_Append

MON_DEFL_BACKCALC_SECT;MON_DEFL_FLEX_BACKCAL_SECT, SECTION,
MON_DEFLECTION_MASTER
qryMON_DEFL_BACKCALC_SECT_Append

MON_DEFL_BACKCALC_PT;MON_DEFL_FLEX_BACKCAL_POINT, SECTION,
MON_DEFLECTION_MASTER
qryMON_DEFL_BACKCALC_PT_Append

MON_DEFL_BACKCALC_LAYER;MON_DEFL_FLEX_BACKCAL_SECT, SECTION,
MON_DEFLECTION_MASTER
qryMON_DEFL_BACKCALC_LAYER_Append

MON_DEFLECTION_DATA_RAW;qryMON_DEFL_DROP_DATA_Union, SECTION,
MON_DEFL_LOC_INFO, MON_DEFLECTION_MASTER
qryMON_DEFLECTION_DATA_RAW_Append

MON_DEFLECTION_DATA_RAW_SENSOR;qryMON_DEFL_DROP_DATA_Union, SECTION,
MON_DEFLECTION_MASTER, tblMON_DEFL_DROP_DATA_Index
qryMON_DEFLECTION_DATA_RAW_SENSOR_Append

Part 3: Instructions for Populating the Database with Data for Non-LTPP Sections

The data for non-LTPP test sections must be entered into the respective tables manually. It is important to populate the “Section Detail” (see Section, Inventory, Construction Events, and Layers from the main switchboard) prior to entering testing, monitoring, and traffic information for the sections.

For New Sections:

- Entries should be initiated via the main switchboard by entering section details in the “Description” and “State Code” field.
- The “Inventory” tab should then be completed, followed by the entries for the “Construction Event” and “Layers” tabs.

For Sections with Existing Entries:

- With a new construction event, the appropriate section should be identified by scrolling through the “Records” on the main switchboard.
- Once the affected section has been identified, click on the “Construction Events” tab, scroll through the “Records,” and identify the last construction event for the section.
- Scroll through the “Records” to insert a new construction event. The new construction event will have a “Construction Number” one greater than the last construction event identified for the section.
- Enter the details for this new construction event.
- If the new construction event resulted in layer structure changes, use the “Layers” tab to enter the layer details for the new construction event.
- For the latest construction number, include only the layer changes made during the specific construction event. For example, if an overlay was the most recent construction event, enter only the information for the overlay. In the event that an existing layer was modified (partially or totally milled and filled), indicate the milling activity in the latest construction event and specify a new layer number for the filling activity. The most recent activity for the mill and fill should indicate a smaller layer thickness for the milled layer when compared to the thickness of the same layer from a previous construction event. For example, if during the milling operation, some or all of an existing layer (already identified in the database) is removed, the remaining existing layer thickness (0 to n inches) should still be identified. The filling activity should be identified with a unique (new) layer number.
- After the “Section Details” have been entered, exit the main switchboard and enter other information (test, monitoring, and traffic) for the section/event.

- The testing information must be entered starting with the entries for the “TST_MASTER” table.
- The monitoring data for non-LTPP sections can be entered in a manner similar to the test information. The monitoring tables are designated with “MON” as a prefix to the table name.

NOTE: The tables “MON_DEFLECTION_MASTER”, “MON_PROFILE_MASTER,” “MON_DISTRESS_MASTER” and MON_RUT_MASTER” should be completed prior to entering deflection, profile, distress and rut information respectively.

- All tables pertaining to test data contain a “TST” prefix before the table name. Open the table by double clicking on the name of the table.
- Go to the bottom of the table (Exhibit 1) to include a new record (blank row).

ID	Section/CN Event/Layer	SAMPLE_NO	FIELD_SET	Age at Sampli	LOC_NO
7229	90 Saskatchewan GPS 6B Section 6410 6410 CN: 1 Layer: 1	BS**	1	9/25/1989	TP2
7230	90 Saskatchewan GPS 6B Section 6410 6410 CN: 1 Layer: 1	BS57	1	9/25/1989	TP2
7231	90 Saskatchewan GPS 6B Section 6410 6410 CN: 1 Layer: 2	BG**	1	9/26/1989	TP1
7232	90 Saskatchewan GPS 6B Section 6410 6410 CN: 1 Layer: 2	BG**	1	9/25/1989	TP2
7234	90 Saskatchewan GPS 6B Section 6410 6410 CN: 1 Layer: 3	BG**	1	9/26/1989	TP1
7233	90 Saskatchewan GPS 6B Section 6410 6410 CN: 1 Layer: 3	BG55	1		TP*
7235	90 Saskatchewan GPS 6B Section 6410 6410 CN: 1 Layer: 3	BG**	1	9/25/1989	TP2
7236	90 Saskatchewan GPS 6B Section 6410 6410 CN: 1 Layer: 4	CA51	1	9/25/1989	A1
7238	90 Saskatchewan GPS 6B Section 6410 6410 CN: 1 Layer: 4	KA01	1	9/26/1989	TP1
7239	90 Saskatchewan GPS 6B Section 6410 6410 CN: 1 Layer: 4	KA02	1	9/25/1989	TP2
7237	90 Saskatchewan GPS 6B Section 6410 6410 CN: 1 Layer: 4	CA52	1	9/25/1989	A2
7240	90 Saskatchewan GPS 6B Section 6410 6410 CN: 1 Layer: 5	CA51	1	9/25/1989	A1
7241	90 Saskatchewan GPS 6B Section 6410 6410 CN: 1 Layer: 5	CA52	1	9/25/1989	A2
7242	90 Saskatchewan GPS 6B Section 6410 6410 CN: 1 Layer: 5	KA01	1	9/26/1989	TP1
7243	90 Saskatchewan GPS 6B Section 6410 6410 CN: 1 Layer: 5	KA02	1	9/25/1989	TP2
7246	90 Saskatchewan GPS 6B Section 6410 6410 CN: 2 Layer: 6	CA52	2	12/5/1990	A2
7244	90 Saskatchewan GPS 6B Section 6410 6410 CN: 2 Layer: 6				
7245	90 Saskatchewan GPS 6B Section 6410 6410 CN: 2 Layer: 6	CA51	2	12/5/1990	A1
7248	90 Saskatchewan GPS 6B Section 6412 6412 CN: 1 Layer: 1	BS55	1	9/26/1989	TP1
7247	90 Saskatchewan GPS 6B Section 6412 6412 CN: 1 Layer: 1	BS**	1	9/26/1989	TP1
7249	90 Saskatchewan GPS 6B Section 6412 6412 CN: 1 Layer: 2	BG**	1	9/26/1989	TP1
7250	90 Saskatchewan GPS 6B Section 6412 6412 CN: 1 Layer: 3	BG**	1	9/26/1989	TP1
7251	90 Saskatchewan GPS 6B Section 6412 6412 CN: 1 Layer: 4	CA51	1	9/26/1989	A2
7252	90 Saskatchewan GPS 6B Section 6412 6412 CN: 1 Layer: 4	KA01	1	9/26/1989	TP1
7253	90 Saskatchewan GPS 6B Section 6412 6412 CN: 1 Layer: 5	CA51	1	9/26/1989	A2
7254	90 Saskatchewan GPS 6B Section 6412 6412 CN: 1 Layer: 5	KA01	1	9/26/1989	TP1
7255	90 Saskatchewan GPS 6B Section 6412 6412 CN: 2 Layer: 6				
7256	90 Saskatchewan GPS 6B Section 6412 6412 CN: 2 Layer: 6	CA51	2	12/5/1990	A1
7257	90 Saskatchewan GPS 6B Section 6412 6412 CN: 2 Layer: 6	CA52	2	12/5/1990	A2
7259	90 Saskatchewan GPS 6B Section 6420 6420 CN: 4 Layer: 3		2		
7258	90 Saskatchewan GPS 6B Section 6420 6420 CN: 4 Layer: 3				
(AutoNumber)					

Open the TST_MASTER table and scroll down to the end of the table.

Exhibit 1

- Using the drop down menu, choose the “Section/CN Event/Layer” details (Exhibit 2) for the new entry intended.

ID	Section/CN Event/Layer	SAMPLE_NO	FIELD_SET	Age at Sample	LOC_NO
7241	90 Saskatchewan GPS 6B Section 6410 6410 CN: 1 Layer: 5	CA52	1	9/25/1989	A2
7242	90 Saskatchewan GPS 6B Section 6410 6410 CN: 1 Layer: 5	KA01	1	9/26/1989	TP1
7243	90 Saskatchewan GPS 6B Section 6410 6410 CN: 1 Layer: 5	KA02	1	9/25/1989	TP2
7246	90 Saskatchewan GPS 6B Section 6410 6410 CN: 2 Layer: 6	CA52	2	12/5/1990	A2
7244	90 Saskatchewan GPS 6B Section 6410 6410 CN: 2 Layer: 6				
7245	90 Saskatchewan GPS 6B Section 6410 6410 CN: 2 Layer: 6	CA51	2	12/5/1990	A1
7248	90 Saskatchewan GPS 6B Section 6412 6412 CN: 1 Layer: 1	BS55	1	9/26/1989	TP1
7247	90 Saskatchewan GPS 6B Section 6412 6412 CN: 1 Layer: 1	BS**	1	9/26/1989	TP1
7249	90 Saskatchewan GPS 6B Section 6412 6412 CN: 1 Layer: 2	BG**	1	9/26/1989	TP1
7250	90 Saskatchewan GPS 6B Section 6412 6412 CN: 1 Layer: 3	BG**	1	9/26/1989	TP1
7251	90 Saskatchewan GPS 6B Section 6412 6412 CN: 1 Layer: 4	CA51	1	9/26/1989	A2
7252	90 Saskatchewan GPS 6B Section 6412 6412 CN: 1 Layer: 4	KA01	1	9/26/1989	TP1
7253	90 Saskatchewan GPS 6B Section 6412 6412 CN: 1 Layer: 5	CA51	1	9/26/1989	A2
7254	90 Saskatchewan GPS 6B Section 6412 6412 CN: 1 Layer: 5	KA01	1	9/26/1989	TP1
7255	90 Saskatchewan GPS 6B Section 6412 6412 CN: 2 Layer: 6				
7256	90 Saskatchewan GPS 6B Section 6412 6412 CN: 2 Layer: 6	CA51	2	12/5/1990	A1
7257	90 Saskatchewan GPS 6B Section 6412 6412 CN: 2 Layer: 6	CA52	2	12/5/1990	A2
7259	90 Saskatchewan GPS 6B Section 6420 6420 CN: 4 Layer: 3				
7258	90 Saskatchewan GPS 6B Section 6420 6420 CN: 4 Layer: 3				

Select “Section/CN Event/Layer” using drop down list.

Exhibit 2

- Enter the sample details (Exhibit 3) requested in the table. After completing the entry, exit this table.

ID	Section/CN Event/Layer	SAMPLE_NO	FIELD_SET	Age at Sample	LOC_NO
+ 7249	90 Saskatchewan GPS 6B Section 6412 6412 CN: 1 Layer: 2	BG**	1	9/26/1989	TP1
+ 7250	90 Saskatchewan GPS 6B Section 6412 6412 CN: 1 Layer: 3	BG**	1	9/26/1989	TP1
+ 7251	90 Saskatchewan GPS 6B Section 6412 6412 CN: 1 Layer: 4	CA51	1	9/26/1989	A2
+ 7252	90 Saskatchewan GPS 6B Section 6412 6412 CN: 1 Layer: 4	KA01	1	9/26/1989	TP1
+ 7253	90 Saskatchewan GPS 6B Section 6412 6412 CN: 1 Layer: 5	CA51	1	9/26/1989	A2
+ 7254	90 Saskatchewan GPS 6B Section 6412 6412 CN: 1 Layer: 5	KA01	1	9/26/1989	TP1
+ 7255	90 Saskatchewan GPS 6B Section 6412 6412 CN: 2 Layer: 6				
+ 7256	90 Saskatchewan GPS 6B Section 6412 6412 CN: 2 Layer: 6	CA51	2	12/5/1990	A1
+ 7257	90 Saskatchewan GPS 6B Section 6412 6412 CN: 2 Layer: 6	CA52	2	12/5/1990	A2
+ 7259	90 Saskatchewan GPS 6B Section 6420 6420 CN: 4 Layer: 3		2		
+ 7258	90 Saskatchewan GPS 6B Section 6420 6420 CN: 4 Layer: 3				
+ 7341	30 Geyser E CN: 1 Layer: 4	AC20	1	5/2/2002	AFT65
* (AutoNumber)					

Enter relevant data for each field using the keyboard.

Exhibit 3

- Open the testing table in which the actual test data will be entered. For example, aggregate gradation for a hot mix asphalt concrete layer will be entered in table "TST_HMA_AGGREGATE." Open the tables by double clicking on the name of the table, then scroll down to the end of the table (Exhibit 4).

ID	Section/SampleNo/LayerNo	TEST_DATE	Phase	Percent passing 3/4"	Percent passing 3/8"
53967	81 A901 Alberta SPS 9N Section 1 Sample: CA01A01 Layer: 3	2/1/1997	In-Situ	77	4
53968	81 A901 Alberta SPS 9N Section 1 Sample: CA08A01 Layer: 3	2/1/1997	In-Situ	83	4
53969	81 A901 Alberta SPS 9N Section 1 Sample: CA01C01 Layer: 3	2/2/1997	In-Situ	82	4
53970	81 A901 Alberta SPS 9N Section 1 Sample: CA08C01 Layer: 3	2/2/1997	In-Situ	81	4
53971	81 A902 Alberta SPS 9N Section 2 Sample: CA02A02 Layer: 3	2/1/1997	In-Situ	74	2
53972	81 A902 Alberta SPS 9N Section 2 Sample: CA33A02 Layer: 3	2/1/1997	In-Situ	81	3
53973	81 A902 Alberta SPS 9N Section 2 Sample: CA01C02 Layer: 3	2/2/1997	In-Situ	61	2
53974	81 A902 Alberta SPS 9N Section 2 Sample: CA08C02 Layer: 3	2/2/1997	In-Situ	75	2
53975	81 A903 Alberta SPS 9N Section 3 Sample: CA01A03 Layer: 3	2/1/1997	In-Situ	81	3
53976	81 A903 Alberta SPS 9N Section 3 Sample: CA08A03 Layer: 3	2/1/1997	In-Situ	82	3
53977	81 A903 Alberta SPS 9N Section 3 Sample: CA01C03 Layer: 3	2/2/1997	In-Situ	85	3
53978	81 A903 Alberta SPS 9N Section 3 Sample: CA08C03 Layer: 3	2/2/1997	In-Situ	82	3
53979	90 6410 Saskatchewan GPS 6B Section 6410 Sample: KA01 Layer: 4	10/27/1990	In-Situ	100	4
53980	90 6410 Saskatchewan GPS 6B Section 6410 Sample: KA02 Layer: 4	10/27/1990	In-Situ	100	4
53981	90 6410 Saskatchewan GPS 6B Section 6410 Sample: KA01 Layer: 5	10/27/1990	In-Situ	100	4
53982	90 6410 Saskatchewan GPS 6B Section 6410 Sample: KA02 Layer: 5	10/27/1990	In-Situ	100	4
53983	90 6410 Saskatchewan GPS 6B Section 6410 Sample: CA51 Layer: 6	8/14/1991	In-Situ	100	7
53984	90 6410 Saskatchewan GPS 6B Section 6410 Sample: CA52 Layer: 6	8/14/1991	In-Situ	100	4
53985	90 6412 Saskatchewan GPS 6B Section 6412 Sample: KA01 Layer: 4	10/10/1990	In-Situ	100	4
53986	90 6412 Saskatchewan GPS 6B Section 6412 Sample: KA01 Layer: 5	10/10/1990	In-Situ	100	4
53987	90 6412 Saskatchewan GPS 6B Section 6412 Sample: CA51 Layer: 6	8/14/1991	In-Situ	100	4
53988	90 6412 Saskatchewan GPS 6B Section 6412 Sample: CA52 Layer: 6	8/14/1991	In-Situ	100	7
53989	90 6801 Saskatchewan GPS 6A Section 6801 Sample: KA01 Layer: 2	3/5/1991	In-Situ	100	7
53990	90 6801 Saskatchewan GPS 6A Section 6801 Sample: KA02 Layer: 2	3/5/1991	In-Situ	100	4
53991	90 6801 Saskatchewan GPS 6A Section 6801 Sample: KA01 Layer: 3	3/4/1991	In-Situ	100	7
53992	90 6801 Saskatchewan GPS 6A Section 6801 Sample: KA02 Layer: 3	3/4/1991	In-Situ	100	4
53994	30 Vaughn Sample: BA09 Layer: 5	6/23/2005	In-Situ	60	2
53995	30 Vaughn Sample: BA09 Layer: 4	6/23/2005	In-Situ	75	2
(AutoNumber)					

Open the TST_HMA_AGGREGATE table,
 and scroll down to the end of the table.

Exhibit 4

- Using the drop down menu, insert a record for the given "Section/Sample No/Layer No" (Exhibit 5).

The screenshot shows a data table with the following columns: ID, Section/SampleNo/LayerNo, TEST_DATE, Phase, Percent passing 3/4", Percent passing 3/8", and Perc %. A dropdown menu is open over the 'Section/Sample No/Layer No' column, showing a list of options including '30 Geyser E Sample: AC10 Layer: 4' through '30 Silver City W Sample: BS** Layer: 1'. The table contains various records with IDs ranging from 53963 to 53995. The status bar at the bottom indicates 'Record: 280 of 280' and 'TST_LAYER_MASTER row ID number.'.

ID	Section/SampleNo/LayerNo	TEST_DATE	Phase	Percent passing 3/4"	Percent passing 3/8"	Perc %
53963	81 2812 Alberta GPS 2 Section 2812 Sample: CA61 Layer: 3	6/27/1991	In-Situ	100	82	
53964	81 2812 Alberta GPS 2 Section 2812 Sample: KA90 Layer: 3	6/27/1991	In-Situ	100	77	
53965	81 8529 Alberta GPS 2 Section 8529 Sample: CA61 Layer: 3	7/1/1991	In-Situ	100	82	
53966	81 8529 Alberta GPS 2 Section 8529 Sample: KA90 Layer: 3	6/27/1991	In-Situ	100	85	
53967	81 A901 Alberta SPS 9N Section 1 Sample: CA01A01 Layer: 3	2/1/1997	In-Situ	77	42	
53968	81 A901 Alberta SPS 9N Section 1 Sample: CA08A01 Layer: 3	2/1/1997	In-Situ	83	50	
53969	81 A901 Alberta SPS 9N Section 1 Sample: CA01C01 Layer: 3	2/2/1997	In-Situ	82	49	
53970	81 A901 Alberta SPS 9N Section 1 Sample: CA08C01 Layer: 3	2/2/1997	In-Situ	81	48	
53971	81 A902 Alberta SPS 9N Section 2 Sample: CA02A02 Layer: 3	2/1/1997	In-Situ	74	26	
53972	81 A902 Alberta SPS 9N Section 2 Sample: CA33A02 Layer: 3	2/1/1997	In-Situ	81	31	
53973	81 A902 Alberta SPS 9N Section 2 Sample: CA01C02 Layer: 3	2/2/1997	In-Situ	61	24	
53974	81 A902 Alberta SPS 9N Section 2 Sample: CA08C02 Layer: 3	2/2/1997	In-Situ	75	29	
53975	81 A903 Alberta SPS 9N Section 3 Sample: CA01A03 Layer: 3	2/1/1997	In-Situ	81	31	
53976	81 A903 Alberta SPS 9N Section 3 Sample: CA08A03 Layer: 3	2/1/1997	In-Situ	82	32	
53977	81 A903 Alberta SPS 9N Section 3 Sample: CA01C03 Layer: 3	2/2/1997	In-Situ	85	33	
53978	81 A903 Alberta SPS 9N Section 3 Sample: CA08C03 Layer: 3	2/2/1997	In-Situ	82	32	
53979	90 6410 Saskatchewan GPS 6B Section 6410 Sample: KA01 L	10/27/1990	In-Situ	100	81	
53980	90 6410 Saskatchewan GPS 6B Section 6410 Sample: KA02 L	10/27/1990	In-Situ	100	82	
53981	90 6410 Saskatchewan GPS 6B Section 6410 Sample: KA01 L	10/27/1990	In-Situ	100	85	
53982	90 6410 Saskatchewan GPS 6B Section 6410 Sample: KA02 L	10/27/1990	In-Situ	100	85	
53983	90 6410 Saskatchewan GPS 6B Section 6410 Sample: CA51 L	8/14/1991	In-Situ	100	79	
53984	90 6410 Saskatchewan GPS 6B Section 6410 Sample: CA52 L	8/14/1991	In-Situ	100	82	
53985	90 6412 Saskatchewan GPS 6B Section 6412 Sample: KA01 L	10/10/1990	In-Situ	100	84	
53986	90 6412 Saskatchewan GPS 6B Section 6412 Sample: KA01 L	10/10/1990	In-Situ	100	89	
53987	30 Geyser E Sample: AC10 Layer: 4	1/14/1991	In-Situ	100	81	
53988	30 Geyser E Sample: AC11 Layer: 4	1/14/1991	In-Situ	100	79	
53989	30 Geyser E Sample: AC12 Layer: 4	3/5/1991	In-Situ	100	77	
53990	30 Geyser E Sample: AC13 Layer: 4	3/5/1991	In-Situ	100	80	
53991	30 Geyser E Sample: AC14 Layer: 4	3/4/1991	In-Situ	100	74	
53992	30 Geyser E Sample: AC00 Layer: 4	7/27/1991	In-Situ	100	80	
53994	30 Geyser E Sample: AC20 Layer: 4	7/34/1991	In-Situ	60	29	
53995	30 Silver City W Sample: BS** Layer: 1	7/29/2005	In-Situ	75	29	

Select "Section/Sample No/Layer No" using the drop down list.

Exhibit 5

- Fill in the details (Exhibit 6) of the test, and exit the form.

ID	Section/SampleNo/LayerNo	TEST_DATE	Phase	Percent passing 3/4"	Percent passing 3/8"	Perc
53988	90 6412 Saskatchewan GPS 6B Section 6412 Sample: CA52 L	8/14/1991	In-Situ	100		79
53989	90 6801 Saskatchewan GPS 6A Section 6801 Sample: KA01 L	3/5/1991	In-Situ	100		77
53990	90 6801 Saskatchewan GPS 6A Section 6801 Sample: KA02 L	3/5/1991	In-Situ	100		80
53991	90 6801 Saskatchewan GPS 6A Section 6801 Sample: KA01 L	3/4/1991	In-Situ	100		74
53992	90 6801 Saskatchewan GPS 6A Section 6801 Sample: KA02 L	3/4/1991	In-Situ	100		80
53994	30 Vaughn Sample: BA09 Layer: 5	6/23/2005	In-Situ	60		29
53995	30 Vaughn Sample: BA09 Layer: 4	6/23/2005	In-Situ	75		29
53997	30 Geysers E Sample: AC20 Layer: 4	6/25/2006	In-Situ			
(AutoNumber)						

Enter relevant data for each field using the keyboard or the drop down list (where available).

Exhibit 6

150 copies of this public document were produced at an estimated cost of \$3.20 each, for a total cost of \$479.48. This includes \$177.84 for postage and \$301.64 for printing.